

# **Non-invasive Imaging and 3D Visualization Techniques for the Study of Sea Urchin Internal Anatomy**

Dissertation  
zur Erlangung des Grades  
des Doktors der Naturwissenschaften  
am Fachbereich Biologie, Chemie und Pharmazie  
der Freien Universität Berlin

vorgelegt von  
Alexander Ziegler  
aus Lörrach

November 2008

**Gutachter**

Erster Gutachter:

Prof. Dr. Klaus Hausmann  
Institut für Biologie  
Fachbereich Biologie, Chemie und Pharmazie  
Freie Universität Berlin

Zweiter Gutachter:

Prof. Dr. Thomas Bartolomaeus  
Institut für Evolutionsbiologie und Ökologie  
Mathematisch-Naturwissenschaftliche Fakultät  
Rheinische Friedrich-Wilhelms-Universität Bonn

Datum der Disputation:

19. Dezember 2008

### **Erklärung**

Hiermit erkläre ich, dass ich die vorliegende Arbeit ohne die unzulässige Hilfe Dritter und ohne die Verwendung anderer als der angegebenen Hilfsmittel angefertigt habe. Die aus anderen Quellen direkt oder indirekt übernommenen Daten und Konzepte sind unter Angabe der Quelle gekennzeichnet.

Die Arbeit wurde bisher weder im In- noch im Ausland in gleicher oder ähnlicher Form einer anderen Prüfungsbehörde vorgelegt.

Berlin, den 24. November 2008

Alexander Ziegler

## Danksagung

Herrn Prof. Dr. Thomas Bartolomaeus möchte ich für die Aufnahme in seine Arbeitsgruppe und die Betreuung dieser Dissertation herzlich danken. Herrn Prof. Dr. Klaus Hausmann sei an dieser Stelle für seine freundliche Bereitschaft gedankt, das Koreferat dieser Dissertation sowie die abschließende Betreuung nebst Kommissionsleitung zu übernehmen.

Diese Arbeit wurde ermöglicht durch ein Promotionsstipendium des Landes Berlin (NaFöG) sowie durch ein Stipendium der Friedrich-Naumann-Stiftung für die Freiheit aus Mitteln des Bundesministeriums für Bildung und Forschung. Für die umfassende Förderung meines Dissertationsvorhabens möchte ich mich bei beiden Stipendiengebern sehr bedanken.

Bei der gesamten AG Systematik und Evolution der Tiere möchte ich mich für die Unterstützung und die vielen interessanten Diskussionen und Gespräche herzlich bedanken. Es hat mir große Freude bereitet, dass ich die letzten Jahre mit Euch verbringen durfte. Besonders möchte ich mich bei Herrn Dr. Björn Quast für seine Hilfe bei den alltäglichen Problemchen und so manche Fachsimpelei bedanken. Den Insassen der Diplomanden- und Doktorandenzimmer sei herzlich gedankt für die notwendige Zerstreung und Kurzweil, ohne die ich die letzten Jahre nicht hätte überleben können!

Nicht unerwähnt bleiben dürfen die Kooperationspartner im In- und Ausland, die mich bei der Erforschung von Seeigeln und den Möglichkeiten der 3D-Visualisierung immens unterstützt haben: Peter Adam (Berlin), Dr. Nadia Améziante (Paris), Dr. Frank Angenstein (Magdeburg), Andrew Cabrinovic (London), Prof. Dr. Chantal De Ridder (Bruxelles), Prof. Dr. Cornelius Faber (Münster), Dr. Peter Grobe (Berlin), Pravin Kumar (Berlin), Dr. Carsten Lüter (Berlin), Dr. Richard J. Mooi (San Francisco), Susanne Mueller (Berlin), Dr. Jérôme Murienne (Cambridge), Prof. Dr. Claus Nielsen (København), Dr. David L. Pawson (Washington D.C.), Dr. Bernhard Ruthensteiner (München), Dr. Andreas Schmidt-Rhaesa (Hamburg), Dr. Andrew B. Smith (London) sowie Dr. Louis G. Zachos (Washington D.C.).

Meiner Familie danke ich abermals für die grenzenlose Geduld und kompromisslose Unterstützung bei meinem Anliegen, ein passabler Akademiker zu werden, und widme ihr diese Arbeit.

## Zusammenfassung

Die Echinoidea (Seeigel) sind eine Gruppe von marinen Invertebraten, welche zu den Echinodermaten (Stachelhäutern), einem Taxon innerhalb der Deuterostomia, gehört. Obwohl umfassende Daten zur Larval- und Hartteilanatomie vorliegen, sind die Kenntnisse der Weichteilstrukturen der Seeigel aus verschiedenen Gründen noch bruchstückhaft. Darauf weisen u.a. gravierende Unterschiede in der Literatur bezüglich des Vorhandenseins von Strukturen wie beispielsweise des Siphons, des Caecums oder der Tiedemann'schen Körperchen bei verschiedenen Seeigeltaxa hin.

Das wesentliche Ziel der vorliegenden Studie war die Ermittlung des Potentials von zwei nicht-invasiven bildgebenden Verfahren, nämlich der Magnetresonanztomographie (MRT) sowie der Mikro-Computertomographie ( $\mu$ CT), zur Darstellung von inneren Strukturen der Seeigel in Kombination mit modernen 3D-Visualisierungstechniken. Eine umfassende vergleichende Analyse sollte durch die Verwendung von seltenem Museumsmaterial ermöglicht werden.

Für die Darstellung von internen Strukturen bei Wirbellosen, speziell von Weichteilen, stellte sich die MRT als ein geeignetes Verfahren heraus, da hier Strukturen bei einer isotropen Auflösung bis weit unter 100  $\mu$ m analysiert werden konnten. Aufgrund der relativ einfachen Vorbereitung des Tiermaterials konnte ein hoher Probendurchsatz realisiert werden. Anhand der Daten wurden 3D-Modelle zur Visualisierung von ausgewählten Weichteilmerkmalen erstellt. Die Darstellung von Weichteilen war mit Hilfe der  $\mu$ CT auf Grund des dort angewandten Röntgenverfahrens nicht möglich. Allerdings konnten interne Hartteilstrukturen mit einer isotropen Auflösung bis unter 20  $\mu$ m dargestellt werden, welche die MRT-Daten sinnvoll ergänzten. Dieser Ansatz ist vor allen Dingen bei Echinodermaten erfolgversprechend, da hier sowohl Weich- als auch Hartteilstrukturen vorliegen.

Um neue Wege bei der Kommunikation und der Speicherung der Daten zu beschreiten, wurden diese per Internet öffentlich zugänglich gemacht sowie als interaktive 3D-Modelle direkt in wissenschaftliche Publikationen eingebettet. Dieser Ansatz beinhaltete auch die Verwendung von Daten aus einer zentralen Datenbank mit Proteinstrukturen.

Zur Verdeutlichung der Anwendungsmöglichkeiten von nicht-invasiven bildgebenden Verfahren wurden die erhobenen MRT-Daten zum Axialkomplex, einer hochspezialisierten Struktur bei Echinodermaten, mit Resultaten aus histologischen Schnittserien sowie einer umfassenden Literaturrecherche verknüpft. Die Ergebnisse belegen eine strukturelle Interdependenz des Axialkomplexes und verschiedener anderer Weichteile bei Seeigeln.

Schlussendlich sollte das Potential der Weichteilstrukturen von Seeigeln zur Erweiterung der bestehenden morphologischen Datenmatrix untersucht werden. Eine Auswahl von Weichteilmerkmalen wurde daher eingehend analysiert und für eine umfassende Anzahl von Seeigeltaxa beschrieben. Die Ergebnisse zeigen die phylogenetische Relevanz dieser Strukturen und eröffnen die Aussicht auf eine umfassende kladistische Analyse basierend auf Hartteil-, Larval-, und molekularen Merkmalen in Kombination mit Weichteilmerkmalen.

## Summary

Echinoidea (sea urchins) are a group of benthic marine invertebrates that belong to the deuterostome taxon Echinodermata. Although extensive data have been gathered on larval and adult hard-part anatomy of sea urchins, for several reasons the knowledge of echinoid soft tissue anatomy is still fragmentary. For example, published works report differences in various taxa regarding the presence or absence of prominent internal organs such as the primary siphon, the gastric caecum, or the spongy bodies.

The major aim of the present study was therefore to evaluate the potential of two non-invasive imaging techniques, namely magnetic resonance imaging (MRI) and micro-computed tomography ( $\mu$ CT), to visualize, in combination with advanced 3D modeling protocols, internal structures of sea urchins and to apply these techniques for large-scale comparative morphological analyses. In order to significantly extend taxon sampling, valuable specimens from museum collections were selected to be included in this study.

MRI proved to be ideally suited to depict internal structures of invertebrates non-invasively, especially soft tissues, at isotropic resolutions well below 100  $\mu$ m. Due to the simple specimen preparation as well as straight-forward imaging protocols, a high specimen throughput could be accomplished. Based on the digital tomographic datasets, 3D models were assembled in order to visualize selected features of echinoid soft tissue anatomy. Although imaging of soft tissues was practically impossible using conventional desktop  $\mu$ CT equipment due to the physical properties inherent in X-ray technology, this technique was successfully employed to visualize sea urchin hard-part anatomy at isotropic resolutions below 20  $\mu$ m. MRI and  $\mu$ CT can therefore be seen as complementary non-invasive imaging techniques, especially for echinoderm specimens in which soft- and hard-part anatomy are equally present.

To explore novel ways of communication and deposition of the acquired datasets as well as 3D models, these were made publicly available through the Internet and by integrating 3D data into PDF-based scientific publications. This approach included also the use of data from a central data repository for protein structures.

The axial complex, a highly specialized organ also found in other echinoderm taxa, was then selected for an exemplary comparative study involving dozens of sea urchin species in order to highlight the possibilities offered by non-invasive imaging techniques combined with dissection, histology, and a reappraisal of information from published work. The results suggest an architectural interdependence of the axial complex with various other internal organs present in sea urchins.

Finally, an attempt was made to evaluate the potential of echinoid soft tissue structures to extend the current list of morphological characters used for phylogenetic inferences. A set of selected soft tissue characters was therefore assembled and evaluated for every major sea urchin taxon. The results provide significant phylogenetic information and open the prospect for a comprehensive cladistic analysis including hard-part, larval and molecular characters as well as extensive soft tissue anatomy.

## List of Publications

Publications describing parts of this thesis:

Ziegler A, Angenstein F (2007): Analyse von Seeigeln (Echinoidea) mit Hilfe der bildgebenden Magnetresonanztomographie. *Mikrokosmos* 96: 49-54

Ziegler A, Mueller S, Bartolomaeus T: Sea urchin (Echinoidea) anatomy revealed by magnetic resonance imaging and 3D visualization. In: Harris L, ed. Conference Proceedings, 12<sup>th</sup> International Echinoderm Conference, in press

Ziegler A, Faber C, Mueller S, Bartolomaeus T (2008): Systematic comparison and reconstruction of sea urchin (Echinoidea) internal anatomy: a novel approach using magnetic resonance imaging. *BMC Biology* 6: 33

Ziegler A, Faber C, Mueller S (2008): 3D visualization of sea urchin anatomy. In: Smith AB, ed. The Echinoid Directory. Internet publication. <http://www.nhm.ac.uk/research-curation/research/projects/echinoid-directory/index.html>

Ziegler A, Zachos LG (2008): *Echinoneus cyclostomus*, *Mespilia globulus*, *Moira atropos* & *Psammechinus miliaris*. In: Rowe T, ed. The Digital Morphology Library. Internet publication. <http://www.digimorph.org/index.phtml>

Murienne J, Ziegler A, Ruthensteiner B (2008): A 3D revolution in communicating science. *Nature* 453: 450

Kumar P\*, Ziegler A\*, Ziegler J, Uchańska-Ziegler B, Ziegler A (2008): Grasping molecular structures through publication-integrated 3D models. *Trends in Biochemical Sciences* 33: 408-412 (\* Joint first authors)

Ziegler A, Faber C, Bartolomaeus T: Evolution of the axial complex and interdependence of internal organ systems in sea urchins (Echinodermata: Echinoidea). Submitted

## List of Abbreviations

2D	two-dimensional
3D	three-dimensional
BAH	Biologische Anstalt Helgoland, Helgoland, Germany
B.C.	before Christ
CAS	California Academy of Sciences, San Francisco, USA
CD	interradius between the echinoderm radii C and D
CLSM	confocal laser scanning microscopy
CPU	central processing unit
CT	computed tomography
DICOM	Digital Imaging and Communications in Medicine
DigiMorph	The Digital Morphology Library
ECM	extracellular matrix
FLASH	Fast Low-Angle Shot
Fig.	figure
Figs.	figures
FOV	field of view
HC	heavy chain
HLA	human leukocyte antigen
ID	identification
JPEG	Joint Photographic Experts Group
MDEFT	Modified Driven Equilibrium Fourier Transform
$\mu$ CT	micro-computed tomography
Mio.	<i>Million</i> (German): million
MorphDBase	Morphological Description Data Base
MNHN	Muséum Nationale de la Histoire Naturelle, Paris, France
MR	magnetic resonance
MRI	magnetic resonance imaging
MRM	magnetic resonance microscopy
MRT	<i>Magnetresonanztomographie</i> (German): magnetic resonance imaging
nanoCT	nano-computed tomography
NHM	Natural History Museum, London, United Kingdom
NMR	nuclear magnetic resonance
N.N.	<i>nomen nescio</i> or <i>nomen nominandum</i> (Latin): name not known
OCT	optical coherence tomography
PC	personal computer
PD	proton density
PDB	Protein Data Bank



PDF	Portable Document Format
RARE	Rapid Acquisition and Relaxation Enhancement
RF	radio frequency
sp.	species – singular form
spp.	species – plural form
T	Tesla
Tab.	table
$T_E$	echo time
TEM	transmission electron microscopy
TIFF	Tagged Image File Format
$T_R$	repetition time
U3D	Universal 3D
ULB	Université Libre de Bruxelles, Bruxelles, Belgium
US	ultrasonography
USNM	National Museum of Natural History, Washington DC, USA
VRML	Virtual Reality Modeling Language
WB	wide-bore
ZMB	Systematische Zoologie am Museum für Naturkunde, Berlin, Germany
ZMH	Zoologisches Institut und Museum, Hamburg, Germany
ZSM	Zoologische Staatssammlung, München, Germany

## Table of Contents

<b>Gutachter</b> .....	i
<b>Erklärung</b> .....	ii
<b>Danksagung</b> .....	iii
<b>Zusammenfassung</b> .....	iv
<b>Summary</b> .....	v
<b>List of Publications</b> .....	vi
<b>List of Abbreviations</b> .....	vii
<b>Table of Contents</b> .....	ix
<b>1. Introduction</b> .....	1
1.1. Echinoidea (sea urchins): general overview .....	1
1.2. Sea urchin internal anatomy: historical outline .....	2
1.3. Non-invasive imaging techniques and 3D visualization .....	7
1.4. Aims of the present study .....	10
<b>2. Analysis of Sea Urchins Using MRI</b> .....	11
2.1. Summary .....	11
2.2. Publication (Mikrokosmos 2007) .....	12
<b>3. Sea Urchin Internal Anatomy Revealed by MRI</b> .....	18
3.1. Summary .....	18
3.2. Publication (Conference Proceedings, 12th IEC) .....	19
<b>4. Systematic Reconstruction of Sea Urchin Internal Anatomy</b> .....	25
4.1. Summary .....	25
4.2. Publication (BMC Biology 2008) .....	26
<b>5. Sea Urchin Models on the Internet</b> .....	43
5.1. Summary .....	43
5.2. Publication (The Echinoid Directory 2008) .....	44
5.3. Publication (The Digital Morphology Library 2008) .....	53
<b>6. Embedding 3D Models into PDF-based Publications</b> .....	56
6.1. Summary .....	56
6.2. Publication (Nature 2008) .....	57
6.3. Publication (Trends in Biochemical Sciences 2008) .....	58
<b>7. Evolution of the Axial Complex</b> .....	63
7.1. Summary .....	63
7.2. Manuscript (submitted).....	64

<b>8. Sea Urchin Comparative Soft Tissue Anatomy</b> .....	114
<b>9. Final Discussion and Conclusions</b> .....	159
9.1. Comparative morphological analyses using MRI and $\mu$ CT .....	159
9.2. Communicating 3D datasets .....	161
9.3. Suitability of echinoid soft tissues for phylogenetic inferences .....	162
9.4. Concluding remarks .....	167
<b>Bibliography (Chapters 1, 8, 9)</b> .....	169

# 1. Introduction

## 1.1. Echinoidea (sea urchins): general overview

Sea urchins are a group of marine benthic organisms belonging to the phylum Echinodermata (marine spiny-skinned animals). The Echinodermata are a large deuterostome clade and share a common ancestor with such diverse taxa as Pterobranchia, Enteropneusta (acorn worms), Tunicata (sea squirts), Cephalochordata (lancelets), and Vertebrata (vertebrates). Echinoderms are characterized by a specialized coelomic compartment, the water vascular system, that distinguishes them from all other taxa. It is composed of the ring canal as well as five radial canals, indicative of a pentameric symmetry. This pentamery, another apomorphy of the Echinodermata, is a secondary character of the adult organism since the echinoderm larva displays a bilateral symmetry. Furthermore, echinoderms do not possess a central nervous centre. Their nervous system consists of nerve cords located around the mouth as well as along the ambulacra. About 6500 echinoderm species are currently known (Goldschmid 2007), with ~620 species assigned to the Crinoidea (sea lilies and feather stars), ~1500 to the Asteroidea (sea stars), ~2000 to the Ophiuroidea (brittle stars and basket stars), ~1500 to the Holothuroidea (sea cucumbers), and about 950 to the Echinoidea (sea urchins, lamp urchins, sand dollars, and heart urchins).

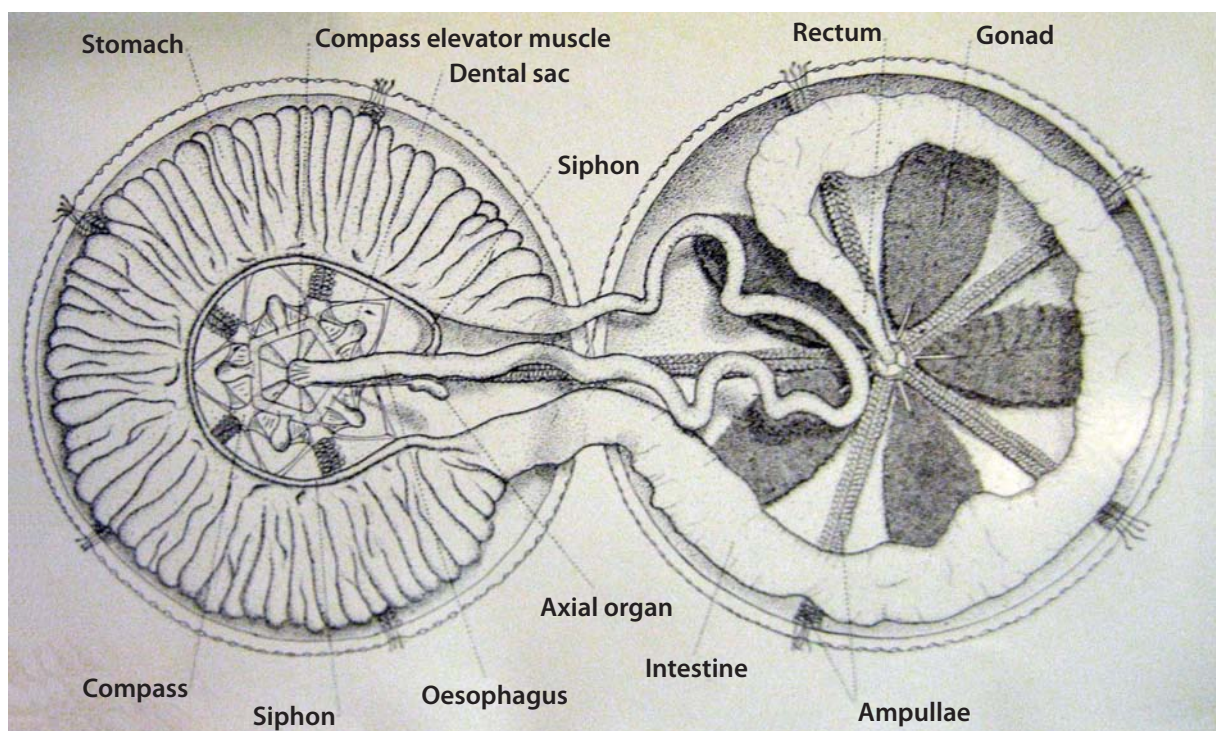
The Echinoidea are a well-defined monophyletic group of echinoderms that form, together with their sister taxon, the Holothuroidea, the taxon Echinozoa. In contrast to sea cucumbers, sea urchins are characterized by a solid globular calcite endoskeleton composed of fused skeletal ossicles. Further characters distinguishing the echinoids from other echinoderm taxa are the presence of a peristome, the apical system with periproct, the perignathic girdle, and the prominent feeding apparatus, known as Aristotle's lantern. The name of this group of animals is derived from the Greek, meaning "hedgehog of the sea" and was coined by Aristoteles (384-322 B.C.) in his *Historia Animalium*.

Echinoid taxonomy and phylogeny are traditionally based on hard-part morphology, i.e. characters of the calcite endoskeleton as well as Aristotle's lantern. Both provide a wealth of phylogenetically informative characters. Moreover, these calcite structures readily fossilize, permitting to integrate the more than 10,000 known fossil species into phylogenetic inferences. The geological record of this group of invertebrates is extremely well known and the monophyly of the Echinoidea is undisputed (e.g. Jensen 1981, Littlewood et al. 1997).

Modern cladistic analyses have combined morphological and molecular datasets, resulting in an improved understanding of echinoid phylogeny (e.g. Littlewood & Smith 1995, Smith et al. 2006). These studies reveal a number of sister-group relationships, e.g. between the Cidaroida and the Euechinoidea as well as between the Echinacea and the Irregularia. However, although the interrelationships of the various higher echinoid taxa are relatively well documented, a number of areas with uncertainty remain, especially at the base of the

euechinoid, acroechinoid and echinacean lineages (Fig. 1 in Chapter 7, p. 96, provides a generalized tree of the Echinoidea). Here, hard-part as well as molecular analyses have so far not been able to successfully resolve phylogenetic relationships. This circumstance can be attributed to the fact that the present set of morphological characters has reached a certain degree of exhaustion. In addition, further molecular studies are complicated due to the problematic logistics that systematists are often confronted with, e.g. in the case of deep-sea taxa. A character set that so far has received comparatively little attention in sea urchin phylogenetic studies is the internal anatomy of sea urchins.

Adult sea urchins are composed of hard-part as well as soft tissue structures. Like all echinoderms, sea urchins can anatomically be divided into radial and interradial zones, termed ambulacra and interambulacra, respectively. The ambulacra are characterized by the presence of the radial canals of the water vascular system, whereas the interambulacra give rise to the reproductive organs. The major internal soft tissue structures include the dominant alimentary canal, reproductive organs, the various muscles of Aristotle's lantern, the water vascular system, and the axial complex (Fig. 1).



**Fig. 1:** *Arbacia punctulata* (Echinoidea: Arbacioida). Major internal soft tissue structures of a “regular” sea urchin. Modified after Coe (1912).

## 1.2. Sea urchin internal anatomy: historical outline

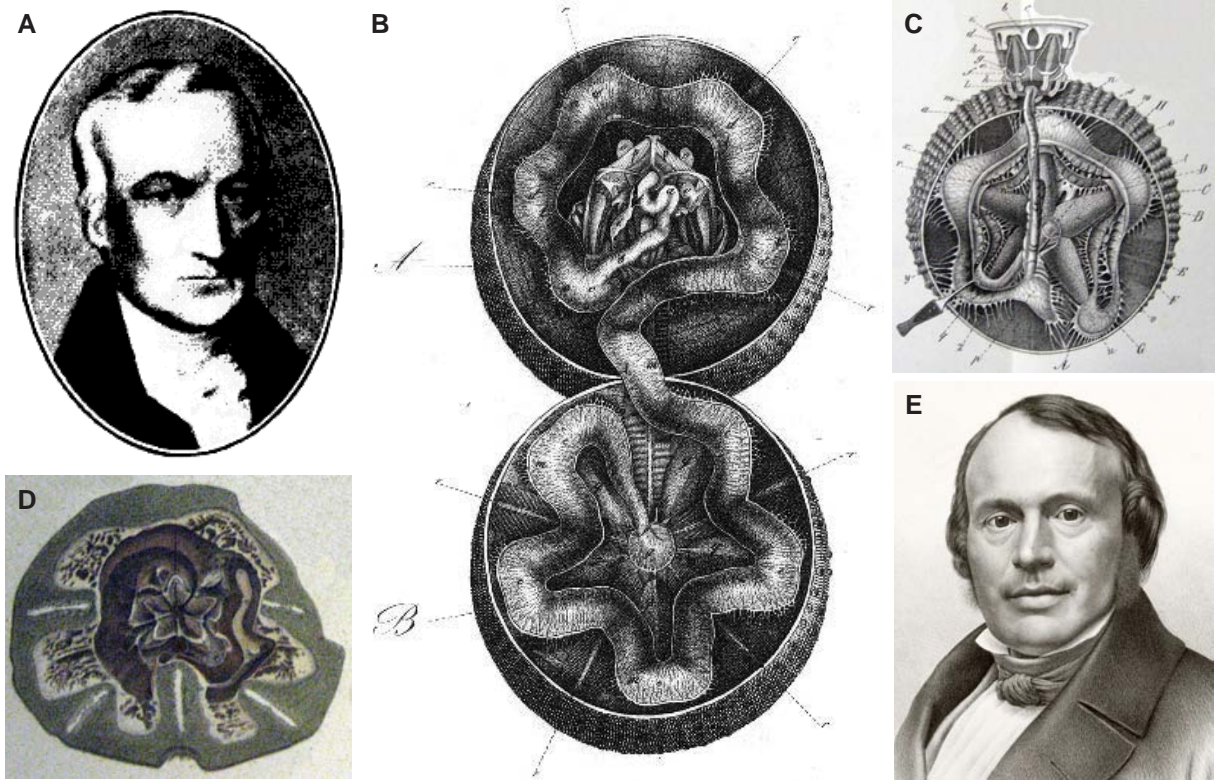
Sea urchin internal anatomy has been a matter of study for almost 2500 years, starting with the early text-based descriptions of Aristoteles (*Historia Animalium*, *De Partibus Animalium*, *De Generatione Animalium*) and Plinius (*Historia Naturalium*). However, the first figure to depict the internal anatomy of a sea urchin was provided by Guillaume Rondelet (also



**Fig. 2:** A Guillaume Rondelet. C Conrad Gesner. E Ulisse Aldrovandi. B, D, F Drawings of a dissected sea urchin taken from the works of the three masters.

known as Rondeletius, 1507-1566) in 1554 and is shown in his monumental work *De Piscibus Marinis* (Fig. 2). This drawing probably represents the earliest figure of a dissected invertebrate (Harvey 1956). The image was copied by Conrad Gesner (Gesnerus, 1516-1565) in his famous *Fischbuch* from 1563 (published first in Latin in 1558 as *De Piscium et Aquatilium Animantium Natura*) as well as by Ulisse Aldrovandi (Aldrovandus, 1522-1605) in one of his works published after his death, *De Reliquis Animalibus Exsanguinibus* from 1606, very likely cases of early plagiarism.

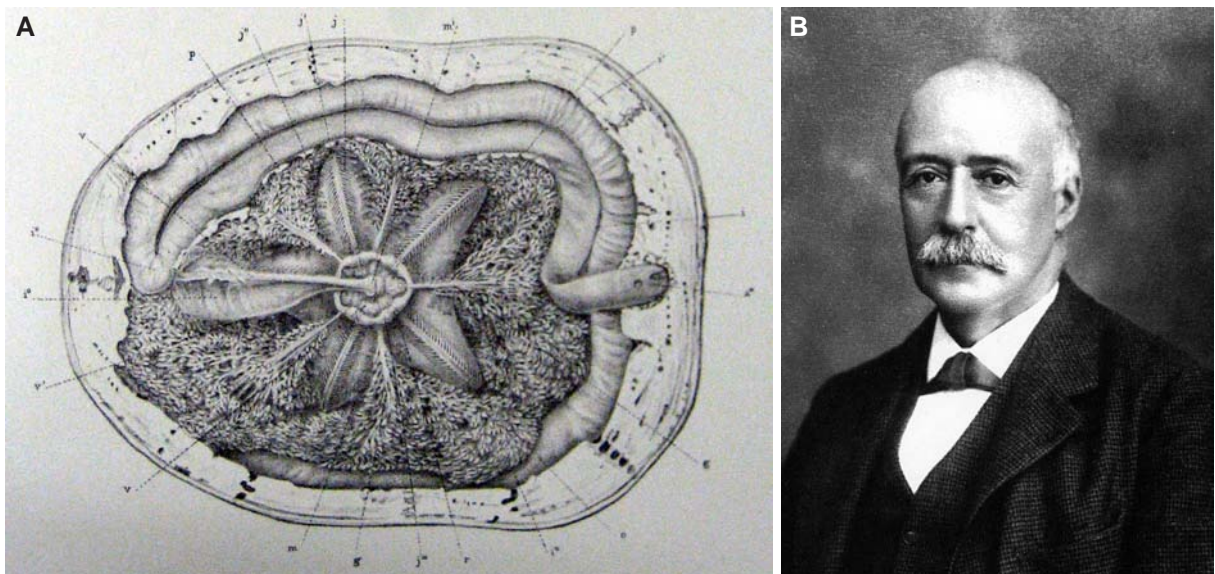
Although other naturalists such as Georg Eberhard Rumpf (Rumphius, 1627-1702), Johann Philipp Breyne (Breynius, 1680-1764), and Jacob Theodor Klein (1685-1759) also described sea urchin anatomy, they did not provide any drawings of internal structures. Over two-hundred years after Aldrovando's work, employing the descriptive and portraying techniques he had learned during his years in medical school, Friedrich Tiedemann (1781-1861) drew several views of the internal anatomy of *Paracentrotus lividus* (Lamarck, 1816) in his award-winning work on echinoderm comparative anatomy from 1816 (Fig. 3). The next sea



**Fig. 3:** **A** Friedrich Tiedemann. **B** *Paracentrotus lividus*, from Tiedemann (1816). **C** *Echinus esculentus*, from Valentin (1841). **D** *Mellita quinquesperforata*, from Agassiz (1841). **E** Jean Louis Rodolphe Agassiz.

urchin species to be portrayed in great detail both from the in- and the outside was *Echinus esculentus* Linnaeus, 1758 as published by Gabriel Gustav Valentin (1810-1883) in one of the monographic series of the great Swiss naturalist Jean Louis Rodolphe Agassiz (1807-1873), *Monographies d'Echinodermes*. In this particular work, Agassiz himself included a drawing of the internal anatomy of a sand dollar, *Mellita quinquesperforata* (Leske, 1778).

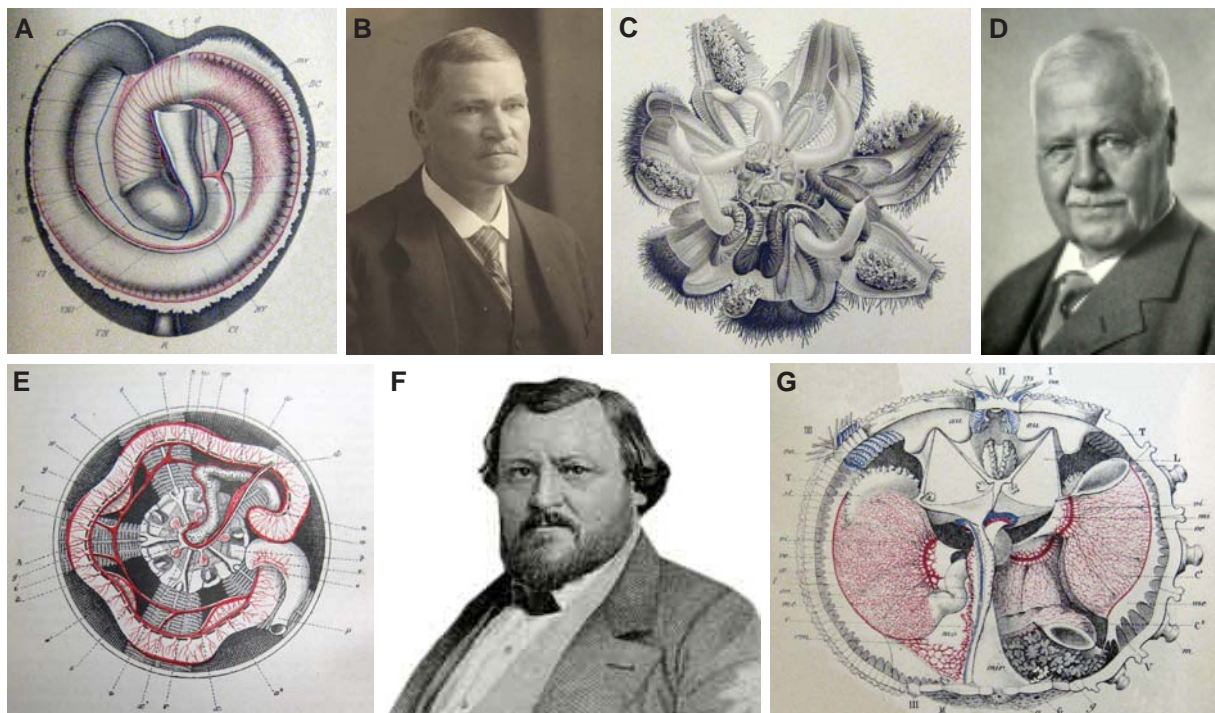
Agassiz' work was continued by his son, Alexander Emmanuel Agassiz (1835-1910) who, just like his father, became director of the Museum of Comparative Zoology at Harvard



**Fig. 4:** **A** *Clypeaster subdepressus*, from Agassiz (1872-1873). **B** Alexander Emmanuel Agassiz, from Summers et al. (1999)

University in Cambridge, USA. Alexander Agassiz published numerous papers and books on sea urchins and other echinoderms and also included many drawings of their internal anatomy (Fig. 4). The drawing presented here was taken from his authoritative work *Revision of the Echini* that was published in 1872-1873.

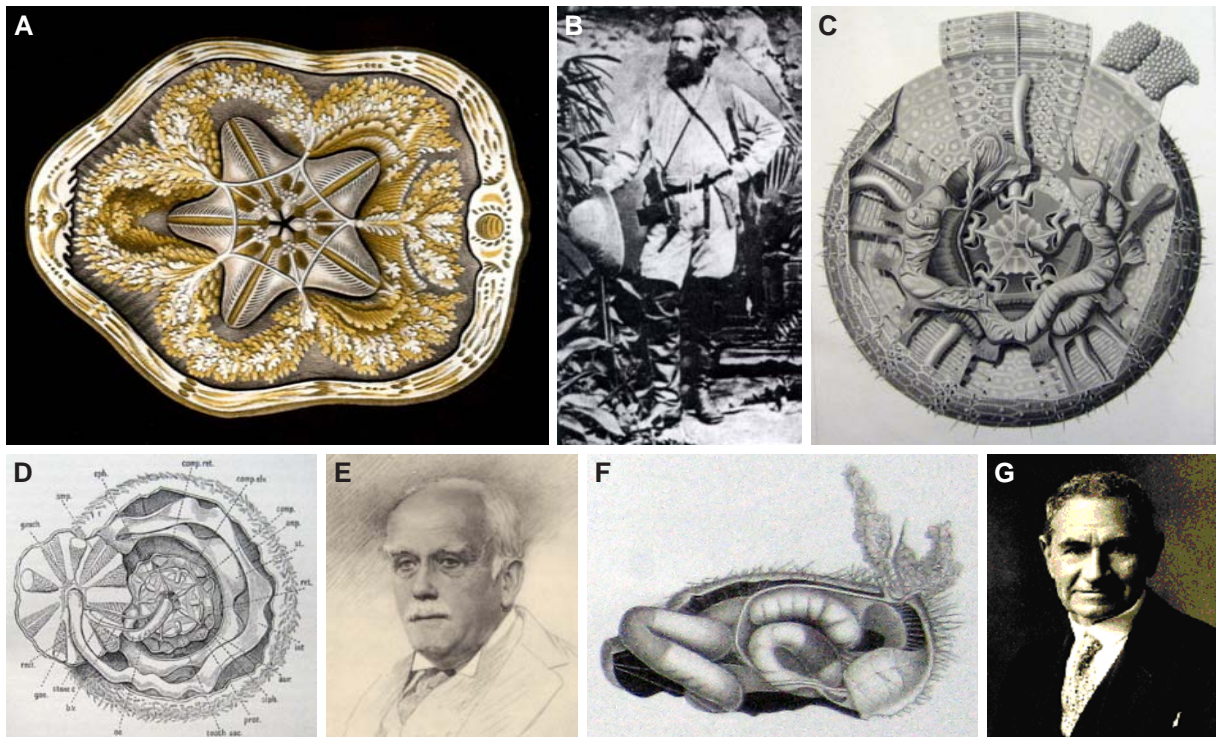
The two last decades of the 19<sup>th</sup> century saw a remarkable increase in knowledge on sea urchin diversity, based largely on the extensive cruises conducted during the years of imperialist expansion. Notable publications on sea urchins and their internal anatomy include works by Jean Baptiste Francois René Koehler (1860-1931), Paul Sarasin (1856-1929) and Karl Friedrich Sarasin (1859-1942), Henri Prouho (1854-1921), as well as August Christoph Carl Vogt (1817-1895) and Émile Yung (1854-1918) (Fig. 5).



**Fig. 5:** **A** *Spatangus purpureus*, from Koehler (1883). **B** Paul Sarasin. **C** *Asthenosoma varium*, from Sarasin & Sarasin (1887). **D** Karl Friedrich Sarasin. **E** *Paracentrotus lividus*, from Vogt & Yung (1888). **F** August Christoph Carl Vogt. **G** *Cidaris cidaris*, from Prouho (1887).

The study of sea urchin internal anatomy at the beginning of the 20<sup>th</sup> century was characterized by a continuation of the work done in the decades before. Based on the large collections assembled during the various scientific cruises, museum curators and other researchers at institutions around the world dissected sea urchins and depicted their internal anatomy in a number of monographs and articles. Understandably, the beauty of the internal and external symmetry of sea urchins did not escape Ernst Heinrich Philipp August Haeckel (1834-1919) and so, in his *Kunstformen der Natur*, he depicted also, apart from external views of sea urchins, the reproductive organs as well as Aristotle's lantern of a dissected *Clypeaster rosaceus* (Linnaeus, 1758). Like Haeckel, further authorities on echinoderm morphology and systematics such as Ernest William MacBride (1866-1940), Walther Schurig, Johannes Wagner and others conducted their research based largely on sea urchin species found in the



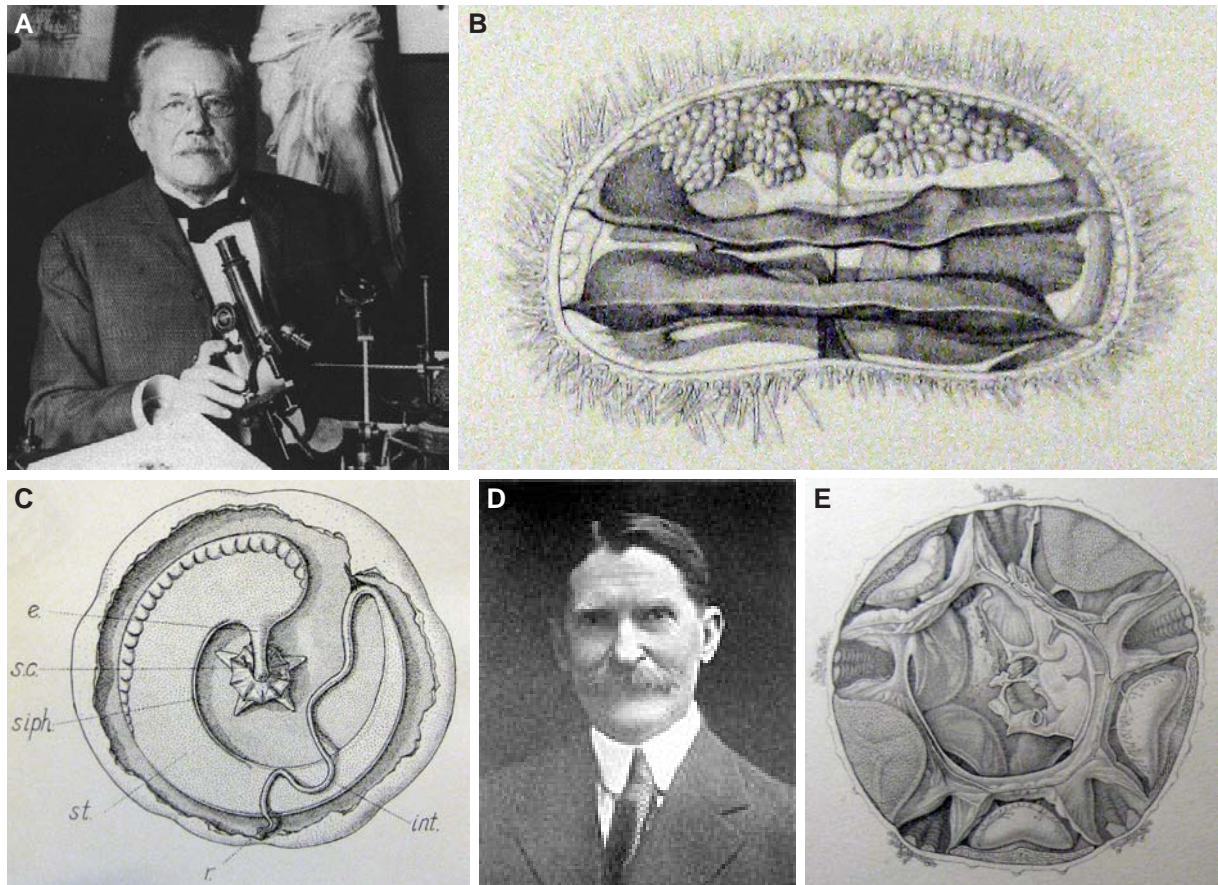


**Fig. 6:** **A** *Clypeaster rosaceus*, from Haeckel (1904). **B** Ernst Heinrich Philipp August Haeckel. **C** *Sperosoma biseriatum*, from Schurig (1906). **D** *Echinus esculentus*, from MacBride (1906). **E** Ernest William MacBride, from Calman (1941). **F** *Pourtalesia jeffreysi*, from Mortensen (1907). **G** Ole Theodor Jensen Mortensen.

European and Atlantic waters (Fig. 6). Drawings of sea urchin internal anatomy were also provided by the presumably most productive author on sea urchin diversity and systematics, Ole Theodor Jensen Mortensen (1868-1952). At the same time, in the United States, Hubert Lyman Clark (1870-1947), Andreas Magnus Westergren, Wesley Roswell Coe (1869-1960) and others worked on species that had been dredged, collected and found in the Atlantic as well as the Pacific Ocean (Fig. 7).

During the later years of the 20<sup>th</sup> century, studies of the internal anatomy of sea urchins became rather uncommon, partly due to new foci of scientific interest and the development of new types of investigation such as electron microscopy that permitted the study of tissues in much greater detail. A comprehensive review of the contemporary knowledge on internal sea urchin structures was provided by Libbie Henrietta Hyman (1888-1969) in her work *The Invertebrates* (1955). However, the golden age of studies on sea urchin gross morphology had clearly come to an end. Nevertheless, a number of recent authors, notably Bonnet (1925), Aiyar (1938), Strenger (1973), De Ridder & Jangoux (1993), and Kaburek & Hilgers (1999) depicted their findings from dissections, thereby contributing to our understanding of the complex internal anatomy of these animals.

One reason that soft tissues have so far been almost entirely neglected in phylogenetic inferences is due to the restriction of reliable information on soft tissues to the more readily accessible sea urchin taxa found along the coasts of Europe and Northern America. Another reason can be found in the scarcity of certain echinoid taxa collected during deep-sea expedi-



**Fig. 7:** **A** Andreas Magnus Westergren, from Summers et al. (1999). **B** *Echinoneus cyclostomus*, from Westergren (1911). **C** *Echinarachnius parma*, from Coe (1912). **D** Wesley Roswell Coe. **E** *Echinothrix diadema*, from Agassiz & Clark (1909).

tions and that are now part of museum collections. Since these animals are available for study only in very small numbers, traditional invasive techniques usually cannot be applied.

All the above-mentioned results were gathered using dissection, a technique which inevitably leads to the destruction of the analyzed specimen. However, modern imaging techniques permit now to look “inside” a specimen without the need to open or even destroy it, thus allowing, in principal, to conduct analyses on valuable and rare museum material.

### 1.3. Non-invasive imaging techniques and 3D visualization

Non-invasive imaging techniques have successfully been employed in medical diagnostics for over one hundred years. Since technical advances in the last decades had led to an increase in image resolution, several non-invasive imaging techniques have also been used for the study of invertebrates. Prominent examples of such methods include confocal laser scanning microscopy (CLSM), optical coherence tomography (OCT), ultrasonography (US), micro-computed tomography ( $\mu$ CT), and magnetic resonance imaging (MRI). All of these methods are capable of delivering three-dimensional representations of biological samples non-invasively at resolutions relevant to invertebrate anatomy and, potentially, also to physiology.

CLSM produces high-resolution optical images of fluorescent slices or whole specimens. In-plane resolution may be as high as 250 nm (Amos & White 2003). Unfortunately, isotropic resolution (i.e. uniform resolution in all directions) at this level is impossible to obtain due to the error inherent in certain optical components of the imaging system. Nevertheless, following point-by-point image acquisition and computer-based image reconstruction, 3D models can in principal be obtained. CLSM is a scanning imaging technique and has also been used for 3D reconstructions of whole specimens based on the autofluorescence of the arthropod cuticula (Klaus & Schawaroch 2006, Michels 2007). This approach is restricted to small specimens and usually does not reveal internal structures. Like CLSM, OCT is also an optical tomographic technique. It is based upon the principle of echo-location and can therefore be best described as optical ultrasound (Huang et al. 1991). Reflections from within biological samples are measured with only the coherent reflections being detected. Resolutions may be as high as 10  $\mu\text{m}$  (Schmitt 1999). However, specimen size as well as tissue penetration depth severely limit the application of OCT. In contrast to OCT, ultrasonography is a widely used technique in medical diagnostics. Like the former technique, it is based on the principle of echo-location, although here ultrasound is emitted into a biological sample and the reflections are measured. 3D imaging is made possible through the application of this technique at different angles and the later processing of the raw data using advanced computers. Overall resolution of ultrasonography is fairly low and rarely exceeds 300  $\mu\text{m}$  (Bushberg 2002).

Considerably higher resolutions – in-plane as well as isotropic – can be acquired using  $\mu\text{CT}$ . This method is based upon a radiographic technique (X-ray) and has become a standard in studies of fossil specimens and skeletons (Attwood 2006). 3D volume datasets are created from a large series of 2D X-ray images that are taken around a single axis of rotation. The isotropic resolutions feasible with  $\mu\text{CT}$  range from 1 mm in clinical imaging down to 400 nm in experimental setups. Due to the form of electromagnetic radiation employed,  $\mu\text{CT}$  systems reveal primarily hard tissue structures such as bone or calcite. However, modern setups have been used to display soft tissue as well. These novel approaches include X-ray synchrotron microtomography and very-high-resolution X-ray computed tomography (Tafureau et al. 2006, Sutton 2008).

Magnetic resonance imaging (MRI) is a further tomographic technique. It relies on the principal of nuclear magnetic resonance (NMR). This physical phenomenon is based upon the intrinsic quantum mechanical property of the spin of certain nuclei. These nuclei are present in elements with an odd number of protons and neutrons, e.g.  $^1\text{H}$ ,  $^{13}\text{C}$ ,  $^{15}\text{N}$ ,  $^{19}\text{F}$ , and  $^{23}\text{Na}$ . In pre-clinical and clinical MRI, it is typically the density of  $^1\text{H}$  protons within the sample that is assessed by excitation of water molecules using radio-frequency waves, combined with spatially varying magnetic fields (the so-called gradient system). The image contrast is based upon the strength of the NMR signal from different locations within a sample. This signal varies according to the physical properties of the tissues. A number of parameters

influence image contrast, giving MRI considerable flexibility in depicting distinct internal structures. Isotropic resolution of high-field clinical scanning systems is currently around 1 mm, whereas high-field experimental scanners may reach isotropic resolutions down to 5  $\mu\text{m}$ . A comprehensive review of MRI principles and applications is provided by Callaghan (1991). Although MRI is primarily used to display soft tissue structures, hard-part anatomy can be analyzed as well in cases where the surrounding tissues generate a negative delineation. The principal feasibility of MRI studies to reveal soft tissue characteristics of invertebrates was demonstrated by studies on molluscs and arthropods (Brouwer et al. 1992, Bock et al. 2001, Gozansky et al. 2003, Davenel et al. 2006, Pohlmann et al. 2007).

Representations of internal structures of biological specimens have traditionally been made following observations during dissections or been based on series of histological sections. These procedures are technically demanding as well as time-consuming and irretrievably alter or even destroy the specimen. Further complications arise from the difficult 3D reconstruction of the structures observed (Ruthensteiner 2008). Artefacts, for example the deformation or compression of histological slices, and the problematic alignment of sections, make 3D reconstructions a laborious and often highly subjective procedure. In addition, the application of these traditional techniques leads to a gap in data transparency, since the original material on which the conclusions are based is usually not available for later examination.

In contrast, the non-invasive imaging techniques described above provide the researcher with digital datasets. The original data can therefore be stored, deposited or even made publicly accessible, so that the results based thereon may later be scrutinized. Apart from this important step towards total data transparency, digitally acquired datasets of morphological structures can readily be used for computerized 3D reconstructions. This applies especially to datasets with isotropic resolution, since the distance between the virtual slices, and thus the information content, is identical in all directions. Here, the individual volume elements (voxels) are cubical and thus facilitate exact measurements during data processing and visualization. These digital isotropic 3D datasets can easily be segmented into virtual 3D objects whose geometry (e.g. size and volume) can be quantitatively assessed.

It must be noted, however, that 3D visualizations of complex structures are currently limited. Today, the communication of 3D models is usually accomplished through a dissemination of movies based on rotating 3D models through the Internet or during presentations. In addition, static 2D images are being used to convey an idea of complex structures in scientific publications. However, a truly interactive access is limited to highly sophisticated software that is inaccessible to scientists without specialized knowledge of visual imagery, let alone the non-scientific community.

## 1.4. Aims of the present study

The aims of this study were, firstly, to evaluate the potential of modern non-invasive imaging techniques, in particular MRI and  $\mu$ CT, to display the internal anatomy of selected species of a marine invertebrate taxon, the Echinoidea.

Secondly, a crucial aspect regarding future comparative data management was to correlate the preliminary MRI results with conclusions derived from histological techniques. In addition, a set of imaging protocols had to be established that could be used for further standardized analyses at higher isotropic resolutions.

The third aim was to significantly extend taxon sampling through the inclusion of museum material. This aim would be achieved if the proven capacity of MRI and  $\mu$ CT techniques to display also the internal anatomical structures could be extended to old, preserved specimens. This approach included the application of contrast agents as well as improved imaging protocols. Based on the digital datasets acquired, 3D models of the internal and external anatomy of sea urchins were to be created.

However, during the computer-based 3D reconstruction process, it became apparent that novel communication channels would be essential in order to fully convey the acquired results. Therefore, bio-structures other than invertebrate anatomical structures were included in the analysis to underline the principal characters of the chosen approach.

Based on a successful application of non-invasive imaging techniques, a study was then to be undertaken that would focus on an important internal structure of sea urchins, which had been analyzed previously using histology and dissection. This large-scale comparative morphological analysis would then serve as a basis for further studies on sea urchin internal anatomy involving various other organ systems. The axial complex was chosen for this exemplary study.

Finally, an attempt was made to evaluate the potential of sea urchin internal organs for phylogenetic inferences in general based on a combination of results derived from non-invasive imaging, dissection, and a comprehensive literature search.

List of image sources taken from the internet:

Fig. 2C: <http://www.nndb.com/people/643/000050493/gesnerus75.jpg>

Fig. 2E: <http://de.wikipedia.org/wiki/Aldrovandi>

Fig. 3A: [http://de.wikipedia.org/wiki/Friedrich\\_Tiedemann](http://de.wikipedia.org/wiki/Friedrich_Tiedemann)

Fig. 3E: [http://de.wikipedia.org/wiki/Louis\\_Agassiz](http://de.wikipedia.org/wiki/Louis_Agassiz)

Fig. 5B: [http://www.ethbib.ethz.ch/aktuell/galerie/sarasin/Portr\\_gross.jpg](http://www.ethbib.ethz.ch/aktuell/galerie/sarasin/Portr_gross.jpg)

Fig. 5D: [http://www.stadtarchiv-schaffhausen.ch/Bildklein/45651.jpg\\_t.jpg](http://www.stadtarchiv-schaffhausen.ch/Bildklein/45651.jpg_t.jpg)

Fig. 5F: [http://de.wikipedia.org/wiki/Carl\\_Vogt](http://de.wikipedia.org/wiki/Carl_Vogt)

Fig. 6B: [http://caliban.mpiz-koeln.mpg.de/~stueber/haeckel/ceylon\\_e/habitus.jpg](http://caliban.mpiz-koeln.mpg.de/~stueber/haeckel/ceylon_e/habitus.jpg)

Fig. 7D: [http://www.peabody.yale.edu/images/archives/ypmbios/Coe\\_WR.jpg](http://www.peabody.yale.edu/images/archives/ypmbios/Coe_WR.jpg)

## 2. Analysis of Sea Urchins Using MRI

### 2.1. Summary

Magnetic resonance imaging (MRI) has become a standard tool in medical diagnostics within the last 30 years, with the imaging quality improving exponentially. The increase in resolution of modern MRI scanners has triggered research on small animals as well, especially mice and rats. These animals are used as model organisms in a great variety of research fields, e.g. neurology and pharmacology. The aim of the work described in the following article was to evaluate the principal feasibility of MRI studies using sea urchins, both *in vivo* and *in vitro*. With a 4.7 T horizontal wide-bore scanner (Bruker BioSpec 47/20), specimens of the species *Psammechinus miliaris* (Müller, 1771) were analyzed in order to obtain data-sets of their internal anatomy and to compare these with results derived from an invasive technique, histology. The resolution achieved was relatively low and comparable to results derived from classical dissection techniques. However, the first images from within a living sea urchin specimen were obtained and a simple surface-rendered model of the internal anatomy was produced using manual segmentation and 3D imaging techniques. Based on these successful preliminary results, the decision was made to continue MRI studies on sea urchins using high-field MRI scanners.

### 2.2. Publication

Ziegler A, Angenstein F (2007): Analyse von Seeigeln (Echinoidea) mit Hilfe der bildgebenden Magnetresonanztomographie. *Mikrokosmos* 96: 49-54

## Analyse von Seeigeln (Echinoidea) mit Hilfe der bildgebenden Magnetresonanztomographie

Alexander Ziegler und Frank Angenstein

**Die Magnetresonanztomographie (MRT) hat sich in den letzten Jahren neben ihrer ständig zunehmenden Bedeutung für den medizinisch-diagnostischen Bereich auch zu einem veritablen Instrument in der zoologischen Grundlagenforschung entwickelt. Diese Entwicklung ist in erster Linie der rasanten Steigerung des Auflösungsvermögens der Geräte zuzuschreiben. Mit modernen MRT-Geräten lassen sich mittlerweile auch die inneren Strukturen von Wirbellosen darstellen, was diesem nicht-invasiven Verfahren neue Anwendungsgebiete eröffnet.**

**B**ei den Seeigeln (Echinoidea) handelt es sich um eine knapp eintausend Arten starke Tiergruppe innerhalb der Stachelhäuter (Echinodermata) mit einem Durchmesser von 5,5 mm (*Echinocyamus scaber*) bis 35 cm (*Sperosoma giganteum*). Die Seeigel zeichnen sich durch ein kugelförmiges, kalzifiziertes Plattenskelett, einen ebenfalls aus Kalk bestehenden Greif- und Baggerapparat, die so genannte Laterne des Aristoteles, sowie die zahlreichen Stacheln aus. Mit Hilfe des Greifapparates werden Algen vom Substrat abgeweidet – die meisten Seeigel sind daher herbivor. Die adulten Tiere weisen den für Stachelhäuter typischen fünfstrahligen (pentameren) Körperbau auf. Im Verlauf der Evolution hat ein Teil der Seeigel, die Irregularia, sekundär wieder einen bilateralen Körperbau angenommen. Dies hängt mit der veränderten Lebens- und Ernährungsweise der Tiere zusammen: Sie gehören zur Infauna, bewohnen also das Sediment, welches sie mit ihren spezialisierten Stacheln durchwühlen. Dabei nehmen sie große Mengen des Sediments auf und filtern die darin befindlichen Mikroorganismen als Nahrung heraus. Im Verlauf der Anpassung an diese Lebensweise entwickelten sie eine gerichtete Bewegung, was sich strukturell im bilateralen Körperbau ausdrückt.

Mikrotomen geschnitten werden zu können, zusätzlich entkalkt werden. Die Auflösung des Kalks setzt jedoch große Mengen an Kohlenstoffdioxid frei, was durch die starke Blasenbildung oftmals zur Zerstörung von Strukturen führt. Aufgrund ihrer Ernährungsweise sind zudem die irregulären Seeigel für die konventionelle Histologie eine im wahrsten Sinne des Wortes harte Nuss: Der Darm ist voll mit Sediment und die Tiere widersetzen sich hartnäckig allen Schneideversuchen.

Möchte man solch komplexe innere Strukturen wie das Nervennetz oder die Coelomräume mit Hilfe von Computern darstellen, ist die komplette Schnittserie eines intakten Tieres vonnöten. Eine computergestützte Rekonstruktion der Tiere wird dann aber zusätzlich dadurch erschwert, dass es beim Schneiden der Tiere zu Verzerrungen im Gewebe kommt. Diese Verzerrungen können nur durch aufwändige und zeitraubende Handarbeit am Computer korrigiert werden. All diese Schwierigkeiten ließen sich umgehen, wenn man, ohne das Tier zerstören zu müssen, einen Blick in sein Inneres werfen könnte. Ein solches Verfahren kommt seit vielen Jahren in der medizinischen Diagnostik zur Anwendung: Die Magnetresonanztomographie.

### **Problematische histologische Analysen von Seeigeln**

Histologische Untersuchungen erweisen sich bei den Seeigeln als kompliziert. Nach dem Fixieren müssen die Tiere, um mit Hilfe von

### **Historisches**

Das Phänomen der Magnetresonanz wurde 1946 von Bloch und Purcell entdeckt, wofür sie 1952 den Nobelpreis für Physik erhielten. In den siebziger Jahren des letzten Jahrhunderts

## 50 A. Ziegler und F. Angenstein

entwickelten dann Lauterbur und Mansfield Gradientensysteme sowie erste computergestützte Verfahren zur Bildgebung. Auch diese Leistungen wurden mit dem Nobelpreis (2003) ausgezeichnet.

### Ein wenig Theorie

Bei der Magnetresonanztomographie wird die physikalische Tatsache genutzt, dass die Atomkerne aller Elemente mit ungerader Anzahl von Protonen (und Neutronen) aufgrund des Eigendrehimpulses von Protonen, dem so genannten Spin, ein magnetisches Moment erhalten. Wird ein solcher Kern einem starken homogenen und statischen Magnetfeld ausgesetzt, dann richten sich seine Protonen entlang der Feldlinien aus – ähnlich wie bei einem Stabmagneten – was zu einer Magnetisierung führt. Allerdings richten sich die Protonen nicht exakt nach den Feldlinien aus, sondern kreisen (präzidieren) um ihre Achse mit einer spezifischen Resonanzfrequenz – der Larmor-Frequenz. Diese Frequenz ist abhängig vom Element sowie von der Feldstärke des Magneten.

Wird nun ein hochfrequenter Anregungsimpuls mit der passenden Larmor-Frequenz quer zum Hauptmagnetfeld eingestrahlt, kommt es zu einer Auslenkung der Spins um 90°. Die Nettomagnetisierung der Protonen, die sich nun im rechten Winkel zum Hauptmagnetfeld befinden, kann mit einer speziellen Empfangsspule gemessen werden. Das Rotieren des magnetischen Moments der Protonen induziert in der Spule einen Strom mit der entsprechenden Larmor-Frequenz. Dieses Signal nimmt exponentiell ab, allerdings abhängig vom Gewebetyp mit unterschiedlicher Geschwindigkeit, was zu

einer unterschiedlichen Signalstärke der einzelnen Gewebe führt. Mit Hilfe eines magnetischen Gradientensystems lassen sich nun einzelne Körperschichten mit der Larmor-Frequenz gezielt anregen; nur in der angeregten Schicht kommt es dann zur Auslenkung der Protonen. Legt man drei Gradientensysteme (x, y, z) an, dann lässt sich das Signal der relaxierenden Protonen auch räumlich darstellen. Dieser Signalmix wird durch leistungsfähige Computer mittels einer Fourier-Transformation aufgelöst und kann schließlich als Bild dargestellt werden.

In der konventionellen Magnetresonanztomographie werden Wasserstoffprotonen als Signalgeber genutzt. Somit ist die Magnetresonanztomographie eigentlich die Darstellung einer Verteilung von Wasser im untersuchten Objekt. Der Kontrast ergibt sich aus der Fähigkeit des jeweiligen Gewebes, das Signal der relaxierenden Wasserstoffprotonen zu beeinflussen.

### Auflösungsvermögen

Als Auflösungsvermögen bezeichnet man in der Optik die Unterscheidbarkeit feiner Strukturen, also den gerade noch wahrnehmbaren Abstand zwischen zwei Punkten. Das Auflösungsvermögen eines Magnetresonanztomographen variiert je nach Stärke des eingesetzten Magneten, der Beschaffenheit der Hochfrequenz- und Empfangsspulen sowie der Dauer der Aufnahmen. Aus Tabelle 1 lässt sich eine Reihe von bildgebenden Verfahren mit ihrem jeweiligen Auflösungsvermögen entnehmen.

Mit den herkömmlichen experimentellen MRT-Geräten kann man, abhängig von der Magnet-

**Tabelle 1: Bildgebende Verfahren und ihr derzeitiges Auflösungsvermögen.**

Technik	Auflösungsvermögen (1 mm $\triangleq$ 1.000 $\mu$ m $\triangleq$ 1.000.000 nm)
Menschliches Auge	200 $\mu$ m
Lichtmikroskop	200 nm
Konfokales Laserscanningmikroskop	50–250 nm
Rasterelektronenmikroskop	10 nm
Transmissionselektronenmikroskop	0,8–2 nm
Klinische Magnetresonanztomographie	1 mm
Experimentelle Magnetresonanztomographie	10–150 $\mu$ m
$\mu$ -Computertomographie	1–5 $\mu$ m
Nano-Computertomographie	400 nm



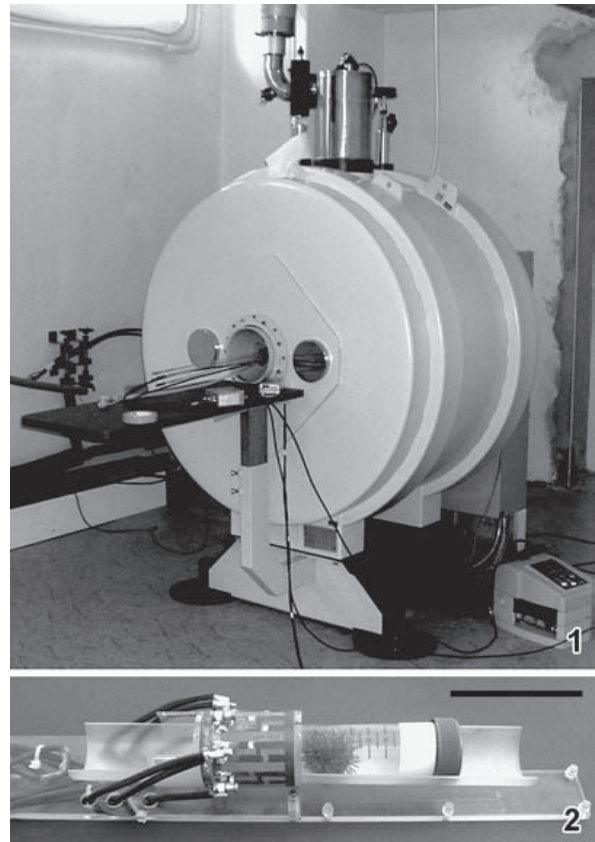
## Analyse von Seeigeln (Echinoidea) mit Hilfe der bildgebenden Magnetresonanztomographie 51

feldstärke, Auflösungen von 10–150  $\mu\text{m}$  erzielen. Welche Strukturen sich mit diesem Auflösungsvermögen bei Seeigeln darstellen lassen, sollten die folgenden Untersuchungen zeigen.

### Seeigel im MRT

Untersucht wurden mehrere Exemplare von *Psammechinus miliaris*, welche unter dem Trivialnamen Strandseeigel besser bekannt sind und auch in heimischen Gewässern vorkommen. Für die Untersuchung wurde ein Tierscanner (BioSpec 47/20) der Firma Bruker Biospin GmbH (Ettlingen, Deutschland) verwendet (Abb. 1). Die Signale wurden mit einer Doty®-Litzcage-Spule (Doty Scientific Corp., Columbus, SC, USA) gemessen. Der zu untersuchende Seeigel wurde in ein Plastikröhrchen gegeben, welches für *in vivo*-Untersuchungen mit Seewasser oder für Untersuchungen mit fixiertem Material mit Fixativ (4–7% Formol) gefüllt war. Das Röhrchen wurde daraufhin in die Empfangsspule eingeschoben (Abb. 2), welche dann ihren Platz in der Bohrung des Magneten fand. Abhängig von Schnittdicke, Schnitzzahl und Größe des Betrachtungsfeldes nahmen die Messungen Minuten oder mehrere Stunden in Anspruch. Die an die Empfangsspulen angeschlossenen Computersysteme berechneten die Bildstapel, welche anschließend mit herkömmlicher Bildbearbeitungssoftware nachbearbeitet und mit Hilfe von spezieller Software (amira™, Mercury Computer Systems) dreidimensional aufbereitet wurden.

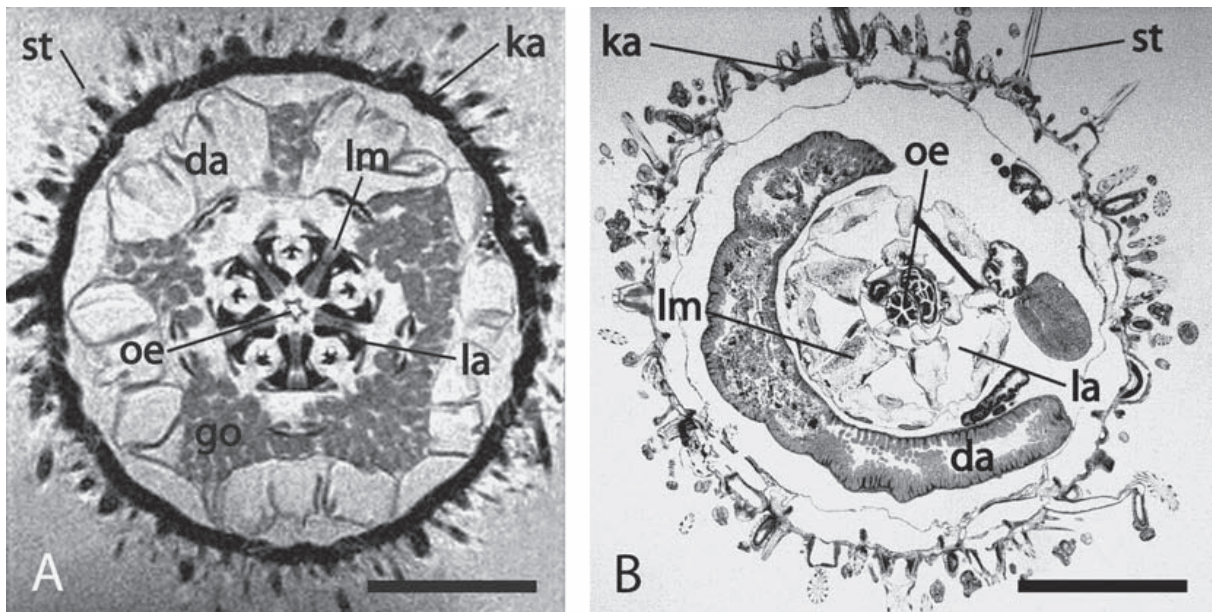
Mit der technisch möglichen Auflösung der verwendeten Apparatur ließen sich die folgenden Strukturen identifizieren: Gonaden, Darm, Laternen, Laternenmuskulatur, Kalkaußenskelett sowie Stacheln, wie die mit Hilfe des Magnetresonanztomographen erzielte horizontale Aufnahme zeigt (Abb. 3A). Die mit Hilfe eines Stereomikroskops hergestellte Aufnahme eines histologischen Schnittes zeigt zwar, dass mit herkömmlichen histologischen Verfahren zum Teil noch bessere Auflösungen zu erzielen sind (Abb. 3B), jedoch aber auch, dass für höhere Auflösungen unter Verwendung von Lichtmikroskopen digitale Übersichtsdarstellungen von größeren Tieren nicht trivial sind. Einzelaufnahmen müssen in sehr rechenintensiven Schritten unter Verwendung spezieller Software (z. B. AnalySIS) per Hand zusammengefügt werden. Interessant ist auch, dass durch die beiden Tech-



**Abb. 1: Magnetresonanztomograph Modell BioSpec 47/20, Bruker Biospin GmbH. Ein MRT mit 4,7 T Magnetfeldstärke und 20 cm Bohrung.**  
**Abb. 2: Empfangsspule mit eingelegtem Probenröhrchen. Der Seeigel befindet sich komplett im Fixativ. Maßstrich 7 cm.**

niken einige Strukturen in unterschiedlichem Maße hervorgehoben werden (Abb. 3A, B). Möchte man nun einzelne Strukturen dreidimensional darstellen, werden auf der Grundlage eines 3D-Datenstapels aus dem Tomographen weitere Arbeitsschritte notwendig. Die identifizierten Strukturen werden per Hand auf jedem der Schnitte gesondert markiert. Jeder markierten Struktur wird eine beliebige Farbe (hier: Graustufe) zugeordnet. Hat man den gesamten Bildstapel bearbeitet, kann der Computer für jede Struktur ein Oberflächen-rendering durchführen: Er verbindet die Markierungen der einzelnen Schnitte und überzieht sie quasi mit einer Haut – die jeweilige Struktur wird als ein zusammenhängendes Objekt dargestellt. Mehrere mit dieser Technik bearbeitete Strukturen zeigen den inneren Aufbau der untersuchten Probe (Abb. 4A–F).

## 52 A. Ziegler und F. Angenstein



**Abb. 3:** *Psammechinus miliaris*. **A** Horizontaler MRT-Schnitt durch ein lebendes Tier. Maßstrich 1 cm. **B** Horizontaler histologischer Schnitt durch ein fixiertes Tier. Maßstrich 2 mm. da Darm, go Gonade, ka Kalkaußenskelett, la Laterne des Aristoteles, lm Laternenmuskulatur, oe Ösophagus, st Stachel.

### Vor- und Nachteile der Methode

Als eindeutiger Vorteil dieser Methode ist sicherlich die geringe Dauer der Analysen zu sehen. Innerhalb von zwei Tagen lassen sich die MRT-Aufnahmen sowie eine 3D-Rekonstruktion der Tiere bewerkstelligen, was einem die Durchsicht von vielen unterschiedlichen Vertretern einer Tiergruppe in relativ kurzer Zeit ermöglicht. Die Daten liegen von Beginn an digital vor und können somit jederzeit durch geeignete Software bearbeitet werden. Des Weiteren ist die Tatsache von Vorteil, dass die Tiere für die Aufnahmen nicht getötet werden müssen und selbst fixiertes Material, beispielsweise Unikate aus wertvollen Museumssammlungen, mit diesem nicht-invasiven Verfahren analysiert werden kann. Die eingesetzte Technik erlaubt darüber hinaus eine beliebige Schnittführung (sagittal, horizontal, vertikal, etc.). Als nachteilig erweist sich jedoch das im Vergleich zu herkömmlichen histologischen Verfahren zurzeit noch niedrige Auflösungsvermögen der Geräte (siehe Tab. 1) sowie ihre Verfügbarkeit. Bei einem Stückpreis jenseits von 1 Mio. € und einem hohen Wartungsaufwand sind solche Apparaturen nur in Universitätskliniken und den Forschungsabteilungen von Pharmakonzernen anzutreffen.

### Ausblick

Die angesprochene geringe Auflösung lässt sich mit Kontrastmitteln aus der medizinischen Diagnostik vermutlich noch steigern. Von Interesse sind hierbei beispielsweise das Nervensystem hervorhebende Substanzen wie Manganionen. Sie werden in den Nervenzellen angereichert und lassen so zuvor nicht erkennbare Strukturen sichtbar werden (Herberholz et al., 2004). Mit einem weiteren Verfahren wird man in Zukunft sogar gezielt bestimmte Gewebe hervorheben können: Von einem Polymer ummantelte Eisenpartikel, so genannte Nanocarrier, werden mit einem Protein gekoppelt (z.B. einer viralen Proteinhülle: Allen et al., 2005), welches spezifisch an ein korrespondierendes Oberflächenprotein bindet.

### Fazit

Die Magnetresonanztomographie besitzt das Potential, zu einer zukunftsweisenden Methode in der zoologischen Morphologie zu werden. Technische Weiterentwicklungen und eine Verfeinerung der Analysemethoden werden das Auflösungsvermögen der Geräte verbessern und konventionelle histologische Verfahren

## Analyse von Seeiegeln (Echinoidea) mit Hilfe der bildgebenden Magnetresonanztomographie 53

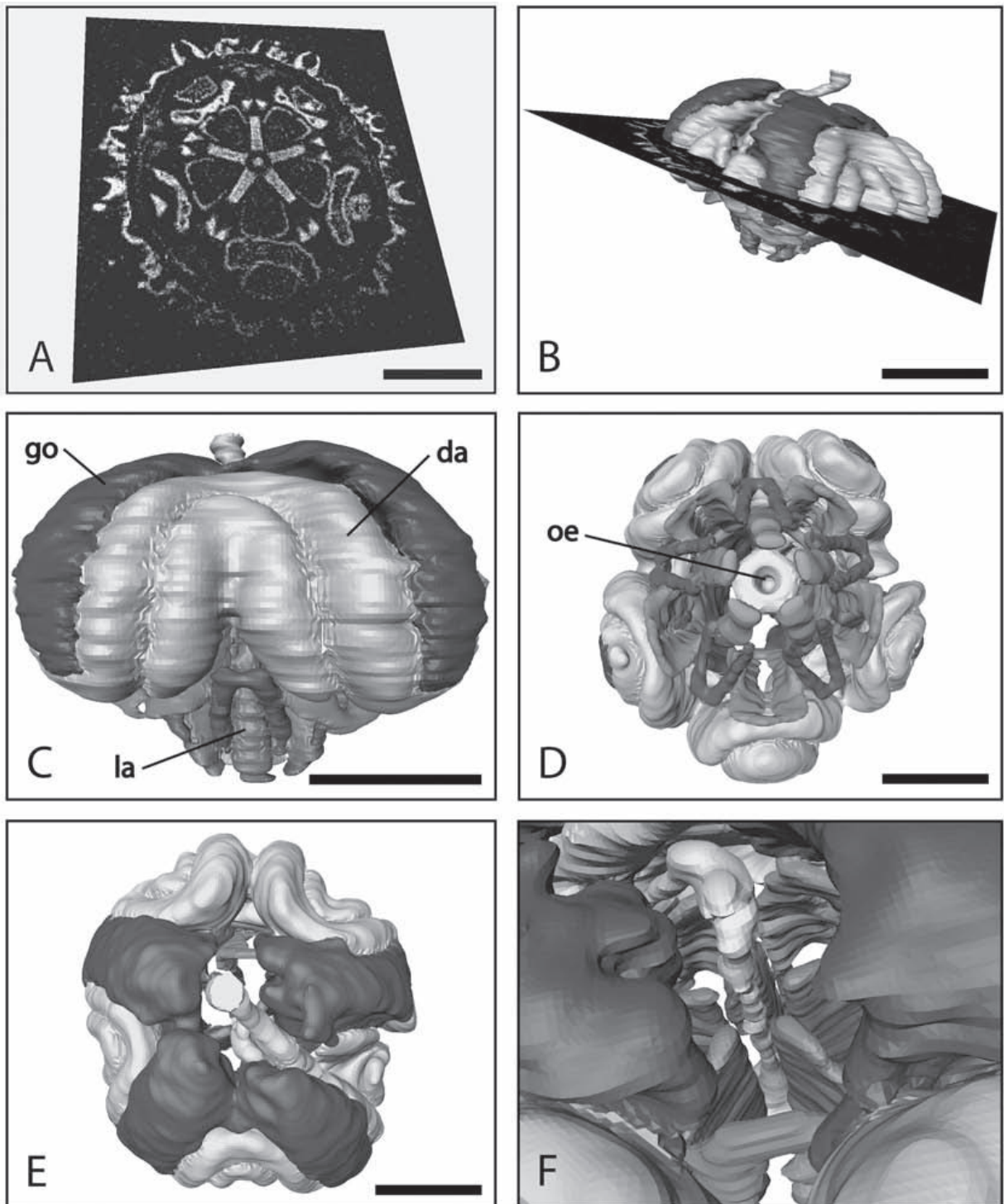


Abb. 4: 3D-Visualisierung der Anatomie eines Seeiegels. A Horizontaler MRT-Schnitt. B Oberflächen-rendering-Modell mit Lage des Schnittes aus A. C Lateralansicht. D Ventralansicht. E Dorsalansicht. F Blick entlang der Gonaden auf Ösophagus und Laterne des Aristoteles. Maßstrich 5 mm. da Darm, go Gonade, la Laterne des Aristoteles, oe Ösophagus.

---

**54 A. Ziegler und F. Angenstein**

---

sinnvoll ergänzen oder sogar ersetzen können. Die dreidimensionale Aufbereitung der Daten erlaubt eine anschauliche Darstellung gerade von komplexen Strukturen.

**Danksagung**

Die Seeigel wurden dankenswerterweise von Frau Margret Krüß, Biologische Anstalt Helgoland, zur Verfügung gestellt. Der Erstautor dankt Herrn Prof. Dr. Thomas Bartolomaeus für die Aufnahme in seine Arbeitsgruppe und die Möglichkeit, Geräte und Software des Instituts für Biologie/Zoologie nutzen zu können.

**Literaturhinweise**

- Allen, M., Bulte, J. W. M., Liepold, L., Basu, G., Zywicke, H. A., Frank, J. A., Young, M., Douglas, T.: Paramagnetic viral nanoparticles as potential high-relaxivity magnetic resonance contrast agents. *Magnetic Resonance in Medicine* 54, 807–812 (2005).
- Brinkley, C. K., Kolodny, N. H., Kohler, S. J., Sandeman, D. C., Beltz, B. S.: Magnetic resonance imaging at 9.4 T as a tool for studying neural anatomy in non-vertebrates. *Journal of Neuroscience Methods* 146, 124–132 (2005).
- Hart, A. G., Bowtell, R. W., Köckenberger, W., Wenseleers, T., Ratnieks, F. L. W.: Magnetic resonance imaging in entomology: a critical review. *Journal of Insect Science* 3, 1–9 (2003).
- Herberholz, J., Mims, C. J., Xiadong, Z., Xiaoping, H., Edwards, D. H.: Anatomy of a live invertebrate revealed by manganese-enhanced magnetic resonance imaging. *The Journal of Experimental Biology* 207, 4543–4550 (2004).

*Verfasser:* Dipl.-Biol. Alexander Ziegler, Systematik und Evolution der Tiere, Institut für Biologie/Zoologie, Freie Universität Berlin, Königin-Luise-Str. 1–3, 14195 Berlin, und Dr. Frank Angenstein, Speziallabor Nicht-Invasive Bildgebung, Leibniz-Institut für Neurobiologie, Universität Magdeburg, Brenneckestraße 6, 39118 Magdeburg.

## **3. Sea Urchin Internal Anatomy Revealed by MRI**

### **3.1. Summary**

Since the preliminary results had revealed the principal feasibility of MRI studies on sea urchins, further non-invasive imaging experiments were conducted using formalin- and alcohol-fixed specimens of *Psammechinus miliaris* (Müller, 1771). The decision to use fixed material was based on the fact that 3D reconstruction ideally requires isotropic datasets and that higher resolutions would ultimately lead to extended scanning times in the range of several hours. Therefore, in order to prevent movement artefacts, freshly fixed specimens were selected for scanning. Imaging experiments were conducted with a 7 T horizontal wide-bore scanner (Bruker Pharmascan 70/16). Using various scanning protocols, isotropic and non-isotropic datasets were gathered and compared with each other as well as with the results derived from our previous histological analyses. The higher field strength of the scanner, paired with a strong gradient system, permitted to achieve isotropic resolutions close to  $(100 \mu\text{m})^3$ , the minimum resolution deemed essential for further comparative analyses. Based on the results from this work, the decision was made to extend the morphological studies to other sea urchin taxa.

### **3.2. Publication**

Ziegler A, Mueller S, Bartolomaeus T: Sea urchin (Echinoidea) anatomy revealed by magnetic resonance imaging and 3D visualization. In: Harris L, ed. Conference Proceedings, 12<sup>th</sup> International Echinoderm Conference, in press

Pages 19-24

## Sea urchin (Echinoidea) anatomy revealed by magnetic resonance imaging and 3D visualization

A. Ziegler & T. Bartolomaeus

*Institut für Biologie, Freie Universität Berlin, Germany*

S. Mueller

*Klinik für Neurologie, Berlin Neuroimaging Centre, Charité-Universitätsmedizin, Berlin, Germany*

**ABSTRACT:** Histological analyses of sea urchins (Echinoidea) confront the researcher with a number of problems such as compression and deformation of the object. In addition, the process is time-consuming and irretrievably alters the specimen. In our study we show that *in vitro* non-invasive analyses using Magnetic Resonance Imaging (MRI) are feasible for sea urchins and yield data that can be easily used for three-dimensional (3D) reconstruction of soft- and hard-part anatomy. With the achieved isotropic resolution of 117  $\mu\text{m}$ , gross anatomical features such as gonads, digestive tract, Aristotle's lantern, calcite endoskeleton, and even mesenteries can be identified. We propose a number of applications for further studies involving sea urchins and MRI.

### 1 INTRODUCTION

The phylogeny of sea urchins (Echinoidea) is currently based on well-founded and extensive molecular, palaeontological and morphological character sets. However, the morphological characters are "...based almost entirely upon hard-part anatomy." (Littlewood & Smith 1995). Comparative soft-tissue anatomy is therefore usually not available for sea urchins, clearly a void in the quest to reconstruct echinoid evolution. Gathering histological data from sea urchins presents a number of problems, some being intrinsic to echinoderm histology and others to histology in general. These problems include compression and deformation of the object due to mechanical stress exerted by the microtome blade, while others include the deformation of the object due to emission of  $\text{CO}_2$  during the process of calcite dissolution. Most of all, histological analyses are time- and specimen-consuming (see Cavey & Yeung 1991 for detailed histological procedures). The data generated in form of sections has to be manually digitized for later three-dimensional (3D) reconstruction and visualization – an often frustrating and time-consuming process. For our comparative studies we sought to gather anatomical data sets for 3D visualization using a non-invasive, destruction-free method.

Unlike histology, Magnetic Resonance Imaging (MRI), a complex technology based on the application of high magnetic fields, transmission of radiofrequency (RF) waves and detection of RF signals

from excited protons, is an objective, non-user specific, unbiased method requiring little sample preparation and allowing for a relatively large sample size. For a short review on the MRI physical principle refer to Natt & Frahm (2005) and for an in-depth explanation to Callaghan (1991). MRI analyses are especially suited to reveal soft tissue anatomy since hard tissue like bone or the echinoderm calcite endoskeleton do not generate a signal, while soft tissue like muscles or fat generate a strong signal due to free protons. Nonetheless, the calcareous structures are made visible as well because the surrounding media - which are rich in free protons - generate a negative delineation.

In the last years, a number of reports on marine invertebrates being analyzed with MRI have been published (e.g., Bock et al. 2001, Brinkley et al. 2005, Gozansky et al. 2003, Herberholz et al. 2004). To the best of our knowledge, no echinoderms have been analyzed to date using MRI, except for a small preliminary study (Ziegler & Angenstein 2006). Here it was shown that by using MRI data in combination with 3D visualization, morphological traits of sea urchins can be made visible without having to destroy the specimens. However, the resolution acquired in these experiments was not satisfactory and since resolution improves linearly with magnetic field strength, we developed methods for *in vitro* anatomical studies of sea urchins at 7 T.

Recent MRI studies suggest a number of confounding terms for the study of anatomical features using

small animal scanners at high magnetic field strengths: MR microscopic imaging, NMR microscopy, small animal MRI,  $\mu$ MRI, MR histology, MR $\mu$ I, and MR microscopy. All these terms refer to modalities for the study of small animals; high-resolution MRI is commonly referred to as any isotropic resolution below 100  $\mu$ m (Callaghan 1991). In that sense our data does not represent high-resolution data, although at 117  $\mu$ m isotropic resolution, the gross anatomical features of sea urchins can easily be discerned.

The purpose of our study was to establish 3D MRI protocols for sea urchins at 7 T and to evaluate the potential of this technique to study echinoid soft and hard-part anatomy and compare it with results from classical histological methods.



Figure 1. Bruker Pharmascan 70/16 AS. The specimen is inserted into the horizontal bore of the magnet.

## 2 MATERIALS AND METHODS

### *Animals*

All experiments were performed using specimens of the sea urchin species *Psammechinus miliaris* (Müller, 1771) (Echinodermata: Echinoidea). Specimens were dredged from depths of 10-50 m in the North Sea off Helgoland island, Germany (54°20' N, 7°90' E) in April 2005 and April 2006 and were sub-

sequently transferred to a salt-water aquarium at the Institut für Biologie-Zoologie, Berlin. Approval by an ethics committee was not required for the studies of invertebrates.

### *Light Microscopy*

For light microscopy, four specimens were fixed in Bouin's fluid for 24 hours, decalcified in 2% nitric acid, dehydrated in an alcohol series, methylbenzoate and butanol and embedded in Paraplast (Kendall). Complete series of 8  $\mu$ m thin sections were made using a microtome (Reichert-Jung 2050 Supercut) with steel blades and later stained using Azan stain. For overview histology, series of sections were digitally recorded using a Leica MZ16A stereo microscope equipped with a Leica DC300 digital camera.

### *Magnetic Resonance Imaging*

For MRI, three specimens were fixed in a 37% formaldehyde solution for 3-4 min and then were transferred to a 7% formaldehyde solution. For imaging, the animals were placed into a 50 ml Falcon tube (Becton Dickinson GmbH), which required removal of some spines at the lateral sides. The tube was filled with a 7% formaldehyde solution until no more air bubbles were visible and sealed tightly with Parafilm (American Can Company).

Imaging experiments were conducted at the Berlin Neuroimaging Center at 7 Tesla ( $^1$ H-resonance-frequency 300 MHz) using a Bruker Pharmascan 70/16 AS (Bruker Biospin, Ettlingen, Germany) (Fig. 1). The system consisted of a 160 mm horizontal bore magnet and a shielded gradient set with an inner diameter of 90 mm and a maximum gradient strength of 300 mT/m. A commercial linear  $^1$ H-radio-frequency volume resonator with an inner diameter of 38 mm was used for excitation and for the detection of signal intensity. The images described here were acquired at  $\sim$ 18°C. Image processing was carried out with Paravision 3.0.2 (Bruker, Ettlingen, Germany). Several imaging protocols were tested. The best results were achieved using an RF-spoiled, T1-weighted segmented gradient echo sequence (MDEFT) in coronal view. Protocol parameters are given in Table 1.

### *MRI 3D Visualization*

3D image reconstruction and visualization was performed by converting the generated MRI data (DICOM Standard) into a TIFF image sequence (ImageJ 1.36b) and by using 3D imaging software (Amira 3.0, Mercury Computer Systems). Segmentation was carried out manually by using the brush tool in the Image Segmentation Editor. Detection of

borderlines and organ designation were done based on Strenger (1973) and our own histological data. The segmentation was done using the data generated with the MDEFT protocol.

Table 1. Parameters for sea urchin imaging at 7 T. See Natt & Frahm (2005) for an explanation of the parameters and protocols.

Protocol/ Parameters	MDEFT	RARE	FLASH
Signal weighting	T1	PD	T2*
Repetition time	21.16 ms	2500 ms	1500 ms
Echo time	3.9 ms	11.82 ms	6 ms
Flip angle	19°	90°	30°
Averages	6	1	4
Total scan time	5h4m16s	1h22m40s	0h25m36s
Mode (2D/3D)	3D	3D	2D
Field of view	3x3x3 cm <sup>3</sup>	3x3x3 cm <sup>3</sup>	3x3x3 cm <sup>3</sup>
Matrix size	256 <sup>3</sup>	256 <sup>3</sup>	256 <sup>2</sup>
Slice thickness	-	-	0.5 mm
Resolution	117 µm iso	117 µm iso	117 µm
Direction	Coronal	Coronal	Coronal
Figure	Fig. 3	Fig. 4	Fig. 5

### 3 RESULTS

#### Light Microscopy

Classical histological sectioning allows for a relatively high magnification and as shown in Fig. 2, anatomical details such as the intestine and its interior composition can be discerned. Ambulacral feet, spines and pedicellariae can easily be identified and their internal anatomy is made visible in some cases.

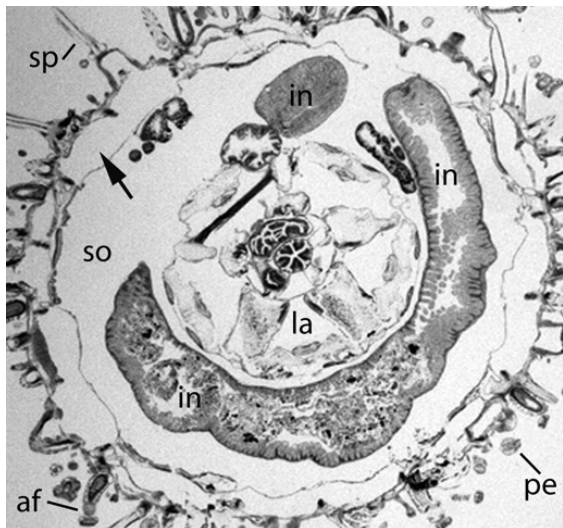


Figure 2. *Psammechinus miliaris*. Histological section at the height of intestine and Aristotle's lantern. The arrow depicts the area where the dissolved calcite has left an open space. af = ambulacral foot, in = intestine, la = lantern, pe = pedicellarium, so = somatocoel, sp = spine.

Yet, the mesenteric suspension of the digestive tract is not visible, although this structure should be clearly within the range of light microscopical resolution. This is likely to be an artifact caused by either decalcification or mechanical stress exerted by the microtome blade. Another striking feature observed is the blank space in-between epidermal and somatocoelomic tissue, where huge gap artifacts are created because of the dissolution of calcite (arrow in Fig. 2). The same occurs inside the lantern and within the spines, both strongly calcified structures.

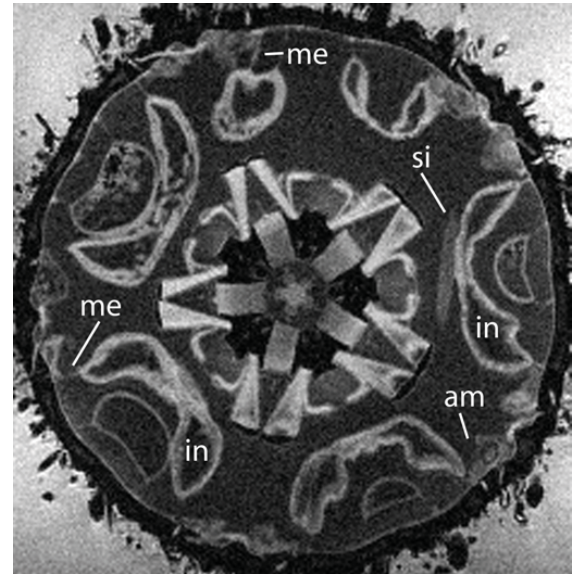


Figure 3. *Psammechinus miliaris*. MRI image taken at the height of Aristotle's lantern and digestive tract using a T1 weighted MDEFT protocol with an isotropic resolution of 117 µm. am = ampulla, in = intestine, me = mesentery, si = siphon.

#### Magnetic Resonance Imaging

The situation of internal and external organs of *P. miliaris* acquired with MRI is shown in Figs. 3-5. In Fig. 3, results from a 3D MDEFT protocol are shown. The T1 weighting generates a strong tissue signal which is improved in contrast due to the weak signal generated by the liquid (somatocoel) surrounding soft tissue. The mesenteric suspension of all digestive tract constituents as well as the outlines of the ampullae of the water vascular system are made visible. In the lower right of the image, an ambulacral foot penetrating the calcite endoskeleton can be depicted. Due to the signal generated by all materials with free protons (including the outer medium), all hard tissue becomes visible, including the calcite endoskeleton and lantern components. Spines, ambulacral feet and most of the pedicellariae are poorly visible. Clearly, the best resolution and contrast is achieved within the animal. Fig. 4 shows



an MRI picture taken with a 3D RARE protocol using the same animal. The proton density (PD) weighting used in this protocol makes the teeth as well as the perignathic girdle at the site of the insertion of the lantern retractor muscles visible - the calcified components of the lantern are more highly resolved here. Yet, the mesenteries are not easy to identify, and they are sometimes even invisible. The same applies to the ampullae of the water vascular system. Where ambulacral feet are penetrating the calcite endoskeleton, a thin line is sometimes visible. External morphological features are only poorly resolved.

The 2D FLASH protocol with T2\* weighting and a slice thickness of 0.5 mm using the same animal is in some parts blurred (Fig. 5). Since the individual sections are about four times thicker than those in the 3D protocols used, a stronger but less finely resolved signal is generated. Although the ampullae are practically invisible, thin structures like the mesenteries can be discerned. External morphological structures such as spines and ambulacral feet are only poorly resolved. In the upper third of the image an unfocused horizontal band can be identified – an artifact caused by the MRI gradient system.

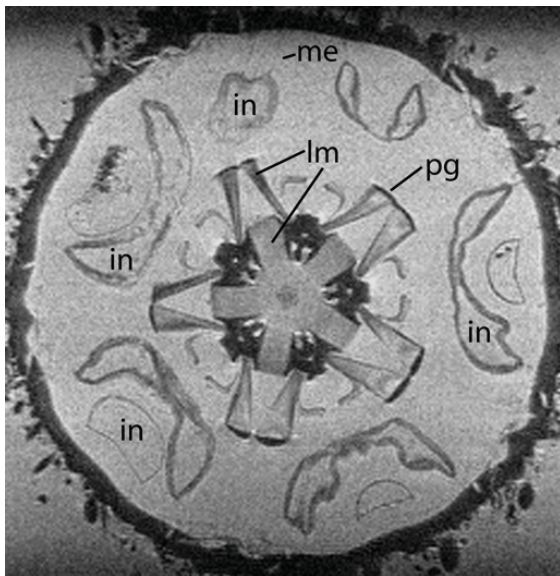


Figure 4. *Psammechinus miliaris*. MRI image taken at the height of Aristotle's lantern and digestive tract using a PD weighted RARE protocol with an isotropic resolution of 117  $\mu\text{m}$ . in = intestine, lm = lantern muscles, me = mesentery, pg = perignathic girdle.

### 3D Visualization

Fig. 6 shows an angled 3D model of the digestive tract of *P. miliaris* reconstructed from MRI images using data processing software. The relation of up-

per and lower intestinal loop and the siphon are made well visible. Our digital data allows for real-time rotation of this complex 3D structure, making examinations from any possible angle feasible. Other internal organs such as gonads, muscles, axial complex and the Aristotle's lantern (data not shown) have been reconstructed as well. The organs are labeled separately during the course of segmentation and can thereafter be made transparent for an unobstructed view on other anatomical features.

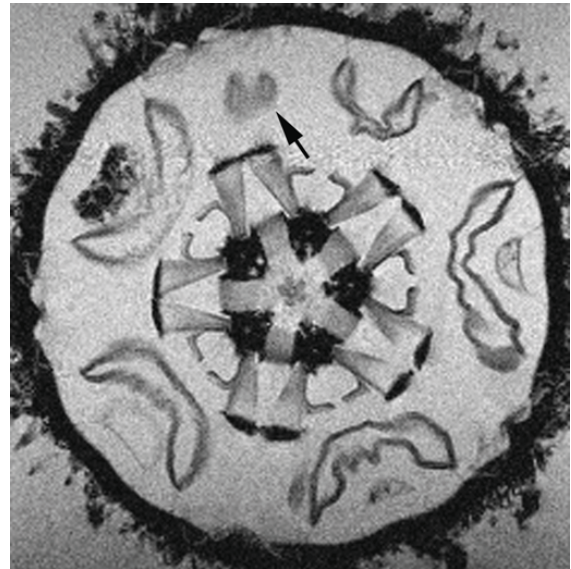


Figure 5. *Psammechinus miliaris*. MRI image taken at the height of Aristotle's lantern and digestive tract using a T2\* weighted FLASH protocol with an in-plane resolution of 117  $\mu\text{m}$ . Note blurred areas around digestive tract due to the slice thickness of 0.5 mm (arrow).

## 4 DISCUSSION

Our MRI studies can clearly depict a number of internal anatomical features of the sea urchin *Psammechinus miliaris*. Especially soft tissues such as muscles, digestive tract, gonads can be made visible with a number of distinct MRI protocols. Due to the signal of surrounding media, hard-part anatomy of the sea urchin is accessible to study as well, depending on the protocol used. The differences observed between results from the various protocols can be made use of when trying to get as much information out of image series with an in-plane resolution of 117  $\mu\text{m}$ . For 3D visualization we used the MDEFT data, referring to the RARE data set when structures or outlines were not clearly visible. The 3D MDEFT protocol we used seems to offer the best trade-off between resolution, contrast and total scan time. In comparison to our histological data it becomes obvious that MRI data with the achieved in-plane resolu-

tion cannot compete with the potential resolution of 200 nm achievable with light microscopy. However, one goal of our study was to generate data suitable for 3D reconstruction and visualization. Digital images derived from overview histology need to be manually aligned in a time-consuming process. This alignment is necessarily biased as each researcher will determine different points of reference. In contrast, MRI data packages are aligned from the beginning and do not have to be altered before 3D image processing is carried out. Furthermore, for a 3D visualization of general sea urchin morphology, overview histology is indispensable, thereby limiting resolution and the size of the object. Another important disadvantage of histological methods is that it is almost impossible to achieve an intact series of histological sections of a given specimen, especially if decalcification is necessary. Therefore, the data needs to be correlated with sections from other specimens, resulting in an even further prolongation of the 3D visualization process.

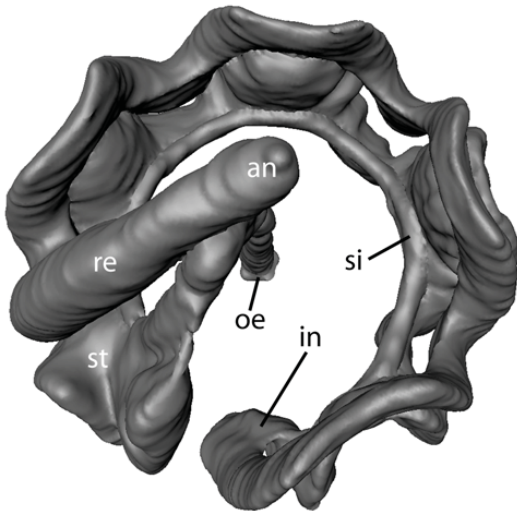


Figure 6. *Psammechinus miliaris*. 3D visualization of the digestive tract. Slightly angled perspective as seen from an aboral position. an = anus, in = intestine, oe = oesophagus, re = rectum, si = siphon, st = stomach.

In terms of artifacts, a number of MRI-specific problems have to be considered when analyzing small animals. Such artifacts include signal amplification or reduction at tissue and solution interfaces. As another source for artifacts, the biology of the animal must be kept in mind, since especially the intake of paramagnetic substances (e.g., manganese) may alter the images. For further information on artifacts refer to Callaghan (1991).

#### *Observations and recommendations*

Since the specimen cannot be visually inspected once inside the magnet, we recommend using a

TRI\_PILOT sequence to determine the position of the probe. After that the data acquisition geometry is determined (e.g., for coronal imaging) and verified using a fast imaging protocol with low resolution and a total scan time of under a minute. Now the desired 2D or 3D imaging sequence can be applied, at best in overnight scans, since most MRI machines are used for medical or pharmaceutical studies during the day.

#### *Significance*

It has to be stressed that our study represents a purely methodological approach yielding to date no scientific data *de novo*. Using this method we are able to visualize structures that have been identified before with classical histological techniques. The relevant achievement in our eyes is the non-invasive and destruction-free approach that requires fewer specimens and, most importantly, less time to generate satisfactory anatomical data from a large number of specimens. We strongly believe that our data can complement and in some cases even replace histology.

### 5 FUTURE PERSPECTIVES

The protocols and procedures developed in our study will serve as a basis for further studies involving MRI and sea urchins. Our research will address primarily the prospect to increase in-plane and isotropic image resolution using higher magnetic fields. First results acquired using a 17.6 T vertical bore system are promising (Ziegler & Faber, unpublished observations). Another aim will be to establish the application of selective and non-selective contrast agents, such as e.g. manganese, Magnevist or Gadovist (for an overview see Weinmann et al. (2003)) on both living and fixed sea urchin specimens. In order to carry out our experiments using living organisms, we will look further into the application of anaesthetic substances in order to decrease movement artifacts. The data generated with 3D visualization software will further increase the potential of MRI picture series, e.g. with regard to the possibility to quantify structures in terms of volume and surface.

Since MRI studies are feasible with fixed sea urchin material, we will broaden our anatomical studies to the screening of valuable museum specimens, including holotypes, as previously done on a beetle by Hörschemeyer et al. (2006). An obstacle for these studies might be the need to remove some spines laterally as done with *P. miliaris* during our studies, since only an optimal use of the given volume inside the tube can yield maximal resolution. Another interesting field will be the correlation of 3D MRI data

with results by other non-invasive imaging techniques such as micro-computed tomography ( $\mu$ CT) and optical coherence tomography (OCT).

### Applications

The use of MRI depends mainly on the type of results expected from a study. MRI experiments are used in an expanding number of scientific fields including anatomy (Herberholz et al. 2004, Hörnschemeyer et al. 2006, Jasanoff & Sun 2002), physiology (Bock et al. 2001, Slowik et al. 1997), developmental investigations (Michealis et al. 2005, Price et al. 1999) and fishery, such as oyster cultivation (Davenel et al. 2006). More and more (marine) invertebrates are being studied with this technique, increasing the number of protocols and imaging parameter sets. Nonetheless, further technical improvements are necessary if MRI is to become a mainstream technology for the study of invertebrate anatomy.

Apart from the interest in original research we would like to hint at the possibilities for teaching that are opened up with the 3D visualization of such complex internal structures as found in sea urchins – knowing that “one picture says it all”.

### ACKNOWLEDGEMENTS

We would like to thank the staff of the Biologische Anstalt Helgoland for supplying us with living sea urchin specimens and for the use of their facilities. AZ thanks the Senate of Berlin for financial support through a NaFöG-fellowship.

### REFERENCES

- Bock, C., Frederich, M., Wittig, Rolf-M. & Pörtner, Hans-O. 2001. Simultaneous observations of haemolymph flow and ventilation in marine spider crabs at different temperatures: a flow weighted MRI study. *Magnetic Resonance Imaging* 19: 1113-1124.
- Brinkley, C.K., Kolodny, N.H., Kohler, S.J., Sandeman, D.C. & Beltz, B.S. 2005. Magnetic resonance imaging at 9.4 T as a tool for studying neural anatomy in non-vertebrates. *Journal of Neuroscience Methods* 146: 124-132.
- Callaghan, P.T. 1991. *Principles of Nuclear Magnetic Resonance Microscopy*, Oxford: Clarendon Press.
- Cavey, M.J. & Yeung, E.C. 1991. Histological and ultrastructural techniques for the examination of soft tissues in the heavily calcified ambulacrum of the starfish. In: Yanagisawa et al. (eds.), *Biology of Echinodermata*, Rotterdam: Balkema.
- Davenel, A., Quéllec, S. & Pouvreau, S. 2006. Noninvasive characterization of gonad maturation and determination of the sex of Pacific oysters by MRI. *Magnetic Resonance Imaging* 24: 1103-1110.
- Gozansky, E.K., Ezell, E.L., Budelmann, B.U. & Quast, M.J. 2003. Magnetic resonance histology: in situ single cell imaging of receptor cells in an invertebrate (*Lolliguncula brevis*, Cephalopoda) sense organ. *Magnetic Resonance Imaging* 21: 1019-1022.
- Herberholz, J., Mims, C.J., Xiaodong Zhang, Xiaoping Hu & Edwards, D.H. 2004. Anatomy of a live invertebrate revealed by manganese-enhanced Magnetic Resonance Imaging. *The Journal of Experimental Biology* 207: 4543-4550.
- Hörnschemeyer, T., Goebbel, J., Weidemann, G., Faber, C. & Haase, A. 2006. The head morphology of *Ascioplaga mimeta* (Coleoptera: Archostemata) and the phylogeny of Archostemata. *European Journal of Entomology* 103: 409-423.
- Jasanoff, A. & Sun, P.Z. 2002. In vivo magnetic resonance microscopy of brain structure in unanesthetized flies. *Journal of Magnetic Resonance* 158: 79-85.
- Littlewood, D.T.J. & Smith, A.B. 1995. A combined morphological and molecular phylogeny for sea urchins (Echinozoa: Echinodermata). *Philosophical Transactions of the Royal Society of London, Series B* 347: 213-234.
- Michealis, T., Watanabe, T., Natt, O., Boretius, S., Frahm, J., Utz, S. & Schachtner, J. 2005. In vivo 3D MRI of insect brain: cerebral development during metamorphosis of *Manduca sexta*. *NeuroImage* 24: 596-602.
- Natt, O. & Frahm, J. 2005. In vivo magnetic resonance imaging: insights into structure and function of the central nervous system. *Measurement Science and Technology* 16, R17-R36.
- Price, W.S., Kobayashi, A., Ide, H., Natori, S. & Arata, Y. 1999. Visualizing the postembryonic development of *Sarcophaga peregrina* (flesh fly) by NMR microscopy. *Physiological Entomology* 24: 386-390.
- Slowik, T.J., Green, B.L. & Thorvilson, H.G. 1997. Detection of Magnetism in the Red Imported Fire Ant (*Solenopsis invicta*) Using Magnetic Resonance Imaging. *Bioelectromagnetics* 18: 396-399.
- Strenger, A. 1973. *Sphaerechinus granularis* (Violetter Seeigel), Anleitung zur makroskopischen und mikroskopischen Untersuchung. In: Siewing, R. (ed.), *Großes Zoologisches Praktikum, Band 18*, Stuttgart: Gustav Fischer Verlag.
- Weinmann, H., Ebert, W., Misselwitz, B. & Schmitt-Willich, H. 2003. Tissue-specific MR contrast agents. *European Journal of Radiology* 46: 33-44.
- Ziegler, A. & Angenstein, F. 2007. Analyse von Seeigeln (Echinozoa) mit Hilfe der bildgebenden Magnetresonanztomographie. *Mikrokosmos* 96 (1): 49-54.

## 4. Systematic Reconstruction of Sea Urchin Internal Anatomy

### 4.1. Summary

The RARE and FLASH protocols established during the preliminary analyses on the 7 T scanner system were further improved and finally resulted in fixed MRI protocols that were used for the following large-scale scanning experiments. Adequate sea urchin material was obtained from various European and American museum collections. Every specimen was scanned using a short pilot sequence. Specimens without obvious artefacts were then selected for high-resolution overnight scanning. Using the 7 T as well as a 17.6 T vertical wide-bore scanner refitted for proton imaging (Bruker Avance 750 MHz WB NMR spectrometer), tomographic datasets of over 40 sea urchin species were obtained. The resolutions that were achieved ranged from  $(96 \mu\text{m})^3$  down to approximately  $(18 \mu\text{m})^3$  at a field of view of up to  $(3.3 \text{ cm})^3$ , permitting to differentiate various soft tissue structures within the specimens. Imaging was conducted on specimens ranging from freshly fixed animals to those of over 130 years of age.

For the following publication, a representative species of every high-ranking sea urchin taxon was selected for 3D modelling. The results unequivocally demonstrate the possibility to systematically visualize the internal anatomy of invertebrates in a reasonable time-frame using MRI and advanced modelling software. Apart from this approach, additional datasets were gathered using  $\mu\text{CT}$ . However, with the scanning parameters employed here, this technique proved to be unsuccessful for soft tissue imaging. MRI and  $\mu\text{CT}$  datasets as well as 3D models based thereon have been made publicly available through interactive Internet publications (see also Chapter 5).

### 4.2. Publication

Ziegler A, Faber C, Mueller S, Bartolomaeus T (2008): Systematic comparison and reconstruction of sea urchin (Echinoidea) internal anatomy: a novel approach using magnetic resonance imaging. *BMC Biology* 6: 33

# BMC Biology

Research article

## Systematic comparison and reconstruction of sea urchin (Echinoidea) internal anatomy: a novel approach using magnetic resonance imaging

Alexander Ziegler\*<sup>1</sup>, Cornelius Faber<sup>2,3</sup>, Susanne Mueller<sup>4</sup> and Thomas Bartolomaeus<sup>1</sup>

Address: <sup>1</sup>Institut für Biologie, Freie Universität Berlin, Königin-Luise-Straße, 14195 Berlin, Germany, <sup>2</sup>Experimentelle Physik 5, Universität Würzburg, Am Hubland, 97074 Würzburg, Germany, <sup>3</sup>Institut für Klinische Radiologie, Universitätsklinikum Münster, Waldeyerstraße, 48149 Münster, Germany and <sup>4</sup>Berlin NeuroImaging Center, Charité-Universitätsmedizin Berlin, Charitéplatz, 10117 Berlin, Germany

Email: Alexander Ziegler\* - [aziegler@zoosyst-berlin.de](mailto:aziegler@zoosyst-berlin.de); Cornelius Faber - [faberc@uni-muenster.de](mailto:faberc@uni-muenster.de); Susanne Mueller - [susanne.mueller1@charite.de](mailto:susanne.mueller1@charite.de); Thomas Bartolomaeus - [tbartol@zoosyst-berlin.de](mailto:tbartol@zoosyst-berlin.de)

\* Corresponding author

Published: 23 July 2008

Received: 12 February 2008

BMC Biology 2008, 6:33 doi:10.1186/1741-7007-6-33

Accepted: 23 July 2008

This article is available from: <http://www.biomedcentral.com/1741-7007/6/33>

© 2008 Ziegler et al; licensee BioMed Central Ltd.

This is an Open Access article distributed under the terms of the Creative Commons Attribution License (<http://creativecommons.org/licenses/by/2.0>), which permits unrestricted use, distribution, and reproduction in any medium, provided the original work is properly cited.

### Abstract

**Background:** Traditional comparative morphological analyses and subsequent three-dimensional reconstructions suffer from a number of drawbacks. This is particularly evident in the case of soft tissue studies that are technically demanding, time-consuming, and often prone to produce artefacts. These problems can partly be overcome by employing non-invasive, destruction-free imaging techniques, in particular micro-computed tomography or magnetic resonance imaging.

**Results:** Here, we employed high-field magnetic resonance imaging techniques to gather numerous data from members of a major marine invertebrate taxon, the sea urchins (Echinoidea). For this model study, 13 of the 14 currently recognized high-ranking subtaxa (orders) of this group of animals were analyzed. Based on the acquired datasets, interactive three-dimensional models were assembled. Our analyses reveal that selected soft tissue characters can even be used for phylogenetic inferences in sea urchins, as exemplified by differences in the size and shape of the gastric caecum found in the Irregularia.

**Conclusion:** The main focus of our investigation was to explore the possibility to systematically visualize the internal anatomy of echinoids obtained from various museum collections. We show that, in contrast to classical preparative procedures, magnetic resonance imaging can give rapid, destruction-free access to morphological data from numerous specimens, thus extending the range of techniques available for comparative studies of invertebrate morphology.

### Background

For centuries, comparative zoomorphological analyses have formed the backbone of phylogenetic inferences. Data on the external and internal morphology of specimens were obtained by dissecting and sectioning selected

representative species. These traditional procedures are technically demanding as well as time-consuming and irretrievably alter or even destroy the specimen. Further complications arise from the difficult three-dimensional (3D) reconstruction of the structures observed. Artefacts,

for example deformation or compression of histological slices, and the problematic alignment of sections make 3D reconstructions a laborious and often highly subjective procedure. The problems encountered are further aggravated by the logistic challenges that arise when comparative studies on selected species of a whole taxon are to be carried out. For example, in case of sea urchins (Echinoidea, Echinodermata), some species are deep-sea dwellers or confined to remote regions of the world. It is therefore a considerable problem to obtain these animals in a freshly fixed state. Understandably, the desirable use of specimens from museum collections is usually not permitted for invasive and destructive analyses.

The application of non-invasive imaging techniques such as micro-computed tomography ( $\mu$ CT; see, for example, [1-8]) or magnetic resonance imaging (MRI; see below) has substantially increased in basic morphological research. Whereas  $\mu$ CT is mainly used to display hard tissue such as bone or calcite structures, MRI provides images depicting primarily soft tissue anatomy. MRI is based on the principles of nuclear magnetic resonance (NMR) and is predominantly used to measure the distribution of hydrogen protons within a sample. Image contrast is achieved due to the different physical properties of tissues. Both  $\mu$ CT and MRI produce standardized digital data, principally permitting an interactive access through virtual collections or voxel libraries as envisaged previously [9,10]. This data represents the unaltered structural composition of the specimen, in contrast to classical histological or dissection techniques and apart from fixation. In the light of these and other recent technological advances, Budd and Olsson [11] refer to the renaissance of morphology, calling for a more extensive use of non-invasive and non-destructive imaging techniques and 3D applications. Since many of the specimens in natural history collections are conserved in alcohol, forming the so-called wet collections, non-invasive imaging techniques might be employed to reveal the internal and external anatomy of preserved, scientifically irreplaceable specimens. This extended use of museum specimens for comparative anatomical studies would allow for a substantial increase in taxon sampling on one hand, and on the other would minimize the ecological impact of such analyses.

The feasibility of MRI studies to reveal soft tissue characteristics of invertebrates was demonstrated by studies on crabs [12,13], squid [14], crayfish [15,16], oysters [17,18], spiders [19], demosponges [20], and insects [21-29] (see also the review by Hart et al. [30]). Ziegler and Angenstein [31] used living and freshly fixed specimens of the sea urchin *Psammechinus miliaris* (Müller, 1771) and showed that members of this taxon are likely to be suitable for detailed MRI studies. These studies yielded imaging results comparable to manual dissection and were corre-

lated with histological data. To achieve better resolved images of the complex internal anatomy of sea urchins, the application of higher magnetic field strengths was proposed [32]. However, all of the studies mentioned above were restricted to the analysis of single specimens or species in a non-systematic context.

For systematic analyses, however, sea urchins appear particularly suitable. Like sea stars or sea cucumbers, they are part of a major deuterostome taxon, the Echinodermata, which shares a common ancestor with diverse groups such as acorn worms (Enteropneusta), tunicates (Tunicata), and vertebrates (Vertebrata) [33]. Owing to the calcified skeleton found in sea urchins, palaeontologists have access to a rich fossil record permitting thorough ground-truthing of phylogenetic hypotheses that are based upon molecular or morphological datasets [34,35]. Recently, the importance of these animals for evolutionary and developmental inferences has been further emphasized by results obtained through the sequencing of the genome of the purple sea urchin, *Strongylocentrotus purpuratus* (Stimpson, 1857) [36].

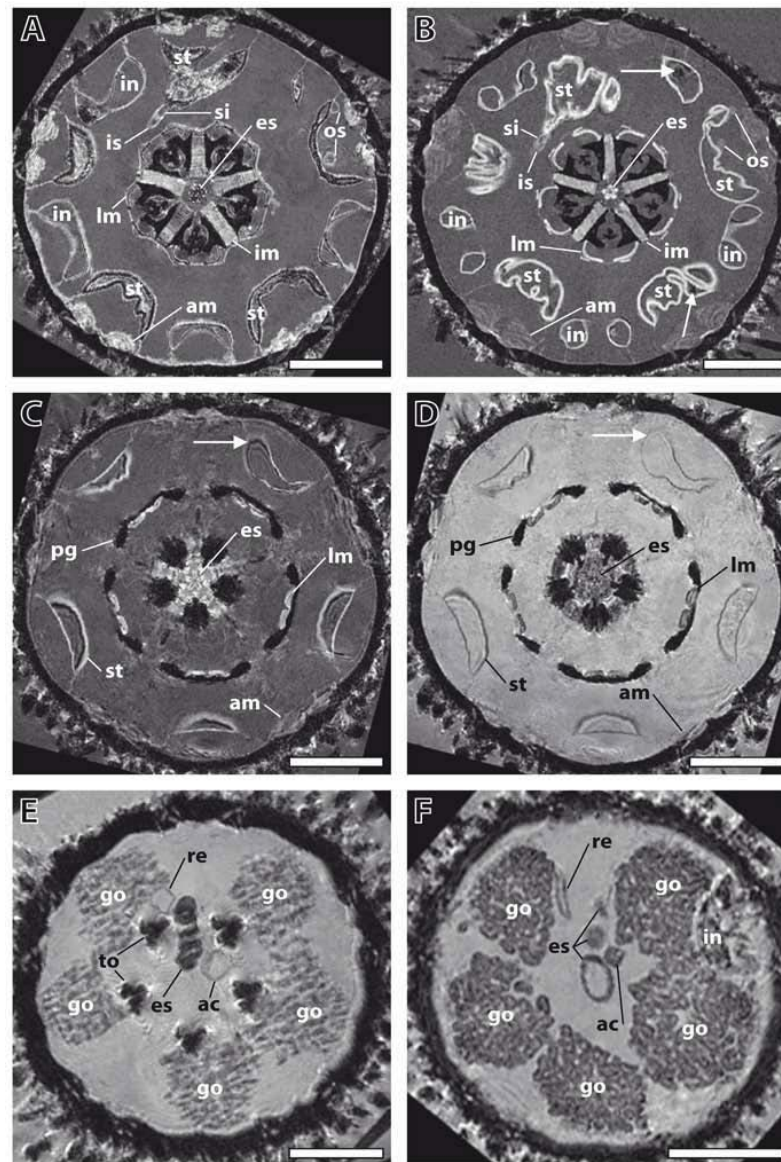
Sea urchins are spherical, oval or flattened free-moving echinoderms covered with spines. Their soft tissue anatomy is characterized by a dominant digestive tract, a varying number of gonads, and the highly specialized water vascular system with its external appendages, the tube or ambulacral feet. The space between the major organ systems is composed of the main body cavities (the so-called perivisceral coeloms) that are filled with coelomic fluid [37]. Therefore, echinoids possess several of the internal structures encountered in most other taxa, although a number of highly specialized organs are present as well. This taxon can thus serve as a model for analyses using non-invasive imaging techniques on a broad systematic scale.

The purpose of our study was to explore the possibility of generating high-resolution 3D MRI datasets from selected specimens of a major invertebrate taxon. For the first time, a non-invasive imaging technique is employed for systematic comparative analyses. We show that MRI permits the rapid acquisition of digitized morphological data on a broad scale and the construction of 3D models that can be made interactively accessible on the Web. In addition, our approach can be employed to compare the internal anatomy of sea urchins to evaluate such datasets for evolutionary inferences.

## Results

### Establishment of imaging conditions

Initially, freshly fixed as well as museum specimens of *Psammechinus miliaris* (Müller, 1771), a common species in the North Sea, were used in order to establish imaging

**Figure 1**

**Establishment of imaging conditions using specimens of *Psammechinus miliaris*.** (A), (B) Comparison of two freshly fixed specimens. Magnetic resonance imaging (MRI) sections at the height of Aristotle's lantern and digestive tract. Resolution:  $(81 \mu\text{m})^3$ , no contrast agent added. The two specimens show a high degree of similarity in their overall internal architecture. Arrows indicate paramagnetic gut content. (C), (D) Effects of a contrast agent on image quality. MRI sections at the height of perignathic girdle and lower stomach. Resolution:  $(81 \mu\text{m})^3$ . This freshly fixed specimen was scanned (C) before and (D) after the application of a contrast agent, Magnevist. Arrows indicate susceptibility artefacts. (E), (F) Comparison of a freshly fixed and a museum specimen. MRI sections at the height of gonads and upper oesophagus. Resolution:  $(81 \mu\text{m})^3$ . The 135-year-old museum specimen (F) gives imaging results comparable to the freshly fixed specimen (E). Both specimens were scanned with contrast agent added. Orientation: ambulacrum II facing upwards. Scale bar: 0.5 cm. ac, axial complex; al, Aristotle's lantern; am, ampulla; es, oesophagus; go, gonad; im, interpyramidal muscle; in, intestine; is, inner marginal sinus; lm, lantern muscle; os, outer marginal sinus; pg, perignathic girdle; re, rectum; si, siphon; st, stomach; to, tooth.

and contrasting protocols for broader systematic analyses. Living specimens of *P. miliaris* were made available through the Biologische Anstalt Helgoland, Germany (BAH). Several dozen sea urchins were kept in the aquarium facilities of the Institut für Biologie, Freie Universität Berlin, Germany, for subsequent scanning and contrasting experiments.

The first set of analyses was conducted to compare different specimens of freshly fixed sea urchins. Imaging was performed initially at a resolution of  $(81 \mu\text{m})^3$  using different imaging protocols with specimens of almost identical size. This analysis showed that although slight differences in anatomical makeup did occur, localization, arrangement and overall shape of the internal organs did not differ significantly. In the specimens depicted (Figure 1A and 1B), this is exemplified by the almost identical shapes of both Aristotle's lanterns and the localization and shape of the digestive tract components. The structure of the wall of the sea urchin lower gut loop (also termed the stomach) was undulated in both specimens, whereas the horizontal sections of the upper gut loop (also termed the intestine) showed a smooth structure. The digestive tract of one specimen was partly filled (Figure 1A), while the digestive tract of the other specimen was empty, apart from tiny objects (Figure 1B). Another striking similarity was the almost exactly identical location of the inner and outer marginal sinus of the haemal system in both specimens. However, some differences were discernable, for example the distinct shapes of the ampullae and the thickness of the interpyramidal muscles, indicating that, ideally, several specimens of a given species should be scanned. Similar comparative experiments were performed on a total of 18 echinoid species (data not shown). In all cases, the overall internal architecture of two specimens of a given species resembled each other more closely than that of other species.

The next set of experiments served to assess the effects of a gadolinium-based contrast agent (Magnevist, a standard in clinical and pre-clinical MRI studies) on image quality. Using the same specimen of *P. miliaris* and the same imaging protocol, we found that the application of the contrast agent resulted in enhanced contrast, although some thin-walled structures, such as the ampullae or the oesophagus, became less visible (Figure 1C and 1D). Another advantage of the use of this contrast agent was that some of the artefacts caused by paramagnetic gut content were reduced due to the stronger water signal. Therefore, most specimens were scanned both before and after the application of the contrast agent (see Additional file 1 for details).

The final set of experiments for establishing a standard set of imaging conditions was designed to compare imaging

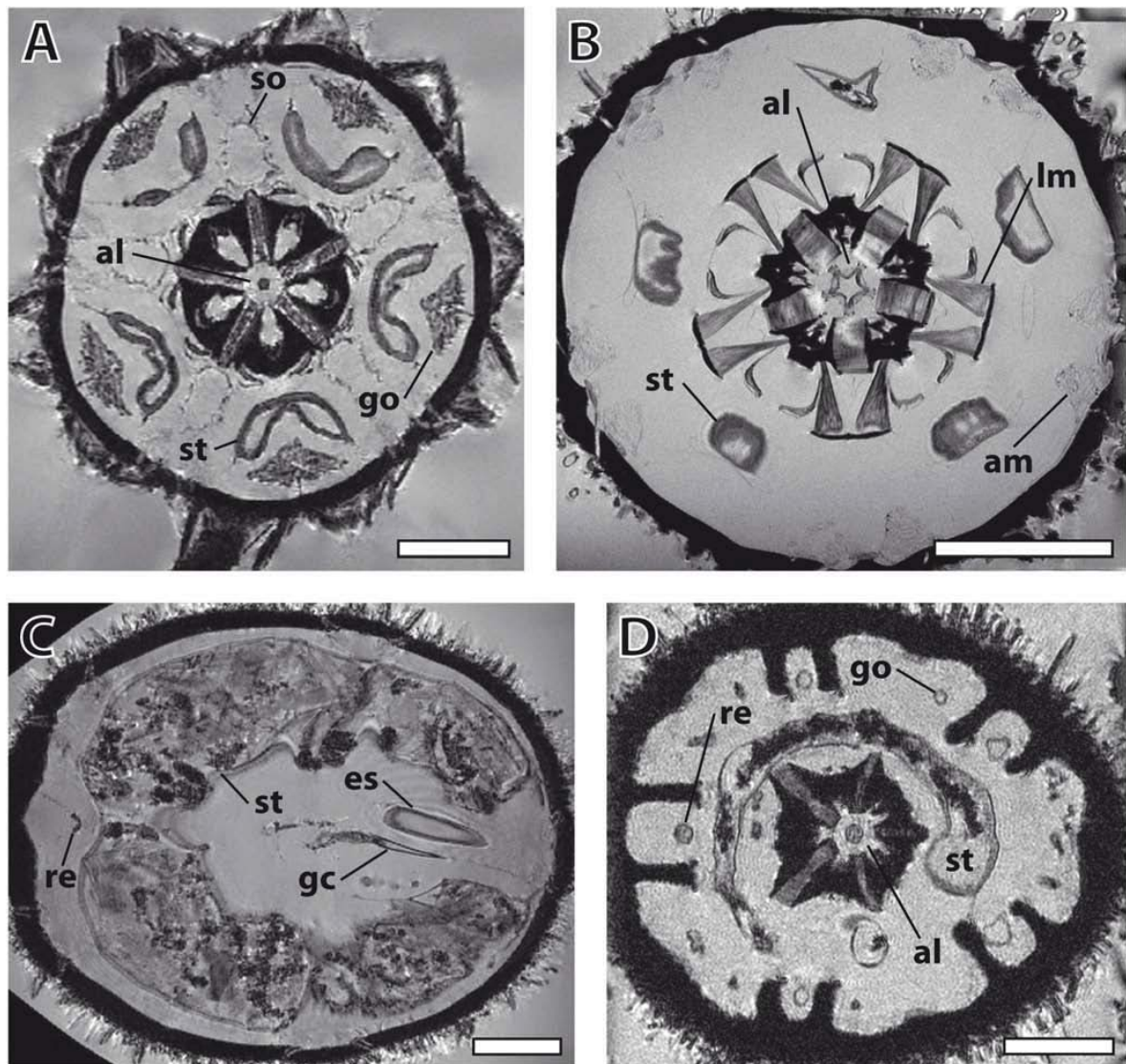
results obtained from freshly fixed and museum specimens of the same species. Prior to the present MRI studies, several museum specimens from the wet collection of the Systematische Zoologie am Museum für Naturkunde, Berlin, Germany (ZMB) were dissected in order to assess the state of preservation after decades or even more than a century of alcohol conservation (*Strongylocentrotus dröbachiensis* (Müller, 1776), *Sphaerechinus granularis* (Lamarck, 1816), *Schizaster lacunosus* (Linnaeus, 1758), and *Brissopsis lyrifera* (Forbes, 1841)). Their state of preservation was surprisingly good and seemed mainly to depend on the mode of collection, the fixation mode, and the subsequent preservation in alcohol. Following the dissections, MRI experiments using freshly fixed and museum specimens of *P. miliaris* were carried out. Structures visible in the freshly fixed specimen (Figure 1E) were recognizable also in the 135-year-old museum specimen (Figure 1F). The size and location of the anatomical features varied slightly, but this had been observed among different specimens of freshly fixed animals as well. Despite these differences, the results confirmed our assumption that museum material, even if more than a hundred years old, can be used for systematic MRI studies.

#### Scanning of selected members of high-ranking echinoid subtaxa

After an initial assessment of the suitability (that is, size, state of preservation, and availability) of specimens in natural history collections worldwide, MRI studies were carried out using selected species of the 14 currently recognized echinoid subtaxa (orders). In three cases, freshly fixed animals were employed for the analysis (see Additional file 2 for details).

The full datasets from two 'regular' sea urchins (*Eucidaris metularia* (Lamarck, 1816) and *P. miliaris*) as well as two irregular sea urchins (*Echinoneus cyclostomus* (Leske, 1778) and *Echinocyamus pusillus* (Müller, 1776)) are presented here as interactive videos (Additional files 3, 4, 5, 6; Figure 2 shows images of selected sections). The four image datasets range in spatial resolution from  $20 \times 18 \times 18 \mu\text{m}^3$  to  $(86 \mu\text{m})^3$  and represent the current state-of-the-art in high-field MRI at a field of view of up to  $(3.3 \text{ cm})^3$ . In *E. metularia* (Figure 2A) and *P. miliaris* (Figure 2B), the pentameric symmetry of echinoderms becomes easily visible when looking at the five gonads or the lantern muscles that form a five-tipped star. Moving down from the aboral to the oral side, the following internal and external structures can be identified, amongst others (Additional files 3, 4, 5, 6): madreporic plate, gonads, spines, intestine, compass elevator muscles, Aristotle's lantern with corresponding muscles, and the stomach. Some parts of the gut of *P. miliaris* were filled with paramagnetic sediment of unknown composition (possibly iron or manganese resi-



**Figure 2**

**Selected horizontal magnetic resonance imaging sections of different sea urchin species taken from Additional files 3, 4, 5, 6.** (A) *Eucidaris metularia*. Resolution:  $(81 \mu\text{m})^3$ . Aristotle's lantern, gonads, Stewart's organs, and stomach can be seen. (B) *Psammechinus miliaris*. Resolution:  $(44 \mu\text{m})^3$ . Aristotle's lantern, lantern muscles, stomach, and ampullae are visible. (C) *Echinoneus cyclostomus*. Resolution:  $(86 \mu\text{m})^3$ . Digestive tract with oesophagus, gastric caecum, stomach, and rectum are shown. (D) *Echinocyamus pusillus*. Resolution:  $20 \times 18 \times 18 \mu\text{m}^3$ . Aristotle's lantern, gonads, stomach, and rectum are represented. Scale bar: (A)-(C) 0.5 cm; (D): 1 mm. al, Aristotle's lantern; am, ampulla; es, oesophagus; gc, gastric caecum; lm, lantern muscle; re, rectum; so, Stewart's organ; st, stomach.

dues) that caused artefacts by altering the homogeneity of the magnetic field inside the MRI instrument.

In *E. cyclostomus* (Figure 2C) and *E. pusillus* (Figure 2D), the secondarily developed bilateral symmetry found in the Irregularia is obvious when looking at the gonads (reduced to four). The digestive tract of *E. cyclostomus* is characterized by a dominant gastric caecum, localized at the beginning of the stomach, and a long rectum, leading down to the anus which is situated at the oral side of the animal. *E. pusillus*, in common with all members of the Clypeasteroidea, the so-called sand dollars, possesses a modified Aristotle's lantern. Other structures that can be identified in the irregular species include relatively small spines, one dominant (*E. pusillus*) or two huge (*E. cyclostomus*) gut loops, filled with debris and detritus, and an axial complex running straight down from the madreporic plate to the adoral part of the oesophagus (*E. cyclostomus*). In addition to soft tissues, the delineation of calcareous structures caused by the signal-providing surrounding fluids and tissues adds some information on hard-part anatomy to the virtual sections as well.

Although several specimens of the echinoid taxon missing in our study, the Echinothurioida (or leather urchins), were found in museum collections, their shape prevented successful soft tissue imaging. These sea urchins possess a flexible calcite endoskeleton as well as specialized internal muscles that contract when the animal is fixed, resulting in a pancake-like shape of the organism. For a reliable comparison of internal structures it would be necessary to scan specimens prior to contraction of these powerful muscles.

### 3D reconstruction of selected internal organs

The 3D reconstructions presented here are limited to the major soft tissue structures identifiable in all datasets, if present in the respective species (Figure 3C–E and 4C–E): digestive tract, Stewart's organs, axial complex, siphon, gonads, buccal sacs (or 'gills') and gastric caecum.

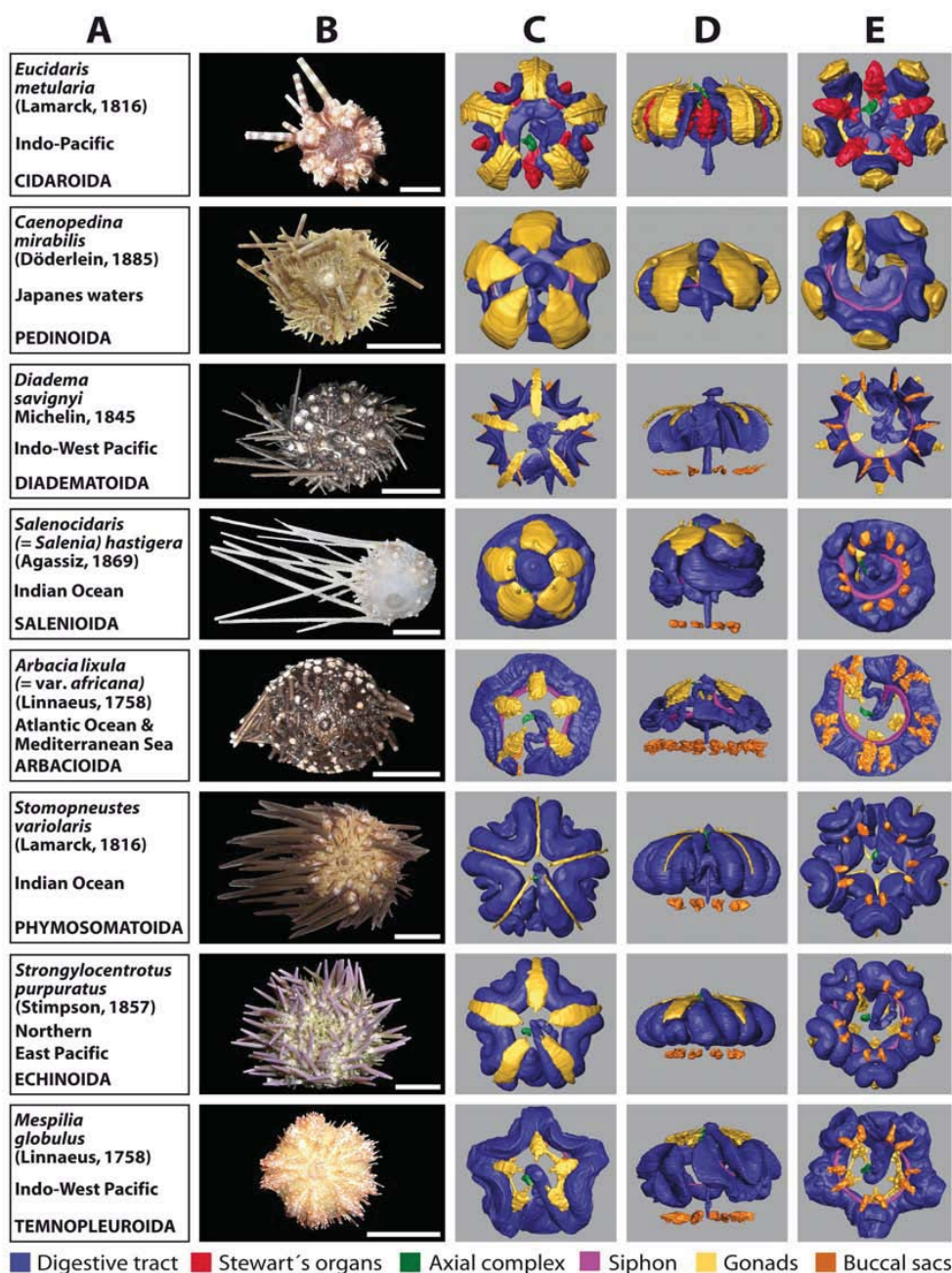
Two of the immediately recognizable features are size and shape of the gonads. Both differ substantially between the analyzed species and usually constitute a character set of high intraspecific variability. This becomes evident from the analysis of animals from a given species in distinct developmental stages (data not shown). The specimen of *Stomopneustes variolaris* (Lamarck, 1816) (Figure 3) shown here was fixed before gonad maturation. In the case of the highly branched gonads found in *E. pusillus* (Figure 4), depicted here for the first time, the advantages offered by the digitized reconstruction of morphological structures become obvious: a 3D reconstruction of such complex structures would be particularly demanding using traditional techniques. In contrast to the gonads, clearly dis-

tinct shapes are revealed when the guts of 'regular' (Figure 3) and irregular (Figure 4) sea urchin specimens are compared. After the scanning process, a digital photograph was taken of every specimen selected for this study (Figures 3B and 4B).

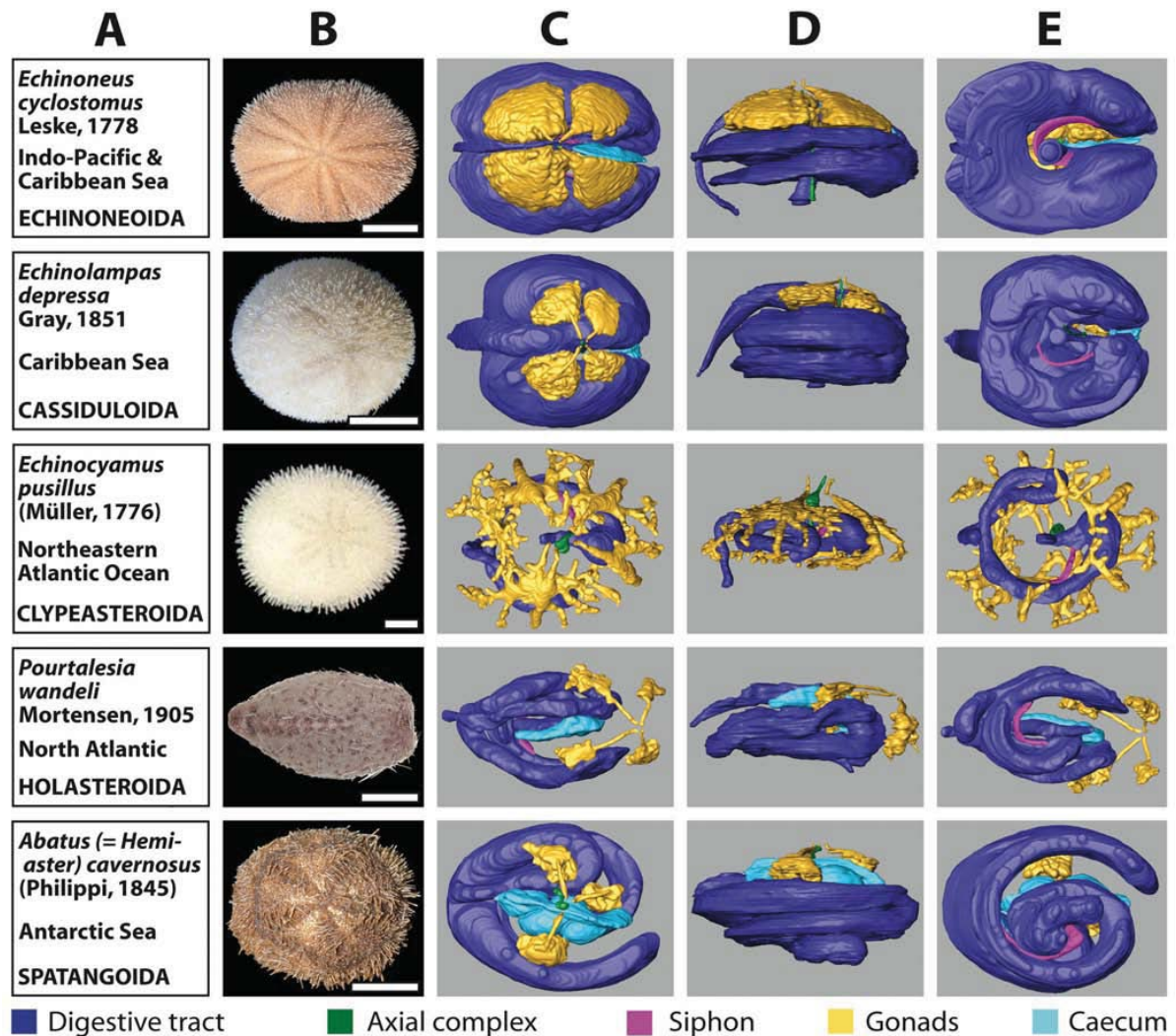
MRI also revealed a striking difference regarding the architecture of the gastric caecum. Except for the two clypeasteroid subtaxa Laganina and Scutellina, this structure can be found in all irregular taxa (Figure 4C–E), located at the beginning of the stomach. Its presence correlates with the feeding habits of this group of sea urchins: most of these animals are partially or completely covered by sediment which they ingest to filter out organic material. Although the precise function of the gastric caecum is still a matter of discussion, it appears to have a major role in digestion (see, for example, [38,39]). In specimens of comparable size, substantial differences in its size and shape were found (Figure 5). The highly reduced gastric caecum consisting of numerous smaller blindly ending sacs that can be observed in *Echinolampas depressa* Gray, 1851 (Figure 5B) appears to be a common characteristic which sets the Cassiduloida apart from other taxa (Figure 5A,C and 5D) of the Irregularia. This is emphasized by the presence of a similar, highly reduced gastric caecum in the cassiduloid species *Cassidulus caribearum* Lamarck, 1801 (data not shown; as described also by Gladfelter [40]) and *Rhyncholampas pacificus* Agassiz, 1863 (as shown in [41]). A comprehensive description and comparative analysis of sea urchin internal anatomy will be published elsewhere (Ziegler et al., publication in preparation).

### Interactive viewing of selected species in three dimensions

To illustrate the opportunities offered by digitized reconstructions, Figure 6A–C shows different views of the 3D model of a member of the Cidaroida (or pencil urchins), *E. metularia*. This widely distributed Indo-Pacific species possesses a moderately thick calcite endoskeleton, large primary and short secondary spines. Its internal organization is characterized by the presence of five bushy Stewart's organs, five stalked gonads and a short intestine. The drawing presented in Figure 6D was made by Stewart [42] from a closely related species, *Cidaris cidaris* (= *Dorocidaris papillata*) (Linnaeus, 1758), where he depicts the newly discovered organs that were later named after him. A comparison of his drawing with the digital model in Figure 6C demonstrates that modern imaging protocols in combination with 3D capability may serve as a valuable substitute for laborious and subjective traditional dissection and visualization techniques. The interactive 3D model of *E. metularia* (accessible through a click onto Figure 6 in the 3D PDF version of this article: Additional file 7) permits, apart from standard operations such as zoom and drag, the selection of the numerous reconstructed structures. These elements can individually be made transparent for

**Figure 3**

**Overview chart showing analyzed specimens of 'regular' sea urchins and corresponding 3D reconstructions of selected internal organs.** (A) Information on species name, geographic distribution, and systematics. (B) Photograph of scanned specimen, aboral view. (C)-(E) 3D models of reconstructed selected internal organs, stepwise turned by 90°: (C) aboral view (interambulacrum 5 facing upwards); (D) lateral view (interambulacrum 5 at back); (E) oral view (interambulacrum 5 facing downwards). The buccal sacs of *Caenopedina mirabilis* as well as the siphon of *Stomopneustes variolaris* could not be seen on the magnetic resonance imaging sections. Scale bar: 1 cm. The colour legend specifies organ designation.

**Figure 4**

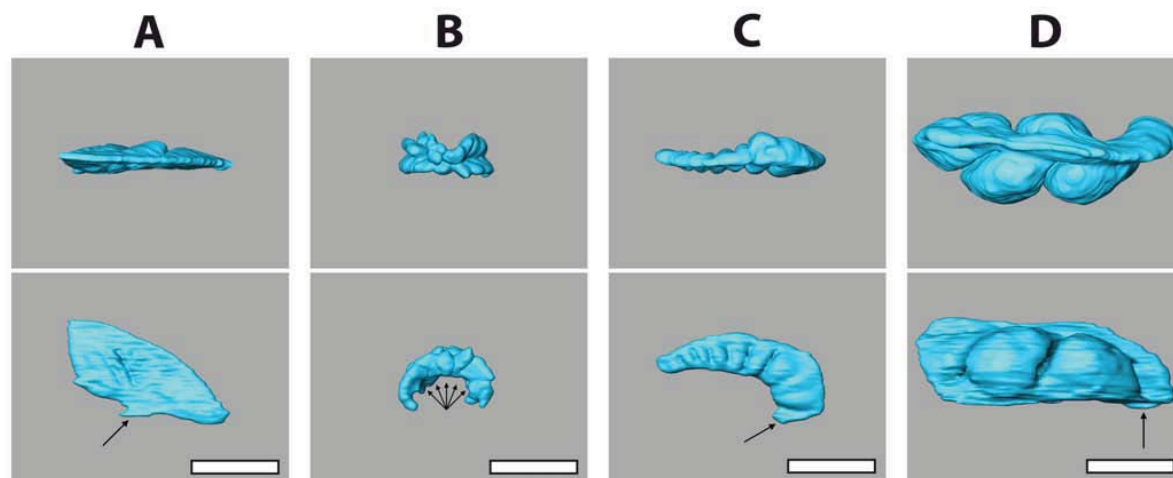
**Overview chart showing analyzed specimens of irregular sea urchins and corresponding 3D reconstructions of selected internal organs.** (A) Information on species name, geographic distribution, and systematics. (B) Photograph of scanned specimen, aboral view. (C)-(E) 3D models of reconstructed selected internal organs, stepwise turned by 90°: (C) aboral view (ambulacrum III facing to the right); (D) lateral view (ambulacrum III facing to the right); (E) oral view (ambulacrum III facing to the right). Scale bar: 1 cm, except for *Echinocyamus pusillus*: 1 mm. The colour legend specifies organ designation.

an unobstructed view on all organs they may occlude. Several pre-installed views can be selected as well. The creation of this model, including MRI data acquisition, took less than three full work days. All other models shown in Figures 3 and 4 are available for download and interactive viewing on The Echinoid Directory [43].

## Discussion

### Methodology

The initial phase of our study served to determine the proper imaging conditions using high-field MRI instruments. In order to achieve resolutions below  $(100 \mu\text{m})^3$ , we employed 7 T and 17.6 T small animal scanners. We were able to obtain resolutions ranging from  $20 \times 18 \times 18 \mu\text{m}^3$  to  $(86 \mu\text{m})^3$  with specimens ranging from 5 mm to

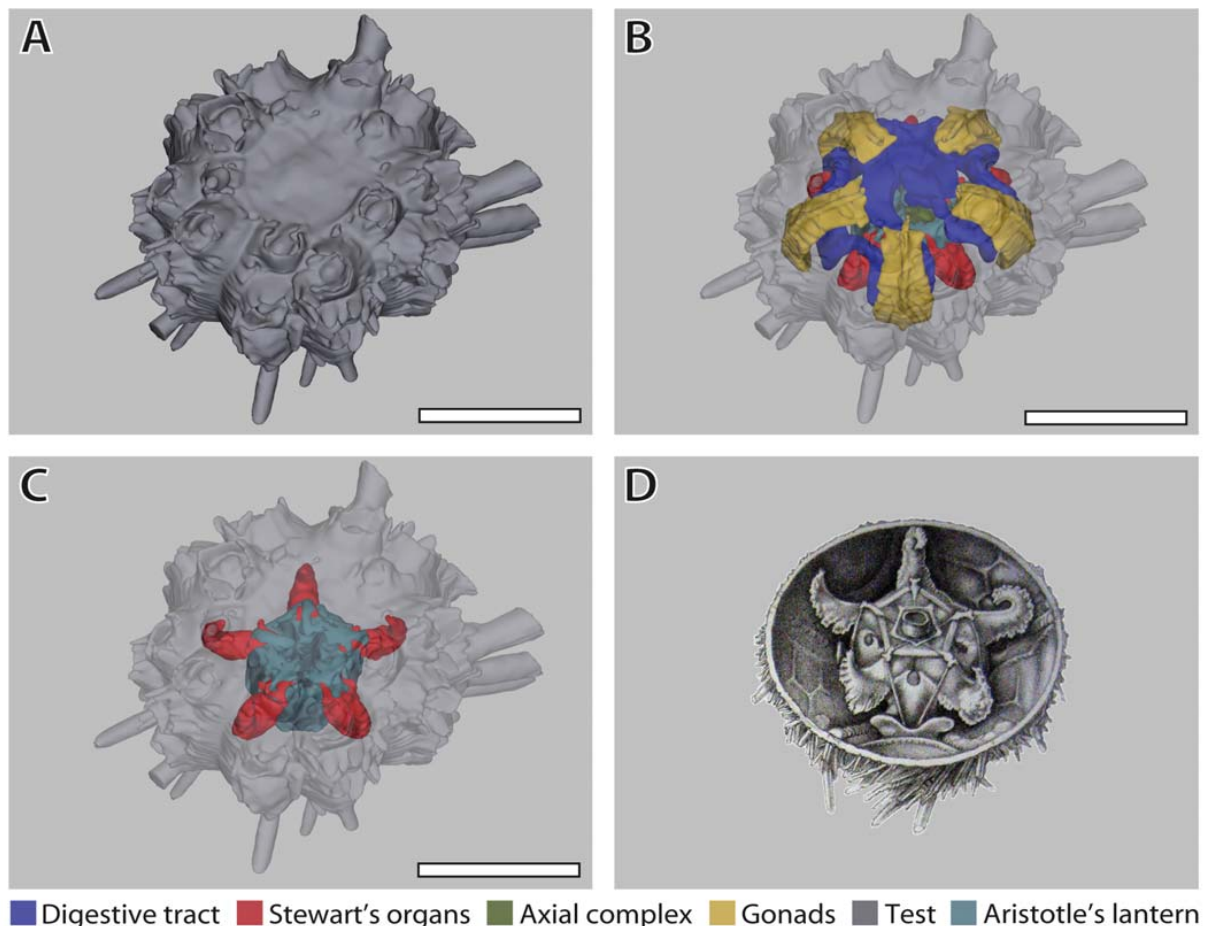


**Figure 5**  
**3D reconstructions of the gastric caecum of selected irregular sea urchin species.** The gastric caecum is a translucent body free of sediment and probably constitutes one of the main sites of digestion [38,39]. The upper diagrams show an aboral view, the lower diagrams a lateral view with the anterior side (ambulacrum III) oriented towards the right-hand side. Arrows indicate the position of the junction of the gastric caecum with the stomach. (A) *Echinoneus cyclostomus*, Echinoneoidea. (B) *Echinolampas depressa*, Cassiduloidea. Species of this sea urchin taxon presumably all possess a highly reduced gastric caecum consisting of numerous small blindly ending sacs. (C) *Pourtalesia wandeli*, Holasteroidea. (D) *Abatus cavernosus*, Spatangoida. Scale bar: 0.5 cm.

3.4 cm in size. Therefore, in terms of resolution, our data is comparable to results derived from manual dissection techniques in combination with stereomicroscopic observation. Susceptibility artefacts were primarily seen in the sediment-feeding irregular species, with the gut content being the source of these artefacts (see, for example, Additional file 6, *Echinocyamus pusillus* (Müller, 1776)). What sediment component is causing which type of artefact needs to be determined in mineralogical studies on freshly fixed specimens. The effects of the contrast agent made it possible to reduce the negative effects of these artefacts in some cases (Figure 1C and 1D), but a thorough investigation of the potential of selective and non-selective contrast agents [44] is essential for their future application in invertebrate morphology. Other major sources for artefacts were the tendency of spatangoid sea urchins to accumulate ferric iron phosphate in the connective tissues of their digestive tracts [45], and the digestive tract diverticula of scutelline sand dollars known to harbour magnetite [46]. However, the scanning of several specimens of a given species and the matching of their internal structures did in some cases help to overcome these problems.

One of the big advantages of MRI techniques is the extremely simple preparation of fixed specimens, being limited to the watering of the specimens (possibly in the

presence of a contrast agent) and later putting them back into alcohol for storage. No detrimental effects of this procedure were noted during our studies. Apart from morphological studies on fixed specimens, MRI can also be used for *in vivo* analyses of invertebrates where, in contrast to  $\mu$ CT techniques that are based on X-rays, the living specimen is not harmed during the scanning process. Extensive morphological or developmental studies can thus be carried out, although anaesthetic substances may have to be applied to reduce movement artefacts during the long scanning times that are needed for high-resolution datasets and 3D reconstructions. Another very important advantage of non-invasive imaging techniques in general is the fact that the digitally acquired image stacks do not have to be manually aligned, as is the case with digital pictures from histological or electronmicroscopical sections. Although these datasets can be used to generate highly resolved digitized 3D models of invertebrates as well (see, for example, [47,48]), these analyses are extremely demanding in terms of specimen preparation, slice alignment and 3D reconstruction. In comparison, 3D reconstruction of MRI data is simple and highly accurate, but the segmentation process carried out for the present work is still subjective and our primary hypotheses regarding organ designation had to be evaluated against the information available from classical histological literature. However, user-friendly semi-automatic seg-

**Figure 6**

**Comparison of a digital 3D model with a traditional anatomical sketch.** (A)-(C) *Eucidaris metularia*. Selected views taken from the interactive 3D model: (A) external view; (B) external view with transparent test, internal organs visible; (C) external view with transparent test and all internal organs removed except for Stewart's organs and Aristotle's lantern. (D) *Cidaridaris cidaris* (= *Dorocidaridaris papillata*). Image taken from [42] and modified. Stewart's organs constitute extensions of the peripharyngeal coelom. Scale bar: 1 cm. The colour legend specifies organ designation. The interactive 3D mode can be accessed by clicking onto Figure 6 in the 3D PDF version of this article: Additional file 7 (Adobe Reader Version 7.1 or higher required).

mentation [49] as well as artefact and noise reduction [50] algorithms have recently become available, and may further simplify the task of 3D reconstruction. The highly demanding step of obtaining a completely automated segmentation and reconstruction of an entire animal would be very desirable and appears technically feasible, although it is not yet available for comparative morphological studies.

In spite of the many positive features, a number of negative aspects are currently inherent to morphological stud-

ies of small animals using MRI. The achievable resolution is comparatively low, and results derived from the reconstruction of internal structures are currently comparable only to manual dissection. Furthermore, an exact outline of how future experiments on other invertebrate taxa should be performed can only be partially derived from our study, since imaging results of fixed specimens depend on several factors, some of them still not fully understood (for example, susceptibility artefacts or changes to organ systems after fixation). Another drawback is the fact that only limited *in vitro* staining possibil-

ities are available for MRI studies, although some substances (for example manganese) can be used for *in vivo* staining [28]. A further disadvantage of MRI is that specimens cannot currently be scanned in alcohol, since this would require spectroscopic imaging techniques resulting in much longer scanning times at the desirable resolutions below  $(100\ \mu\text{m})^3$ . In addition, in the case of sea urchins, the 3D models generated (see, for example, Figure 6) are practically useless for taxonomic purposes since sea urchin taxonomy is currently based entirely on hard parts. Resolutions well below  $(10\ \mu\text{m})^3$  would be necessary to differentiate between the often miniscule characters of the sea urchin skeleton. However, using  $\mu\text{CT}$ , these datasets can potentially be gathered, as demonstrated by  $\mu\text{CT}$  scans of two sea urchin species, *Strongylocentrotus purpuratus* (Stimpson, 1857) [51] and *Encope michelini* Agassiz, 1841 [52], presented on the Digital Morphology Library (DigiMorph) website [53].

On the other hand, the access to MRI instruments does not appear to be a limiting factor. There are currently more than 1000 experimental small animal MRI instruments worldwide available for pre-clinical imaging. Since all high-field MRI scanners consist of super-conducting electromagnets, overnight and weekend scans as performed during this study would permit an optimal use of this resource.

#### **Internal morphology of sea urchins**

Despite the existence of extensive fossil, morphological and molecular datasets for this taxon, comparatively little systematic knowledge has been gathered on the internal anatomy of sea urchins. However, some authors have greatly extended our knowledge about the internal anatomy of selected, readily available sea urchin species such as *Cidaris cidaris* (Linnaeus, 1758) [54], *Arbacia punctulata* (Lamarck, 1816) [55], *Paracentrotus lividus* (Lamarck, 1816) [56,57], *Echinus esculentus* Linnaeus, 1758 [58], *Sphaerechinus granularis* (Lamarck, 1816) [57,59], *Spatangus purpureus* Müller, 1776 [57] or *Echinocardium cordatum* (Pennant, 1777) [38], not to mention the extensive works of Alexander E Agassiz, Hubert L Clark and Theodor J Mortensen. A common drawback of these studies is that a given author rarely dissected and analysed several species of a single taxon using one consistent method. Only in very few cases have histological sections, dissected specimens and so on, been preserved. The conclusions drawn from the original data can therefore not always be scrutinized.

Furthermore, the results were sometimes biased by prevailing morphological hypotheses. For example, recent histological studies [60] as well as our findings (Figure 3) indicate that the siphon, a canal bypassing the sea urchin stomach that was believed not to be found in the Diade-

matoida (see, for example, [61]), is indeed also present in this group of animals. Distinct features of internal sea urchin anatomy may extend to the sizes and shapes of digestive tract, gonads, ampullae and muscles. A thorough revision of internal structures in the light of recent technological advances will therefore almost certainly change our view of facts that, for years, were taken for granted. Scanning of sea urchins has so far been performed by us on more than 50 species (Ziegler et al., publication in preparation).

The feasibility of comparative morphological studies using MRI is further exemplified by our description of the highly variable shape and size of the gastric caecum found in the Irregularia (Figure 5). Our findings were correlated with the little information available on this structure; the combined data led us to assume that a reduced gastric caecum consisting of several smaller blindly ending sacs might constitute a soft tissue character common to all cassiduloid sea urchins. We therefore predict the presence of a similarly shaped structure in all species of the Echinolampadidae and Cassidulidae. Furthermore, it would be of interest to extend our analyses to members of the Apatopygidae and Neolampadidae, the other two extant families currently assigned to the Cassiduloidea.

Although for some organs high intraspecific variability was detected, in particular in the case of organs with a development-dependent size and shape such as the gonads (Figure 1E and 1F), shape and localization of other organs (for example the digestive tract) did not differ significantly among specimens from a given echinoid species, allowing comparison on various taxic levels (Figures 3 and 4). However, intraspecific variability of internal organs can also be observed in other taxa, for example gastropods (sinistral freak) or humans (situs inversus viscerum). Therefore, like larval and hard-part morphology, which are continuously updated [62,63], morphological character sets derived from internal organs of sea urchins will serve as a useful systematic reference for future studies.

#### **Non-invasive imaging techniques other than MRI**

A number of imaging techniques allow for non-invasive morphological studies on whole specimens. However, only a few of them are able to achieve resolutions that permit detailed morphological analyses in small animals. Confocal laser scanning microscopy (CLSM), in combination with the autofluorescence of the crustacean or insect cuticula, can be used for 3D reconstructions of minuscule body parts or whole specimens [64-66]. The potential of this promising technique must not be underestimated, since the achievable resolutions permit taxonomic studies (based, for example, on chaetotaxy) as well as large-scale systematic morphological analyses. However, this proce-

ture reveals internal structures only in rare cases and is limited to tiny objects.

In contrast to CLSM,  $\mu$ CT has already become a standard tool for detailed non-invasive studies of whole specimens, especially in studies on fossils [67]. It is based on the analysis of a sample by means of X-rays and can primarily be used to reveal hard tissue structures such as bone or calcite. Moreover, recent studies using more advanced techniques such as X-ray synchrotron microtomography and a new setup called very-high-resolution X-ray computed tomography have been employed to display soft tissues, *in vitro* as well as *in vivo* [6,7,68-70] (see also the review by Attwood [4]). Using  $\mu$ CT, isotropic resolutions of less than  $(5 \mu\text{m})^3$  have been achieved on whole specimens, although, technically, resolutions in the nanometre scale are within reach. However, whether these new  $\mu$ CT methods can compete with the ability of MRI to display soft tissue at high resolutions still needs to be evaluated. Our own preliminary studies to generate images of internal organs performed on several sea urchin museum specimens (*Echinoneus cyclostomus* Leske, 1778, *Psammechinus miliaris* (Müller, 1771), *Mespilia globulus* (Linnaeus, 1758), and *Moira atropos* (Lamarck, 1816)) using a desktop high-resolution  $\mu$ CT scanner (Skyscan 1172, Skyscan, Kontich, Belgium) at the Max-Planck-Institut für evolutionäre Anthropologie, Leipzig, Germany were not successful, although these  $\mu$ CT datasets can be used for the reconstruction of hard tissue structures. 3D models based on this data will be made available on the DigiMorph website [53].

These results demonstrate that complementary imaging techniques should ideally be used for comparative morphological analyses, an approach commonly referred to as multimodality.

### Conclusion

Our results extend the use of MRI in invertebrate morphology to a systematic approach using museum specimens of a major marine invertebrate taxon, the sea urchins (Echinoidea). MRI can be employed for the rapid, non-destructive and unbiased acquisition of digital morphological data, and the creation of interactive 3D models accessible both within a publication and via the Web. The revelation of the internal anatomy of echinoid museum specimens at a resolution comparable with manual dissection extends our knowledge of soft tissue characters, permitting phylogenetic inferences.

### Methods

#### Specimen preparation

All specimens analyzed belong to the taxon Echinoidea (sea urchins), one of the five subtaxa of the Echinodermata (marine spiny-skinned animals). The museum spec-

imens were mostly fixed in formalin and all were conserved in alcohol, although in some cases the exact mode of fixation could not be determined. For MR scanning, the museum specimens had to be lowered down to distilled water in a gradual alcohol series. Specimens that were obtained in living state were fixed in a 7% formaldehyde solution. For MR scanning, the freshly fixed specimens were kept in this solution. Results derived from specimens scanned in alcohol and formalin did not appear to differ significantly.

The specimens were placed either inside a custom-built Plexiglas chamber (Berlin), inside a 50 ml Falcon tube (Berlin), or inside NMR tubes with diameters between 5 and 20 mm (Würzburg), depending on the size of the specimen. On some specimens spines had to be dressed for tight fit inside the tubes. Magnevist (Bayer-Schering, Berlin, Germany), a gadolinium-based non-selective contrast agent, was added at a final concentration of 2 mM. This concentration had been employed successfully in preliminary studies (results not shown). The addition of the contrast agent to the museum specimens was discussed beforehand with the curators who judged the risk to the specimens' integrity as negligible. Prior to scanning, samples were degassed at 50 mbar. The freshly fixed specimens used in this study will be deposited as voucher material at the ZMB. Museum specimens will be stored in separate jars for potential later re-scanning. Table 2 lists detailed information on every museum and freshly fixed specimen used in this study.

#### Specimen scanning and photography

##### Berlin

Experiments were conducted at the Berlin NeuroImaging Center, Charité – Universitätsmedizin Berlin, Germany on a 7 T Pharmascan 70/16 AS rodent scanner with a  $^1\text{H}$ -resonance frequency of 300 MHz (Bruker Biospin GmbH, Ettlingen, Germany). The system consisted of a 160 mm horizontal bore magnet, a shielded gradient set with an inner diameter of 90 mm, and a maximum gradient strength of 300 mT/m. A  $^1\text{H}$ -radio frequency linear transmit/receive birdcage resonator with an inner diameter of 38 mm was used for excitation and signal detection. The images described here were acquired at around 18°C. Data acquisition and image processing were carried out with Paravision 4.0.

##### Würzburg

Experiments were conducted at the Physikalisches Institut, Würzburg, Germany at 17.6 T with a  $^1\text{H}$ -resonance frequency of 750 MHz on a Bruker Avance 750WB NMR spectrometer (Bruker Biospin GmbH, Rheinstetten, Germany). The system consisted of an 89 mm vertical bore magnet, a shielded gradient set with an inner diameter of 40 mm, and a maximum gradient strength of 1 T/m. A 20



BMC Biology 2008, 6:33

<http://www.biomedcentral.com/1741-7007/6/33>

mm linear birdcage resonator and a 5 mm linear bird cage resonator were used. The images described here were acquired at around 18°C. Image processing was carried out with Paravision 3.0.2 and involved zero filling to a  $(512)^3$  matrix prior to Fourier transformation.

Scanning protocols employed a 3D gradient echo imaging sequence (FLASH) with parameters depending on the specimen size (see Additional file 2 for details). Almost all scans resulted in datasets with isotropic spatial resolution.

The photos of museum and freshly fixed specimens were made using a digital camera (Casio Exilim) with 7.2 Megapixels. The acquired images were processed using Adobe Photoshop CS2 9.0.

### 3D visualization

3D image reconstruction and visualization were performed by converting the generated MRI data (DICOM standard) into an 8-bit TIFF image sequence (ImageJ 1.38w) and by using 3D imaging software (amira 3.0.2, Mercury Computer Systems, Berlin, Germany). Segmentation was carried out manually by using the brush tool in the amira Image Segmentation Editor. In some cases structures on every other slice were labelled, with subsequent 'interpolation' of structures on intervening slices, followed by a check and correction of segmentation results if necessary. Detection of borderlines and organ designations were performed based on literature, our own histological data and previously acquired MRI data [31,32].

Operations were carried out on a desktop PC (CPU: Intel Core 2 Duo, 2.67 GHz; graphics card: NVIDIA GeForce 8600 GT; operating system: Windows XP; display: WACOM Cintiq 21UX Pen Display). Image processing was performed using Adobe Photoshop CS2 9.0 and Adobe Illustrator CS2 12.0.1. The movies were produced using the ImageJ 1.38w QuickTime export function. The individual 3D structures were saved as Wavefront files and imported into Adobe 3D Toolkit 8.1.0, where they were reassembled and transformed into an interactive 3D PDF. The 3D model was embedded into this publication using the Adobe 3D Toolkit according to the procedures described in [71].

### List of abbreviations

3D: three-dimensional; BAH: Biologische Anstalt Helgoland, Germany; CAS: California Academy of Sciences, San Francisco, USA; CLSM: confocal laser scanning microscopy;  $\mu$ CT: micro-computed tomography; FOV: field of view; MRI: magnetic resonance imaging; NHM: Natural History Museum, London, UK; NMR: nuclear magnetic resonance; USNM: National Museum of Natural History, Washington DC, USA; ZMB: Systematische Zoologie am Museum für Naturkunde, Berlin, Germany.

### Authors' contributions

AZ designed and coordinated the experiments, carried out the dissections, prepared specimens and carried out scanning and 3D modelling. CF and SM prepared and scanned specimens. TB supervised the experiments. All authors contributed to writing the manuscript and approved of the final version.

### Additional material

#### Additional file 1

Table 1 – Scanning parameters for specimens used in this study.

Click here for file

[<http://www.biomedcentral.com/content/supplementary/1741-7007-6-33-S1.pdf>]

#### Additional file 2

Table 2 – List of specimens used in this study.

Click here for file

[<http://www.biomedcentral.com/content/supplementary/1741-7007-6-33-S2.pdf>]

#### Additional file 3

Video 1 – MRI dataset of *Eucidaris metularia* (Lamarck, 1816). Resolution:  $(81 \mu\text{m})^3$ .

Click here for file

[<http://www.biomedcentral.com/content/supplementary/1741-7007-6-33-S3.mov>]

#### Additional file 4

Video 2 – MRI dataset of *Psammechinus miliaris* (Müller, 1771). Resolution:  $(44 \mu\text{m})^3$ .

Click here for file

[<http://www.biomedcentral.com/content/supplementary/1741-7007-6-33-S4.mov>]

#### Additional file 5

Video 3 – MRI dataset of *Echinoneus cyclostomus* Leske, 1778. Resolution:  $(86 \mu\text{m})^3$ .

Click here for file

[<http://www.biomedcentral.com/content/supplementary/1741-7007-6-33-S5.mov>]

#### Additional file 6

Video 4 – MRI dataset of *Echinocyamus pusillus* (Müller, 1776). Resolution:  $20 \times 18 \times 18 \mu\text{m}^3$ .

Click here for file

[<http://www.biomedcentral.com/content/supplementary/1741-7007-6-33-S6.mov>]

#### Additional file 7

3D model – 3D PDF version of the entire article. By clicking anywhere onto Figure 6 the 3D model of *Eucidaris metularia* (Lamarck, 1816) can be interactively accessed. The 3D model is based on the virtual MRI sections seen in Video 1. In order to view the 3D model please install (or upgrade to) Adobe Reader Version 7.1 or higher.

Click here for file

[<http://www.biomedcentral.com/content/supplementary/1741-7007-6-33-S7.pdf>]

BMC Biology 2008, 6:33

<http://www.biomedcentral.com/1741-7007/6/33>

### Acknowledgements

The authors thank Andrew Cabrinovic (NHM), Carsten Lüter (ZMB), David Pawson (USNM), and Rich Mooi (CAS) for the generous supply with sea urchin museum specimens. We sincerely appreciate the help with photography from Peter Adam (Institut für Biologie, Freie Universität Berlin, Germany). Andrew B Smith (NHM) is thanked for introducing AZ to sea urchin systematics and commenting on the manuscript. We are grateful to Heiko Temming (Max-Planck-Institut für evolutionäre Anthropologie, Leipzig, Germany) for carrying out the  $\mu$ CT scans. The authors appreciate the comments by Timothy Rowe (The University of Texas at Austin, Austin, USA) and two anonymous reviewers. We also thank Andreas Ziegler (Institut für Immunogenetik, Freie Universität Berlin, Germany) for critical reading of the manuscript. The 17.6 T NMR spectrometer was funded by the DFG (Ha1232/13). AZ was supported through stipends from the State of Berlin (NaFöG), Germany, and the Friedrich-Naumann-Stiftung für die Freiheit, Potsdam, Germany

### References

- Hörschemeyer T, Beutel RG, Pasop F: **Head structure of *Priacma serrata* Leconte (Coleoptera, Archostemata) inferred from x-ray tomography.** *J Morphol* 2002, **252**:298-314.
- Wirkner CS, Richter S: **Improvement of microanatomical research by combining corrosion casts with microCT and 3D reconstruction, exemplified in the circulatory organs of the woodlouse.** *Microsc Res Tech* 2004, **64**:250-254.
- Burrow CJ, Jones AS, Young G: **X-ray microtomography of 410 million-year-old optic capsules from placoderm fishes.** *Micron* 2005, **36**:551-557.
- Attwood D: **Nanotomography comes of age.** *Nature* 2006, **442**:642-643.
- Betz O, Wegst U, Weide D, Heethoff M, Helfen L, Lee WK, Cloetens P: **Imaging applications of synchrotron X-ray phase-contrast microtomography in biological morphology and biomaterials science. I. General aspects of the technique and its advantages in the analysis of millimetre-sized arthropod structure.** *J Microsc* 2007, **227**:51-71.
- Dierick M, Cnudde V, Masschaele B, Vlassenbroeck J, Van Hoorebeke L, Jacobs P: **Micro-CT of fossils preserved in amber.** *Nucl Instrum Meth Phys Res A* 2007, **580**:641-643.
- Socha JJ, Westneat MW, Harrison JF, Waters JS, Lee WK: **Real-time phase-contrast x-ray imaging: a new technique for the study of animal form and function.** *BMC Biol* 2007, **5**:6.
- Wirkner CS, Richter S: **The circulatory system in Mysidacea – implications for the phylogenetic position of Lophogastrida and Mysida (Malacostraca, Crustacea).** *J Morphol* 2007, **268**:311-328.
- Jones G, Christal M: **The future of virtual museums: on-line, immersive, 3D environments.** 2002 [<http://tinyurl.com/4vt97g>]. Created Realities Group
- Rowe J: **Developing a 3D digital library for spatial data: issues identified and description of prototype.** *RLG DigiNews* 2002, **6**:5.
- Budd GE, Olsson L: **A renaissance for evolutionary morphology.** *Acta Zool* 2007, **88**:1.
- Brouwer M, Engel DW, Bonaventura J, Johnson GA: **In vivo magnetic resonance imaging of the blue crab, *Callinectes sapidus*: effect of cadmium accumulation in tissues on protein relaxation properties.** *J Exp Zool* 1992, **263**:32-40.
- Bock C, Frederich M, Wittig RM, Pörtner HO: **Simultaneous observations of haemolymph flow and ventilation in marine spider crabs at different temperatures: a flow-weighted MRI study.** *Magn Reson Imaging* 2001, **19**:1113-1124.
- Gozansky EK, Ezell EL, Budelmann BU, Quast MJ: **Magnetic resonance histology: in situ single cell imaging of receptor cells in an invertebrate (*Lolliguncula brevis*, Cephalopoda) sense organ.** *Magn Reson Imaging* 2003, **21**:1019-1022.
- Herberholz J, Mims CJ, Zhang X, Hu X, Edwards DH: **Anatomy of a live invertebrate revealed by manganese-enhanced magnetic resonance imaging.** *J Exp Biol* 2004, **207**:4543-4550.
- Brinkley CK, Kolodny NH, Kohler SJ, Sandeman DC, Beltz BS: **Magnetic resonance imaging at 9.4 T as a tool for studying neural anatomy in non-vertebrates.** *J Neurosci Meth* 2005, **146**:124-132.
- Davenel A, Quellec S, Pouvreau S: **Noninvasive characterization of gonad maturation and determination of the sex of Pacific oysters by MRI.** *Magn Reson Imaging* 2006, **24**:1103-1110.
- Pouvreau S, Rambeau M, Cochard JC, Robert R: **Investigation of marine bivalve morphology by in vivo MR imaging: first anatomical results of a promising technique.** *Aquaculture* 2006, **259**:415-423.
- Pohlmann A, Möller M, Decker H, Schreiber WG: **MRI of tarantulas: morphological and perfusion imaging.** *Magn Reson Imaging* 2007, **25**:129-135.
- Müller WEG, Kaluzhnaya OV, Belikov SI, Rothenberger M, Schröder HC, Reiber A, Kaandorp JA, Manz B, Mietchen D, Volke F: **Magnetic resonance imaging of the siliceous skeleton of the demopong *Lubomirskia baicalensis*.** *J Struct Biol* 2006, **153**:31-41.
- Goodman BA, Gordon SC, Chudek JA, Hunter G, Woodford JAT: **Nuclear magnetic resonance microscopy as a non-invasive tool to study the development of lepidopteran pupae.** *J Insect Physiol* 1995, **41**:419-424.
- Mapelli M, Greco F, Gussoni M, Consonni R, Zetta L: **Application of NMR microscopy to the morphological study of the silkworm, *Bombyx mori*, during its metamorphosis.** *Magn Reson Imaging* 1997, **15**:693-700.
- Janoff A, Sun PZ: **In vivo magnetic resonance microscopy of brain structure in unanesthetized flies.** *J Magn Reson* 2002, **158**(1-2):79-85.
- Wecker S, Hörschemeyer T, Hoehn M: **Investigation of insect morphology by MRI: assessment of spatial and temporal resolution.** *Magn Reson Imaging* 2002, **20**:105-111.
- Haddad D, Schaupp F, Brandt R, Manz G, Menzel R, Haase A: **NMR imaging of the honeybee brain.** *J Insect Sci* 2004, **4**:7.
- Huetteroth W, Schachtner J: **Standard three-dimensional glomeruli of the *Manduca sexta* antennal lobe: a tool to study both developmental and adult neuronal plasticity.** *Cell Tissue Res* 2005, **319**:513-524.
- Michaelis T, Watanabe T, Natt O, Boretius S, Frahm J, Utz S, Schachtner J: **In vivo 3D MRI of insect brain: cerebral development during metamorphosis of *Manduca sexta*.** *Neuroimage* 2005, **24**:596-602.
- Watanabe T, Schachtner J, Krizan M, Boretius S, Frahm J, Michaelis T: **Manganese-enhanced 3D MRI of established and disrupted synaptic activity in the developing insect brain in vivo.** *J Neurosci Meth* 2006, **158**:50-55.
- Hörschemeyer T, Goebels J, Weidemann G, Faber C, Haase A: **The head morphology of *Ascioplaga mimeta* (Coleoptera: Archostemata) and the phylogeny of Archostemata.** *Eur J Entomol* 2006, **103**:409-423.
- Hart AG, Bowtell RW, Köckenberger W, Wenseleers T, Ratnieks FLW: **Magnetic resonance imaging in entomology: a critical review.** *J Insect Sci* 2003, **3**:5.
- Ziegler A, Angenstein F: **Analyse von Seeiegeln (Echinoidea) mit Hilfe der bildgebenden Magnetresonanztomographie.** *Mikrokosmos* 2007, **96**:49-54.
- Ziegler A, Mueller S, Bartolomeaus T: **Sea urchin (Echinoidea) anatomy revealed by magnetic resonance imaging and 3D visualization.** In *Proceedings of the 12th International Echinoderm Conference* Edited by: Harris LG. Rotterdam: AA Balkema in press.
- Dunn CW, Hejnal A, Matus DQ, Pang K, Browne WE, Smith SA, Seaver E, Rouse GV, Obst M, Edgcombe GD, Sorensen MV, Hadlock SHD, Schmidt-Rhaesa A, Okusu A, Kristensen RM, Wheeler WC, Martindale MQ, Giribet G: **Broad phylogenomic sampling improves resolution of the animal tree of life.** *Nature* 2008, **452**:745-749.
- Littlewood DTJ, Smith AB: **A combined morphological and molecular phylogeny for sea urchins (Echinoidea: Echinodermata).** *Philos Trans R Soc Lond B Biol Sci* 1995, **347**:213-234.
- Smith AB, Pisani D, Mackenzie-Dodds JA, Stockley B, Webster BL, Littlewood DTJ: **Testing the molecular clock: molecular and paleontological estimates of divergence times in the Echinoidea (Echinodermata).** *Mol Biol Evol* 2006, **23**:1832-1851.
- Sea Urchin Genome Sequencing Consortium: **The genome of the sea urchin *Strongylocentrotus purpuratus*.** *Science* 2006, **314**:941-952.
- Ruppert EE, Fox RS, Barnes RD: *Invertebrate Zoology – A Functional Evolutionary Approach* Belmont: Brooks/Cole-Thomson Learning; 2004.

BMC Biology 2008, 6:33

<http://www.biomedcentral.com/1741-7007/6/33>

38. DeRidder C, Jangoux M: **The digestive tract of the spatangoid echinoid *Echinocardium cordatum* (Echinodermata): morpho-functional study.** *Acta Zool* 1993, **74**:337-351.
39. Thorsen MS: **Abundance and biomass of the gut-living microorganisms (bacteria, protozoa and fungi) in the irregular sea urchin *Echinocardium cordatum* (Spatangoida: Echinodermata).** *Mar Biol* 1999, **133**:335-360.
40. Gladfelter VB: **General ecology of the cassiduloid urchin *Cassidulus caribbearum*.** *Mar Biol* 1978, **47**:149-160.
41. Agassiz A: **Revision of the Echini.** In *Illustrated Catalogue of the Museum of Comparative Zoology at Harvard College, No. VII Volume 1872-1874.* Cambridge: Cambridge University Press :1-761.
42. Stewart C: **On certain organs of the Cidaridae.** *Trans Linn Soc - Lond* 1877, **1**:569-572.
43. **The Echinoid Directory** [<http://tinyurl.com/33bn38>]
44. Shapiro MG, Atanasijevic T, Faas H, Westmeyer GG, Jasanoff A: **Dynamic imaging with MRI contrast agents: quantitative considerations.** *Magn Reson Imaging* 2006, **24**:449-462.
45. Buchanan JB, Brown BE, Coombs TL, Pirie BJS, Allen JA: **The accumulation of ferric iron in the guts of some spatangoid echinoderms.** *J Mar Biol Assoc* 1980, **60**:631-640.
46. Seilacher A: **Constructional morphology of sand dollars.** *Paleobiology* 1979, **5**:191-221.
47. Dacosta S, Cunha CM, Simone LRL, Schrödl M: **Computer-based 3-dimensional reconstruction of major organ systems of a new aeolid nudibranch subspecies, *Flabellina engeli licianae* from Brazil (Gastropoda: Opisthobranchia).** *J Mollus Stud* 2007, **73**:339-353.
48. Ruthensteiner B, Lodde E, Schopf S: **Genital system development of *Williamia radiata* (Gastropoda, Siphonariidae).** *Zoomorphology* 2007, **126**:17-29.
49. Yushkevich PA, Piven J, Hazlett HC, Smith RG, Ho S, Gee JC, Gerig G: **User-guided 3D active contour segmentation of anatomical structures: significantly improved efficiency and reliability.** *Neuroimage* 2006, **31**:1116-1128.
50. Vlassenbroeck J, Dierick M, Masschaele B, Cnudde V, Van Hoorebeke L, Jacobs P: **Software tools for quantification of x-ray microtomography at the UGCT.** *Nucl Instrum Meth Phys Res A* 2007, **580**:442-445.
51. **The Digital Morphology Library - *Strongylocentrotus purpuratus*** [<http://tinyurl.com/5x2apf>]
52. **The Digital Morphology Library - *Encope michelini*** [<http://tinyurl.com/4tfgbl>]
53. **The Digital Morphology Library** [<http://www.digimorph.org>]
54. Prouhu H: **Recherches sur le *Dorocidaris papillata* et quelques autres échinides de la Méditerranée.** *Arch Zool Exp Gén* 1887, **5**:213-380.
55. Coe WR: **Echinoderms of Connecticut.** In *State Geological and Natural History Survey Bulletin No. 19* State of Connecticut; 1912.
56. Valentin G: **Anatomie du genre *Echinus*.** In *Monographies d'Echinodermes* Edited by: Agassiz L. Neuchatel; 1841:1-126.
57. Koehler R: **Recherches sur les échinides des côtes de Provence.** *Ann Mus Hist Natur Marseilles Zool* 1883, **1**:1-139.
58. Chadwick HC: ***Echinus*.** In *L.M.B.C. Memoirs* Edited by: Herdman WA. Liverpool: Liverpool Marine Biology Committee; 1900.
59. Strenger A: ***Sphaerechinus granularis* (Violetter Seeigel), Anleitung zur makroskopischen und mikroskopischen Untersuchung.** In *Großes Zoologisches Praktikum, Band 18* Edited by: Siewing R. Stuttgart: Gustav Fischer; 1973:1-68.
60. Campos LS, Moura RB: **Macrostructure and evolution of the echinoid digestive system.** *Zoomorphology* 2008, **127**:135-141.
61. Holland ND, Ghiselin MT: **A comparative study of gut mucous cells in thirty-seven species of the class Echinoidea (Echinodermata).** *Biol Bull* 1970, **138**:286-305.
62. Mooi R: **Paedomorphosis, Aristotle's lantern, and the origin of the sand dollars (Echinodermata: Clypeasteroidea).** *Paleobiology* 1990, **16**:25-48.
63. Smith AB, Stockley B: **Fasciole pathways in spatangoid echinoids: a new source of phylogenetically informative characters.** *Zool J Linn Soc* 2005, **144**:15-35.
64. Klaus AV, Kulasekera VL, Schawaroch V: **Three-dimensional visualization of insect morphology using confocal laser scanning microscopy.** *J Microsc* 2003, **212**:107-121.
65. Klaus AV, Schawaroch V: **Novel methodology utilizing confocal laser scanning microscopy for systematic analysis in athropods (Insecta).** *Integr Comp Biol* 2006, **46**:207-214.
66. Michels J: **Confocal laser scanning microscopy: using cuticular autofluorescence for high resolution morphological imaging in small crustaceans.** *J Microsc* 2007, **227**:1-7.
67. Sutton MD: **Tomographic techniques for the study of exceptionally preserved fossils.** *Proc R Soc Lond B Biol Sci* 2008, **275**:1587-1593.
68. Nickel M, Donath T, Schweikert M, Beckmann F: **Functional morphology of *Tethya* species (Porifera): I. Quantitative 3D-analysis of *Tethya wilhelma* by synchrotron radiation based x-ray microtomography.** *Zoomorphology* 2006, **125**:209-223.
69. Tafforeau P, Boistel R, Boller E, Bravn A, Brunet M, Chaimanee Y, Cloetens P, Feist M, Hozszowska J, Jaeger JJ, Kay RF, Lazzari V, Marivaux L, Nel A, Nemoz C, Thibault X, Vignaud P, Zabler S: **Applications of x-ray synchrotron microtomography for non-destructive 3D studies of paleontological specimens.** *Appl Phys A: Mater* 2006, **83**:195-202.
70. Penney D, Dierick M, Cnudde V, Masschaele B, Vlassenbroeck J, Van Hoorebeke L, Jacobs P: **First fossil Micropholcommatidae (Araneae), imaged in Eocene Paris amber using x-ray computed tomography.** *Zootaxa* 2007, **1623**:47-53.
71. Ruthensteiner B, Hess M: **Embedding 3D models of biological specimens in PDF publications.** *Microsc Res Tech* in press.

Publish with **BioMed Central** and every scientist can read your work free of charge

"BioMed Central will be the most significant development for disseminating the results of biomedical research in our lifetime."

Sir Paul Nurse, Cancer Research UK

Your research papers will be:

- available free of charge to the entire biomedical community
- peer reviewed and published immediately upon acceptance
- cited in PubMed and archived on PubMed Central
- yours — you keep the copyright

Submit your manuscript here:

[http://www.biomedcentral.com/info/publishing\\_adv.asp](http://www.biomedcentral.com/info/publishing_adv.asp)



Table 1 - Scanning parameters for specimens used in this study.

Specimen	Scanning location	Scanning solution	Spatial resolution	Field of view (FOV)	Matrix size in pixel	Echo time (T <sub>E</sub> )	Repetition time (T <sub>R</sub> )	Average number	Scanning time	Figure in this study
<i>Eucidaris metularia</i> (NHM)	Berlin (7 T)	H <sub>2</sub> O dest. + Magnevist	(81 μm) <sup>3</sup>	(3.12 cm) <sup>3</sup>	(384) <sup>3</sup>	6.7 ms	30 ms	12	15 h	2A, 3, 6A-C, 3D model
<i>Caenopedina mirabilis</i> (USNM)	Berlin (7 T)	H <sub>2</sub> O dest. + Magnevist	(81 μm) <sup>3</sup>	(3.12 cm) <sup>3</sup>	(384) <sup>3</sup>	6.7 ms	30 ms	12	15 h	3
<i>Diadema savignyi</i> (Aquarium store)	Würzburg (17.6 T)	Formalin + Magnevist	(40 μm) <sup>3</sup>	1.7x1.7x1.4 cm <sup>3</sup>	420x420x348	2.84 ms	20 ms	22	18 h	3
<i>Salenocidaris</i> (= <i>Salenia hastigera</i> ) (ZMB)	Berlin (7 T)	H <sub>2</sub> O dest. + Magnevist	(81 μm) <sup>3</sup>	(3.12 cm) <sup>3</sup>	(384) <sup>3</sup>	6.7 ms	30 ms	12	15 h	3
<i>Arbacia lixula</i> (= var. <i>africana</i> ) (NHM)	Würzburg (17.6 T)	H <sub>2</sub> O dest. + Magnevist	(44 μm) <sup>3</sup>	1.7x1.5x1.7 cm <sup>3</sup>	384x340x384	2.57 ms	20 ms	36	26 h	3
<i>Stomopneustes variolaris</i> (USNM)	Berlin (7 T)	H <sub>2</sub> O dest. + Magnevist	(81 μm) <sup>3</sup>	(3.12 cm) <sup>3</sup>	(384) <sup>3</sup>	6.7 ms	30 ms	12	15 h	3
<i>Psammechinus militaris</i> (BAH)	Berlin (7 T)	H <sub>2</sub> O dest. + Magnevist	(81 μm) <sup>3</sup>	(3.12 cm) <sup>3</sup>	(384) <sup>3</sup>	6.7 ms	30 ms	12	15 h	1A-E
<i>Psammechinus militaris</i> (ZMB)	Würzburg (17.6 T)	Formalin + Magnevist	(44 μm) <sup>3</sup>	1.7x1.4x1.7 cm <sup>3</sup>	384x320x384	2.97 ms	20 ms	22	15 h	2B
<i>Strongylocentrotus purpuratus</i> (CAS)	Berlin (7 T)	H <sub>2</sub> O dest. + Magnevist	(81 μm) <sup>3</sup>	(3.12 cm) <sup>3</sup>	(384) <sup>3</sup>	6.7 ms	30 ms	12	15 h	1F
<i>Mespilia globulus</i> (ZMB)	Würzburg (17.6 T)	H <sub>2</sub> O dest. + Magnevist	(36 μm) <sup>3</sup>	(1.4 cm) <sup>3</sup>	(384) <sup>3</sup>	2.65 ms	20 ms	40	33 h	3
<i>Echinoneus cyclostomus</i> (NHM)	Berlin (7 T)	H <sub>2</sub> O dest. + Magnevist	(86 μm) <sup>3</sup>	(3.12 cm) <sup>3</sup>	(384) <sup>3</sup>	6.7 ms	30 ms	12	15 h	2C, 4, 5A
<i>Echinolampas depressa</i> (USNM)	Berlin (7 T)	H <sub>2</sub> O dest. + Magnevist	(81 μm) <sup>3</sup>	(3.12 cm) <sup>3</sup>	(384) <sup>3</sup>	6.7 ms	30 ms	12	15 h	4, 5B
<i>Echinocyamus pusillus</i> (BAH)	Würzburg (17.6 T)	Formalin + Magnevist	20x18x18 μm <sup>3</sup>	5.0x4.5x4.5mm <sup>3</sup>	(256) <sup>3</sup>	3.27 ms	20 ms	32	12 h	2D, 4
<i>Pourtalesia wandeli</i> (NHM)	Berlin (7 T)	H <sub>2</sub> O dest. + Magnevist <sup>®</sup>	(86 μm) <sup>3</sup>	(3.3 cm) <sup>3</sup>	(384) <sup>3</sup>	6.7 ms	30 ms	12	15 h	4, 5C
<i>Abatus</i> (= <i>Hemiaster</i> ) <i>cavernosus</i> (ZMB)	Berlin (7 T)	H <sub>2</sub> O dest. + Magnevist	(81 μm) <sup>3</sup>	(3.12 cm) <sup>3</sup>	(384) <sup>3</sup>	6.7 ms	30 ms	12	15 h	4, 5D

Table 2 - List of specimens used in this study.

Specimen	Specimen ID	Source	Locality	Year collected	Collected by	Identified by	Diameter without spines	Figure in this study
<i>Eucidaris metularia</i> (Lamarck, 1816)	1969.5.1.15-40	NHM	Aldabra, Indian Ocean	1969	J.D. Taylor	Unknown	2.0 cm	2A, 3, 6A-C, 3D model
<i>Caenopedina mirabilis</i> (Döderlein, 1885)	31182	USNM	Kii Strait, Pacific Ocean	1906	Northwestern Pacific Expedition	H.L. Clark	1.5 cm	3
<i>Diadema savignyi</i> Michelin, 1845	n/a, one specimen	Aquarium store	Red Sea, Indian Ocean	2006	Seewasser Center Berlin	A. Ziegler	1.9 cm	3
<i>Salenocidaris</i> (= <i>Salenia</i> ) <i>hastigera</i> (Agassiz, 1869)	5816	ZMB	Maldives, Indian Ocean	1898	Valdivia Expedition	Unknown	1.5 cm	3
<i>Arbacia lixula</i> (= var. <i>africana</i> ) (Linnaeus, 1758)	1952.3.26.31-36	NHM	Ghana, Atlantic Ocean	1949	R. Bassindale	Unknown	1.8 cm	3
<i>Stomopneustes variolaris</i> (Lamarck, 1816)	E45930	USNM	Greater Sunda Islands, Indian Ocean	1963	L. Kelts	C. Ahearn	2.2 cm	3
<i>Psammechinus miliaris</i> (Müller, 1771)	n/a, several specimens	BAH	Helgoland, North Sea	2006	BAH	BAH	1.5-2.5 cm	1A-E, 2B
<i>Psammechinus miliaris</i> (Müller, 1771)	2011	ZMB	Arendal, Baltic Sea	1872	Pommerania Expedition	Unknown	1.7 cm	1F
<i>Strongylocentrotus purpuratus</i> (Stimpson, 1857)	5724	CAS	Morro Bay, Pacific Ocean	1972	J.T. Carlton et al.	J.T. Carlton et al.	2.3 cm	3
<i>Mespilia globulus</i> (Linnaeus, 1758)	5620	ZMB	Madang, Pacific Ocean	1909	S. Schöde	Unknown	1.3 cm	3
<i>Echinoneus cyclostomus</i> Leske, 1778	1969.5.1.105	NHM	Aldabra, Indian Ocean	1969	J.D. Taylor	Unknown	Length: 3.4 cm	2C, 4, 5A
<i>Echinolampas depressa</i> Gray, 1851	E32955	USNM	Florida, Gulf of Mexico	1981	Continental Shelf Associates	Continental Shelf Associates	Length: 2.8 cm	4, 5B
<i>Echinocyamus pusillus</i> (Müller, 1776)	n/a, one specimen	BAH	Helgoland, North Sea	2006	BAH	BAH	Length: 5.0 mm	2D, 4
<i>Pourtalesia wandeli</i> Mortensen, 1905	1976.7.30.76-95	NHM	300 mls S of Iceland, Atlantic Ocean	1976	Discovery Expedition	Unknown	Length: 3.3 cm	4, 5C
<i>Abatus</i> (= <i>Hemiaster</i> ) <i>cavernosus</i> (Philippi, 1845)	5854	ZMB	Kerguelen, Indian Ocean	1898	Valdivia Expedition	Unknown	Length: 2.8 cm	4, 5D

## 5. Sea Urchin Models on the Internet

### 5.1. Summary

The MRI and  $\mu$ CT datasets gathered during the previous experiments were scrutinized for resolution and visual quality and only particularly representative species were selected for publication on the Internet. 3D models based on the MRI datasets as well as selected tomographic slices were published in collaboration with Dr. Andrew B. Smith on The Echinoid Directory, an award-winning website of the Natural History Museum, London. The  $\mu$ CT datasets were processed by Dr. Louis G. Zachos, a palaeontologist at the University of Texas at Austin. Based on these datasets, volume rendering models as well as movies of various views of the whole datasets were produced and made publicly accessible on The Digital Morphology Library, an award-winning Internet-based project aimed at providing the scientific and non-scientific communities with 3D models of fossil and extant biological specimens. The additional 3D models shown in Chapter 8 will be added to The Echinoid Directory in the course of the next months.

### 5.2. Publication

Ziegler A, Faber C, Mueller S (2008): 3D visualization of sea urchin anatomy. In: Smith AB, ed. The Echinoid Directory. Internet publication. <http://www.nhm.ac.uk/research-curation/research/projects/echinoid-directory/index.html>

Pages 44-52

### 5.3. Publication

Ziegler A, Zachos LG (2008): *Echinoneus cyclostomus*, *Mespilia globulus*, *Moira atropos* & *Psammechinus miliaris*. In: Rowe T, ed. The Digital Morphology Library. Internet publication. <http://www.digimorph.org/index.phtml>

Pages 53-55



## Welcome to THE ECHINOID DIRECTORY

Designed and created by  
Dr. Andrew B. Smith, The Natural History Museum, London



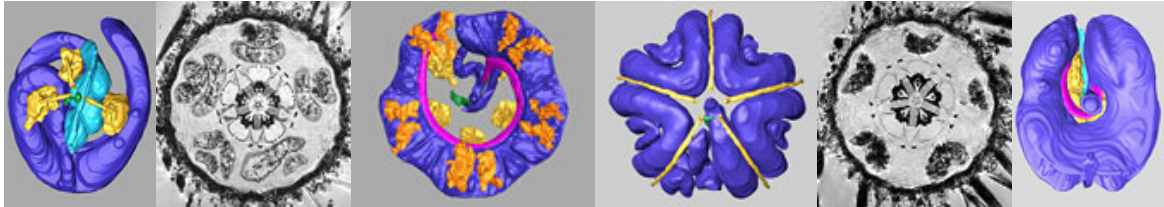
<b>About this site</b>	Scope and aims - how to get the most out of your visit to this site Update of changes (check here for new postings)
<b>Introduction</b>	Sea urchins - what they are, how they live and a brief history of the group
<b>Morphology and morphological terms</b>	An introductory guide to the morphology and terminology used in describing echinoids
<b>Key to the families and genera</b>	An illustrated key that helps you identify echinoids to generic level, and gives more detailed information about the families and orders
<b>Classification</b>	A hierarchical listing of all genera and higher taxa used on this site
<b>3D models of soft tissue anatomy</b>	Images and three-dimensional models of echinoid soft tissue anatomy created by Alexander Ziegler
<b>Index to taxa</b>	Searchable, alphabetic listing of all taxonomic groups to genus level to take you straight to detailed information on that group
	<b>How to cite this site</b>



### 3D visualization of sea urchin anatomy

created by Alexander Ziegler, Institut für Biologie, Freie Universität Berlin, Germany  
In cooperation with:

Cornelius Faber, Experimentelle Physik V, Universität Würzburg, Germany  
Susanne Mueller, Berlin NeuroImaging Center, Charité-Universitätsmedizin, Germany  
Contact: alexander\_ziegler@gmx.net



#### Background

This project systematically visualizes the internal (and external) anatomy of selected sea urchin specimens representing 13 of the 14 currently recognized sea urchin orders. The only specimens that successfully resisted scanning were members of the order Echinothuroidea (or leather urchins). Their flexible endoskeleton and powerful longitudinal muscles result in a pancake shape after fixation.

#### Image pages

Click here to go to an [index of image pages](#) → **Page 47**

#### How to view the 3D images

In order to use the full 3D capability of the models found on our species pages, please download and install the latest Adobe Acrobat Reader ([link below](#)). Once the Reader is installed, open the file and click onto the image to initiate the 3D viewer. Please refer to the Reader Help section for all information regarding handling and manipulation of the 3D models.

#### How the images were created

The technique that was predominantly used in this study is called magnetic resonance imaging (MRI) - for an explanation of the principle behind MRI and further applications please refer to the MRI section of [Wikipedia](#). The freshly fixed and museum sea urchin specimens were put into plastic or glass tubes filled with distilled water or formalin that were then placed inside the coil of the MRI machine. The instruments used in this study are all high-field MRI instruments with 7 T and 17.6 T magnets. For an in-depth explanation regarding all technical parameters of this study please refer to the article by Ziegler et al. (2008). **Page 46**

After the process of image acquisition, the virtual sections were transformed into 3D models using a process called segmentation. Click [here](#) for a demonstration of how a model is generated by segmenting each slice. In most cases, interpolation of structures (e.g. gonads) across several slices allowed for a faster segmentation - however, in some cases each organ had to be manually segmented slice by slice.

#### References and links

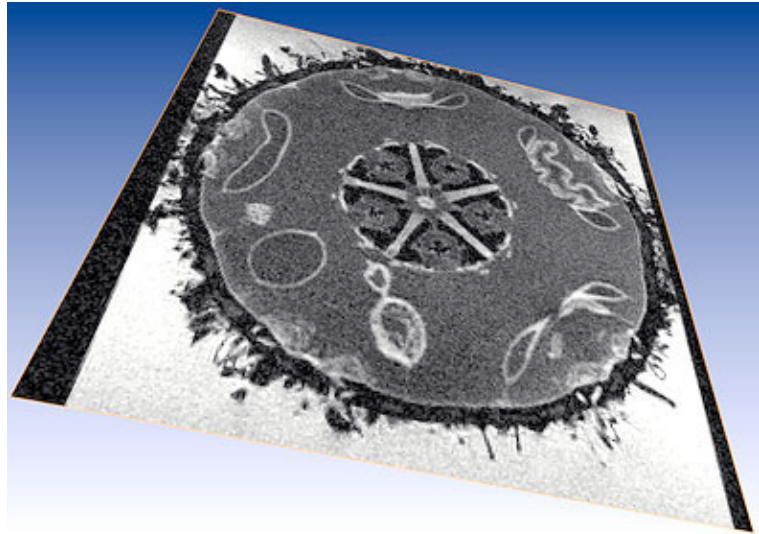
Ziegler, A., Faber, C., Mueller, S. & Bartolomaeus, T. 2008. Systematic comparison and reconstruction of sea urchin (Echinoidea) internal anatomy: a novel approach using magnetic resonance imaging. *BMC Biology* 6:33.

[Adobe Acrobat Reader](#) - get the latest reader to view our 3D models.  
[www.adobe.com/products/acrobat/readstep2.html](http://www.adobe.com/products/acrobat/readstep2.html)

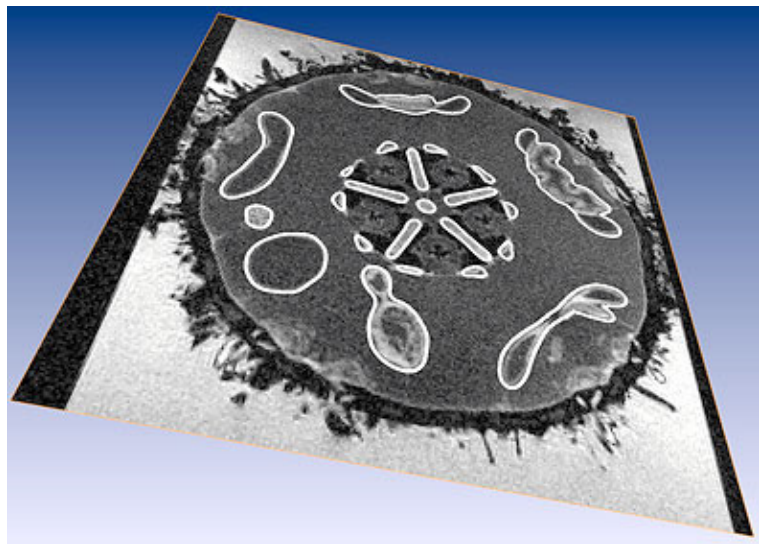


**3D visualization of sea urchin anatomy: creating the 3D models**

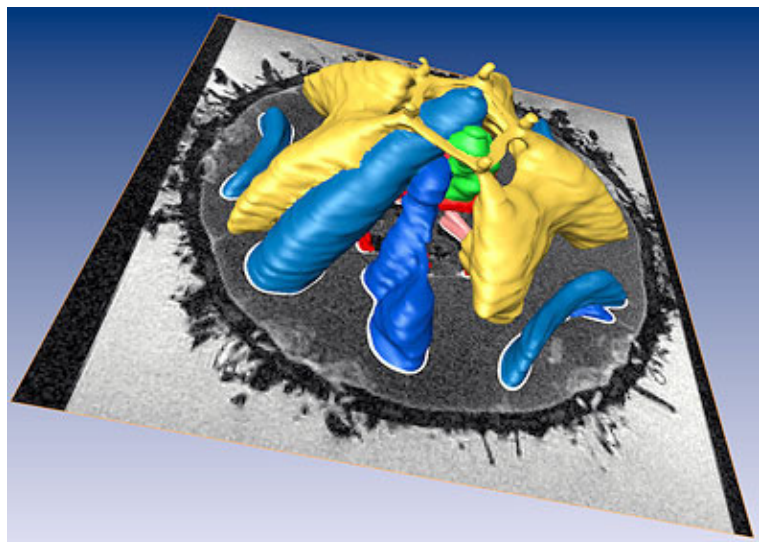
Raw MRI image slice



Organs outlined on slice

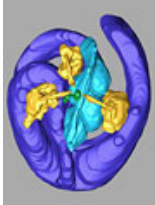

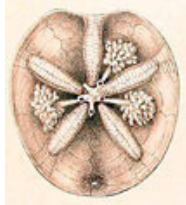
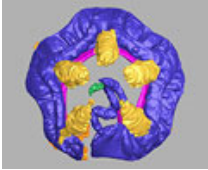
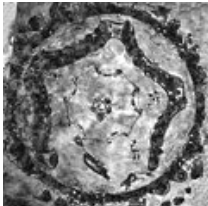
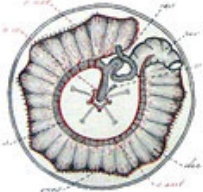

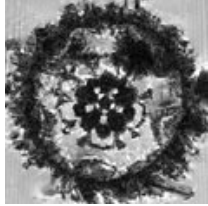

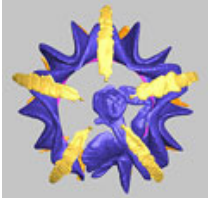
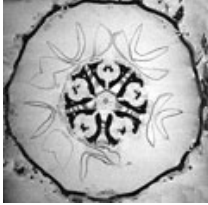

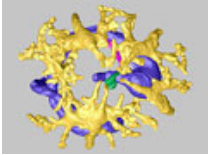



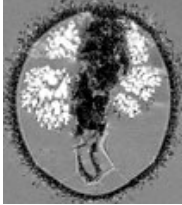



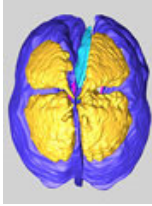
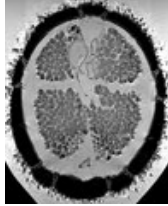
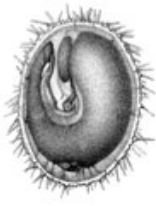
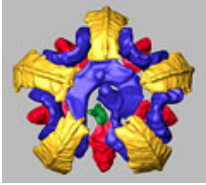


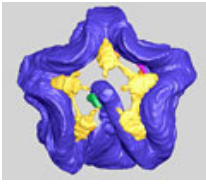


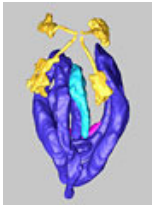


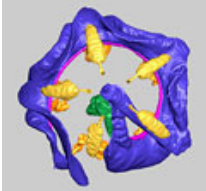

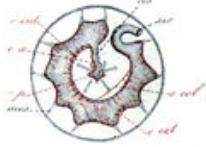
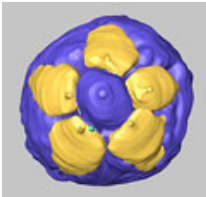
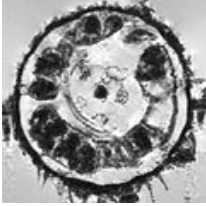
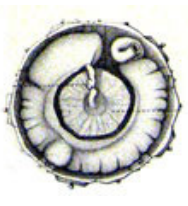
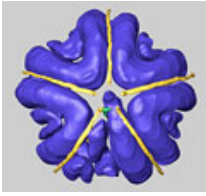


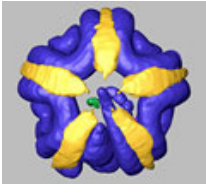


Organs assigned colour and followed through stack of images



### 3D visualization of sea urchin anatomy: index

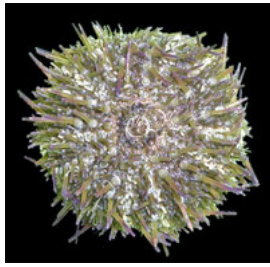
Click on a **NAME** to take you to the **introductory page** with links to the 3D interactive model and to images of internal anatomy taken from the literature, MRI image slices, and static views from the 3D model. Alternately click on any **image** to go direct to the relevant section.

Taxon	3D model (interactive)	3D model (static)	MRI images	Classical anatomy
<b><i>Abatus</i></b> (Spatangoida)	<a href="#">PDF (3.2 Mb)</a>			
<b><i>Arbacia</i></b> (Arbacioida)	<a href="#">PDF (3.9 Mb)</a>			
<b><i>Caenopedina</i></b> (Pedinoida)	<a href="#">PDF (7.0 Mb)</a>			
<b><i>Diadema</i></b> (Diadematoidea)	<a href="#">PDF (8.5 Mb)</a>			
<b><i>Echinocyamus</i></b> (Clypeasteroidea)	<a href="#">PDF (7.8 Mb)</a>			
<b><i>Echinolampas</i></b> (Cassiduloidea)	<a href="#">PDF (6.6 Mb)</a>			

<p><i>Echinoneus</i> (Echinoneioida)</p>	<p><a href="#">PDF (6.7 Mb)</a></p>			
<p><i>Eucidaris</i> (Cidaroida)</p>	<p><a href="#">PDF (8.0 Mb)</a></p>			
<p><i>Mespilia</i> (Temnopleuroida)</p>	<p><a href="#">PDF (8.2 Mb)</a></p>			
<p><i>Pourtalesia</i> (Holasteroida)</p>	<p><a href="#">PDF (6.7 Mb)</a></p>			
<p><b>Psammechinus</b> (Echinoidea)</p>	<p><a href="#">PDF (9.3 Mb)</a></p>			
<p><i>Salenocidaris</i> (Salenioida)</p>	<p><a href="#">PDF (6.7 Mb)</a></p>			
<p><i>Stomopneustes</i></p>	<p><a href="#">PDF (8.9 Mb)</a></p>			
<p><i>Strongylocentrotus</i> (Echinoidea)</p>	<p><a href="#">PDF (7.6 Mb)</a></p>			

Page 49

### *Psammechinus miliaris* (Müller, 1771)



- Common name: English - Shore urchin, Green sea urchin, German - Strand-Seeigel, French - Oursin grimpeur, Oursin des rochers, Petit oursin vert
- Systematics: Parechinidae, Echinoida
- Distribution: Atlantic Ocean
- Diet: Omnivorous, drift algae, encrusting organisms
- Feeding type: Grazer
- Habitat: On sand, gravel, and rocks
- Depth range: Littoral - 100 m
- Maximum test size: 50 mm
- Behaviour: Epifaunal

#### 3D model (interactive)

- [Model](#)

#### 3D model (static)

- [Aboral, lateral and oral views](#) → **Page 50**

#### MRI pictures

- [MRI image slices](#) → **Page 51**

#### Illustrations from literature

- [Internal anatomy](#) taken from Bonnet (1925) → **Page 52**

#### More images

- <http://www.nhm.ac.uk/research-curation/projects/echinoid-directory/taxa/taxon.jsp?id=984>

#### Technical information

- Specimen ID: -
- Expedition: freshly fixed specimen collected by Biologische Anstalt Helgoland (BAH)
- Collected in: 2006, near Helgoland island, North Sea
- Collected by: BAH
- Identified by: BAH
- Specimen test size: 1.7 cm
- Scanning location: Würzburg 17.6T
- Scanning solution: Formalin + Magnevist
- MRI dataset resolution: (44  $\mu\text{m}$ )<sup>3</sup>

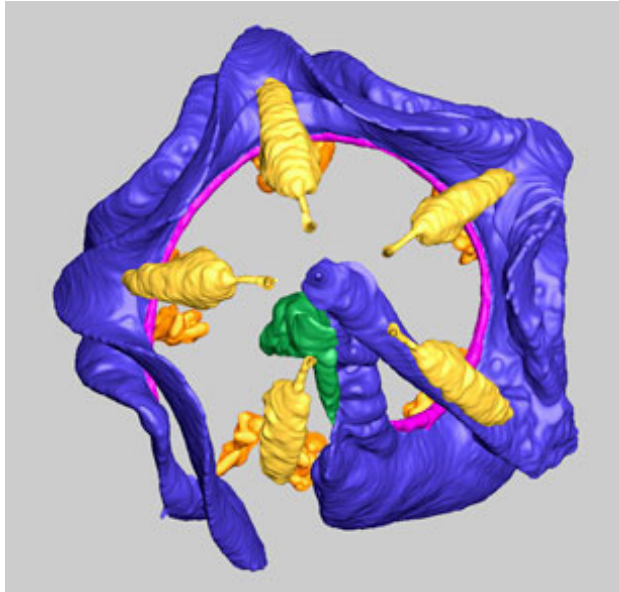
#### Literature cited

- Bonnet, A. 1925. Recherches sur l'appareil digestif et absorbent de quelques échinides réguliers. *Annales de l'Institut Océanographique* 2(2).

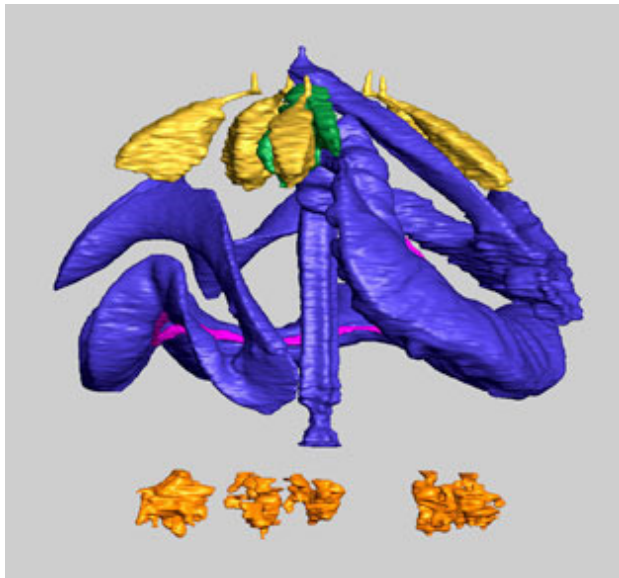
***Psammechinus miliaris* (Müller, 1771): 3D model (static)****Key to colours**

- Dark blue - digestive tract
- Light blue - caecum
- Green - axial complex
- Yellow - gonads
- Pink - siphon
- Dark red - Stewart's organs
- Orange - buccal sacs

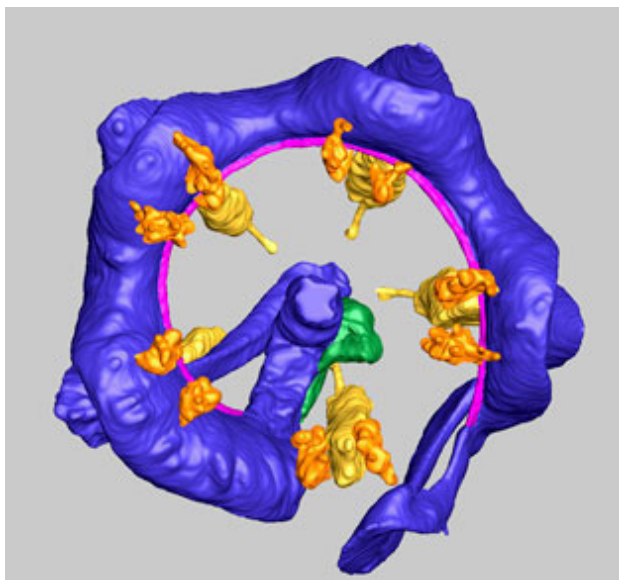
Aboral view



Lateral view

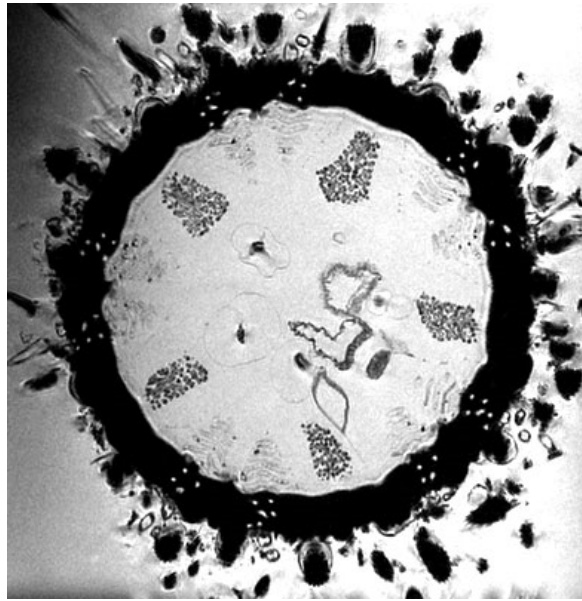


Oral view

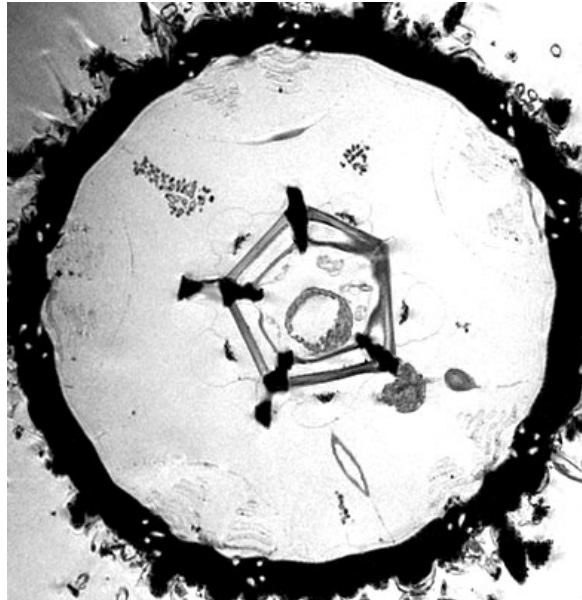


***Psammechinus miliaris* (Müller, 1771): MRI images**

Gonads & rectum, aboral view

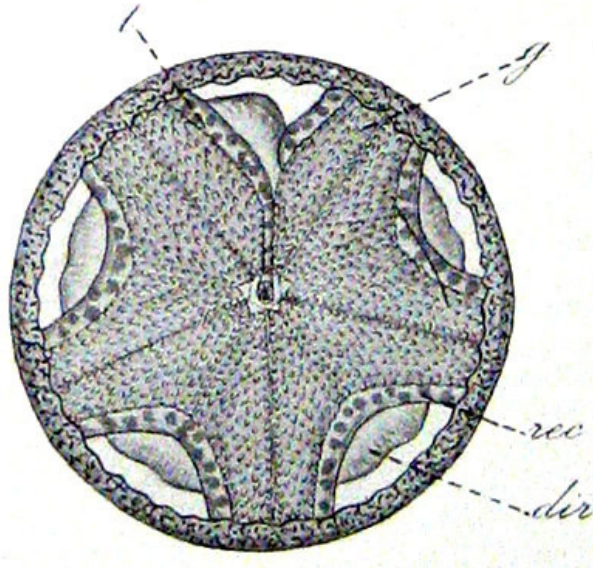


Oesophagus, gonads & Aristotle's lantern, aboral view

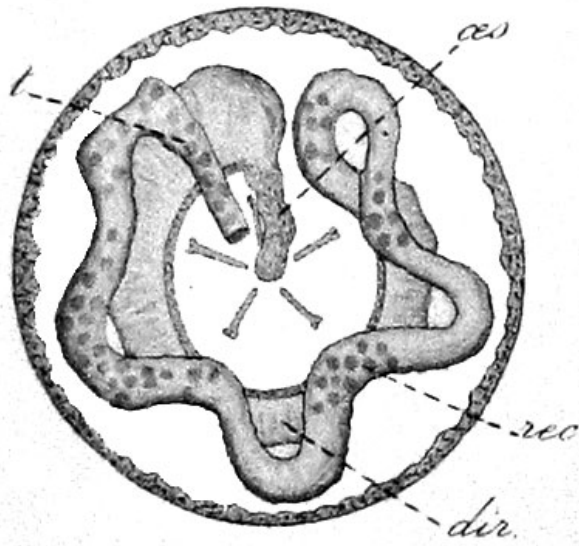


Stomach & Aristotle's lantern, aboral view

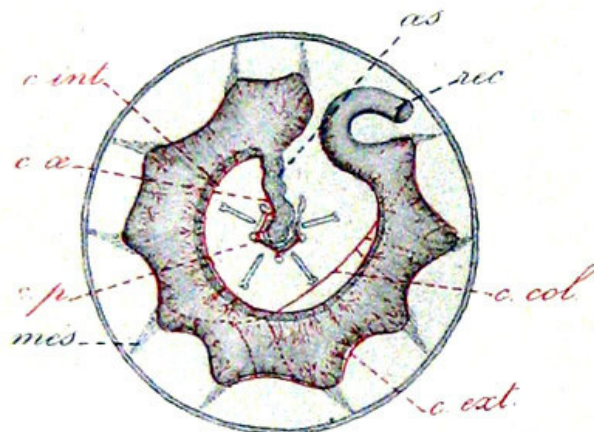


***Psammechinus miliaris* (Müller, 1771)**

Gonads & intestine, aboral view, from Bonnet, A. 1925. Recherches sur l'appareil digestif et absorbent de quelques échinides réguliers. *Annales de l'Institut Oceanographique* 2(2).



Intestine & stomach, aboral view, from Bonnet, A. 1925. Recherches sur l'appareil digestif et absorbent de quelques échinides réguliers. *Annales de l'Institut Oceanographique* 2(2).



Stomach & siphon, aboral view, from Bonnet, A. 1925. Recherches sur l'appareil digestif et absorbent de quelques échinides réguliers. *Annales de l'Institut Oceanographique* 2(2).

# DIGITAL MORPHOLOGY

A National Science Foundation Digital Library at The University of Texas at Austin


## DigiMorph

- [Home](#)
- [About DigiMorph](#)
- [DigiMorph Help](#)
- [Sponsors](#)
- [Links](#)
- [Recent Publications](#)
- [DigiMorph People](#)

## Browse the Library by:

- [Scientific Names](#)
- [Common Names](#)
- [Cladogram](#)
- [What's New?](#)
- [What's Popular?](#)

## Learn More

- [DigiMorph Course](#)
- [X-ray CT](#)
- [3-D Printing](#)

## Overview Pages

- [Dinosaurs](#)
- [Tapirs](#)
- [Horned Lizards](#) \*
- [Endocasts](#)
- [Bats](#)
- [Primates](#)

## A Production of

- [UTCT](#)
- [UT Geosciences](#)
- [CIT](#)
- [TMM](#)
- [DigiMorph Contributors](#)

\* Expert annotation

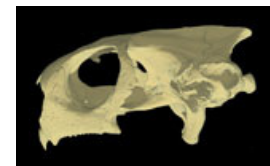
The **Digital Morphology** library is a dynamic archive of information on digital morphology and [high-resolution X-ray computed tomography](#) of biological specimens. Browse through the site and see spectacular imagery and animations and details on the morphology of many representatives of the Earth's biota. **Recent additions or updates to the site include:**



### *Agrionemys horsfieldii*, Russian Tortoise

15-Sep-2008

The Russian tortoise is a member of Testudinidae, a large and diverse clade of extinct and extant terrestrial forms that includes well-known giant species such as the Galápagos and Aldabra tortoises. *Agrionemys horsfieldii* occurs in Pakistan, Iran, and Afghanistan, extending into western China and southeastern Russia. Learn more about the Russian tortoise by reading this account by Dr. Heather Jamniczky of the University of Calgary. [\[more...\]](#)



### Metatherian Mammal, *Herpetotherium cf. fugax*

02-Sep-2008

*Herpetotherium cf. fugax* is a metatherian ('marsupial') from the Oligocene of North America. The recent discovery of well preserved specimens in the Early Oligocene White River Formation of Wyoming has allowed a better understanding of its morphology, phylogenetic position, and locomotor adaptations. Learn more about these remarkably complete fossils, recently described by Horovitz and coauthors in *Palaeontographica Abteilung*. [\[more...\]](#)

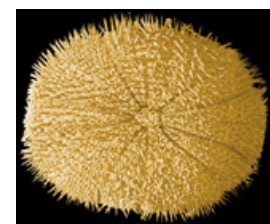


Page 54

### *Echinoneus cyclostomus*, Little Burrowing Urchin

18-Aug-2008

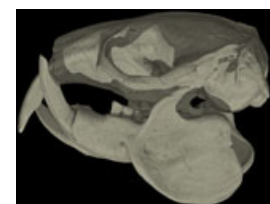
The little burrowing urchin, *Echinoneus cyclostomus*, occurs worldwide throughout the tropics. While it inhabits depths up to 570 m, it is most common in shallow waters. Adult individuals of this species and others in Echinoneidae do not possess a lantern or teeth -- these structures are absorbed during maturation. Learn more about the little burrowing urchin by reading this new account by Mr. Louis Zachos of The University of Texas at Austin. [\[more...\]](#)



### Naked Mole-rat, *Heterocephalus glaber*

04-Aug-2008

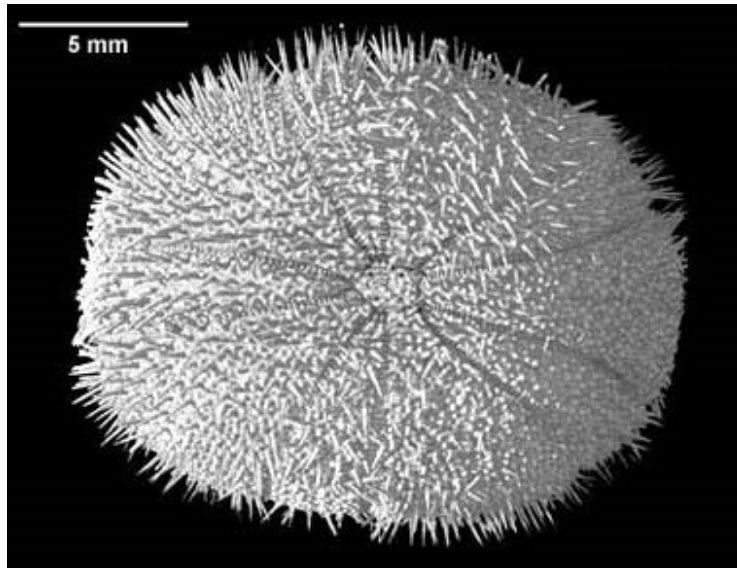
The naked mole-rat, a fossorial rodent endemic to the arid regions of eastern Africa, is a remarkable creature. Although it is a mammal, it lacks the ability to regulate its internal body temperature. It is one of only two mammals to exhibit an advanced social structure called eusociality. And it is the longest-lived rodent species, with individuals living as long as 28 years in captivity. These bizarre attributes have garnered much scientific attention for *Heterocephalus glaber*. Learn more by reading the new DigiMorph account by Nicholas Smith of The University of Texas at Austin. [\[more...\]](#)





## ***Echinoneus cyclostomus*, Little Burrowing Urchin**

[Alexander Ziegler](#) - Freie Universitaet Berlin  
 Louis Zachos, The University of Texas at Austin



Natural History Museum, London (NHM 1969.5.1-105)

Applet, Slices & 3D Models	3D Volume Rendered Movies
----------------------------	---------------------------

- |  |  |
|--|--|
| <p>Java Slice Viewer<br/> <a href="#">inspeCTor</a><br/>                 Slice Movies<br/> <a href="#">Coronal - 4mb</a><br/> <a href="#">Horizontal - 3mb</a><br/> <a href="#">Sagittal - 3mb</a><br/>                 Surface Models<br/>                 STL - n/a<br/>                 3D CT - n/a</p> | <p>Skeleton Only<br/> <a href="#">Roll - 3mb</a><br/> <a href="#">Pitch - 3mb</a><br/> <a href="#">Yaw - 3mb</a><br/>                 With Skin/Matrix<br/>                 Roll - n/a<br/>                 Pitch - n/a<br/>                 Yaw - n/a<br/>                 Dynamic Cutaway<br/> <a href="#">Coronal - 2mb</a><br/> <a href="#">Horizontal - 2mb</a><br/>                 Sagittal - n/a</p> |
|--|--|



**Page 55**

Image processing: [Mr. Louis Zachos](#)  
 Publication Date: 18 August 2008

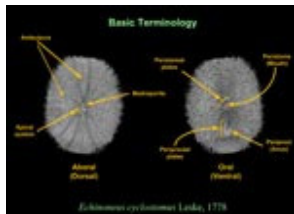
[ITIS](#) [TNS](#) [Google](#) [MSN](#)

<b>About the Species</b>	<b>About this Specimen</b>	<b>About the Scan</b>	<b>Literature &amp; Links</b>	<b>Additional Imagery</b>
--------------------------	----------------------------	-----------------------	-------------------------------	---------------------------

*Echinoneus cyclostomus*, also called the little burrowing urchin or round-mouth bean urchin, is a rather small "irregular" sea urchin. Its spines are short and range from whitish to light brown in color. The tube feet are conspicuously red, and can be found in narrow bands in the ambulacra. The color of the test is white to light brown. The mouth is ovoidal and located in the center of the oral surface of the test. A large anus can be found just posterior to the mouth. *Echinoneus cyclostomus* ingests organic material that adheres to coarse sand and shell fragments. Adult individuals of this species and others in the family Echinoneidae do not possess a lantern or teeth - these structures are absorbed during maturation.



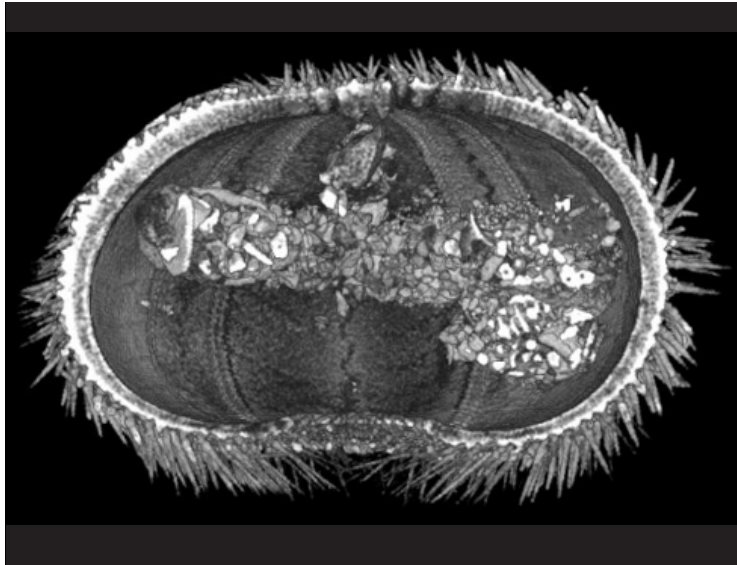
The little burrowing urchin occurs worldwide throughout the tropics. It inhabits waters 5-570 m in depth, but is most common at shallow depths. *Echinoneus cyclostomus* can be found under rock slabs or pieces of coral rubble, living in or on coarse sand. The urchin is never exposed; it may burrow or cling to undersurfaces of rock slabs. It is generally sedentary and moves very slowly even when disturbed.




Click on the thumbnail to the left for an [illustration](#) of the basic morphology of *Echinoneus*.

## Echinoneus cyclostomus, Little Burrowing Urchin

[Alexander Ziegler](#) - Freie Universitaet Berlin  
 Louis Zachos, The University of Texas at Austin



Applet, Slices & 3D Models	3D Volume Rendered Movies
Java Slice Viewer	Skeleton Only
inspeCTor	Roll - 3mb
Slice Movies	Pitch - 3mb
Coronal - 4mb	Yaw - 3mb
Horizontal - 3mb	With Skin/Matrix
Sagittal - 3mb	Roll - n/a
Surface Models	Pitch - n/a
STL - n/a	Yaw - n/a
3D CT - n/a	Dynamic Cutaway
	Coronal - 2mb
	Horizontal - 2mb
	Sagittal - n/a

Natural History Museum, London (NHM 1969.5.1-105)

[ITIS](#) [TNS](#) [Google](#) [MSN](#)

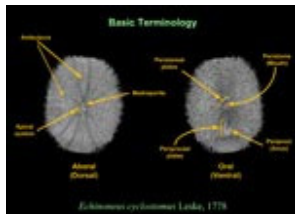
Image processing: [Mr. Louis Zachos](#)  
 Publication Date: 18 August 2008

<b>About the Species</b>	<b>About this Specimen</b>	<b>About the Scan</b>	<b>Literature &amp; Links</b>	<b>Additional Imagery</b>
--------------------------	----------------------------	-----------------------	-------------------------------	---------------------------

*Echinoneus cyclostomus*, also called the little burrowing urchin or round-mouth bean urchin, is a rather small "irregular" sea urchin. Its spines are short and range from whitish to light brown in color. The tube feet are conspicuously red, and can be found in narrow bands in the ambulacra. The color of the test is white to light brown. The mouth is ovoidal and located in the center of the oral surface of the test. A large anus can be found just posterior to the mouth. *Echinoneus cyclostomus* ingests organic material that adheres to coarse sand and shell fragments. Adult individuals of this species and others in the family Echinoneidae do not possess a lantern or teeth - these structures are absorbed during maturation.



The little burrowing urchin occurs worldwide throughout the tropics. It inhabits waters 5-570 m in depth, but is most common at shallow depths. *Echinoneus cyclostomus* can be found under rock slabs or pieces of coral rubble, living in or on coarse sand. The urchin is never exposed; it may burrow or cling to undersurfaces of rock slabs. It is generally sedentary and moves very slowly even when disturbed.



Click on the thumbnail to the left for an [illustration](#) of the basic morphology of *Echinoneus*.

## 6. Embedding 3D Models into PDF-based Publications

### 6.1. Summary

During the production of the 3D models it became apparent that the added information content of three-dimensional structures would be impossible to communicate through two-dimensional publications alone. One way to improve this situation was to include 3D models as well as movies based on rotating models into Internet publications (Chapter 5) and refer to these websites in the article itself. However, once the website would be taken off the Web, the information would be lost to the public. Another approach, already practised during the production of the article in BMC Biology (Chapter 4), was to actually include the 3D model into the article itself. This approach has recently become possible due to the newly developed PDF 1.6 format that permits to include surface-rendered 3D models into PDF publications. The models are embedded into the PDF version of the article and a download of the paper allows the reader to keep the data permanently on the computer. Therefore, the necessity to access the Internet and search for the appropriate supplementary material becomes superfluous. The implications of this new approach for the entire scientific community are obvious and the experience acquired during the development of the sea urchin models was employed to create an exemplary 3D model based on a publicly accessible dataset of a protein structure.

### 6.2. Publication

Murienne J, Ziegler A, Ruthensteiner B (2008): A 3D revolution in communicating science. *Nature* 453: 450

Page 57

### 6.3. Publication

Kumar P\*, Ziegler A\*, Ziegler J, Uchańska-Ziegler B, Ziegler A (2008): Grasping molecular structures through publication-integrated 3D models. *Trends in Biochemical Sciences* 33: 408-412 (\* Joint first authors)

Pages 58-62

The cover page of the September 2008 issue of *Trends in Biochemical Sciences* (TiBS) as well as an Editorial by Dr. Jonathan Tyzack (TiBS 33: 405-407) refer to the article by Kumar et al. (2008) and stress the many opportunities and challenges offered by the approach of integrating 3D models into PDF publications.

or spare time (*sic*) of researchers to mobilize data into the public domain.

One proposal discussed recently (<http://tinyurl.com/6elpq4>) concerned the building of a realistic measure for use of database elements and a 'cite me' button for a dynamic composite web page. The Global Biodiversity Information Facility (GBIF, [www.gbif.org](http://www.gbif.org)) is investigating the assignment of 'life-science identifiers' to allow accreditation not only to data sets, but also to the individual datum and its author. Simplified mechanisms are needed that make it easy for individuals to assign these identifiers to their data.

We believe that scientists' productivity also needs to be gauged through data publishing, which requires a culture change in the recognition of scientific output. An industry-standard identifier, such as that proposed by the GBIF, could be part of publishers' referencing systems, and authors could provide 'citation identifiers' for all data records and data sets. Such a mechanism would achieve increased data mobilization and increased accreditation, both desirable to scientists.

**Dave Roberts** The Natural History Museum, Cromwell Road, London SW7 5BD, UK

**Vishwas Chavan** GBIF Secretariat, Universitetsparken 15, DK-2100 Copenhagen, Denmark

## Name variations can hit citation rankings

SIR — The Correspondence 'Give south Indian authors their true names' (*Nature* 452, 530; 2008) and earlier News Feature 'Identity crisis' (*Nature* 451, 766–767; 2008) are highly relevant to calculations of PubMed citations and h-index (the number  $n$  of a researcher's papers that have received at least  $n$  citations).

For example, I used to use the south Indian form of my name:

T. Biji Kurien, with Biji being my personal name. I have seven publications cited incorrectly in PubMed as being by 'Kurien, T. B.', 'Bijikurien, T.' or 'Kurien, B.'. Four of these entries were cited often enough to be counted towards my h-index computation. As I had by then changed my name to conform with Western style, these publications unfortunately do not appear in the Web of Science or PubMed under my current name format. Consequently, my h-index ranking has fallen by 25%.

It is of paramount importance to adhere to a consistent name pattern right from the start, in order to maintain a correct list of publications in the public databases as well as the right h-index rankings.

**Biji T. Kurien** Arthritis and Immunology, Oklahoma Medical Research Foundation, 825 NE 13th Street, Oklahoma City, Oklahoma 73104, USA

## Names: dropped to avoid prejudice, now useful again

SIR — The Correspondence 'Give south Indian authors their true names' (*Nature* 452, 530; 2008), incorrectly states that people from the south do not traditionally have surnames.

I am from southern India and have a proper surname — as do all the families in my region. Besides Patil, surnames such as Naidu, Reddy, Rao and Gouda are common in the different states of southern India. One of the authors of the Correspondence has the surname Kuttly.

Surnames have widely fallen into disuse because our fathers and forefathers avoided using them to prevent discrimination on grounds of caste.

It doesn't make sense in this case to use only an author's first name in scientific publications and to devise a special system to accommodate a different naming format. Instead, editors should

encourage these authors to revive the use of their surnames.

**Prabhu B. Patil** E307, Centre for Cellular and Molecular Biology, Hyderabad 500007, India

*Readers are welcome to comment at the Nature India blog Indigenus, <http://tinyurl.com/58r9wf>*

## Open-access more harm than good in developing world

SIR — The traditional 'publish for free and pay to read' business model adopted by publishers of academic journals can lead to disparity in access to scholarly literature, exacerbated by rising journal costs and shrinking library budgets. However, although the 'pay to publish and read for free' business model of open-access publishing has helped to create a level playing field for readers, it does more harm than good in the developing world.

Authors by no means have a level playing field, even in the traditional publishing model. The dynamics of peer review make it hard to ensure that publication of an article is a function of only its quality, uninfluenced by factors such as topicality or the author's name and affiliation. The open-access model makes the playing field for authors even more uneven.

Page charges may be waived for authors who cannot afford to pay, but a model that depends on payment by authors can afford only a few such waivers. And why should anyone want to survive on charity? The argument that it is the granting agency and not the author that pays does not wash either. If anything, the playing field for grants is even more uneven. Besides, this will undermine, rather than encourage, the whole area of grant-free research.

Page charges make extra difficulties for authors, while the old problems associated with peer review persist. They could be disastrous for the underdeveloped

world, encouraging people to remain as consumers (readers), rather than to become producers (authors) of knowledge.

A 'publish for free, read for free' model may one day prove to be viable. Meanwhile, if I have to choose between the two evils, I prefer the 'publish for free and pay to read' model over the 'pay to publish and read for free' one. Because if I must choose between publishing or reading, I would choose to publish. Who would not?

**Raghavendra Gadagkar** Centre for Ecological Sciences, Indian Institute of Science, Bangalore 560012, India

## A 3D revolution in communicating science

SIR — Since the release of Adobe Systems' Portable Document Format (PDF) version 1.6 in 2004, it has become possible to view interactively three-dimensional models that are embedded into PDF files. This attribute will dramatically increase information content as well as data transparency in scientific papers. Additionally, replacing multiple two-dimensional figures of a three-dimensional structure with one integrated interactive three-dimensional model will reduce the need for supplementary material.

The potential of this technological advance for all science is obvious. Because of the foreseeable rise in demand by the scientific community, publishers and scientific institutions need to work hand in hand to support the implementation of this highly desirable technique.

**Jérôme Murielle** UMR 5202, Département Systématique et Evolution, case 50, Muséum national d'Histoire naturelle, 45 rue Buffon, 75005 Paris, France  
**Alexander Ziegler** Institut für Biologie, Freie Universität Berlin, Königin-Luise-Straße 1-3, 14195 Berlin, Germany  
**Bernhard Ruthensteiner** Zoologische Staatssammlung München, Münchhausenstraße 21, 81247 München, Germany

# Grasping molecular structures through publication-integrated 3D models

Pravin Kumar<sup>1,\*</sup>, Alexander Ziegler<sup>2,\*</sup>, Julian Ziegler<sup>1,3</sup>, Barbara Uchanska-Ziegler<sup>1</sup> and Andreas Ziegler<sup>1</sup>

<sup>1</sup>Institut für Immungenetik, Charité–Universitätsmedizin Berlin, Campus Benjamin Franklin, Freie Universität Berlin, Thielallee 73, 14195 Berlin, Germany

<sup>2</sup>Institut für Biologie, Freie Universität Berlin, Königin-Luise-Strasse 1-3, 14195 Berlin, Germany

<sup>3</sup>Current address: Meister-Francke-Strasse 8, 22309 Hamburg, Germany

**Although the need for communicating 3D data using simple and intuitive means extends to disciplines as diverse as biology, engineering sciences and the visual arts, none of the currently available molecular-visualization programs depicting potentially highly complex structures are compatible with the portable document format (PDF), the current gold standard of electronic publishing. Therefore, it is highly desirable for authors to be able to provide their readers with a basic 3D display of structures that can be accessed without the need for specialized visualization software. Here, we describe how an interactive 3D model of a molecular complex can be embedded directly into a PDF, thus providing readers with important and educational visual information that would otherwise be more difficult to disseminate.**

## Benefits of portable document format (PDF)-integrated 3D models

How multidimensional research data are presented in a scientific publication will often be crucial for an in-depth understanding. This is not only the case in structural biology where molecular features have been accessible in print format for many years through static and ‘stereo’ images [1–5], but is also the case in many other disciplines, such as chemistry, physics or medicine. However, complete access to a 3D model of a molecule that enables direct interaction with all its components, requires not only adequate hardware, but also the skill to operate a molecular-visualization tool appropriately, including the ability to effectively obtain and extract the precise information that is desired. Because these programs are often complicated to handle, there is an urgent need for a simple, effective and interactive representation of 3D structures that would enable both non-specialist and specialist readers of scientific publications to gain access to the most important aspects of the information contained within such structures. This requirement has already been recognized but there is as yet no consensus as to which presentation format is best suited [6,7].

Some examples of attempts to address this issue include internet browser plug-ins, such as Protein Explorer [4] and Jmol [7,8], which provide the possibility of integrating

interactive 3D models into scientific and educational web-pages, and the iSee platform [6], which offers a unified access system to a variety of components of structural genomics data from genes to complete structures. However, all these technologies require installation of programs or plug-ins by the user before the relevant information can be accessed and, crucially, the information is only accessible when online. The alternative or complementary mechanism is to provide a pre-rendered film of the molecule in a downloadable video format. Although improving the ‘viewability’ for the reader of the 3D information relative to that of static 2D images, this prevents any direct interaction with the structure, thus limiting its potential educational benefit and restricting the reader to scenes of the molecule dictated by the author. An additional problem for both of these approaches is that the information has to be supplied as a supplement to the original article rather than as a part of it, thus proving an impediment to the reader’s access. Significantly, none of these technologies are compatible with the Adobe Systems’ PDF, the universally accepted standard of electronic publications. A recent article [9] exemplifies these problems: although a 3D viewer (‘FirstGlance in Jmol’) with several different viewing options can be activated through a supplementary attachment, all attributes are only available online in a standardized manner through Jmol, precluding any integration into a PDF file, the format by which the article is distributed.

To simplify communication between the author and the reader, the aim must therefore be to depict structural data with the maximum of information about the molecules described but integrated within the electronic publication itself. Here, we show how an interactive, highly informative 3D model that fulfils these requirements can now be assembled and integrated into PDF documents. In addition to the typical 2D representations of static figures, this leads to enhanced, directly accessible 3D information in the content of publications in which structural data are described, thus combining the benefits of all other approaches to the dissemination of 3D structural information into a single, standard format file.

## The HLA-B\*2705–pVIPR complex

To demonstrate how a 3D model can be created and integrated into a PDF file, we chose the structure [Protein

\*Corresponding author: Ziegler, A. (andreas.ziegler@charite.de)

\* Joint first authors.

## Opinion

Trends in Biochemical Sciences Vol.33 No.9

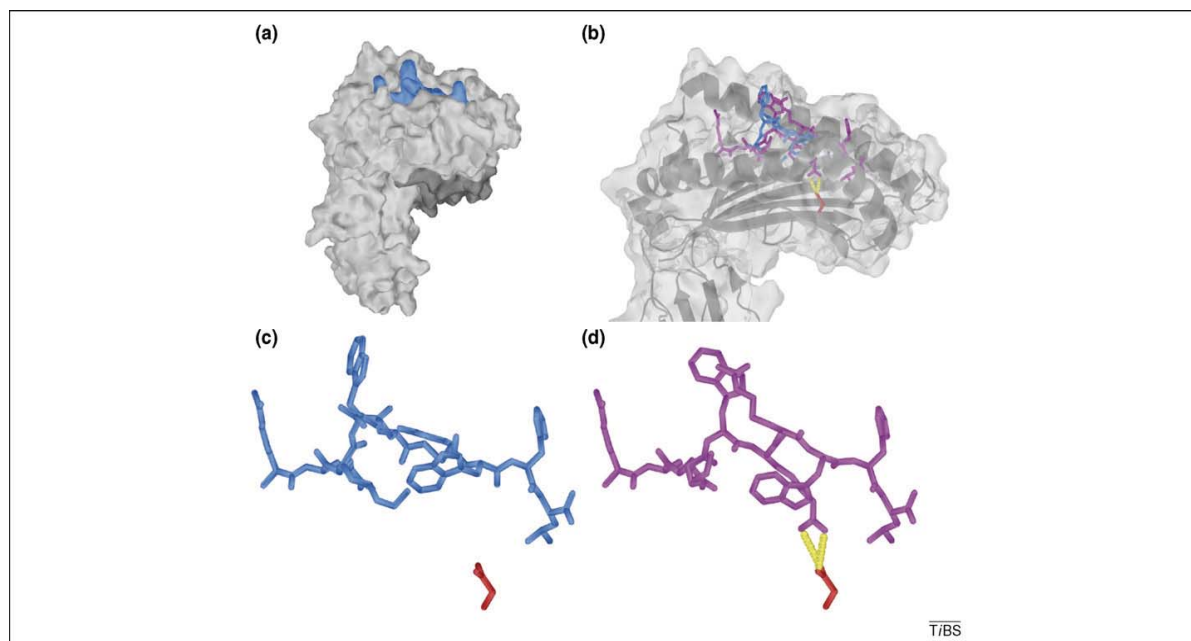
Data Bank (PDB) accession code 1ogt] of the human histocompatibility antigen HLA-B\*2705 in complex with a peptide (pVIPR; RRKWRRWHL) that is derived from vasoactive intestinal peptide type 1 receptor, residues 400–408. A peculiarity of this molecular complex is the presence of the peptide in two equally occupied binding modes that differ considerably from each other, although all HLA-B\*2705 heavy chain (HC) and  $\beta_2$ -microglobulin ( $\beta_2$ m) residues essentially retain the same conformations (there is a C $\alpha$  root mean square deviation of 0.2 Å between the two complexes) [10].

In a traditional article, the following would be typical of how the structural information is presented to the reader: the heterotrimer consists of HC,  $\beta_2$ m and the self-peptide pVIPR (Figure 1). Although the ends of pVIPR [peptide residues 1 (p1) and p2, and p8 and p9] are bound identically in both conformations, the middle of the peptide (p3 to p7) diverges considerably. This is a consequence of the presence of the HC residue Asp116 (coloured red in Figure 1b–d), which binds to pArg5 by a bidentate salt bridge (yellow in Figure 1b,d) in one of the conformations. In this binding mode (termed non-canonical or p6 $\alpha$ ; coloured magenta in Figure 1), the main chain  $\phi$  and  $\psi$  torsion angles occur in  $\alpha$ -helical conformation only at p6, whereas, in the other, conventional peptide-binding mode (termed p4 $\alpha$ ; coloured light blue in Figure 1), this is the case only at p4. In both conformations, the other  $\phi/\psi$  torsion angles, respectively, are as in  $\beta$ -strands. This conformational dimorphism of pVIPR has functional consequences because it is respon-

sible for the inappropriate negative selection of HLA-B\*2705–pVIPR-restricted T cells within the thymus [10,11]. In addition, X-ray crystallographic and functional studies show that the non-canonical conformation of pVIPR, but not its canonical counterpart, participates in HLA-B27 subtype-dependent molecular mimicry [10,12–14]. Because of the dual conformation of the peptide, the HLA-B\*2705–pVIPR complex is a particularly instructive example to illustrate the advantages offered by PDF-integrated 3D models.

### 2D and 3D representations of the HLA-B\*2705–pVIPR complex

The 2D images shown in Figure 1a,d provide the reader with a general idea of the structure of the HLA-B\*2705–pVIPR complex, as would be typical for any other 3D structure presented in an academic paper. A surface representation of the entire molecule is shown in Figure 1a, followed by a view of the binding groove with pVIPR in both binding modes (Figure 1b, semi-transparent surface and cartoon representation). The bidentate salt bridge between HC Asp116 and pArg5 that characterizes the p6 $\alpha$ -binding mode is also shown. Finally, Figure 1c,d demonstrate that an omission of HC,  $\beta_2$ m and one of the peptide conformations leads to an unobstructed, simplified view of the remaining pVIPR-binding mode. Representations like these provide the bare minimum of information that must be available for an evaluation of the structure of a molecule. In a conventional



**Figure 1.** An interactive 3D model of the HLA-B\*2705 molecule in complex with the pVIPR peptide. The HLA-B\*2705 HC is shown in light grey,  $\beta_2$ m in dark grey and the two conformations of the pVIPR peptide in light blue (p4 $\alpha$ ) or magenta (p6 $\alpha$ ). The peptide N terminus is always shown on the left and the C terminus on the right. (a) Side view of the molecular surface of the whole molecule (only the p4 $\alpha$  conformation of the peptide is shown). (b) Differential display of the pVIPR peptide (stick representation) in the canonical (light blue) and non-canonical (magenta) conformations in the HLA-B\*2705 binding groove. The anchoring of pVIPR to the floor of the peptide binding groove in the p6 $\alpha$  conformation is through a bidentate salt bridge (yellow) between pArg5 and the side chain of Asp116 (red). After removal of HC and  $\beta_2$ m, pVIPR is depicted in p4 $\alpha$  (c) or p6 $\alpha$  (d) conformation together with Asp116 and the salt bridge (only d). 3D functions can be activated by clicking on any part of the image in the interactive PDF version of the article (note, to end the 3D view, right-click the 3D display and select 'Disable 3D' from the contextual menu). Components of the 3D model can be accessed using the model tree icon. The model can be manipulated interactively using the mouse (options for selecting rotating, panning and zooming tools are available in the toolbar or contextual menu) and readers can see the preset views by clicking on the respective designations assigned by the authors (through the middle section of the model tree when it is displayed, the drop-down menu in the toolbar or the contextual menu).

## Opinion

publication, Figure 1 would therefore have to be complemented by several additional images providing more structural detail (see, e.g. Ref. [10]).

The alternative and more enlightening approach that we advocate here involves the use of the freely available Adobe Reader (Version 7.1 or later) to access the 3D model of the molecule in an interactive manner – this is achieved by clicking on any part of Figure 1 in the interactive PDF version of this publication (see [Supplementary Material](#) online). An introduction into the possibilities that are offered is provided when the ‘Help’ option within the program is addressed. Already the ‘basic’ tools, such as zoom, rotation in freely chosen directions or hiding of structural elements (e.g. HC,  $\beta_2m$  or one of the pVIPR conformations) permit an interactive access that facilitates a better understanding of many structural features. In this case, it is particularly helpful to be able to compare the peptide conformations by zooming in and by rotating the two structures with the HC component hidden (by toggling its visibility off in the model tree), both in surface and ball and stick view (which can be alternated easily, also by toggling the view options in the model tree). In this way, it becomes obvious immediately that the C $\alpha$  backbones and side chains of pVIPR are distinct between the two conformations from p3 to p7, whereas they are virtually identical at the ends of the peptide [10].

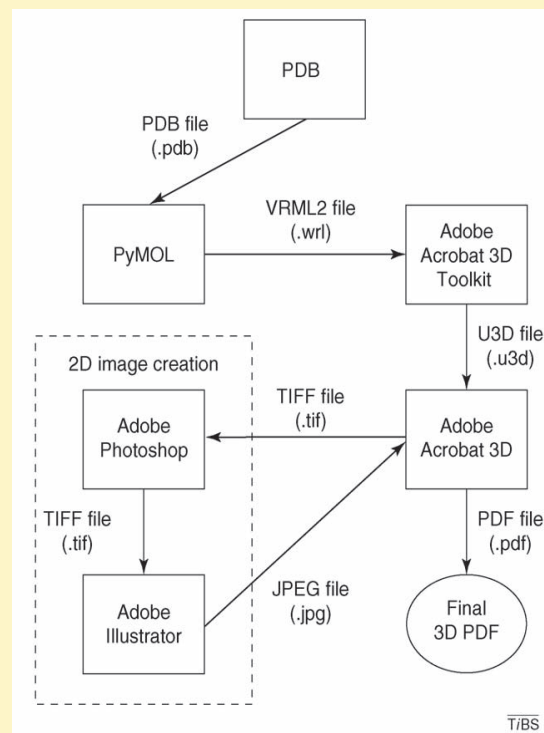
With the included preset views, an author-generated ‘tour’ of the molecule is made available to the reader. This tour provides the reader with the equivalent views that would be typical of a pre-rendered video file of the structures, which is offered normally as supplementary material for download, yet it still enables full interaction with the structures at each stage of the tour. In our case, the tour begins by depicting the entire complex and then shows a ‘skeletal’ view of all components, zooms into the peptide-binding groove, disentangles the molecular assembly more and more, using various side and top views, and concentrates finally on the two peptide conformations. The HC residue Asp116 and the salt bridge that it forms with pArg5 only in the p6 $\alpha$  conformation of pVIPR are also shown. The educational aspect of this tour makes it particularly suited for presentations and teaching without the necessity for online access. Despite these features, the file size of the present publication, including the combined 2D and 3D figure, is not greater than ~3 MB.

### Creating an interactive 3D model and integrating it into PDF files

A detailed description of how to build such a model is provided in [Box 1](#). In summary, the HLA-B\*2705–pVIPR structure was divided into its individual components. Interactive vector graphics objects of each component were then created using PyMOL, followed by the import of the image objects into the Adobe Acrobat 3D Toolkit and their reassembly. The Toolkit was further used to design the model ‘tree’ (which is a hierarchy of components of the molecule that enables the reader to set their individual visibility and display style), name sub-structures and select colours for each object. The model was then saved in Adobe Systems’ Universal 3D (U3D) file format and the

### Box 1. How the PDF-integrated 3D model was created

The 3D model was assembled in a step-by-step manner, which is outlined in [Figure 1](#). Initially, the raw PDB file (1ogt) was downloaded from PDB ([www.rcsb.org/pdb/home/home.do](http://www.rcsb.org/pdb/home/home.do)) and opened using PyMOL version 1.0r1 (<http://pymol.sourceforge.net/>) in an OpenSUSE 13.2 Linux environment. Here, the components to be shown in the final 3D model were selected (HLA-B\*2705 HC,  $\beta_2m$ , HC residue Asp116, the bidentate salt bridge between pArg5 and Asp116 of the HC and the two peptide conformations) and each saved separately in VRML2 format, followed by loading into Adobe Acrobat 3D Toolkit 8.1.0 (Adobe Systems, CA, USA) by drag and drop. Once loaded, the mesh size (i.e. the amount of data representing the surface) of each object was reduced as far as possible by a process of trial and error (down to ~30% of the original size) to keep the final file size to a minimum. The separate objects were then designated (e.g.  $\beta_2m$ ), an object hierarchy (i.e. model tree) was created and different colours were assigned to each. The model was saved in the Adobe Universal 3D file format, which was then opened in Adobe Acrobat 3D. The four images shown in [Figure 1a–d](#) were created from TIFF-format desktop screenshots of the desired model views and were modified in Adobe Photoshop CS3 to show the desired information (i.e. cropped to size). After combining these TIFF files, a single JPEG-format image file was generated using Adobe Illustrator CS3. Following this operation, the raw U3D file was opened in Adobe Acrobat 3D and the single 2D JPEG image file was combined with it. Then all final viewing settings were defined, such as background colour, standard render mode and lighting. The next step consisted of selecting the preset views using the camera tool and defining a standard view that would be shown after activation of the 3D mode. Finally, the model was saved as a PDF file. An overview of the minimum system requirements needed to create and view 3D PDF models can be obtained through the following websites from Adobe Systems: Adobe Acrobat 3D and Adobe Acrobat 3D Toolkit ([www.adobe.com/products/acrobat3d/systemreqs](http://www.adobe.com/products/acrobat3d/systemreqs)), and Adobe Reader ([www.adobe.com/products/reader/productinfo/systemreqs](http://www.adobe.com/products/reader/productinfo/systemreqs)).



**Figure 1.** Flow diagram depicting the creation process of a PDF-integrated 3D model ‘hidden’ behind a single 2D image file ([Figure 1a–d](#)) of the HLA-B\*2705–pVIPR complex. Note: the processes on the left of the flow chart are ones that will hopefully become redundant in the future if the Adobe Acrobat 3D software is ever updated to be able to perform these tasks itself.

## Opinion

Trends in Biochemical Sciences Vol.33 No.9

U3D file imported directly into a PDF file, using Adobe Acrobat 3D. This program was also used to assign additional features of the model, such as its rendering mode or lighting. The 2D representations in Figure 1a–d were also created during this stage. The last step consisted of preparing and designating the preset views for the reader.

**Concluding remarks**

It should be noted that the Adobe Acrobat 3D Toolkit enables authors to incorporate many more features into 3D models, such as the labelling of components of the structure, measuring distances, variable lighting options and several additional model-render modes. We have deliberately limited the options that are available in the model presented here to enable the reader to concentrate on the principal features that distinguish the conventional 2D representations of Figure 1a–d from the PDF-integrated 3D models of the molecular structures. These are the 3D-viewing capability, platform-independence, accessibility and, probably of greatest importance, its interactivity that enables the reader to delve into aspects of the structure that would otherwise not be available to them readily. However, it must be pointed out that the program does not yet offer several options available in standard molecular-visualization software (Box 2). These shortcomings of the Adobe Acrobat 3D programs might, in part, be due to their current focus on technical applications rather than the biochemical sciences (i.e. computer-aided design and computer-aided manufacturing). However, other molecular-visualization programs are also not problem-free. For example, when the structure of the HLA-B\*2705–pVIPR complex is accessed with 'FirstGlance in Jmol', only the canonical-binding mode of pVIPR can be seen, thereby precluding an understanding of the dual conformation's immunological implications.

Our example demonstrates that the integration of 3D models into electronic publications provides the reader with the ability to visualize complex structures in an interactive, yet intuitive, manner, without having to rely on the often highly sophisticated programs used by structural biologists [1–8]. A wide dissemination of this technology is made possible by the platform independence of programs, such as Adobe Reader. The potential that is thus offered has also not escaped the attention of astrophysicists and zoologists, as two recent reports demonstrate [15,16]. We believe that the incorporation of 3D files into electronic publications will also be of importance in many disciplines of clinical medicine, such as neurology, cardiology and oncology, in which the original data are not accessible through databases, such as PDB.

Several improvements will be needed to establish this procedure as a mainline tool in electronic publishing (Box 2). For example, although a direct export of the PDB file into Adobe Acrobat 3D Toolkit is possible in principle, for the purposes of our article, we had to use a deviation through PyMOL to be able to display the molecule in the commonly used ribbon or surface representations. Therefore, the import options of the relevant PDF-creation programs as well as the export functions of molecular-visualization

**Box 2. PDF-integrated 3D models: caveats and desirable improvements**

Despite the advantages offered by PDF-integrated 3D models, several problems do remain. These belong to three areas: (i) viewing options, (ii) ease of creating the PDF-integrated 3D model and (iii) file-size limitations.

Owing to their design explicitly for structural biology, current molecular visualization programs [1–8] offer far more viewing options than are available for the 3D model shown here. However, many of the features provided might not be essential to convey the most important message about a structure, such as the conformational dimorphism of pVIPR in the HLA-B\*2705 subtype. For example, in our case, the omission of the non-canonical pVIPR conformation by 'FirstGlance in Jmol' must be considered a more severe problem than the inability of our PDF-integrated 3D model to display the 'rainbow' viewing option that is offered by the former program for colouring the three chains of the complex. However, the lack of all the display settings available in current specialist software could still be a problem in other cases, so a 'complete' set of viewing options is desirable.

As the flow diagram (Box 1, Figure 1) demonstrates, the process of creating a 3D PDF of a molecular structure is presently not as easy as one would hope and a simplification of this procedure would be highly desirable. This could be approached either by developing a U3D to PDF export function in standard molecular visualization programs or by providing the Adobe Acrobat 3D Toolkit with a more advanced import function for raw PDB files (the current import options are unsatisfactory). Clearly, having to use third-party software (here: PyMOL; see also Box 1, Figure 1) to obtain the necessary output for the structures is laborious and the current need to perform this step will hopefully become unnecessary in the future.

Finally, it must be stressed that the integration of 3D models into electronic publications results in an extended publication file size, which in some cases might be too large (e.g. if numerous 3D structures need to be included in a single article), especially as many scientific institutions have download limits for individual files of 5–10 MB.

software need to be scrutinized and improved. Apart from these issues, we have to stress that a considerable responsibility rests with the model-creating author because the diverging interests and program-handling capabilities of the readers must be anticipated.

**Note added in proof**

During the final processing stage of this manuscript, Adobe Systems announced the launch of new Adobe Acrobat and Adobe Reader versions for July 2008 (both in version 9). We have not been able to evaluate the advantages (or disadvantages) offered by these new versions in any depth. However, the links we provide in our article are still valid, the one directing the reader to the Adobe Reader download page, the other link directing the reader to the Adobe Acrobat Version 9 homepage. According to the sales staff at Adobe Systems, the functions of the Adobe Acrobat 3D Toolkit have been incorporated into the new 'Adobe 3D Reviewer' which is sold as part of the new 'Adobe Acrobat Version 9 Pro Extended' package.

**Acknowledgements**

This work was supported by the VolkswagenStiftung (I/79 983 and a stipend to P.K.) and the Friedrich-Naumann-Stiftung für die Freiheit (fellowship to A.Z.). We thank T. Bartolomeaus (Berlin, Germany) for support and J.A. López de Castro (Madrid, Spain) for his helpful comments on the manuscript.



## Opinion

Trends in Biochemical Sciences Vol.33 No.9

**Supplementary data**

Owing to the necessity to provide a standard-format PDF to institutions for their archives, this version of the article cannot currently include the interactive Figure 1. Instead, the fully interactive version of this article is available as Supplementary material in the online version, at doi:10.1016/j.tibs.2008.06.004

**References**

- 1 Kraulis, P.J. (1991) MOLSCRIPT: a program to produce both detailed and schematic plots of protein structures. *J. Appl. Crystallogr.* 24, 946–950
- 2 Merritt, E.A. and Bacon, D.J. (1997) Raster3D: photorealistic molecular graphics. *Methods Enzymol.* 277, 505–524
- 3 DeLano, W.L. (2002) *The PyMOL Molecular Graphics System*. DeLano Scientific
- 4 Martz, E. (2002) Protein Explorer: easy yet powerful macromolecular visualization. *Trends Biochem. Sci.* 27, 107–109
- 5 Fenn, T.D. *et al.* (2003) POVScript+: a program for model and data visualization using persistence of vision ray-tracing. *J. Appl. Crystallogr.* 36, 944–947
- 6 Abagyan, R. *et al.* (2006) Disseminating structural genomics data to the public: from a data dump to an animated story. *Trends Biochem. Sci.* 31, 76–78
- 7 Cammer, S. (2007) SChISM2: creating interactive web page annotations of molecular structure models using Jmol. *Bioinformatics* 23, 383–384
- 8 Herráez, A. (2006) Biomolecules in the computer: Jmol to the rescue. *Biochem. Educ.* 34, 255–261
- 9 Röthlisberger, D. *et al.* (2008) Kemp elimination catalysts by computational enzyme design. *Nature* 453, 190–197
- 10 Hülsmeier, M. *et al.* (2004) Dual. *HLA-B27 subtype-dependent conformation of a self-peptide*. *J. Exp. Med.* 199, 271–281
- 11 Fiorillo, M.T. *et al.* (2000) CD8(+) T-cell autoreactivity to an HLA-B27-restricted self-epitope correlates with ankylosing spondylitis. *J. Clin. Invest.* 106, 47–53
- 12 Fiorillo, M.T. *et al.* (2005) Allele-dependent similarity between viral and self-peptide presentation by HLA-B27 subtypes. *J. Biol. Chem.* 280, 2962–2971
- 13 Rückert, C. *et al.* (2006) Conformational dimorphism of self-peptides and molecular mimicry in a disease-associated HLA-B27 subtype. *J. Biol. Chem.* 281, 2306–2316
- 14 Ziegler, A. *et al.* Implications of structural and thermodynamic studies of HLA-B27 subtypes exhibiting differential association with ankylosing spondylitis. In: *Molecular Mechanisms of Spondyloarthropathies* (López-Larrea, C., ed.), Landes Bioscience (in press)
- 15 Barnes, D.G. and Fluke, C.J. (2008) Incorporating interactive three-dimensional graphics in astronomy research papers. *N. Astron.* 13, 599–605
- 16 Ruthensteiner, B. and Hess, M. Embedding 3D models of biological specimens in PDF publications. *Microsc. Res. Tech.* (in press)

## **7. Evolution of the Axial Complex**

### **7.1. Summary**

Based on the comparative morphological datasets of several high-ranking echinoid taxa, an internal organ complex of special interest was further analyzed, the axial complex. Previous histological and electron microscopical studies had revealed discrepancies between the morphology observed and descriptions in the literature. For example, the reasons underlying the drastically altered architecture of the axial complex reported for several irregular sea urchin taxa were still lacking an explanation. Given the opportunity to virtually dissect the analyzed species based on isotropic MRI datasets, a re-evaluation of the axial complex and the internal organs in contact with it was undertaken. These analyses reveal that the morphological variations observed are mainly restricted to some of the derived irregular taxa. The changes are predominantly caused by an altered anatomy of other internal organs, notably the gastric caecum as well as mesenteric strands suspending the digestive tract. Due to the availability of datasets incorporating representative species of almost all high-ranking echinoid taxa, a thorough comparative analysis could be accomplished.

### **7.2. Manuscript**

Ziegler A, Faber C, Bartolomaeus T: Evolution of the axial complex and interdependence of internal organ systems in sea urchins (Echinodermata: Echinoidea). Submitted

Pages 64-113

# **Evolution of the axial complex and interdependence of internal organ systems in sea urchins (Echinodermata: Echinoidea)**

Alexander Ziegler<sup>1\*</sup>, Cornelius Faber<sup>2</sup>, and Thomas Bartolomaeus<sup>1</sup>

<sup>1</sup>Institut für Biologie, Freie Universität Berlin, Königin-Luise-Straße 1-3, 14195 Berlin, Germany

<sup>2</sup>Institut für Klinische Radiologie, Universitätsklinikum Münster, Waldeyerstraße 1, 48149 Münster, Germany

\* Corresponding author. E-mail: [aziegler@zoosyst-berlin.de](mailto:aziegler@zoosyst-berlin.de)

## **Abstract**

The axial complex of echinoderms (Echinodermata) is composed of various primary and secondary body cavities that interact with each other. In sea urchins (Echinoidea), structural differences of the axial complex in “regular” and irregular species have been observed, but the reasons underlying these differences are not fully understood. In addition, a better knowledge of axial complex diversity could not only be useful for phylogenetic inferences, but improve also an understanding of the function of this enigmatic structure. We therefore analyzed numerous species of almost all sea urchin orders by magnetic resonance imaging, dissection, histology, and transmission electron microscopy and compared the results with findings from published studies spanning almost two centuries. These combined analyses demonstrate that the axial complex is present in all sea urchin orders and has remained structurally conserved for a long time, at least in the “regular” species. Within the Irregularia, a considerable morphological variation of the axial complex can be observed with gradual changes in topography, size, and internal architecture. These modifications are related to the growing size of the gastric caecum as well as to the rearrangement of the morphology of the digestive tract as a whole. The structurally most divergent axial complex can be observed in the highly derived Atelostomata in which the reorganization of the digestive tract is most pronounced. Our findings demonstrate a structural interdependence of various internal organs, including digestive tract, mesenteries, and the axial complex.

## Introduction

“Das Dorsalorgan ist von jeher das Schmerzenskind der Anatomen gewesen.” (Johannes Wagner 1903)

All echinoderms (Echinodermata) possess an axial complex as part of their coelomic and haemal system. This organ complex is characterized by a structural, functional and topographic interaction between various primary and secondary body cavities and is composed of derivatives of the three paired larval coeloms, i.e. the protoel and the mesocoel, both surrounded by the lining epithelia of the metacoel. The different coelothelia rest on the connective tissue matrix that is crossed by numerous haemal spaces and lacunae. The various sub-structures forming the axial complex have been successfully homologized in all echinoderm taxa (Fedotov 1924; Erber 1983a, b).

Sea urchins (Echinoidea) – see Fig. 1 for the present view on sea urchin phylogeny based largely on hard-part morphology and molecular data – also possess a well-developed axial complex. The morphological data obtained for this structure are based to a large extent on findings in the more easily accessible “regular” sea urchins such as *Arbacia punctulata*, *Psammechinus miliaris*, *Sphaerechinus granularis*, and *Strongylocentrotus purpuratus*. However, historical (Hoffmann 1871, Koehler 1883, Hamann 1887, Prouho 1887, Wagner 1903), as well as more recent (De Ridder & Jangoux 1993, Kaburek & Hilgers 1999) studies have revealed that the axial complex found in irregular sea urchins differs in its gross morphology and histology from that found in “regular” taxa. This is exemplified by the work of Kaburek and Hilgers (1999), who reported that *Schizaster canaliferus* possesses a specialized axial complex exhibiting pronounced structural changes including loss of sub-structures. However, more recent studies on sea urchin soft tissues indicate that there is good reason to believe that the axial complex found in *Schizaster canaliferus* might not be typical for all Irregularia. In the more primitive irregular species *Echinoneus cyclostomus*, for example, the gross morphology of the axial complex is more similar to the “regular” type (Ziegler *et al.* 2008). A number of questions therefore arise from previous studies: (i) What are the major changes affecting the architecture of the axial complex within the Echinoidea? (ii) Can differences in its structure be observed also among the “regular” species? (iii) What could have caused the drastic changes found in some taxa? (iv) Does a better understanding of axial complex morphology reveal information about its function? And finally, (v) Can characters be deduced from comparative observations of the axial complex that might be useful for phylogenetic inferences?

Using non-invasive imaging techniques that permit large taxon sampling (Ziegler & Angenstein 2007, Ziegler *et al.* 2008), we analyzed numerous species from almost all sea urchin orders to infer the structure of their axial complex. These data were extended employing invasive techniques such as dissection, histology, as well as transmission electron microscopy, and included also findings from published studies spanning almost two centuries. The

combined analysis suggests an interdependence of soft tissue organ systems in sea urchins that we believe to be ultimately responsible for the structural changes of the axial complex observed in irregular taxa.

Since part of the confusion regarding axial complex morphology can be attributed to the bewildering terminology applied by different authors and in different languages to the same anatomical entities, we also suggest a list of definitions and provide a multilingual compilation for echinoid axial complex components to facilitate further comparative studies.

## Material and Methods

The specimens referred to in this study are listed in Table 1 together with information on the current systematic classification of each species (see also Fig. 1), the source of the data used in the study, specimen ID where applicable, and literature references.

### *Magnetic resonance imaging*

Magnetic resonance imaging (MRI) was performed using the methods described by Ziegler and co-workers (2008). Imaging was carried out in Berlin, Germany and Würzburg, Germany using high-field small animal MRI scanners equipped with 7 T and 17.6 T super-conducting electromagnets. The resolution of the datasets varied between  $20 \times 18 \times 18 \mu\text{m}^3$  and  $(86 \mu\text{m})^3$ . Table 1 lists the resolutions achieved for every species analyzed by MRI. Image processing was carried out using ImageJ 1.38w and its Volume Viewer plugin. All datasets are available from the authors upon request.

### *Dissection*

Dissection was performed on freshly fixed as well as museum specimens under direct observation through a stereo-microscope equipped with a digital camera for documentation.

### *Histology*

Histological analyses were performed on four echinoid species: *Eucidaris tribuloides*, *Diadema setosum*, *Psammechinus miliaris*, and *Echinocyamus pusillus*. *Eucidaris tribuloides* was collected at Twin Cayes, Belize in June 2002. *Psammechinus miliaris* and *Echinocyamus pusillus* were dredged from depths of 10-50 m in the North Sea off Helgoland, Germany in April 2005. *Diadema setosum* was purchased at a tropical fish store in Berlin, Germany in May 2005. One juvenile of *Eucidaris tribuloides*, one juvenile and three adults of *Diadema setosum*, five adults of *Psammechinus miliaris*, and three adults of *Echinocyamus pusillus* were used in this study. For light microscopy, the specimens were fixed in Bouin's fluid for 24 h, decalcified in 2% nitric acid, dehydrated in an alcohol series, methylbenzoate and butanol, and embedded in paraplast (Kendall). Complete series of  $8 \mu\text{m}$  thick sections were made using a microtome (Reichert-Jung 2050 Supercut) with steel blades (ThermoShandon

Coated High Profile Disposable Blades) and later stained using Azan stain. Series of sections were digitally recorded with an Olympus BX 2 microscope equipped with a Color View II camera (Soft Imaging Systems).

#### *Electron microscopy*

For transmission electron microscopy (TEM), several specimens of *Psammechinus miliaris* and *Echinocardium cordatum* were dredged from depths of 10-50 m in the North Sea off Helgoland, Germany in April 2005. The specimens were dissected and their axial complexes were fixed at 4°C in 2.5% glutaraldehyde in 0.1 M sodium cacodylate buffer at pH 7.4 for 2 h. The tissue samples were washed thrice in the same buffer, subsequently post-fixed for 1 h in 1% OsO<sub>4</sub> buffered in 0.1 M sodium cacodylate, dehydrated in an acetone series and embedded in Araldite. Silver interference coloured sections (75 nm) were made with a diamond knife using an ultramicrotome (LEICA UC6), automatically stained with 2% uranyl acetate and 2% lead citrate using a semi-automatic ultrastaining machine (Phoenix), and observed with a transmission electron microscope (Philips CM 120 BioTWIN). Micrographs were made on digital imaging plates (Ditabis) and electronically processed with the software Adobe Photoshop CS3.

#### *Systematic classification*

The systematic classification used throughout this study is based upon results obtained by Jensen (1981, 1988), Littlewood & Smith (1995), Littlewood *et al.* (1997), Ax (2003), Smith (2005), Stockley *et al.* (2005), and Smith *et al.* (2006). Sea cucumbers (Holothuroidea) constitute the sister taxon to sea urchins, while Cidaroida are the most primitive taxon within the Echinoidea and sister taxon to Euechinoidea. The “Regularia” are a paraphyletic clade, while the Echinacea and the Irregularia each form a monophyletic taxon (Fig. 1). “Hemiasterina” and “Paleopneustina” presumably are paraphyletic clades. Resolution at the base of the Euechinoidea as well as for the Echinacea is still considered relatively poor (Smith *et al.* 2006).

## **Results**

#### *Developmental origin of the axial complex*

Primary and secondary body cavities can be distinguished at the ultrastructural level by their lining (Ruppert 1991, Bartolomaeus 1994, Rieger & Purschke 2005): a primary body cavity is lined by extracellular matrix (ECM), whereas a secondary body cavity is lined by an epithelium consisting of basal lamina and epithelial cells. In echinoderms, the primary body cavities form the haemal system, whereas the secondary body cavities develop to constitute the coelom and are thus also termed coelomic cavities. Historically, the second-

ary body cavities found in echinoderms have been termed axocoel (proto-coel), hydrocoel (mesocoel), and somatocoel (metacoel) (Heider 1912).

The echinoid axial complex is part of this tripartite coelomic system. In its most basic form, the axial complex lies vertically within the oral-aboral axis – hence the term “axial complex” – of interradius CD and is surrounded by the oral and aboral somatocoel. It consists of derivatives of axocoel and hydrocoel. During ontogenesis, these two cavities have different fates: while the right hydrocoel degenerates, the left hydrocoel gains connection to the left axocoel via the stone canal. During further ontogenesis, the left hydrocoel becomes the ring canal that gives rise to the radial canals of the ambulacral (or water vascular) system, while the stone canal connects the ring canal with the madreporic ampulla. The latter is connected to the exterior by a number of small ductules, the madreporic pore canals. These canals penetrate the madreporic plate, their distal regions being lined by an ectodermally derived epithelium, the epidermis. As in asteroids (Ruppert & Balser 1986), the lining of the proximal madreporic pore canal sections is of mesodermal origin, since madreporic ampulla and axial coelom ontogenetically originate from the left larval axocoel.

The axial coelom is an orally oriented part of the axocoel that partly enwraps the stone canal as well as the axial organ. The latter structure is a large space within the connective tissue matrix, lined by epithelial cells of the coelomic cavities that surround it. It constitutes in fact a hypertrophy of the mesenteries that attach part of the digestive tract to the calcite endoskeleton. Since the haemal structures of the axial complex are mainly located within the dorso-ventral mesentery, bounded by the lining of the somatocoel, the axial organ is surrounded by the somatocoel on one side and by the axocoel on the other. The axial organ is an integral component of the echinoid haemal system (Vogt & Yung 1888). An aboral extension of the axial organ, however, is surrounded by the so-called dorsal sac, a derivative of the right larval axocoel. This aboral extension is termed the head process and consists of a large compartment within the connective tissue matrix between somatocoel and dorsal sac. Axial organ and head process are crossed by numerous anastomosing haemal lacunae that aborally join with the anal haemal ring and the genital lacunae. In addition, the axial organ is crossed by numerous canaliculi that constitute invaginations of the axial coelom and somatocoelomic epithelia. Adorally, the axial organ does not end entirely blindly, but extends into the perioesophageal haemal ring either directly or through connecting haemal lacunae.

#### *Definition of components of the echinoid axial complex*

In its primary structure, the echinoid axial complex consists of the following components: madreporic ampulla, dorsal sac, head process, pulsating vessel, axial coelom, axial organ, canaliculi, haemal lacunae, and stone canal. Figure 2 depicts a semi-schematic representation of the axial complex of *Sphaerechinus granularis*, probably the best-studied echinoid species in terms of axial complex morphology (e.g. Leipoldt 1893, Strenger 1973). The

designations and definitions referring to components of the echinoid axial complex as well as the developmental origin of each structure are provided in Table 2. A trilingual compilation of synonymous terms to facilitate comparative studies is provided in Table 3.

### *Morphological findings*

In this section, the results derived from our own analyses are combined with results derived from the literature available on the axial complex as well as its mesenterial suspension. For a given species, these different contributions may vary considerably, and Table 1 provides a compilation.

## **Cidaroida**

In lateral view, the axial complex found in *Cidaris cidaris* and *Eucidaris metularia* is almost straight and it lies directly underneath the madreporic plate (Figs. 3A, 5). Throughout its entire course it maintains more or less the same width, only slightly bulging in the middle. It is suspended by the dorso-ventral and the free mesentery (Fig. 6). The dorso-ventral mesentery is strongly developed and connects axial complex, oesophagus, and the peripharyngeal (or lantern) coelom with the endoskeleton. The free mesentery connects the peripharyngeal coelom with axial complex and rectum. The axial complex is thus attached to two mesenteries over its entire length in *Cidaris cidaris* and *Eucidaris metularia* (Fig. 4A, B). In the juvenile specimen of *Eucidaris tribuloides*, however, the free mesentery is lacking at the level of the axial organ (Fig. 7B).

A madreporic plate is present in cidaroid species and numerous madreporic pore canals connect the exterior with the madreporic ampulla underneath the madreporic plate. Below the madreporic ampulla lies the roundish-elongated dorsal sac (Fig. 7A). Its epithelium is only slightly muscularized and mainly glandular according to Prouho (1887) and Leipoldt (1893). However, the presence of glands at this location seems unlikely due to the enclosed nature of the dorsal sac.

The head process, located within the dorsal sac (Fig. 8), is lined by myoepithelial cells. It extends adorally into the pulsating vessel of the axial organ. The madreporic ampulla opens adorally into the axial coelom and the stone canal. The axial coelom is a blindly-ending cavity that is located between stone canal and axial organ (Fig. 9) and that extends towards Aristotle's lantern. The width of the axial coelom does not vary much, remaining large towards the adoral end in *Cidaris cidaris* (Prouho 1887, Leipoldt 1893). In *Eucidaris tribuloides*, the axial coelom in general is reduced to a thin cavity (Fig. 7B). It is lined by an epithelium with numerous podocytes. These podocytes are found to be restricted to that side of the axial coelom in *Eucidaris* sp. that borders the axial organ (Welsch & Rehkämper 1987).

In all cidaroid species analyzed to date, the axial organ is a haemal structure composed of a connective tissue matrix filled with coelomocytes and anastomosing haemal lacunae. Canaliculi extend into its interior from the lining somatocoelomic and axocoelomic epithe-



lia. The axial organ sends out a well-developed haemal lacuna towards the perioesophageal haemal ring that is in close contact with the ring canal. The stone canal is a tubular structure connecting the madreporic ampulla with the ring canal. At its adoral end, the stone canal forms several dilatations that converge with the ring canal. Ultrastructural investigations of the stone canal of *Eucidaris* sp. reveal a prismatic epithelium with ciliated, myoepithelial, and granulated cells that probably represent secretory neurons (Rehkämper & Welsch 1988).

### **Echinothurioida**

The axial complex of echinothurioids is straight in lateral view, located directly underneath the madreporic plate. Schurig (1906) and Sarasin & Sarasin (1887) report it to be spirally winding in *Phormosoma bursarium*, *Asthenosoma varium*, *Hygrosoma hoplacantha*, and *Sperosoma biseriatum* (Fig. 5). It is suspended by two mesenteries (Fig. 6), of which the dorso-ventral mesentery is strongly developed, connecting the axial complex, the oesophagus, and the peripharyngeal coelom with the endoskeleton. The free mesentery connects the axial complex with the rectum and terminates halfway down the axial complex in *Phormosoma bursarium* and *Asthenosoma varium* (Sarasin & Sarasin 1887, Schurig 1906, Fig. 6).

A madreporic ampulla lies underneath the madreporic plate and opens into the axial coelom and the stone canal. Sarasin & Sarasin (1887) report the madreporic ampulla of *Asthenosoma varium* to be connected by a canal to another small cavity lying underneath the madreporic plate. However, these structures were not reported for *Phormosoma bursarium* (Schurig 1906), and we believe this isolated observation to be an artefact that will not be further considered in this analysis. The dorsal sac (Fig. 8) lies underneath the madreporic plate and is lined by a slightly muscularized epithelium that is mainly glandular (Sarasin & Sarasin 1887, Schurig 1906). As in cidaroids, the presence of glands at this location seems unlikely.

The head process is lined by a muscularized epithelium as well and continues adorally in the form of the also muscularized pulsating vessel (Schurig 1906). The axial coelom parallels stone canal and axial organ (Fig. 9) and extends from the madreporic ampulla towards the ring canal where it ends blindly. Its width at the base is comparable to its middle part, at least in *Asthenosoma varium* and *Phormosoma bursarium*.

The axial organ is a structure composed of a haemal tissue mesh crossed by anastomosing haemal lacunae and canaliculi. As in Cidaroida, the stone canal forms several dilatations at its junction with the ring canal.

### **Pedinoida**

In lateral view, the axial complex found in *Caenopedina mirabilis* is extending straight from the lantern adapically and then obliquely in its apical part (Figs. 3B, 5). While the upper part broadens, the lower part is of the same size as the middle part of the axial complex. It is suspended by two mesenteries (Fig. 4C), the dorso-ventral and the free mesentery. The former is strongly developed and connects axial complex, oesophagus, and the peripharyngeal

coelom with the endoskeleton, while the free mesentery connects the axial complex with the rectum and terminates halfway down the axial complex, thus resembling the situation found in Echinothurioida (Fig. 6). A madreporic plate is present and numerous madreporic pore canals connect the exterior with the madreporic ampulla underneath the madreporic plate.

### **Aspidodiadematidae**

The axial complex of *Aspidodiadema hawaiiense* and *Plesiadiadema indicum* is mostly straight when viewed laterally and only slightly oblique in its upper half (Figs. 3C, 5). On the level of the first curvature of the oesophagus, the axial complex tapers out adorally towards the ring canal. The axial complex is attached to the dorso-ventral and the free mesentery (Fig. 4D). The dorso-ventral mesentery is strongly developed and connects axial complex, oesophagus, and the peripharyngeal coelom with the endoskeleton. The free mesentery connects the axial complex with the rectum and terminates halfway down the axial complex (Fig. 6). In its lower half, it appears that the axial complex consists only of the stone canal and the haemal lacuna(e) that connect(s) the axial organ and the perioesophageal haemal ring. The axial organ itself seems to be restricted to the upper half of the axial complex. It is spindle-shaped and bulges in its middle part (Figs. 3C, 5).

### **Diadematidae**

In lateral view, the axial complex found in *Diadema setosum* is extending straight down from the madreporic plate to the ring canal. The relatively large Aristotle's lantern found in this species (as well as in most other diadematids) squeezes the axial complex between lantern and the apical endoskeleton (Fig. 5). The axial complex is suspended by the dorso-ventral and the free mesentery. The former is strongly developed and connects axial complex, oesophagus, and the peripharyngeal coelom with the endoskeleton, while the free mesentery connects the rectum with the axial complex in its uppermost part close to dorsal sac and head process. It is not present in the middle and lower parts of the axial complex (Fig. 6). In the juvenile specimen of *Diadema setosum*, the dorso-ventral mesentery interconnects peripharyngeal coelom, oesophagus, axial complex as well as the rectum (Fig. 7C, D).

The madreporic plate is perforated by numerous madreporic pore canals that connect the exterior with the madreporic ampulla. Right underneath the madreporic ampulla lies the dorsal sac that encloses the compact and roundish-elongated head process. The dorsal sac extends further adorally, paralleling axial coelom and stone canal in its lower part (Figs. 7C, 8). The head process is more prominent in its adapical part and is lined by a strong myoepithelium. It sends out the pulsating vessel into the lumen of the axial coelom in *Diadema setosum* and *Diadema antillarum*. The axial coelom is a large cavity located between axial organ and stone canal (Fig. 8). It ends blindly towards the adoral end of the axial complex.

The axial organ bulges in the middle part of the axial complex and shows considerable infolding into the axial coelom (Fig. 7D). The stone canal is a tubular structure that con-

stantly decreases in diameter on its way down towards the ring canal. It joins the ring canal through a number of small canals.

### **Arbacioida**

In lateral view, the axial complex is straight, extending down from the madreporic plate to the ring canal (Coe 1912, Bonnet 1925) (Fig. 5). In the vicinity of the oesophagus, the adoral part of the axial complex tapers out and reaches the surface of Aristotle's lantern. Its mesenterial suspension resembles the diadematid/echinacean type (Fig. 6). The madreporic plate is perforated by numerous madreporic pore canals. A pulsating vessel constitutes the adoral extension of the head process. Schematic representations of horizontal sections of the axial organ, axial coelom as well as stone canal of *Arbacia lixula* and *Arbacia punctulata* illustrate the internal morphology of the arbacioid axial complex (Fig. 9). The axial organ of *Arbacia lixula* is reported to be surrounded by a large number of haemal lacunae (Millott 1966). The axial complex found in *Stomopneustes variolaris* (incerta sedis, presumably sister taxon to Arbacioida) resembles the arbacioid/echinoid gross morphology.

### **Salenioida**

The axial complex found in *Salenocidaris hastigera* (Figs. 3D, 5) is comparable in its lateral aspect to the axial complex found in aspidodiadematids. The mesenterial suspension resembles the diadematid/echinacean type (Fig. 6).

### **Echinoida**

The axial complex found in the Echinoida is straight in lateral view, situated slightly shifted from the oral-aboral axis underneath the madreporic plate (Figs. 2; 4E, F; 5). At the junction with the oesophagus, the axial complex gradually tapers out towards the ring canal. Above this junction, a conspicuous swelling is visible that is widest in its middle part, giving the axial complex a spindle-shaped appearance. The mesenterial suspension resembles the diadematid/echinacean type (Figs. 4E, F; 6).

The madreporic plate is perforated by numerous madreporic pore canals that are lined by a ciliated epithelium and that merge adorally to form the madreporic ampulla (Fig. 8). The latter is lined by a ciliated epithelium as well. The diameter of the madreporic ampulla becomes gradually smaller towards its adoral end and it basally diverges into stone canal and axial coelom. The dorsal sac lies laterally underneath the madreporic ampulla and surrounds the globular head process (Figs. 8, 11A). The dorsal sac is a closed cavity and is not connected to either madreporic ampulla, stone canal or the axial coelom. Boolootian & Campbell (1964), however, report a divergent morphology of the dorsal sac in *Strongylocentrotus purpuratus* in which the dorsal sac communicates with the somatocoel via a small slit and is divided into two contractile chambers. We believe this isolated finding to be an artefact and will not consider it any further in our analysis.

A strong pulsating vessel is present in all echinoid species studied so far, its ultrastructure resembling that of the head process. The axial coelom is located in-between stone canal and axial organ (Fig. 9), extending adorally before ending blindly above the ring canal. The axial organ of Echinoida is spindle-shaped in vertical section and shows characteristic infolding, with an enlarged surface towards the axial coelom with numerous digitations that protrude into the lumen of the latter.

The stone canal is located at the lateral edge of the axial complex (Fig. 9). After its gradual opening at the lower end of the madreporic ampulla, it runs down towards the ring canal, while exhibiting a diameter that varies only slightly and a shape that is almost circular in cross-section. At the lower end of the axial complex, the haemal lacuna(e) of the axial organ adorally merge(s) with the perioesophageal haemal ring while the stone canal directly opens into the ring canal. In numerous echinoid species of Echinoida the stone canal was found to pulsate.

#### Echinoida: ultrastructural findings

In *Psammechinus miliaris*, a ciliated, pseudostratified monolayer lines the dorsal sac (Fig. 10A). While only some of the peripheral lining cells are epithelio-muscle cells, those resting on the matrix of the head process form a strong myoepithelium (Fig. 11E). Here, the epithelio-muscle cells contain strong, basally located bundles of myofilaments that form a regular network of rectangularly arranged outer circular and inner longitudinal bundles that are embedded in the voluminous matrix of the head process. The perikarya deeply extend into the dorsal sac lumen, which indicates that the organ was apparently fixed during contraction. The state of contraction can be estimated from the position of the apical adhaerens junctions between adjacent cells. Intraepithelial nerve fibre processes were found interspersed among the lining cells, but podocytes were never found.

The head process contains primary body cavities lined by the matrix of the head process. Numerous cells with homogenous cytoplasm and relatively big nuclei float inside this cavity, and some haematocytes could be recognized by their large number of lysosomes and residual bodies.

The axial organ begins at the level of the first curvature of the oesophagus and is surrounded by numerous haemal lacunae (Fig. 11B). That part of the axial organ which bulges into the axial coelom contains numerous deep crypts and invaginations in *Psammechinus miliaris*, so that the axocoelomic surface of the axial organ is tremendously enlarged. Inside the canaliculi, the entire lumen seems to be occupied by microvilli (Fig. 10B). Only a few cells are found inside the lumen, most of them coelomocytes. Haematocytes at different stages of differentiation are present within the matrix. They contain residual bodies and lysosomes of different rank.

Numerous podocytes rest on the axial coelomic side of the matrix (Figs. 10C, 11F). Their pedicels are bridged by electron-dense diaphragmata. Each podocyte has a single cilium

with a  $(9 \times 2) + 2$  axoneme that adheres to the cell body by a basal body, short rootlets and an accessory centriole perpendicular to the basal body. A circle of 9-12 strong microvilli surrounds each cilium (Fig. 10D). Additional microvilli emanate from the surface of the perikaryon and only seldom from the pedicels. In *Echinometra* sp., the podocytes within the axial coelom lining are irregularly distributed and not restricted to the side covering the axial organ (Welsch & Rehkämper 1987).

The stone canal lining in *Psammechinus miliaris* is a monolayered columnar epithelium (Fig. 11C). Each of these epithelial cells bears a long cilium with a  $(9 \times 2) + 2$  axoneme that adheres to the cell body with a basal body and three rootlet structures. A circle of 9-12 strong microvilli surrounds each cilium and additional smaller microvilli emanate from the cell surface. A number of glandular cells that show a distinct polarity can be found within the epithelium: some cells of the stone canal lining contain large, electron-densely stained vesicles. These possible secretory granules lie near the apex while other cellular components are located more basally. However, degrading cells can rarely be found among the basal portions of the lining cells, and epithelio-muscle cells, muscle cells or podocytes were never seen to be part of the stone canal epithelium. The somatocoel is lined by a flat epithelium which is only slightly muscularized (Figs. 10D, 11D). The cilia of the somatocoel epithelium show the characteristic composition with a dense microvilli fringe surrounding the axoneme. The epithelial cells are connected to each other via adhaerens junctions and do not show the specializations of the dorsal sac and axial coelom lining.

### **Tennopleuroida**

In lateral view, the axial complex found in *Mespilia globulus* and *Salmacis bicolor* is straight, extending down from the madreporic plate to the ring canal (Fig. 5) (Aiyar 1938). In the vicinity of the oesophagus, the adoral part of the axial complex tapers out and reaches the apical surface of Aristotle's lantern. The mesenterial suspension of the axial complex resembles the diadematid/echinacean type (Figs. 4G, 6). A schematic representation of a horizontal section through the axial complex of *Salmacis bicolor* at the level of the axial organ is shown in Fig. 8. In *Genocidaris maculata*, the course of the axial complex is slightly oblique (Fig. 3G).

### **Irregularia**

Most obviously, irregular sea urchin species are distinguished from animals belonging to "regular" orders by their secondarily developed bilateral symmetry. However, their analysis demonstrates that the shape of the axial complex is primarily not dependent on features of the endoskeleton, but is influenced by the architecture of several internal organs as detailed below.

## Holactypoida

The axial complex found in *Echinoneus cyclostomus* extends from the madreporic plate down to the ring canal in an almost straight line (Figs. 3H, 5). The madreporic plate can be seen bulging slightly into the interior of the animal. In the upper fourth of the axial complex, a conspicuous swelling can be seen, which is interpreted as the axial organ (Westergren 1911). Close to the ring canal, the lower fourth of the axial complex shows a swollen region which has been seen with MRI but has also been described by Westergren (1911). Unfortunately, histological data are currently not available for this taxon.

The mesenterial suspension of the axial complex resembles the aspidodiadematid type (Fig. 6). The dorso-ventral mesentery extends between oesophagus, axial complex, gastric caecum, pentagonal apical membrane (or aboral sinus), and the endoskeleton (Figs. 4H, 6). At the apical pole this mesentery joins the pentagonal apical membrane which forms the connection between the gonoducts and the axial complex. This membrane appears to be present in all irregular sea urchin taxa (Hyman 1955). A second mesentery suspends the axial complex towards the rectum and also forms part of the pentagonal apical membrane. The gastric caecum is not in close contact with the axial complex (Fig. 6).

## “Cassiduloida”

The axial complex found in *Cassidulus caribearum* and *Echinolampas depressa* extends from the madreporic plate down to the ring canal. It is bent anteriorly towards ambulacrum III (Figs. 3I, J; 5). Jensen (1981) has reported similar findings for *Apatopygus recens*. The madreporic plate can be seen bulging only slightly into the interior of the animal. In the upper third, a conspicuous swelling of the axial complex can be seen which is interpreted as the axial organ. During its entire path, the axial complex is attached to the dorso-ventral mesentery. This structure extends between oesophagus, axial complex, gastric caecum, pentagonal apical membrane and the endoskeleton (Fig. 6). A second, smaller mesentery suspends the axial complex towards rectum and aboral endoskeleton as well as the pentagonal apical membrane. The gastric caecum of *Cassidulus caribearum* and *Echinolampas depressa* is reduced to numerous smaller sacs that are located further anteriorly (Ziegler *et al.* 2008) and that are therefore not in close contact with the axial complex. In *Cassidulus caribearum*, a slightly swollen region can be seen in the adoral part of the axial complex (Fig. 3I). Unfortunately, histological data are currently not available for this taxon.

## Clypeasteroida

Due to the flattened aspect of clypeasteroids (sea biscuits and sand dollars), the axial complex is considerably miniaturized. It is located underneath the madreporic plate and has a straight (Fig. 5) to bean-shaped form in lateral view. The madreporic plate is perforated by numerous madreporic pore canals that connect the madreporic ampulla to the exterior. In *Echinocyamus pusillus* (and all other taxa of the Fibulariidae), the madreporic ampulla is in contact with the exterior via a single canal, the hydropore (*sensu* Mortensen 1948). Except

for a small lateral process, the madreporic ampulla is almost tubular so that hydropore and madreporic ampulla seem to be merely an aboral elongation of stone canal and axial coelom in this species. All other clypeasteroids studied so far possess a genuine madreporic plate and a prominent madreporic ampulla, and their axial complex is attached to a single mesentery during its entire course, the dorso-ventral mesentery (Fig. 6). In its upper part, it fuses with the pentagonal membrane at the apical pole. According to Cuénot (1891), clypeasteroid species possess a strongly developed dorsal sac that surrounds the muscularized head process (Figs. 7G, 8). Furthermore, Cuénot (1948) reports that the dorsal sac of *Echinodiscus bisperforatus* communicates with the somatocoel via a small slit. Such a connection could not be found in *Echinocyamus pusillus* and we believe this finding to be a misinterpretation. At least in the latter species, a pulsating vessel could not be detected (Figs. 7H, 9).

The axial coelom originates from the madreporic ampulla directly underneath the madreporic plate. The axial organ can be found to be straight (*Echinocyamus pusillus*) or bean-shaped (*Echinarachnius parma*, *Mellita quinquesperforata*) in lateral view (Fig. 3K). The stone canal's diameter continuously decreases before passing into the ring canal in *Echinocyamus pusillus*. In the few clypeasteroid taxa that possess a gastric caecum, this highly reduced structure is not in close contact with the axial complex.

### Holasteroida

In lateral view, the axial complex found in Holasteroida is C-shaped and extends between madreporic plate and ring canal (Fig. 5). In its upper half, the axial complex runs parallel to the aboral endoskeleton towards interambulacrum 5. The madreporic plate is slightly infolded. The conspicuous swelling right underneath the madreporic plate, interpreted as the axial organ, is in an horizontal position. In its middle section, the previously horizontally oriented axial complex bends towards the mouth, comes into close contact with the oesophagus adorally, and leads in a straight line down towards the ring canal. Another swelling can be observed in its lower third, at least in *Urechinus naresianus* (Fig. 5). Unfortunately, no histological data are currently available for this taxon.

The axial complex is held in place by the dorso-ventral mesentery that attaches digestive tract, axial complex, gastric caecum, and pentagonal membrane to the calcite endoskeleton. Between gastric caecum and axial complex, this mesentery is very thin, so that both structures are in close contact with each other in the aboral part of the animals. A second, smaller mesentery connects the axial complex with rectum, pentagonal apical membrane and endoskeleton. The mesenterial strand that interconnects the first loop of the digestive tract is extending half-ways along the gut loop (Fig. 6). Mortensen (1907) describes the gross morphology of the axial complex in four holasteroid species: *Echinograda paradoxa*, *Pourtalesia jeffreysi*, *Pourtalesia wandeli*, and *Urechinus naresianus*. The axial complexes found in *Antrechinus nordenskjoldi* and *Pourtalesia hispida* closely resemble this description. The large gastric caecum is in close contact with the upper part of the axial complex (Fig. 6).

### “Hemiasterina”

The axial complex found in *Hemiaster expergitus* closely resembles the holasteroid and paleopneustine axial complex in its gross morphology.

### “Paleopneustina”

In lateral view, the axial complex found in *Abatus cavernosus* and *Schizaster canaliferus* is C- to L-shaped and extends down from the madreporic plate to the ring canal close to the mouth (Fig. 5). The following description is based on *Schizaster canaliferus* (Kaburek & Hilgers 1999). The madreporic plate is characterized by two calcareous ridges protruding into the interior of the endoskeleton. The axial complex is attached to the right ridge from where it is extending towards interambulacrum 5. It then bends down towards the mouth and extends along the gastric caecum and later the oesophagus before finally reaching the ring canal. It is primarily suspended by the dorso-ventral mesentery that attaches digestive tract, axial complex, gastric caecum, and pentagonal apical membrane to the calcite endoskeleton. Between gastric caecum and axial complex this mesentery is very thin, so that both structures are in close contact in the aboral part of the specimen (Fig. 6). A second, smaller mesentery attaches the axial complex to rectum, pentagonal apical membrane and endoskeleton.

The madreporic ampulla is reduced to several broadened madreporic pore canals inside the right calcareous ridge, and according to Kaburek & Hilgers (1999), the dorsal sac as well as a pulsating vessel are not present in *Schizaster canaliferus*. However, the structure of the head process resembles that in the “regular” species (Fig. 8). The axial organ is located directly behind the right calcareous ridge and is oriented horizontally, parallel to the endoskeleton. A large uniform axial coelom is not present. The stone canal is tri-partite: its upper part bears a tall-prismatic epithelium, its middle region is muscularized and filled with coelomocytes, while its lower part close to the ring canal is lined by a flat epithelium and is only slightly filled with coelomocytes. The stone canal of *Schizaster canaliferus* is not dilated at its junction with the ring canal and at least its muscularized middle part can pulsate. The mesenterial strand that interconnects the first loops of the digestive tract is extending half-ways along the first gut loop (Fig. 6, bottom line). The large gastric caecum is in close contact with the upper part of the axial complex (Fig. 6).

### Micrasterina

A lateral view reveals that the micrasterine axial complex is roughly S-shaped. Its gross morphology is largely similar in the micrasterine taxa studied so far (Table 1). The madreporic plate protrudes into the interior by two calcareous ridges comparable to the paleopneustine species *Schizaster canaliferus*. Lodged in-between these two ridges and successively emanating from the right ridge, the axial complex is oriented horizontally in its first small part. During its later course, it is closely associated with the large gastric caecum passing along anteriorly towards ambulacrum III. At the junction of the gastric caecum with the oesophagus, the axial complex bends backwards towards interambulacrum 5 before finally moving



again anteriorly towards the ring canal that encircles the mouth (Figs. 5, 6). The micrasterine axial complex is primarily suspended by the dorso-ventral mesentery that attaches digestive tract, axial complex, gastric caecum, and pentagonal membrane to the calcite endoskeleton (Fig. 6). Between gastric caecum and axial complex, this mesentery is very thin, so that both structures are in close contact in the aboral part of the specimens. A second, smaller mesentery suspends the axial complex towards pentagonal apical membrane, rectum, and aboral endoskeleton. The mesenterial strand that interconnects the first loops of the digestive tract is extending far towards ambulacrum III, “dragging” the axial complex along (Fig. 6).

The madreporic plate is perforated by a small number of horizontal and vertical madreporic pore canals (Hamann 1887, Wagner 1903). Underneath and within the right calcareous ridge, a small madreporic ampulla can be seen. Parallel to this structure, a dorsal sac can be found at least in *Echinocardium mediterraneum*, *Heterobrissus niasicus*, and *Spatangus purpureus* (Hamann 1887, Prouho 1887, Wagner 1903). It contains the head process (Fig. 8), which is not pulsatile in *Heterobrissus niasicus* according to Wagner (1903). The head process extends further posteriorly into the axial organ. A pulsating vessel was found in several micrasterine species. Parallel to axial organ and stone canal, the axial coelom extends adorally from the inconspicuous madreporic ampulla.

The gross morphology of the stone canal is known for a number of micrasterine taxa and closely resembles the architecture in *Schizaster canaliferus*. It can be sub-divided into three parts: the first part is in close association with the axial organ and ends at the adoral end of the latter. Here, the stone canal transforms into a canal composed of a mesh-like tissue that is filled with “pigment” (Hamann 1887). It continues in this state parallel to the gastric caecum and the haemal lacunae until reaching the vicinity of the oesophagus where it transforms again to become a hollow canal covered by a thin epithelium. Schurig (1906) states that the water vascular and the haemal systems in *Heterobrissus niasicus* are always clearly separated, the haemal lacuna running parallel to the stone canal before reaching the perioesophageal haemal ring.

#### Micrasterina: ultrastructural findings

In *Echinocardium cordatum*, the axial coelom is lined by flat epithelial cells, each of which bears a single cilium. The ciliary axoneme shows the typical (9x2)+2-pattern and is attached to the basal body. Two ciliary rootlets and a basal foot anchor the cilium to the cell. Both ciliary rootlets are co-axial, running obliquely to the main axis of the basal body. Some fibrillar material secures the connection of the accessory centriole to the longer vertical rootlet and fixes its position underneath the basal foot. The cilia are encircled by a dense fringe of 9-12 strong microvilli (Fig. 10E). Numerous podocytes line the axial coelom and the lumina of the canaliculi inside the axial organ (Fig. 11F). The canaliculi are filled with a huge number of microvilli and cilia that project into their lumen, resulting in a tremen-

dous surface extension (Fig. 10F). Epithelio-muscle cells can be detected sporadically, and sometimes even podocytes seem to bear muscle fibers.

The axial organ consists of a dense matrix and is rich in canaliculi and lacunae (Fig. 9). It is characterized by cells with electron-bright cytoplasm and by the distinct lacunar system. Local increments of the matrix constitute haemal lacunae filled with haemal fluid. A basal lamina demarcates the border of the tissue towards the coelomic epithelium of the axial coelom. Connective tissue cells and an enormous number of phagocytotic cells can be found in the inner parts of the axial organ. The haematocytes are filled with residual bodies as well as lysosomes of different rank. Collagenous and elastic fibers as well as free cells constitute the major part of the axial organ. The somatocoelomic lining is a flat, only slightly muscularized epithelium (Fig. 11D), consisting of a monociliated monolayer overlying the basal lamina of the axial organ. No podocytes could be detected in the somatocoelomic epithelium.

## Discussion

Whereas an extensive comparative study of the axial complex had been undertaken in the sister taxon to Echinoidea, the Holothuroidea (Erber 1983b), such a comparative approach has not yet been applied to the study of the echinoid axial complex. One objective of this study was therefore to obtain an insight into the overall anatomy of the axial complex within a wide selection of sea urchin species. Many of these species can be obtained only with great difficulty as viable specimens, and several others are available only as fixed specimens from museum collections, often precluding their use for dissection, histology or electron microscopy. To partially circumvent these problems, we additionally employed a non-invasive imaging technique (MRI) in conjunction with a thorough review of the relevant literature dating back to the pioneering studies of F. Tiedemann that were published at the beginning of the 19<sup>th</sup> century (Tiedemann 1816). This complementary approach did not allow an analysis of all examined echinoid species with all procedures, but nevertheless permitted to gather results from a representative number of sea urchin species regarding the architecture of the axial complex, thereby forming the basis for an in-depth comparison. To avoid, as much as possible, repetitions with data presented in the Results section, we will attempt to concentrate here on (i) major changes in axial complex architecture, (ii) the possible reasons for these changes, and (iii) the axial complex' potential function as derived from morphological features. Finally, (iv) we address the question whether phylogenetically informative characters can be deduced from comparative observations of the axial complex. It must be borne in mind, however, that the present compilation is far from complete and rests, in a number of orders, on the analysis of only a few or even single species and specimens.

### Major changes in the architecture of the axial complex and its constituent parts

The gross morphology of the axial complex in the analyzed sea urchin taxa varies considerably, although major structural changes are restricted to the more derived irregular species (Fig. 5). However, the form of the axial complex may depend on a number of factors, such as the age or health of the specimen. Furthermore, since the stone canal fuses with the ring canal set atop Aristotle's lantern in the "regular" and clypeasteroid taxa, movement of this feeding apparatus may alter the form of the axial complex considerably. In the Atelostomata, the axial complex is running parallel to the endoskeleton in its upper part before bending down adorally to run along the gastric caecum towards oesophagus and ring canal. This can be considered the most derived condition. Other irregular sea urchin taxa such as the Holoctypoida, "Cassiduloida" and Clypeasteroida have obviously preserved the more plesiomorphic state, exhibiting an axial complex that is comparable in its gross morphology to the condition observed in Aspidodiadematidae or Salenioida, the taxa most closely associated with the ancestor of Irregularia (Fig. 1).

In most species analyzed here, the madreporic plate (Figs. 2, 5) is situated medially on the aboral side and is perforated by numerous madreporic pore canals. However, *Echinocyamus pusillus* does not have a madreporic plate, and its axocoel is connected to the exterior via a single pore. Mortensen (1948) describes the reduction of the madreporic plate as characteristic for the Fibulariidae, a small group within the Clypeasteroida that exhibit strong paedomorphic traits, and the reduction of madreporic pore canals has been considered a derived feature (Mooi 1990).

All examined "regular" species possess a prominent madreporic ampulla (Figs. 2, 5), while the madreporic ampulla is reduced to a system of broadened madreporic pore canals in the spatangoid sea urchins as shown by Kaburek & Hilgers (1999) for *Schizaster canaliferus*. Whether the ampulla-like cavity underneath the madreporic plate that was described by Hamann (1887) and Koehler (1883) in *Spatangus purpureus* can be referred to as a madreporic ampulla must currently be regarded as unclear.

A prominent, in cross-section C-shaped dorsal sac (Figs. 2, 5, 11) is partially enveloping the head process in most species. According to Kaburek & Hilgers (1999), this structure is reduced in *Schizaster canaliferus*. Hamann (1887) and Wagner (1903), however, presented drawings of the dorsal sac and head process in *Echinocardium mediterraneum* and *Heterobrissus niasicus*, which, together with the comparison of the axial complex architecture in several spatangoid taxa presented here, leads us to assume that a misapprehension of its composition may have led Kaburek & Hilgers (1999) to consider that the dorsal sac is missing in *Schizaster canaliferus*. However, we hypothesize that size and form of dorsal sac and head process may be dependent on the sexual maturity of the specimen, since, at least in Asteroidea, the dorsal sac-head process complex was shown to serve the gonads as a local heart (Warnau & Jangoux 1992).

The axial coelom of all species studied ends blindly at the adoral end of the axial organ (Figs. 2, 11). The axial coelom, like dorsal sac and madreporic ampulla, shows a similar

structural pattern within the “regular” sea urchin species as well as the clypeasteroid species examined so far, although it must be noted that species of *Atelostomata* appear again to display a differing condition (see, e.g. Kaburek & Hilgers (1999)).

Rather unclear is the situation regarding the pulsating vessel (Fig. 9). Cidaroid, echinothurioid, diadematoïd, arbacioid, echinoid, as well as temnopleuroïd species have been reported to possess a truly pulsating structure within the axial coelom that constitutes an adoral extension of the muscularized head process. Such pulsations have not been reported for any irregular taxon, although histological sections of the upper axial coelom of spatangoid species reveal a separate haemal lacuna overlying the axial organ that we homologize with the pulsating vessel found in the “regular” taxa. Whether this structure actually pulsates cannot currently be stated with confidence.

The axial organ is present in all echinoid species observed so far and constitutes an integral component of the sea urchin haemal system both in “regular” and irregular taxa (Figs. 2, 7, 11). Its internal structure is comparable in all taxa, its dense connective tissue matrix being crossed by numerous anastomosing haemal lacunae and canaliculi.

The stone canal (Figs. 2, 7, 8, 9, 11) is in fact that sub-structure of the axial complex undergoing the most drastic changes during evolution: in spatangoid species, it is divided into three distinctive parts, its upper part closely resembling the stone canal found in “regular” taxa. At the adoral end of the axial organ it transforms to become a chambered structure filled with numerous coelomocytes. This part of the stone canal is additionally surrounded by smooth muscle fibers and might therefore pulsate. The lower part is again unchambered, but also filled with coelomocytes. Kaburek & Hilgers (1999) believe that the stone canal in *Schizaster canaliferus* may assume functions of the axial organ. This, however, would imply a mixing of different body fluids at this location which we believe to be highly unlikely.

The columnar epithelium of the stone canal is a distinctive feature in comparison to the flat epithelia of axial coelom and somatocoel (Fig. 11). The interior of the stone canal is filled with numerous cilia that cause an active and directed transport of coelomic fluid (Ludwig 1890, Rehkämper & Welsch 1988, Ferguson 1996). Another difference to the other coelomic cavities can be seen in the presence of glandular cells, which Rehkämper & Welsch (1988) consider to be neuro-secretory cells. Neither muscular tissue or podocytes within nor contractions by the stone canal could be observed by us in “regular” or irregular sea urchins.

In conclusion, it can be stated that presumably all sea urchin taxa possess an axial complex as part of their haemal system. The axial complexes found in all “regular” species are comparable to a large degree, consisting of a straight to slightly oblique structure located in interradius CD extending vertically down from the madreporic plate to the ring canal. In the irregular sea urchin species an evolutionary trend towards miniaturization and horizontal alignment of the axial organ in conjunction with a bending of the axial complex as a whole (Fig. 5) can be observed. However, despite these drastic changes in axial complex gross

morphology, its internal composition has largely remained the same, so that the plesiomorphic Cidaroida share numerous similarities with the derived Atelostomata.

### **Reasons underlying the observed changes in axial complex architecture**

The mesenterial suspension of the axial complex and of the digestive tract components is straightforward in the “regular” taxa: Cidaroida possess an axial complex supported by two mesenteries, of which the free mesentery is successively reduced in the other “regular” taxa (Fig. 6). The situation observed in the juvenile specimen of *Eucidaris tribuloides*, where only the dorso-ventral mesentery is suspending the axial complex in its middle part (Fig. 7B), might hint at a similar development within Cidaroida or might be due to the early developmental stage of the specimen. In *Psammechinus miliaris*, both mesenteries seem to be reduced completely in the lower middle and lower part of the axial complex (Jangoux & Schaltin 1977, this study), hinting at an even further reduction of mesenterial structures in some taxa within the Echinoida. The mesenteric suspension of the axial complex in the more primitive Irregularia can be described as largely comparable to the condition observed in Aspidodiadematidae and Diadematidae. Whether the smaller mesentery suspending the axial complex towards the rectum can be considered homologous with the respective structure in “regular” sea urchins cannot currently be answered with certainty. Notable is the absence of this mesentery in the Clypeasteroida, a condition that presumably can be ascribed to the laterally displaced position of the rectum. In the Atelostomata, the dorso-ventral mesentery fuses with the large mesenterial strand that interconnects the coils of the first loop of the digestive tract (Fig. 6). However, the precise mesenterial suspension of irregular sea urchins on the whole as well as the homologies of the respective mesenterial structures remain unclear and merit further investigation.

The assumption that a reorganization of the morphology of the axial complex occurred along with the evolution of bilateral symmetry can therefore be ruled out. Rather, the present results suggest a gradual co-evolution of various internal organs within the Irregularia based on their structural interdependence. The underlying reasons for this development can be seen in the altered lifestyles of irregular sea urchins based on the conquering of infaunal habitats and a parallel change in feeding strategies. These changes apparently correspond to the gradual enlargement of the gastric caecum, a structure that constitutes an outgrowth of the proximal stomach, which is thought to be of importance in the digestive process (De Ridder & Jangoux 1993). Due to its topography, the gastric caecum is suspended by the dorso-ventral mesentery as well. Its successive growth inevitably had to lead to a rearrangement of the gross morphology of the axial complex. Since the gastric caecum is most prominent in the Atelostomata, its effect on the structure of the axial complex and the dorso-ventral mesentery should also be most evident here, which is precisely what is observed (Figs. 5, 6). An additional change in digestive tract anatomy is responsible for another highly derived condition seen in Micrasterina: here, the mesentery suspending the first coil of the digestive

tract has expanded and moved in anterior direction towards ambulacrum III, “dragging” the axial complex along, and ultimately leading to the more or less S-shaped form observed in this group of animals (Figs. 5, 6).

Another aspect of importance for the changes in axial complex gross morphology can be seen in the relative position of the apical system of the endoskeleton that accommodates also the madreporic plate. In the Holasteroidea, the apical system is located further anteriorly than in other irregular taxa, which, in combination with the posteriorly orientated gastric caecum, brings about a prolonged and horizontally aligned axial complex in the apical region (Figs. 5, 6).

### **Function of the echinoid axial complex**

In terms of function, the sea urchin axial complex remains as enigmatic as ever, especially so, since these marine invertebrates have been shown to survive its removal for several months (Bamber 1921, Schinke 1951, Millott & Farmanfarmanian 1967), although some specimens do show rapid regeneration of the removed structures (Millot & Farmanfarmanian 1967), suggestive of a beneficial function of this organ for the animal. Historically, a number of functions have been attributed to the echinoid axial complex, including that of a gill (Greeff 1872), an immune organ (e.g. Millott 1966, Millott 1967, Millott 1969, Larson & Bayne 1994), a gland (e.g. Perrier 1875, Koehler 1883, Fedotov 1924, Millott 1964, Boolootian & Campbell 1966), an embryonal organ without function in the adult (Teuscher 1876), a coelomocyte and cell production site (e.g. Carpenter 1885, Hamann 1887, Prouho 1887, Cuenot 1891, Schinke 1951), a cell degradation site (e.g. Jangoux & Schaltin 1977, Bachmann & Goldschmid 1980), a swelling of the water vascular system (Hoffmann 1871), and a heart (e.g. Tiedemann 1816, Valentin 1841, Leydig 1854, Müller 1854, Gegenbaur 1859, Agassiz 1872-1874, Boolootian & Campbell 1964, Boolootian *et al.* 1965). Furthermore, a number of authors have advocated a predominantly excretory role of the axial complex (e.g. Perrier 1875, Koehler 1883, Hamann 1887, Hartog 1887, Sarasin & Sarasin 1887). This hypothesis is supported by recent studies that homologize the left larval axocoel (protocoel) that can be found throughout the “lower” deuterostome taxa (e.g. Balser & Ruppert 1993, Balser *et al.* 1993, Stach 2002). In this context, the finding of podocytes – highly specialized cells that permit selective fluid transfer – in coelomic compartments of the axial complex is indicative of an excretory function (Welsch & Rehkämper 1987).

One aim of our study concerned the possible presence of podocytes in the Irregularia to support the excretion hypothesis as well as to shed light on other functions that have been ascribed to the echinoid axial complex. Since epithelio-muscle cells are found lining the axial coelom in addition to podocytes, their contraction could generate a pressure gradient that allows filtration of the haemal fluid into the axocoel, but it remains unsolved on the basis of the available data whether the ultrafiltrate constitutes primary urine in terms of a metanephridial system (Ruppert & Smith 1988). However, the presence of structures as

highly specialized as podocytes leads us to assume that the axial organ at the junction of haemal and coelomic compartments primarily acts as an excretory structure.

The epithelium of the dorsal sac consists of a strong pseudostratified myoepithelium in the vicinity of the head process in *Psammechinus miliaris*. At least in the “regular” sea urchins ultrastructurally examined so far (Table 1), this can be stated as the common situation. The presence of axons inside the dorsal sac lining of asteroids (Bargmann & von Hehn 1968) clearly supports the assumption that the myoepithelial lining of the dorsal sac is a contractile component of the axial complex. Based on the “local heart-hypothesis” postulated for Asterozoa by Warnau & Jangoux (1992), we hypothesize that the echinoid dorsal sac may serve to spatially separate the contractions of the head process from the neighbouring body cavities. The fact that no podocytes were found lining the dorsal sac is in support of its complete disconnection from other coelomic cavities and the exterior.

The inner composition of the head process with its free cells and elastic fibers resembles that of the axial organ, allowing for the haemal fluid to pass unhindered. The distinct muscularization of the surrounding epithelium as well as the even macroscopically visible contractions in some species (e.g. Bamber 1921, Burton 1964, Boolootian *et al.* 1965, Millott 1966, Strenger 1973) corroborate the axial organ’s function as a local contractile organ. Since the haemal spaces inside the head process are directly connected to the gonadal haemal lacunae, the head process might serve to supply the aborally located gonads with nutrients. If so, enlargement of the digestive tract and reduction of the number of gonads should be accompanied by the reduction of haemal supply lacunae. This can in fact be observed in Spatangoida (DeRidder & Jangoux 1993). The remarkable amplification of the axial organ surface by involution clearly supports the assumption that substances in solution are being absorbed by large areas of the axial organ. This situation leads us to assume that components of all body fluids (haemal fluid and coelomic fluid) might interact inside the axial organ. In addition, the large number of haematocytes in the axial organ points to a removal of corpuscular wastes, such as foreign cells (e.g. bacteria) and cellular remnants of the animal itself. As the genomic analysis of *Strongylocentrotus purpuratus* has revealed the presence of many immune system-related genes (Sea Urchin Genome Sequencing Consortium 2006), it would clearly be interesting whether these exhibit a particularly pronounced expression within components of the axial complex.

### **Phylogenetic implications**

Based on the comparative morphological results, a number of characters can be inferred that are phylogenetically informative. However, since we believe all axial complex substructures (Table 2) to be present in all echinoid orders, no informative characters can be deduced from the presence or absence of these.

The overall form of the axial complex shape in lateral view differs considerably in sea urchin taxa and ranges from a straight aspect to a largely S-shaped form in the derived Micrasterina.

A further character that can be used with confidence is the orientation of the axial organ, being vertically oriented in most taxa and horizontally oriented in the Atelostomata only. The mesenteric suspension of the axial complex differs considerably among the observed taxa and clear-cut changes are observed between “regular” and irregular taxa with the free mesentery no longer being part of axial complex suspension in the latter. In addition, a successive reduction of the free mesentery can be observed in the “regular” taxa. The mesenteric suspension in *Micrasterina* further distinguishes this taxon from other Atelostomata with its enlarged mesenteric strand interconnecting the coils of the first gut loop.

A character for which extensive data are available is the composition of the stone canal. In the Atelostomata, the stone canal is tri-partite whereas all “regular” taxa observed so far possess a uniform stone canal. However, the conspicuous swelling observed in the oral part of the stone canal in *Holactypoida* and some “*Cassiduloida*” might hint at a sub-divided stone canal in these taxa as well. Here, more extensive histological examination is required. A further character involving the stone canal is its connection to the ring canal which is dilated in the basal echinoid taxa. Echinacea have presumably developed a single connection. However, the condition is not known in several basal “regular” (e.g. *Pedinoida*, *Aspidodiadematidae*) and irregular taxa (e.g. *Holactypoida*, “*Cassiduloida*”) as well as in the outgroup, *Holothuroidea*. Another character for which no sufficient data are available is the interesting aspect of the diverging distributional pattern of podocytes in *Cidaroida* and *Echinoidea*. To shed light on this phenomenon, extensive ultrastructural analyses are required.

In order to assess whether the above mentioned characters will lead to an extension of the morphological character matrix and thus to a refined echinoid phylogeny, a cladistic analysis based on these and further soft tissue characters is currently in preparation by members of our group. It remains to be determined whether the comparative analysis of further echinoid organs, such as the gut and its various appendages, will result in the recognition of additional features whose architecture is dependent on each other within the *Echinoidea*. However, the present study demonstrates that the type of approach employed here, i.e. to combine all available data on a given organ across a large number of taxa, long in use for hard-part anatomical structures, can be applied to internal organs as well and is very powerful in elucidating interdependent anatomical relationships that are not obvious when the analysis is carried out only with a few species.

## **Abbreviations**

CAS = California Academy of Sciences, San Francisco; MNHN = Muséum Nationale de la Histoire Naturelle, Paris; MRI = magnetic resonance imaging; NHM = Natural History Museum, London; ULB = Université Libre de Bruxelles; USNM = National Museum of Natural History, Washington, D.C.; ZMB = Systematische Zoologie am Museum für



Naturkunde, Berlin; ZMH = Zoologisches Institut und Museum, Hamburg; ZSM = Zoologische Staatssammlung, München.

## Acknowledgements

The authors are grateful to the staff of the Biologische Anstalt Helgoland for access to their facilities and for providing specimens. Nadia Améziane (MNHN), Andrew Cabrinovic (NHM), Carsten Lüter (ZMB), Rich Mooi (CAS), David Pawson (USNM), Bernhard Ruthensteiner (ZSM), and Andreas Schmidt-Rhaesa (ZMH) kindly supplied us with numerous sea urchin specimens from their collections. We thank Susanne Mueller (Charité-Universitätsmedizin, Berlin) for assistance with MR scanning. AZ was supported through a stipend of the Friedrich-Naumann-Stiftung für die Freiheit, Potsdam, Germany.

## References

- Agassiz A. 1872-1873. Revision of the Echini. Illustrated Catalogue of the Museum of Comparative Zoology 7
- Aiyar RG. 1938. Salmacis - The Indian sea urchin. In: Bahl KN, ed. *The Indian Zoological Memoirs on Indian Animal Types, Vol. 7*. Lucknow: Lucknow Publishing House
- Ax P. 2003. Echinodermata. In: *Multicellular animals, Vol. 3*. Heidelberg: Springer
- Bachmann S, Goldschmid A. 1978a. Fine structure of the axial complex of *Sphaerechinus granularis* (Lam.) (Echinodermata: Echinoidea). *Cell and Tissue Research* 193: 107-123
- Bachmann S, Goldschmid A. 1978b. Ultrastructural, fluorescence microscopic and microfluorimetric study of the innervation of the axial complex in the sea urchin, *Sphaerechinus granularis* (Lam.). *Cell and Tissue Research* 194: 315-326
- Bachmann S, Goldschmid A. 1980: The echinoid axial complex and Tiedemann bodies – the different pathways and accumulation sites of coelomocytes with regard to waste disposal in the organism. In: Jangoux M, ed. *Echinoderms: present & past*. Rotterdam: Balkema, 255-257
- Bachmann S, Pohla H, Goldschmid A. 1980. Phagocytes in the axial complex of the sea urchin, *Sphaerechinus granularis* (Lam.). *Cell and Tissue Research* 213: 10-120
- Balser EJ, Ruppert EE, Jaeckle WB. 1993. Ultrastructure of the coeloms of auricularia larvae (Holothuroidea: Echinodermata): evidence for the presence of an axocoel. *Biological Bulletin* 185: 86-96
- Balser EJ, Ruppert EE. 1993. Ultrastructure of axial vascular and coelomic organs in comasterid featherstars (Echinodermata: Crinoidea). *Acta Zoologica (Stockholm)* 74: 87-101

- Bamber RC. 1921. Note on some experiments on the water vascular system of *Echinus*. Proceedings of the Liverpool Biological Society 35: 64-70
- Bargmann W, von Hehn G. 1968. Über das Axialorgan („mysterious gland“) von *Asterias rubens* L. Zeitschrift für Zellforschung 88: 262-277
- Bartolomaeus T. 1994. On the ultrastructure of the coelomic lining in annelids, echiurids and sipunculids. Microfauna Marina 9: 171-220
- Bonnet A. 1925. Documents pour servir à l'étude de la variation chez les échinides. Bulletin de l'Institut Oceanographique a Monaco 462: 1-18
- Booolootian RA, Campbell JL. 1964. A primitive heart in the echinoid *Strongylocentrotus purpuratus*. Science 145: 173-175
- Booolootian RA, Bell A, Campbell JL. 1965. Fine structure of the "heart" of *Strongylocentrotus purpuratus* and *Strongylocentrotus dröbachiensis*. American Zoologist 5: 667A
- Booolootian RA, Campbell JL. 1966. The axial gland complex. Nature 212: 946-947
- Burton MPM. 1964. Haemal system of regular echinoids. Nature 204: 1218
- Carpenter PH. 1883. Notes on echinoderm morphology, No. VI. On the anatomical relations of the vascular system. Quarterly Journal of Microscopical Science 23: 597-616
- Carpenter PH. 1885. Notes on echinoderm morphology, No. IX. On the vascular system of the urchins. Quarterly Journal of Microscopical Science 25: 139-155
- Chadwick HC. 1900. *Echinus*. In: *Liverpool Marine Biology Committee Memoir III*. Liverpool: University Press
- Chadwick HC. 1923. *Asterias*. In: *Liverpool Marine Biology Committee Memoir XXV*. Liverpool: University Press
- Chesher RH. 1963. Contributions to the biology of *Meoma ventricosa* (Echinoidea: Spatangoida). Bulletin of Marine Science 19: 72-110
- Coe WR. 1912. Echinoderms of Connecticut. Connecticut State Geological and Natural History Survey Bulletin 19: 1-152
- Cuénot L. 1886. Sur les fonctions de la glande ovoïde, des corps de Tiedemann et des vésicules de Poli chez les Asterides. Comptes rendus de l'Académie des Science (Paris) 102: 1568-1569
- Cuénot L. 1891. Etudes morphologiques sur les échinodermes. Archives de Biologie (Paris, Bruxelles) 11: 303-680
- Cuénot L. 1948. Anatomie, Éthologie et Systématique des Echinodermes. In: Grassé, PP, ed. *Traité de Zoologie, Vol. 11*. Paris: Masson, 1-363
- De Ridder C, Jangoux M. 1993. The digestive tract of the spatangoid echinoid *Echinocardium cordatum* (Echinodermata): morphofunctional study. Acta Zoologica (Stockholm) 74: 337-351

- Erber W. 1983a. Der Steinkanal der Holothurien: Eine morphologische Studie zum Problem der Protocoelampulle. *Zeitschrift für Zoologische Systematik und Evolutionsforschung* 21: 217-234
- Erber W. 1983b. Zum Nachweis des Axialkomplexes bei Holothurien (Echinodermata). *Zoologica Scripta* 12: 305-313
- Farmanfarmaian A. 1968. The controversial echinoid heart and hemal system – function effectiveness in respiratory exchange. *Comparative Biochemistry and Physiology* 24: 855-863
- Fechter H. 1965. Über die Funktion der Madreporenplatte der Echinoidea. *Zeitschrift für vergleichende Physiologie* 51: 227-257
- Fechter H. 1972. Untersuchungen über den Wasserwechsel der Seeigel und seine Bedeutung für Atmung und Exkretion. *Helgoländer Meeresuntersuchungen* 23: 80-89
- Fechter H. 1973. Die stickstoffhaltigen Stoffwechselendprodukte und ihre Exkretion bei *Paracentrotus lividus*. *Marine Biology* 19: 162-172
- Fedotov DM. 1924. Zur Morphologie des axialen Organkomplexes der Echinodermen. *Zeitschrift für wissenschaftliche Zoologie* 123: 209-305
- Ferguson JC. 1996. Madreporite function and fluid volume relationships in sea urchins. *Biological Bulletin* 191: 431-440
- Gegenbaur C. 1859. *Grundzüge der vergleichenden Anatomie*. Leipzig: Engelmann
- Greeff R. 1872. Über den Bau der Echinodermen. *Sitzungsberichte der Gesellschaft zur Beförderung der Naturwissenschaften zu Marburg* 10: 158-172
- Hamann O. 1885. Die Asteriden, anatomisch und histologisch untersucht. In: *Beiträge zur Histologie der Echinodermen, Heft 2*. Jena: Fischer, 1-126
- Hamann O. 1887. Anatomie und Histologie der Echiniden und Spatangiden. In: *Beiträge zur Histologie der Echinodermen, Heft 3*. Jena: Fischer, 1-176
- Hartog M. 1887. The true nature of the madreporic system of Echinodermata, with remarks on nephridia. *Annual Magazine of Natural History* 20: 321-326
- Heider K. 1912. Über Organverlagerungen bei der Echinodermen-Metamorphose. *Verhandlungen der Deutschen Zoologischen Gesellschaft* 22: 239-251
- Hoffmann CK. 1871. Zur Anatomie der Echinen und Spatangen. *Niederländisches Archiv für Zoologie* 1: 11-112
- Holland ND. 1970. The fine structure of the axial organ of the feather star, *Nemaster rubiginosa* (Echinodermata: Crinoidea). *Tissue & Cell* 2: 625-636
- Huxley TH. 1878. Echinodermata. In: *A manual of the anatomy of invertebrated animals*. London: Churchill, 466-509
- Hyman LH. 1955. IV. Echinodermata. In: *The invertebrates*. New York: McGraw-Hill.

- Jangoux M, Schaltin P. 1977. Le complexe axial de *Psammechinus miliaris* (Gmelin) (Echinodermata, Echinoidea). Archives de Zoologie Experimentale et Générale 118: 285-303
- Jensen M. 1981. Morphology and classification of Euechinoidea Bronn, 1860 – a cladistic analysis. Videnskabelige Meddelelser fra Dansk Naturhistorisk Forening i Kjobenhavn 143: 7-99
- Jensen M. 1988. Functional morphology and systematics of spatangoids (Euechinoidea). In: Burke RD *et al.*, eds. *Echinoderm Biology*. Rotterdam: Balkema, 327-335
- Jourdain S. 1867. Recherches sur l'appareil circulatoire de l'étoile de mer commune (*Asteracanthion rubens*). Comptes rendus de l'Académie des Science (Paris) 65: 1002-1004
- Kaburek M, Hilgers H. 1999. The axial-hydrocoel complex of the endemic Mediterranean heart urchin *Schizaster canaliferus* (Echinoida: Spatangoida). In: Candia Carnevali MD, Bonasoro F, eds. *Echinoderm Research 1998*. Rotterdam: Balkema, 15-20
- Koehler R. 1883. Recherches sur les échinides des côtes de Provence. In: *Annales du Musée d'Histoire Naturelle Marseille – Zoologie, Tome 1, Memoire No. 3*. 1-167
- Larson MK & Bayne CJ 1994. Evolution of immunity: potential immunocompetence of the echinoid axial organ. Journal of Experimental Zoology 270: 474-485
- Leipoldt F. 1893. Das angebliche Exkretionsorgan der Seeigel, untersucht an *Sphaerechinus granularis* und *Dorocidaris papillata*. Zeitschrift für wissenschaftliche Zoologie 55: 4-50
- Leydig F. 1854. Kleinere Mitteilungen zur tierischen Gewebelehre. In: Müller JP, ed. *Archiv für Anatomie, Physiologie und wissenschaftliche Medicin*. Berlin: Veit
- Littlewood DTJ, Smith AB. 1995. A combined morphological and molecular phylogeny for sea urchins (Echinoidea: Echinodermata). Philosophical Transactions of the Royal Society B Biological Sciences 347: 213-234
- Littlewood DTJ, Smith AB, Clough KA, Emson RH. 1997. The interrelationships of the echinoderm classes: morphological and molecular evidence. Biological Journal of the Linnean Society 61: 409-438
- Ludwig H. 1877. Beiträge zur Anatomie der Crinoideen. Zeitschrift für Wissenschaftliche Zoologie 28: 255-353
- Ludwig H. 1878. Beiträge zur Anatomie der Asteriden. Zeitschrift für Wissenschaftliche Zoologie 30: 98-162
- Ludwig H. 1890. Über die Function der Madreporenplatte und des Steincanals der Echinodermen. Zoologischer Anzeiger 13: 377-379
- Ludwig H, Hamann O. 1904. Die Seeigel. In: *Dr. H. G. Bronn's Klassen und Ordnungen des Thier-Reichs. Band 2, Abtheilung 3, Buch 4*. Leipzig: C.F. Winter'sche Verlagshandlung

- MacBride EW. 1903. The development of *Echinus esculentus*, together with some points in the development of *E. miliaris* and *E. acutus*. Philosophical Transactions of the Royal Society of London Series B 195: 285-327
- Millott N. 1964. Axial organ and fluid circulation in echinoids. Nature 204: 1216-1217.
- Millott N. 1966. A possible function for the axial organ of echinoids. Nature 209: 594-596
- Millott N. 1967. The axial organ of echinoids, re-interpretation of its structure and function. Symposia of the Zoological Society of London 20: 53-63
- Millott N. 1969. Injury and the axial organ of echinoids. Experientia (Basel) 25: 756-757
- Millott N, Farmanfarmaian A. 1967. Regeneration of the axial organ of *Arbacia punctulata* and its implications. Nature 216: 1136-1138
- Millott N, Vevers HG. 1964. Axial organ and fluid circulation in echinoids. Nature 204: 1216-1217
- Millott N, Vevers HG. 1967. The morphology and histochemistry of the echinoid axial organ. Philosophical Transactions of the Royal Society B 253: 201-230
- Mooi R. 1990. Paedomorphosis, Aristotle's lantern, and the origin of the sand dollars (Echinodermata: Clypeasteroidea). Paleobiology 16: 25-48
- Mortensen T. 1907. Echinoidea, Part 2. In: *The Danish Ingolf-Expedition 4*. 1-200
- Mortensen T. 1928-1951. A Monograph of the Echinoidea. Copenhagen: Reitzel
- Müller J. 1854. Über den Bau der Echinodermen. Abhandlungen der Preussischen Akademie der Wissenschaften, Berlin 44: 123-219
- Narasimhamurti N. 1931. The development and function of the heart and pericardium in Echinodermata. Proceedings of the Royal Society of London, Series B 764: 471-487
- Perrier E. 1875. Recherches sur l'appareil circulatoire des oursins. Archives de Zoologie Experimentale et Générale 4: 605-643
- Perrier E. 1887. Sur le corps plastidogene ou pretendu coeur des Echinodermes. Comptes rendus de l'Académie des Science (Paris) 104: 180-182
- Pietschmann V. 1906. Zur Kenntnis des Axialorgans und der ventralen Bluträume der Asteriden. Arbeiten des Zoologischen Institutes in Wien 16: 5-24
- Prouho H. 1887. Recherches sur le *Dorocidaris papillata* et quelques autres échinides de la Méditerranée. Archives de Zoologie Expérimentale et Générale 5: 213-380
- Rehkämper G, Welsch U. 1988. Functional morphology of the stone canal in the sea urchin *Eucidaris* (Echinodermata: Echinoidea). Zoological Journal of the Linnean Society 94: 259-269
- Rieger RM, Purschke G. 2005. The coelom and the origin of the annelid body plan. Hydrobiologia 535: 127-137

- Ruppert EE. 1991. Introduction to the aschelminth phyla: a consideration of mesoderm, body cavities, and cuticle. In: Harrison FW, Ruppert EE, eds. *Microscopic Anatomy of Invertebrates, Vol. 4*. New York: Wiley-Liss, 1-17
- Ruppert EE, Balser EJ. 1986. Nephridia in the larvae of hemichordates and echinoderms. *Biological Bulletin* 171: 188-196
- Ruppert EE, Smith PR. 1988. The functional organization of filtration nephridia. *Biological Reviews* 63: 231-258
- Sarasin P, Sarasin F. 1887. Ueber die Anatomie der Echinothuriden und die Phylogenie der Echinodermen. In: *Ergebnisse naturwissenschaftlicher Forschungen auf Ceylon. Band I, Heft 3*. Wiesbaden: Kreidel`s
- Schinke H. 1951. Bildung und Ersatz der Zellelemente der Leibeshöhlenflüssigkeit von *Psammechinus miliaris* (Echinoidea). *Zeitschrift für Zellforschung* 35: 311-331
- Schurig W. 1906. Anatomie der Echinothuriden. In: Chun C, ed. *Wissenschaftliche Ergebnisse der deutschen Tiefsee-Expedition auf dem Dampfer „Valdivia“ 1898-1899. Fünfter Band, dritte Lieferung*. Jena: Fischer
- Sea Urchin Genome Sequencing Consortium. 2006. The genome of the sea urchin *Strongylocentrotus purpuratus*. *Science* 314: 941-952
- Sharpey W. 1836. Echinodermata. In: Todd RB, ed. *Cyclopaedia of Anatomy and Physiology, Vol. 2*. London: Sherwood, Gilbert & Piper, 30-46
- Smith AB. 2005. The Echinoid Directory. World Wide Web electronic publication. <http://www.nhm.ac.uk/palaeontology/echinoids> [accessed: June - October 2008]
- Smith AB, Pisani D, Mackenzie-Dodds JA, Stockley B, Webster BL, Littlewood DTJ. 2006. Testing the molecular clock: molecular and paleontological estimates of divergence times in the Echinoidea (Echinodermata). *Molecular Biology and Evolution* 23: 1832-1851
- Spirlet C, Gosselin P, Jangoux M. 1999. The structure of the axial complex of *Paracentrotus lividus* (Echinodermata: Echinoidea) at the end of post-larval life. In: Candia Carnevali MD, Bonasoro F, eds. *Echinoderm Research 1998*. Rotterdam: Balkema, 229A
- Stach T. 2002. Minireview: on the homology of the protocoel in Cephalochordata and “lower” Deuterostomia. *Acta Zoologica (Stockhom)* 83: 25-31
- Stockley B, Smith AB, Littlewood T, Lessios HA, Mackenzie-Dodds J. 2005. Phylogenetic relationships of spatangoid sea urchins (Echinoidea): taxon sampling density and congruence between morphological and molecular estimates. *Zoologica Scripta* 34: 447-468
- Stott FC. 1955. The food canal of the sea-urchin *Echinus esculentus* L. and its functions. *Proceedings of the Zoological Society London* 125: 63-86

- Strenger A. 1973. *Sphaerechinus granularis* (Violetter Seeigel), Anleitung zur makroskopischen und mikroskopischen Untersuchung. In: Siewing R, ed. *Großes Zoologisches Praktikum, Band 18*. Stuttgart: Fischer, 1-68
- Tiedemann F. 1816. Anatomie der Röhren-Holothurie (*Holothuria tubulosa*), des Pomerantzfarbigen Seesterns (*Astropecten aurantiacus*) und des Stein-Seeigels (*Echinus saxatilis*). Landshut: Joseph Thomannsche Buchdruckerei, Verlag der Landshuter Zeitung, 1-98
- Teuscher R. 1876. Beiträge zur Anatomie der Echinodermen. *Jenaische Zeitschrift für Medizin und Naturwissenschaften* 10: 493-528
- Valentin GG. 1841. Anatomie du genre *Echinus*. In: Agassiz L, ed. *Livraison des Monographies d' Echinodermes vivants et fossiles*. Neuchatel: Petitpierre, 1-126
- Vevers HG. 1967. The histochemistry of the echinoid axial organ. *Symposia of the Zoological Society of London* 20: 65-74
- Vogt KC, Yung E. 1888. Echinodermata. In: *Lehrbuch der praktischen Vergleichs-Anatomie*. Braunschweig: Vieweg, 581-618
- von Ubisch L. 1913. Die Entwicklung von *Strongylocentrotus lividus*. (*Echinus microtuberculatus*, *Arbacia pustulosa*). *Zeitschrift für wissenschaftliche Zoologie* 106: 409-448
- Wagner J. 1903. Anatomie des *Palaeopneustes niasicus*. In: Chun C, ed. *Wissenschaftliche Ergebnisse der Deutschen Tiefsee-Expedition auf dem Dampfer „Valdivia“ 1898-1899. Fünfter Band, erste Lieferung*. Jena: Fischer
- Warnau M, Jangoux M. 1992. Fine structure of the upper part of the axial complex (head process and dorsal sac) in the asteroid *Asterias rubens* L. (Echinodermata). In: Scalera Liaci L, Canicatti C, eds. *Echinoderm Research 1991*. Rotterdam: Balkema, 53-57
- Welsch U, Rehkämper G. 1987. Podocytes in the axial organ of echinoderms. *Journal of Zoology (London)* 213: 45-50
- Westergren AM. 1911. Echinoneus and Micropetalon. In: *Echini. Reports on the scientific results of the expedition „Albatross“*. *Memoirs of the Museum of Comparative Zoology Volume 39, No. 2*
- Ziegler A, Angenstein F. 2007. Analyse von Seeigeln (Echinoidea) mit Hilfe der bildgebenden Magnetresonanztomographie. *Mikrokosmos* 96: 49-54
- Ziegler A, Faber C, Mueller S, Bartolomaeus T. 2008. Systematic comparison and reconstruction of sea urchin (Echinoidea) internal anatomy: a novel approach using magnetic resonance imaging. *BMC Biology* 6: 33

## Figure legends

Figure 1. Current understanding of sea urchin phylogeny. The hypotheses of echinozoan and echinoid relationships are based on multiple sources of morphological and molecular datasets (see Material and Methods section for references). This tree has not been generated using a consensus or numerical technique and reflects the views and biases of the authors.

Figure 2. Semi-schematic representation of the apical region in interradius CD of *Sphaerechinus granularis* (Echinoidea) showing madreporic plate, ring canal, axial complex, and rectum [after Leipoldt (1893) and Strenger (1973), modified]. Aboral haemal ring, Aristotle's lantern, gonads, gonoducts, and Tiedemann's (or spongy) bodies not shown. Not to scale.

Figure 3. Vertical magnetic resonance imaging (MRI) sections of various sea urchin specimens depicting the axial complex (arrow). A *Cidaris cidaris* (Cidaroida). B *Caenopedina mirabilis* (Pedinoida). C *Plesiadiadema indicum* (Aspidodiadematidae). D *Salenocidaris hastigera* (Salenoida). E *Strongylocentrotus purpuratus* (Echinoidea). F *Lytechinus variegatus* (Echinoidea). G *Genocidaris maculata* (Temnopleuroidea). H *Echinoneus cyclostomus* (Holectypoida). I *Cassidulus caribearum* ("Cassiduloida"). J *Echinolampas depressa* ("Cassiduloida"). K *Echinarachnius parma* (Clypeasteroida). Table 1 lists isotropic resolutions for each MRI dataset.

Figure 4. Horizontal magnetic resonance imaging (MRI) sections of various sea urchin specimens at the level of gonads and upper digestive tract, and axial complex (arrow). Note the differing mesenterial suspensions of the axial complex. A *Cidaris cidaris* (Cidaroida). B *Eucidaris metularia* (Cidaroida). C *Caenopedina mirabilis* (Pedinoida). D *Aspidodiadema hawaiiense* (Aspidodiadematidae). E *Strongylocentrotus purpuratus* (Echinoidea). F *Lytechinus variegatus* (Echinoidea). G *Mespilia globulus* (Temnopleuroidea). H *Echinoneus cyclostomus* (Holectypoida). Table 1 lists isotropic resolutions for each MRI dataset.

Figure 5. Schematic representation of the gross morphology of the axial complex in various higher sea urchin taxa. All other internal organs have been omitted, the ring canal is depicted in part only, and the anus is not shown. The gray-scale legend denominates every structure shown.

Figure 6. Schematic representation of the mesenterial suspension of the echinoid axial complex in various higher sea urchin taxa and the impact of the gastric caecum (gc) on the architecture of the axial complex. Upper three lines: dorso-ventral mesentery always depicted on the right-hand side. Dashed lines indicate course of the oesophagus or the axial complex (Micrasterina). Lower line: Ventral view of the digestive tract and the axial complex in the



vicinity of the oesophagus of highly derived irregular sea urchin taxa (Atelostomata) – note the extension of the mesentery. The gray-scale legend denominates every structure shown.

Figure 7. Horizontal light-microscopic sections through the axial complex. A, B *Eucidaris tribuloides* (Cidaroida); C, D *Diadema setosum* (Diadematidae); E, F *Psammechinus miliaris* (Echinoida); G, H *Echinocyamus pusillus* (Clypeasteroida). Left column: section at the level of head process and dorsal sac. Right column: section at the level of axial organ and axial coelom. ac = axial coelom, ao = axial organ, dm = dorso-ventral mesentery, ds = dorsal sac, fm = free mesentery, go = gonad, hp = head process, ma = madreporic ampulla, oe = oesophagus, pv = pulsating vessel, re = rectum, sc = stone canal, so = somatocoel.

Figure 8. Schematic representation of the axial complex at the level of head process and dorsal sac based on light-microscopic sections. Note that although changes in shape do occur, the internal composition remains largely the same. For better comparison, the stone canal is shown towards the top of each image. The gray-scale legend denominates every structure shown.

Figure 9. Schematic representation of the axial complex at the level of axial organ and axial coelom based on light-microscopic sections. Note that although changes in shape do occur, the internal composition remains largely the same. For better comparison, the stone canal is depicted towards the top of each image. The gray-scale legend denominates every structure shown.

Figure 10. Horizontal electron-microscopic sections of the axial complex. A-D *Psammechinus miliaris* (Echinoida) and E, F *Echinocardium cordatum* (Micrasterina). A Dorsal sac epithelium with myoepithelial cells. B Heavily ciliated canaliculus inside the axial organ. C Axial coelom epithelium with podocyte and haemal lacunae. D Somatocoelomic epithelium. E Axial coelom epithelium with podocyte and haemal lacunae. F Heavily ciliated canaliculus inside the axial organ. ac = axial coelom, aj = adhaerens junctions, bl = basal lamina, cf = collagenous fibers, ci = cilium, cm = circumciliary microvillum, ds = dorsal sac, ec = epithelial cell, hl = haemal lacuna, mf = myofibrils, mv = microvillum, nu = nucleus, pe = pedicel, po = podocyte, so = somatocoel.

Figure 11. Schematic representation of sections through the axial complex of *Sphaerechinus granularis* (Echinoida). A Horizontal section through the echinoid axial complex at the level of head process and dorsal sac. B Horizontal section through the echinoid axial complex at the level of the axial organ. The insert between A and B (compare Fig. 2) roughly outlines where the virtual sections were made. C Schematic representation of the columnar epithelium of the stone canal. D Schematic representation of the flat epithelium of the somatocoel. E

Schematic representation of the myoepithelium that lines head process and pulsating vessel. F Schematic representation of the specialized epithelium with podocytes found in the axial coelom. ac = axial coelom, ao = axial organ, bl = basal lamina, ca = canaliculus, ci = cilium, ct = connective tissue, dm = dorso-ventral mesentery, ds = dorsal sac, ec = epithelial cell, fm = free mesentery, hl = haemal lacuna, hp = head process, pv = pulsating vessel, sc = stone canal, so = somatocoel.

### Table legends

Table 1. List of species included in this study. Systematic classification based on current hypotheses. The table provides information on every species studied so far with regard to the axial complex, the method(s) used to infer axial complex anatomy from this and older studies, the specimen ID of museum specimens where applicable, and the respective references. Numbers in brackets behind “MRI” represent the isotropic resolution of the dataset. An overview of scanning parameters is provided by Ziegler *et al.* (2008).

Table 2. Definition of technical terms assigned to the axial complex of echinoids used in this manuscript in terms of body cavity involved, developmental origin, and topography. A primary body cavity is always lined by extracellular matrix, whereas a secondary body cavity is lined by a mesothel (i.e. mesodermally derived epithelium). Axocoel = proto-coel, hydrocoel = mesocoel, somatocoel = metacoel (Heider 1912).

Table 3. Trilingual list of technical terms that have been used so far in publications dealing with the echinoid (as well as echinoderm) axial complex including madreporic plate and madreporic pore canals. The terms used in this study are printed in bold. The author(s) that first established a certain term appear after it in brackets. Where no reference is provided, the creator (author) of the respective term could not be identified with certainty.

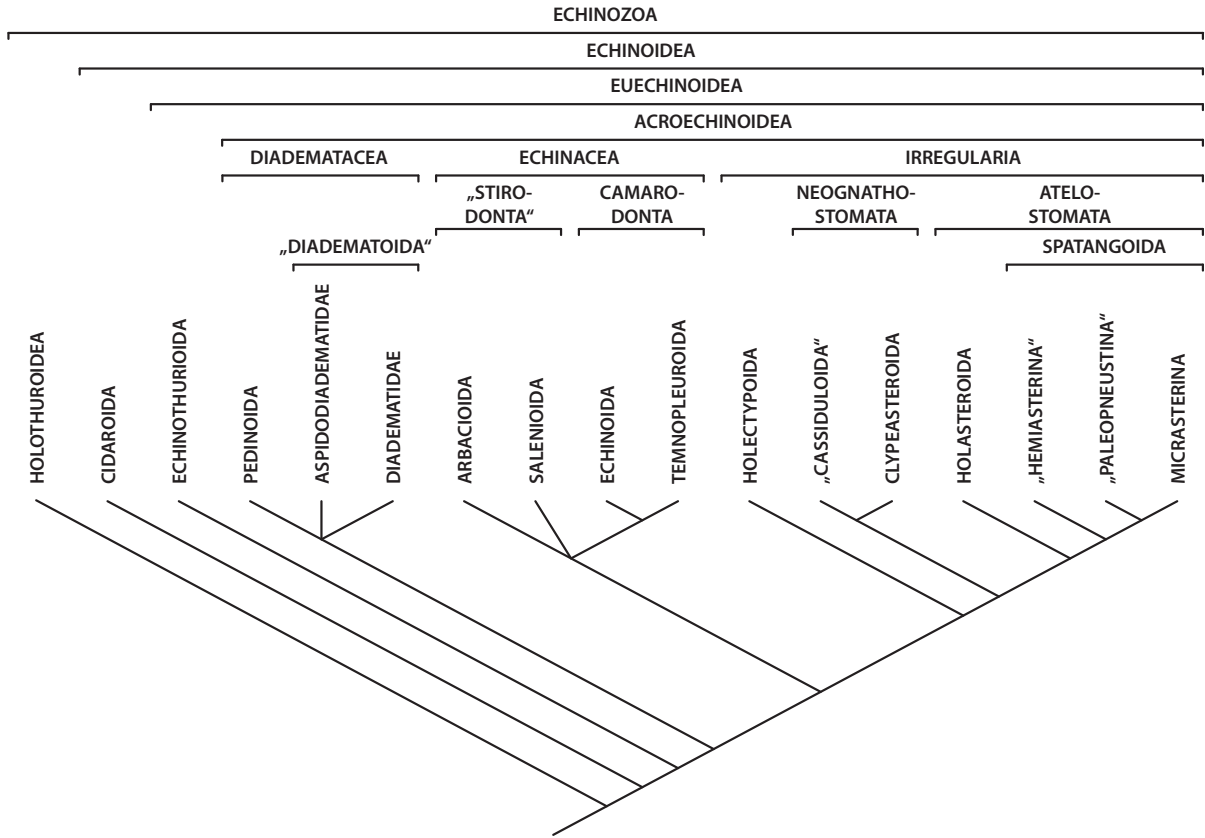


Figure 1

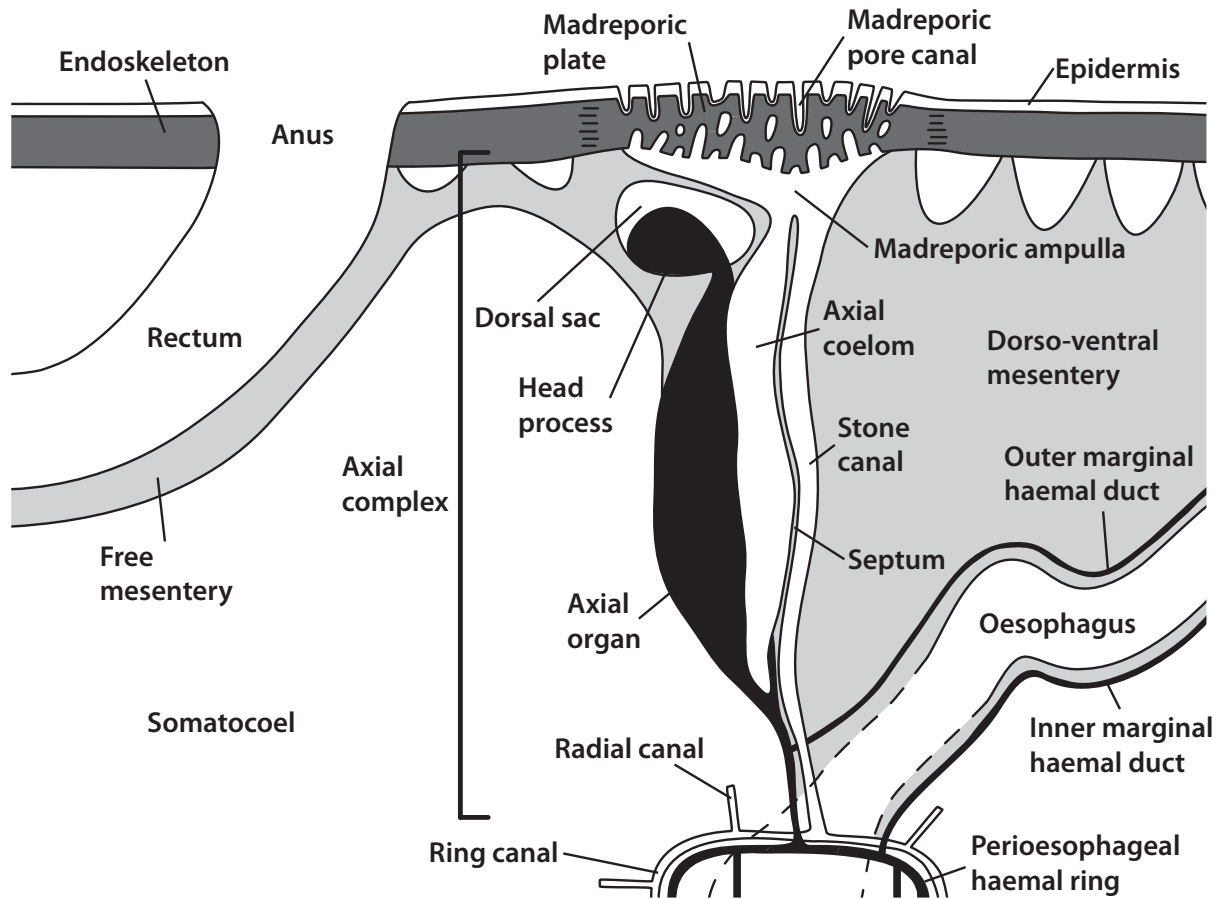


Figure 2

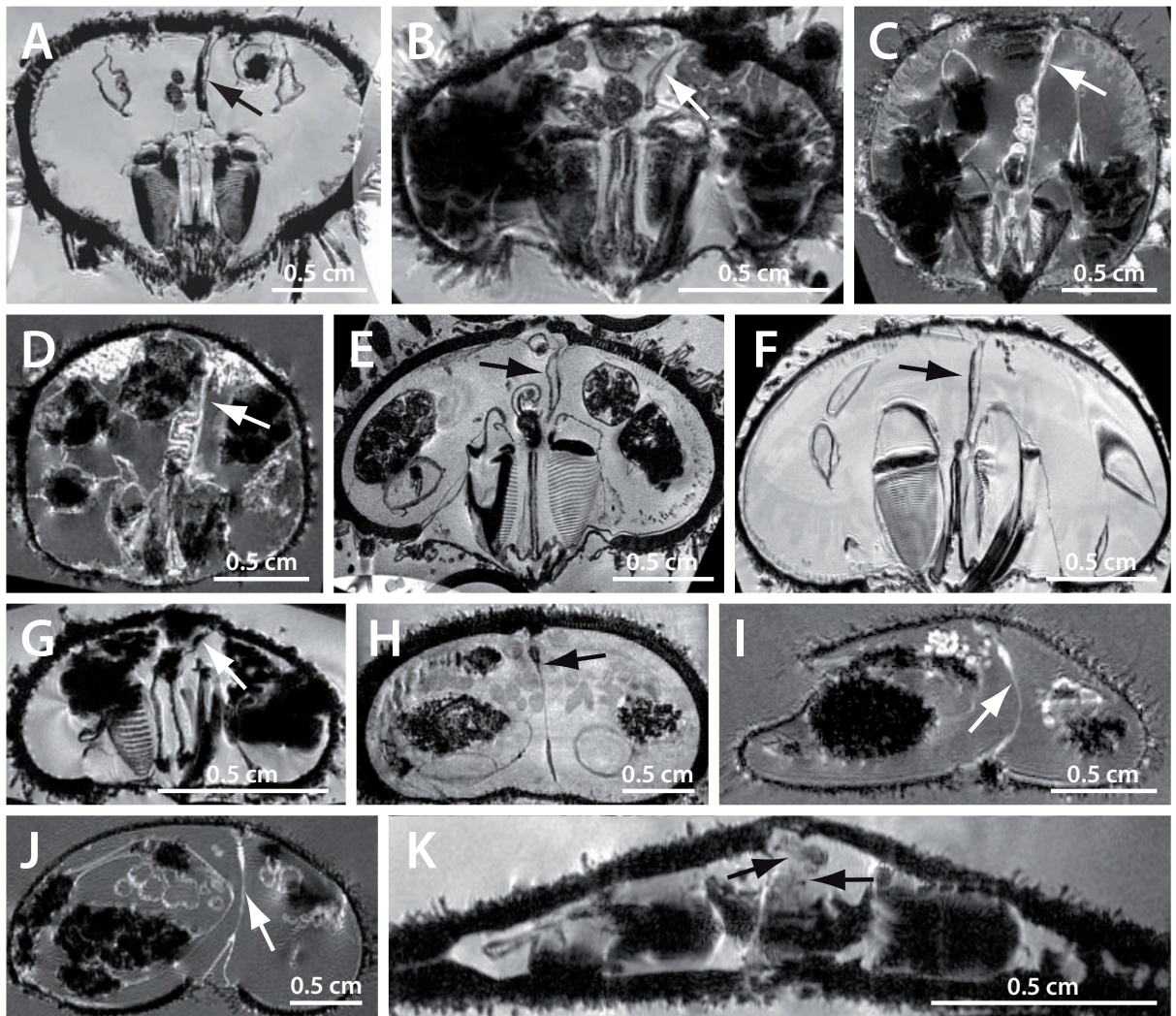


Figure 3

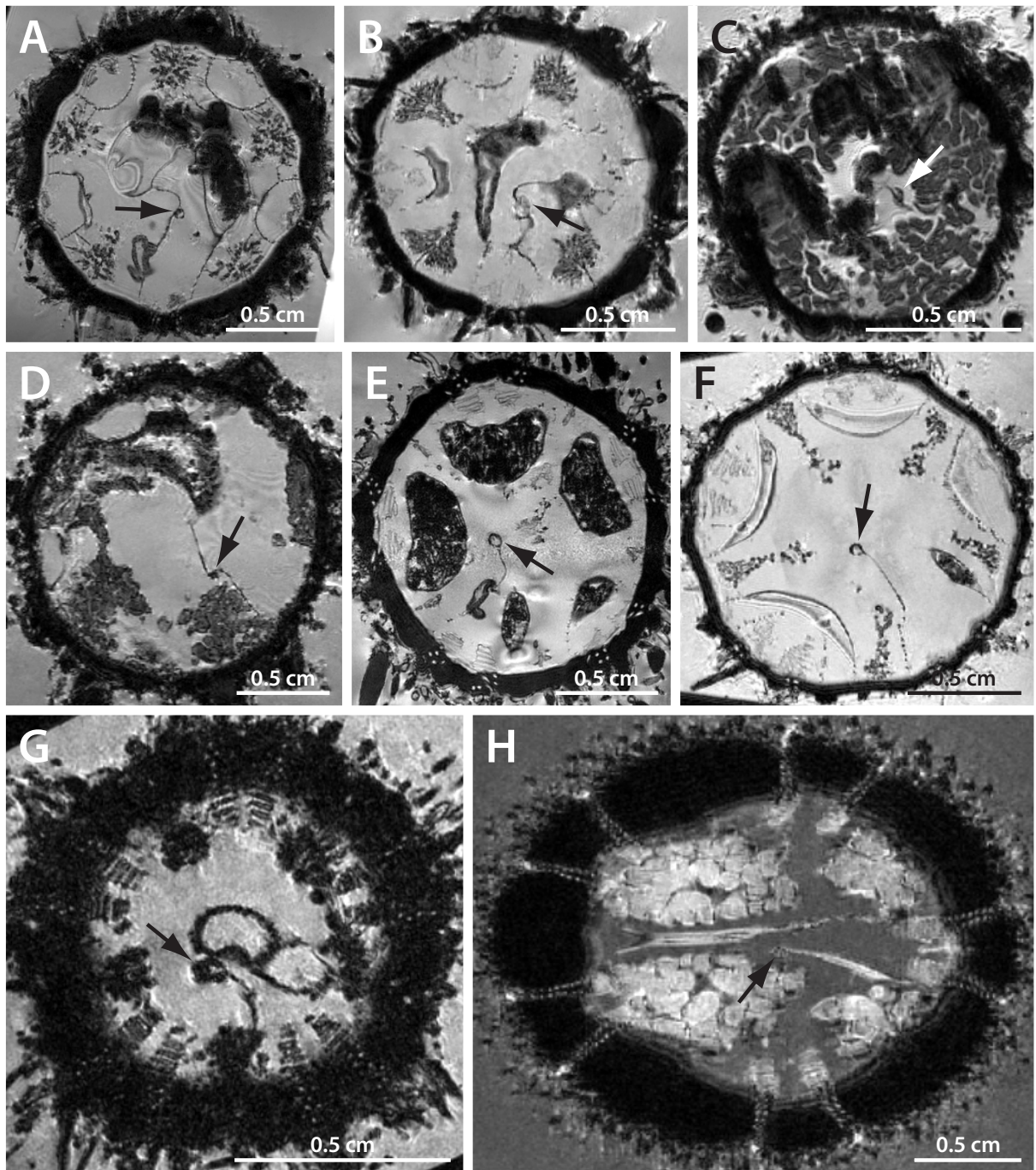
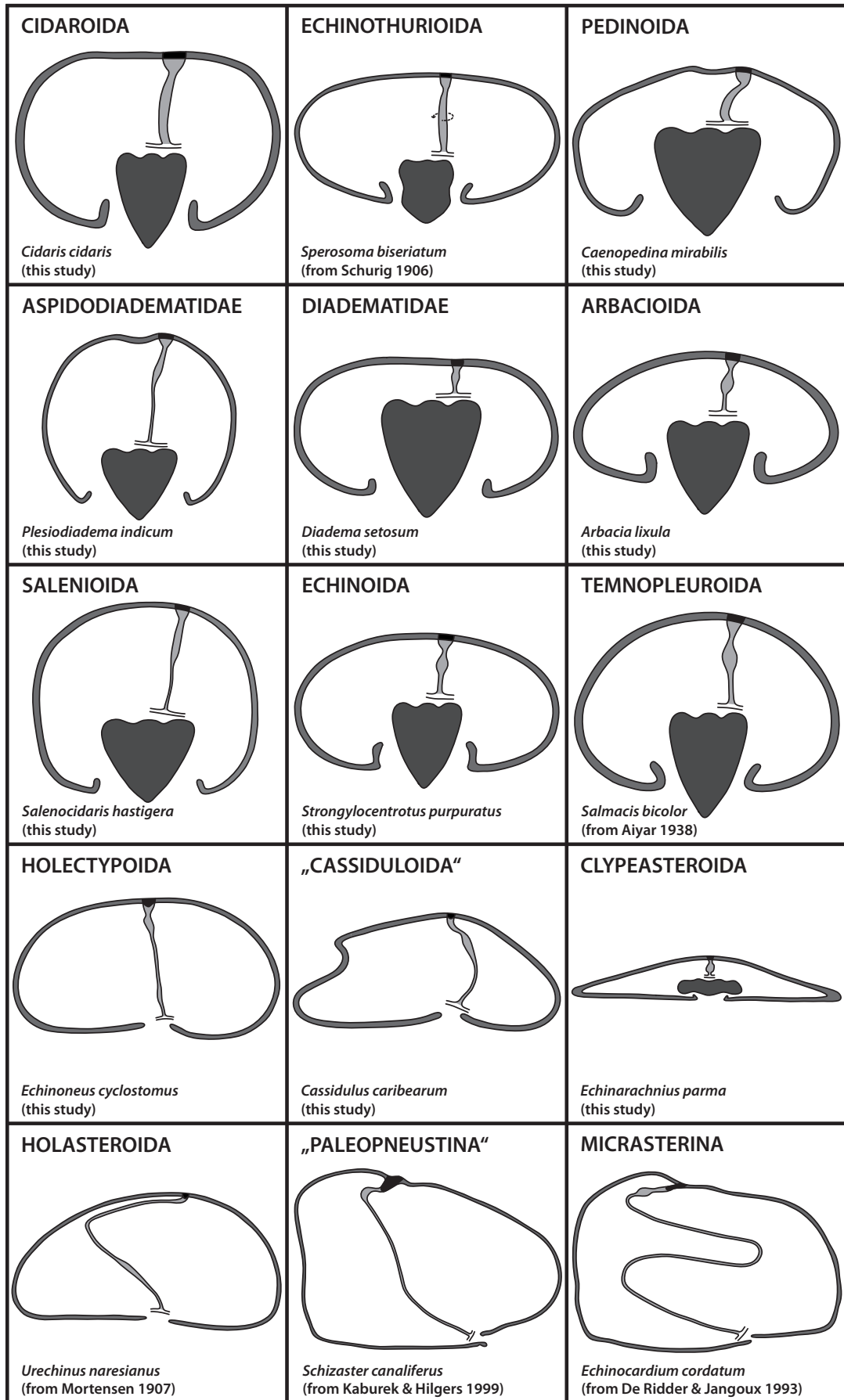


Figure 4



Madreporic plate
  Aristotle's lantern
  Endoskeleton
  Axial complex

Figure 5

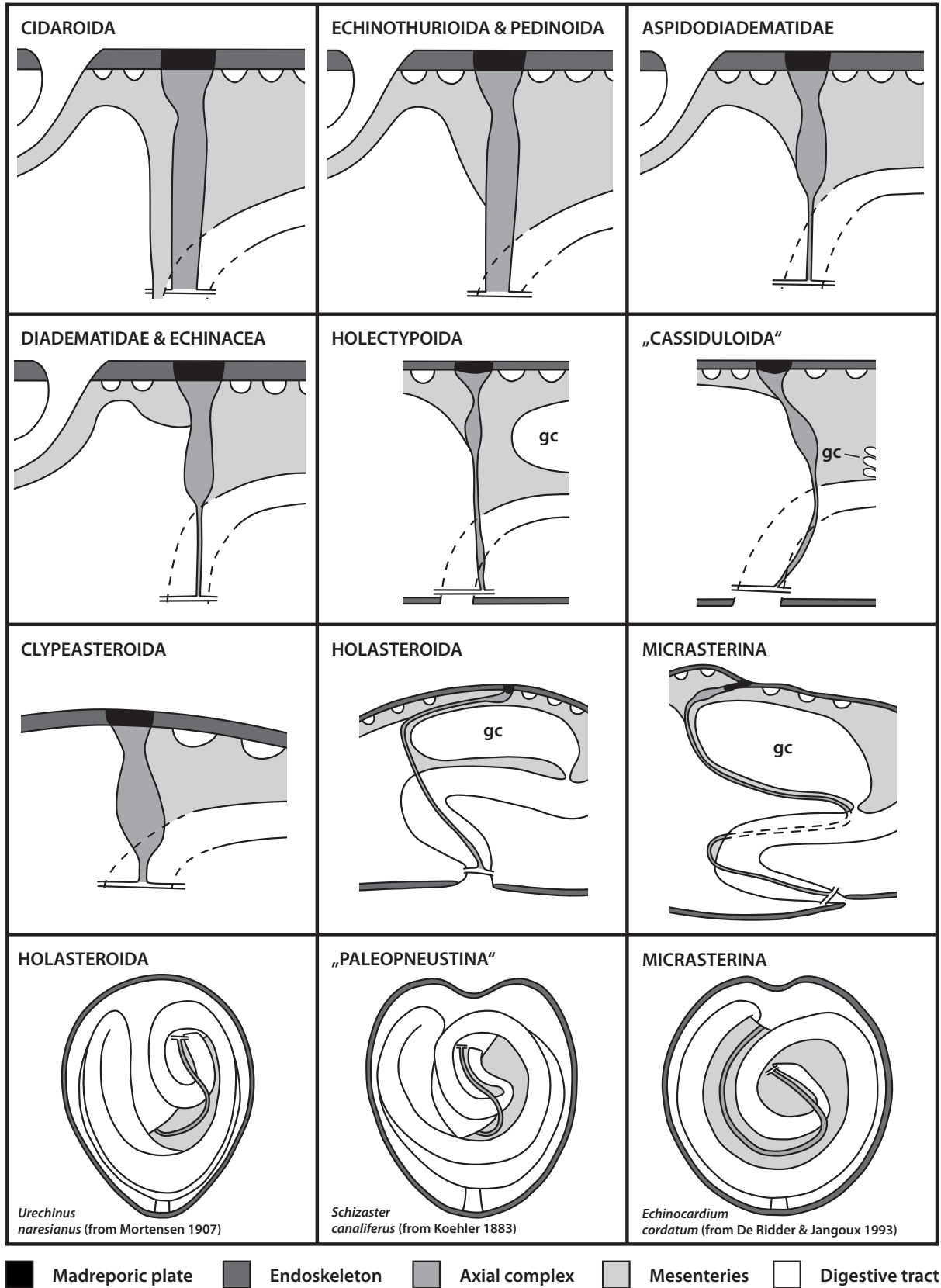


Figure 6



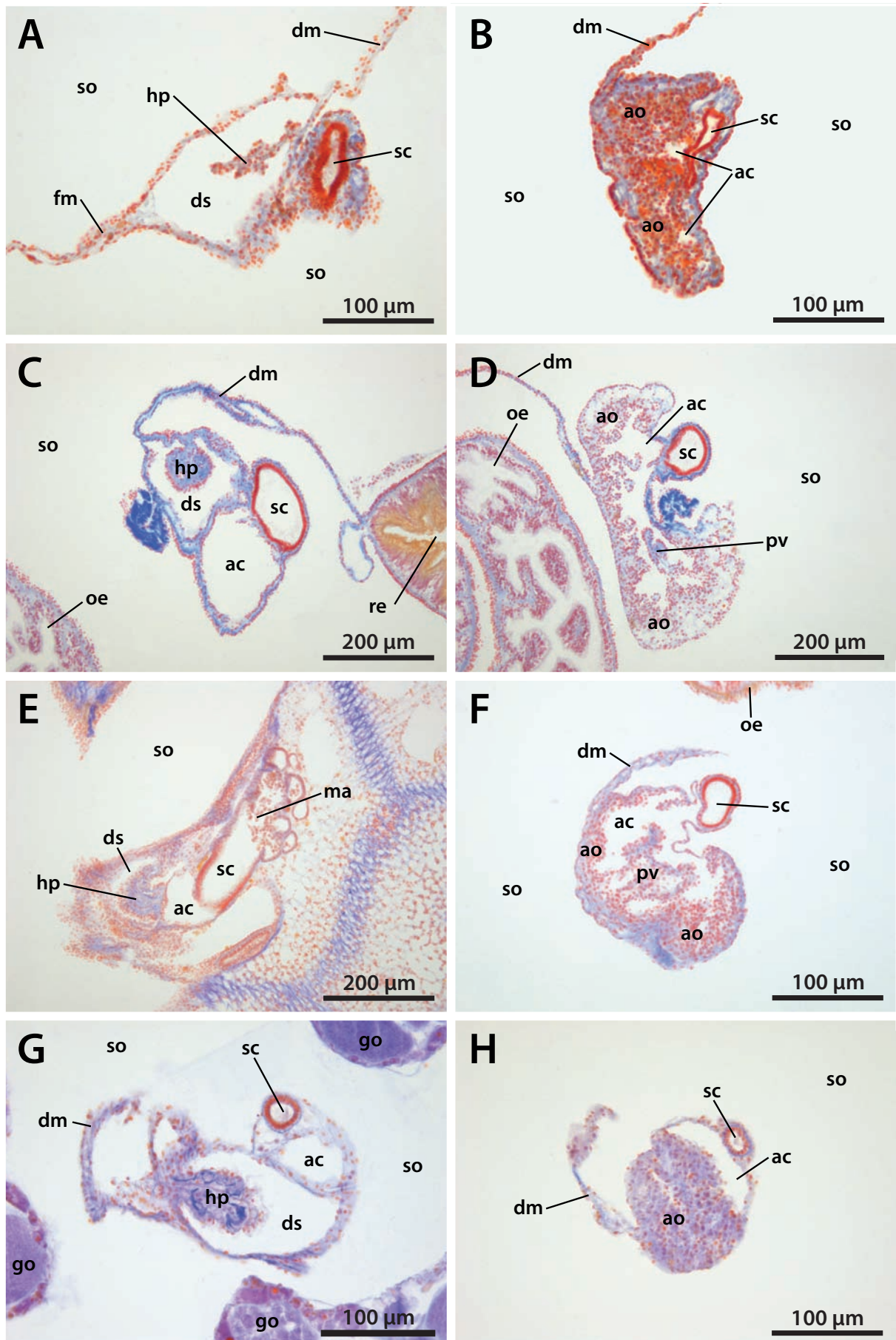


Figure 7

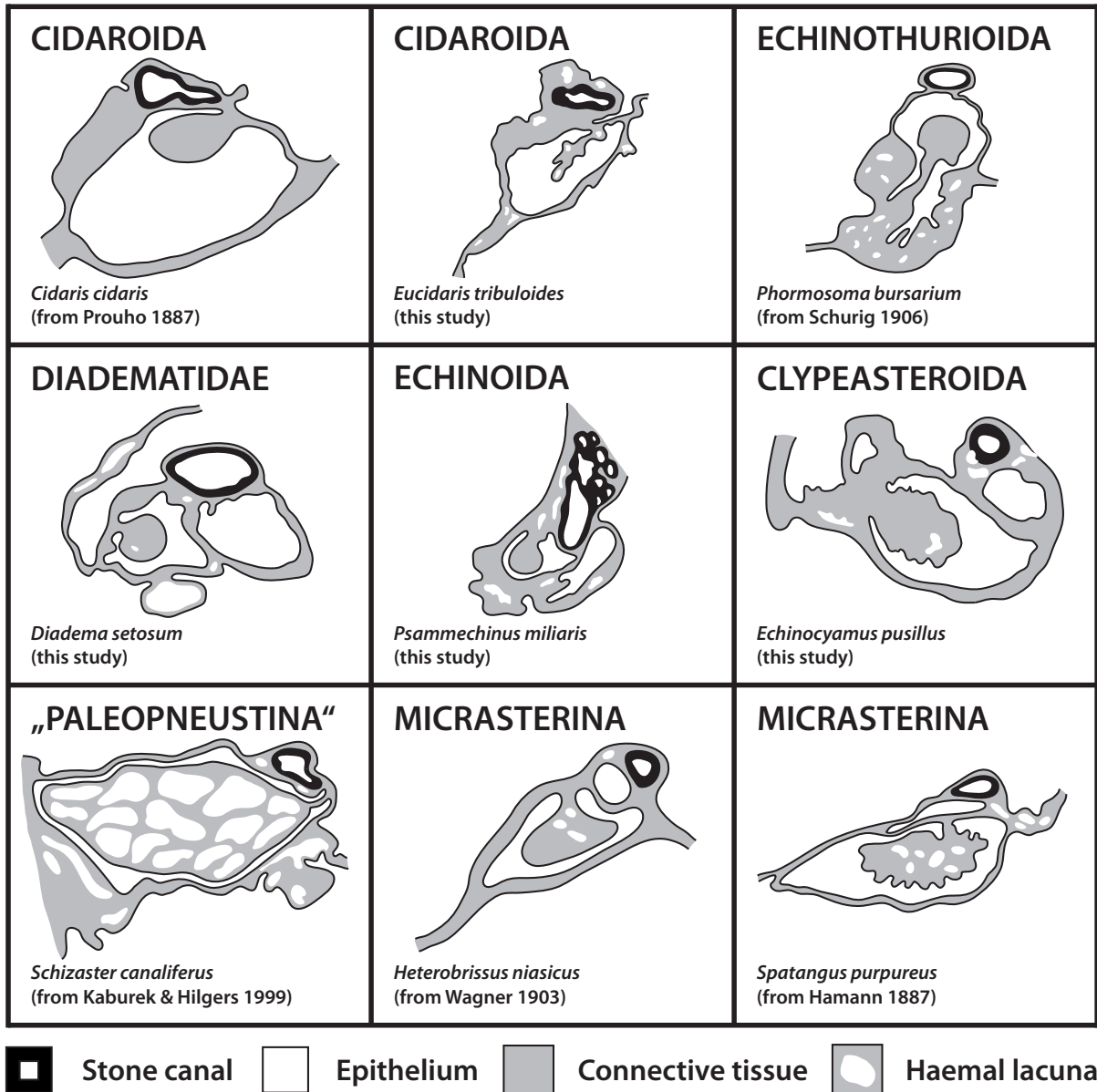


Figure 8

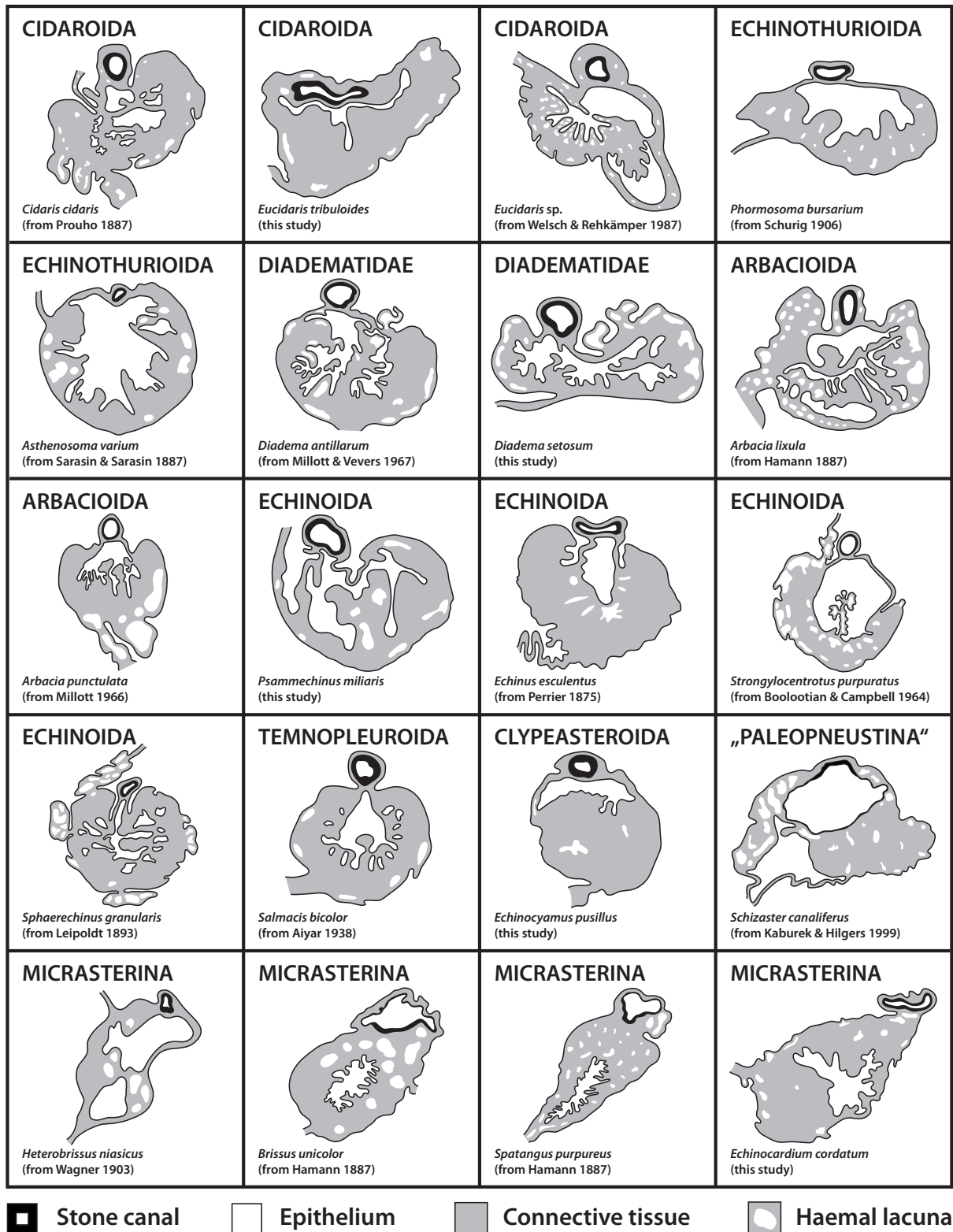


Figure 9

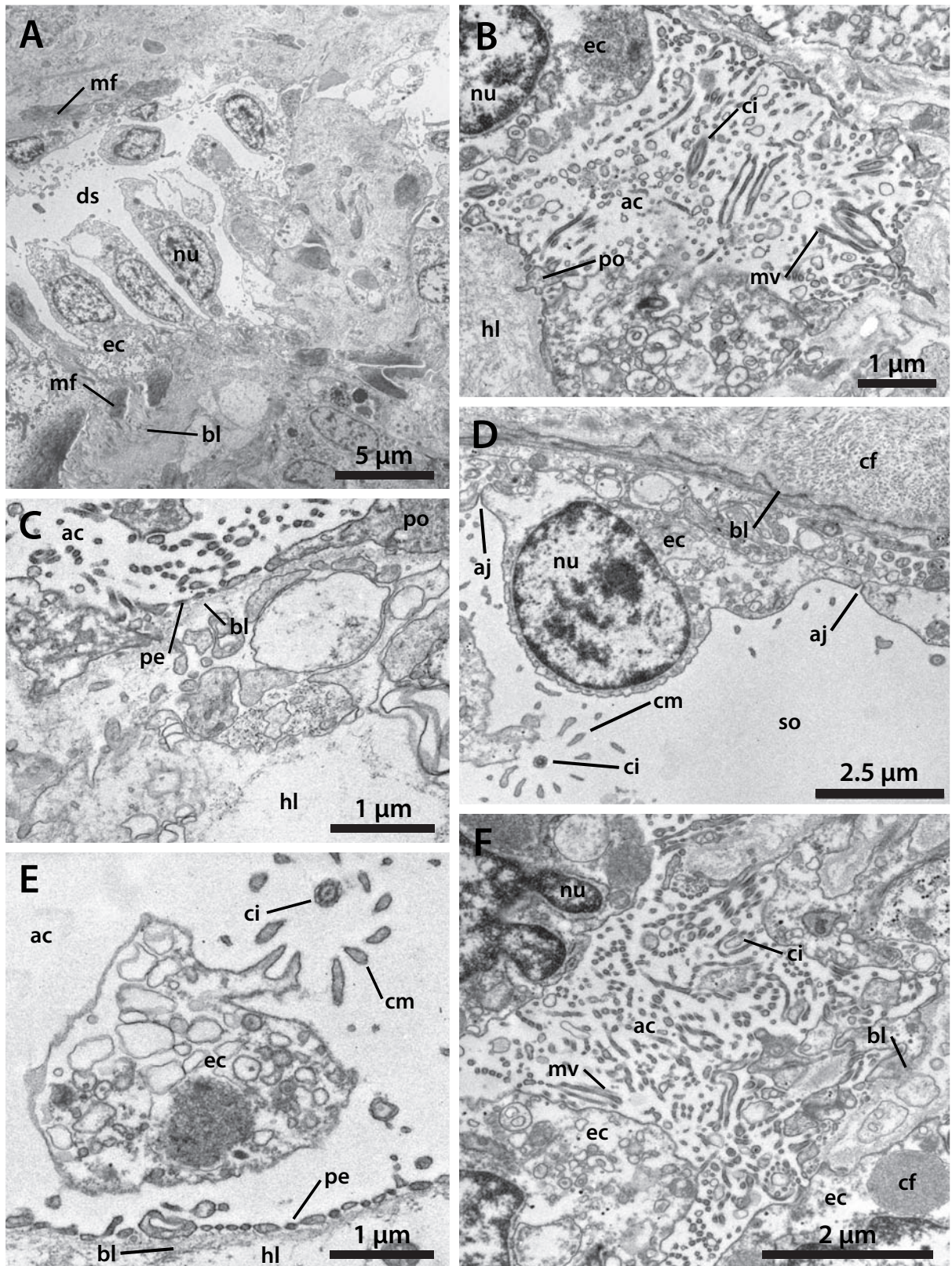


Figure 10

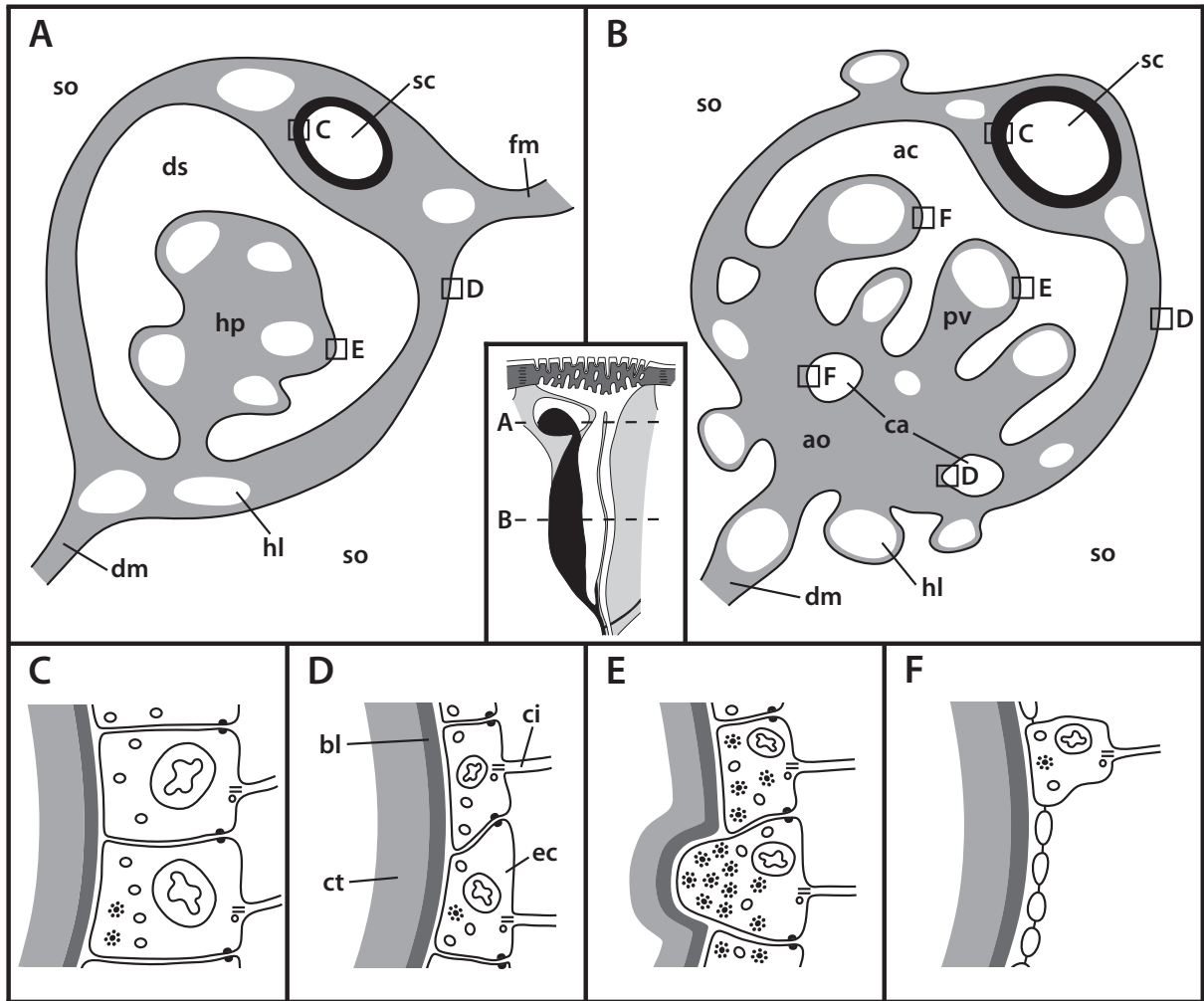


Figure 11

Table 1

Order	Family	Species	Method used	Specimen ID	Reference
Cidaroida Claus, 1880	Histocidaridae Lambert, 1900	<i>Histocidaris elegans</i> (Agassiz, 1879)	MRI (81 µm) <sup>3</sup>	ZMH E907	this study
	Cidaridae Gray, 1825	<i>Cidaris cidaris</i> (Linnaeus, 1758)	MRI (81 µm) <sup>3</sup> , dissection, histology	NHM 1925.10.30.10 3-113	Koehler 1883, Prouho 1887, Leipoldt 1893, this study
		<i>Eucidaris metularia</i> (Lamarck, 1816)	MRI (81 µm) <sup>3</sup>	NHM 1969.5.1.15-40	Ziegler <i>et al.</i> 2008, this study
		<i>Eucidaris</i> sp.	Histology, ultrastructure	-	Welsch & Rehkämper 1987, Rehkämper & Welsch 1988
		<i>Eucidaris tribuloides</i> Desmoulins, 1835	Dissection, histology	-	Ludwig 1877, this study
Echinothurioida Claus, 1880	Phormosomatidae Mortensen, 1934	<i>Phormosoma bursarium</i> Agassiz, 1881	Dissection, histology	-	Schurig 1906
	Echinothuriidae Wyville Thomson, 1872	<i>Asthenosoma varium</i> Grube, 1868	Dissection, histology	-	Sarasin & Sarasin 1887, Schurig 1906
		<i>Hygrosoma hoplacantha</i> (Wyville Thomson, 1877)	Dissection	-	Schurig 1906
		<i>Sperosoma biseriatum</i> Döderlein, 1901	Dissection	-	Schurig 1906
Pedinoida Mortensen, 1939	Pedinidae Pomel, 1883	<i>Caenopedina mirabilis</i> (Döderlein, 1885)	MRI (81 µm) <sup>3</sup> , dissection	USNM 31178, USNM 31182	this study
Diadematoida Duncan, 1889	Aspidodiadematidae Duncan, 1889	<i>Aspidodiadema hawaiiense</i> Mortensen, 1939	MRI (81 µm) <sup>3</sup> , dissection	USNM 27590	this study
		<i>Plesiadiadema indicum</i> (Döderlein, 1901)	MRI (81 µm) <sup>3</sup>	ZMB 7232	this study
	Diadematidae Gray, 1855	<i>Diadema antillarum</i> Philippi, 1845	Histology	-	Millott & Vevers 1967
		<i>Diadema savignyi</i> Michelin, 1845	MRI (40 µm) <sup>3</sup>	-	this study
		<i>Diadema setosum</i> (Leske, 1778)	Dissection, histology	-	this study
Salenioida Delage & Herouard, 1903	Saleniidae Agassiz, 1838	<i>Salenocidaris hastigera</i> (Agassiz, 1869)	MRI (81 µm) <sup>3</sup>	ZMB 5816	Ziegler <i>et al.</i> 2008, this study
Arbacioida Gregory, 1900	Arbaciidae Gray, 1855	<i>Arbacia lixula</i> (Linnaeus, 1758)	MRI (81 µm) <sup>3</sup> , histology	-	Hamann 1887, Bonnet 1925, Millott & Vevers 1967, Ziegler <i>et al.</i> 2008, this study
		<i>Arbacia punctulata</i> (Lamarck, 1816)	Dissection, histology	-	Coe 1912, von Ubisch 1913, Millott 1966, Millott & Farmanfarmaian 1967, Farmanfarmaian 1968, Millott 1969
Incerta sedis	Stomopneustidae Mortensen, 1903	<i>Stomopneustes variolaris</i> (Lamarck, 1816)	MRI (81 µm) <sup>3</sup>	USNM E45930	Ziegler <i>et al.</i> 2008, this study
Echinoida Troschel, 1872	Parechinidae Mortensen, 1903	<i>Paracentrotus lividus</i> (Lamarck, 1816)	MRI (81 µm) <sup>3</sup> , dissection, histology	-	Valentin 1841, Prouho 1887, von Ubisch 1913, Bonnet 1925, Millott & Vevers 1967, Spirlet <i>et al.</i> 1999A, this study

		<i>Psammechinus microtuberculatus</i> (Blainville, 1825)	Dissection, histology	-	Ludwig & Hamann 1904, von Ubisch 1913, Narasimhamurti 1931
		<i>Psammechinus miliaris</i> (Müller, 1771)	MRI (44 µm) <sup>3</sup> , dissection, histology, ultrastructure	-	Tiedemann 1816, Perrier 1875, Burton 1964, Jangoux & Schaltin 1977, this study
	Echinidae Gray, 1825	<i>Echinus esculentus</i> Linnaeus, 1758	MRI (81 µm) <sup>3</sup> , dissection, histology	ZMB 3826	Perrier 1875, Chadwick 1900, Wagner 1903, Bamber 1920, Cuénot 1948, Stott 1955, this study
		<i>Echinus melo</i> Lamarck, 1816	Dissection	-	Bonnet 1925
		<i>Gracilechinus acutus</i> (Lamarck, 1816)	Dissection, histology	-	Hamann 1887, Prouho 1887
	Echinometridae Gray, 1855	<i>Echinometra mathaei</i> (Blainville, 1825)	MRI (81 µm) <sup>3</sup>	NHM 1969.5.1.61-75	this study
		<i>Echinometra</i> sp.	Histology, ultrastructure	-	Welsch & Rehkämper 1987
	Strongylocentrotidae Gregory, 1900	<i>Strongylocentrotus dröbachiensis</i> (Müller, 1776)	Dissection, histology, ultrastructure	-	Fedotov 1924, Boolootian <i>et al.</i> 1965A, Millott 1966, Farmanfarmaian 1968, Ferguson 1996
		<i>Strongylocentrotus purpuratus</i> (Stimpson, 1857)	MRI, dissection, histology, ultrastructure	CAS 5724	Boolootian & Campbell 1964, Burton 1964, Millott & Vevers 1964, Boolootian <i>et al.</i> 1965A, Boolootian & Campbell 1966, Farmanfarmaian 1968, Ferguson 1996, Ziegler <i>et al.</i> 2008, this study
	Toxopneustidae Troschel, 1872	<i>Lytechinus variegatus</i> (Lamarck, 1816)	MRI (81 µm) <sup>3</sup>	-	this study
		<i>Sphaerechinus granularis</i> (Lamarck, 1816)	MRI (81 µm) <sup>3</sup> , dissection, histology, ultrastructure	-	Koehler 1883, Ludwig 1890, Leipoldt 1893, Bonnet 1925, Strenger 1973, Bachmann & Goldschmid 1978a, Bachmann & Goldschmid 1978b, Bachmann & Goldschmid 1980, Bachmann <i>et al.</i> 1980, this study
Temnopleuroida Mortensen, 1942	Trigonocidaridae Mortensen, 1903	<i>Genocidaris maculata</i> Agassiz, 1869	MRI (36 µm) <sup>3</sup>	ZMB 5827	this study
		<i>Trigonocidaris albida</i> Agassiz, 1869	MRI (32 µm) <sup>3</sup>	ZSM 20012468	this study
	Temnopleuridae Agassiz, 1872	<i>Mespilia globulus</i> (Linnaeus, 1758)	MRI (44 µm) <sup>3</sup>	ZMB 5620	Ziegler <i>et al.</i> 2008, this study
		<i>Salmacis bicolor</i> (Agassiz, 1846)	Dissection, histology	-	Aiyar 1938
Holactypoida Duncan, 1889	Echinoneidae Agassiz & Desor, 1847	<i>Echinoneus cyclostomus</i> Leske, 1778	MRI (86 µm) <sup>3</sup> , dissection	NHM 1969.5.1.105	Westergren 1911, Ziegler <i>et al.</i> 2008, this study
Cassiduloida Agassiz & Desor, 1847	Cassidulidae Agassiz & Desor, 1847	<i>Cassidulus caribearum</i> Lamarck, 1801	MRI (81 µm) <sup>3</sup>	CAS 112632	this study

	Echinolampadidae Gray, 1851	<i>Echinolampas depressa</i> Gray, 1851	MRI (81 µm) <sup>3</sup>	USNM E32955	Ziegler <i>et al.</i> 2008, this study
	Apatopygidae Kier, 1962	<i>Apatopygus recens</i> (Mortensen, 1948)	Dissection	-	Jensen (1981)
Clypeasteroidea Agassiz, 1835	Fibulariidae Duncan, 1889	<i>Echinocyamus pusillus</i> (Müller, 1776)	MRI 20 x 18 x 18 µm <sup>3</sup> , histology	-	Cuenot 1891, Ziegler <i>et al.</i> 2008, this study
	Laganidae Agassiz, 1873	<i>Peronella lesueurii</i> Agassiz, 1841	Dissection	MNHN EcEh79	this study
		<i>Peronella orbicularis</i> Leske, 1778	Dissection	-	Cuenot 1891
	Echinarachniidae Lambert, 1914	<i>Echinarachnius parma</i> (Lamarck, 1816)	MRI (44 µm) <sup>3</sup> , dissection	ZSM 20011676	Coe 1912, Mooi (unpublished data), this study
	Mellitidae Stephanini, 1914	<i>Mellita quinquesperforata</i> (Leske, 1778)	Dissection	-	this study
	Astriclypeidae Stephanini, 1911	<i>Echinodiscus bisperforatus</i> Leske, 1778	Histology	-	Cuenot 1891
Holasteroidea Durham & Melville, 1957	Urechinidae Duncan, 1889	<i>Antrechinus nordenskjoldi</i> (Mortensen, 1905)	Dissection	ZMH E7350	this study
		<i>Urechinus naresianus</i> Agassiz, 1879	Dissection	NHM 1903.8.1.100-104	Mortensen 1907, this study
	Pourtalesiidae Agassiz, 1881	<i>Echinosisgra paradoxa</i> Mortensen, 1905	Dissection	-	Mortensen 1907
		<i>Pourtalesia hispida</i> Agassiz, 1879	Dissection	ZMH E7349	this study
		<i>Pourtalesia jeffreysi</i> Wyville Thomson, 1873	Dissection	-	Mortensen 1907
		<i>Pourtalesia wandeli</i> Mortensen, 1905	MRI (86 µm) <sup>3</sup> , dissection	NHM 1976.7.30.76-95	Mortensen 1907, this study
	Plexechinidae Mooi & David, 1996	<i>Plexechinus planus</i> (McKnight, 1974)	Dissection	ZMH E7345	this study
Spatangoida Agassiz, 1840 „Hemiasterina“	Hemiasteridae Clark, 1917	<i>Hemiaster expergitus</i> (Loven, 1874)	Dissection	NHM 1914.1.30.66-9	this study
„Paleopneustina“	Schizasteridae Lambert, 1905	<i>Abatus cavernosus</i> (Philippi, 1845)	MRI (81 µm) <sup>3</sup>	ZMB 5854	Ziegler <i>et al.</i> 2008, this study
		<i>Schizaster canaliferus</i> (Lamarck, 1816)	Dissection, SEM, histology	-	Koehler 1883, Kaburek & Hilgers 1999
Micrasterina	Incerta sedis	<i>Heterobrissus niasicus</i> (Döderlein, 1901)	Dissection, histology	-	Wagner 1903
	Spatangidae Gray, 1825	<i>Spatangus purpureus</i> Müller, 1776	Dissection, histology	-	Hoffmann 1871, Koehler 1883, Hamann 1887, Prouho 1887, this study
	Brissidae Gray, 1855	<i>Brissus unicolor</i> (Leske, 1778)	Dissection, histology	-	Koehler 1883, Hamann 1887
		<i>Meoma ventricosa</i> (Lamarck, 1816)	Dissection	-	Hyman 1955, Chesher 1963
	Brissopsidae Lambert, 1905	<i>Brissopsis lyrifera</i> (Forbes, 1841)	Dissection	-	Koehler 1883, this study
	Echinocardiidae Wythe Cooke, 1942	<i>Echinocardium cordatum</i> (Pennant, 1777)	Dissection, histology, ultrastructure	-	De Ridder & Jangoux 1993, this study



---

		<i>Echinocardium flavescens</i> (Müller, 1776)	Dissection	-	Koehler 1883
		<i>Echinocardium mediterraneum</i> (Forbes, 1844)	Dissection, histology	-	Hamann 1887

Table 2

Structure	Type of body cavity involved	Developmental origin of body cavity	Topography
Axial complex	Primary and secondary body cavities	Left larval axocoel Right larval axocoel Left larval hydrocoel Right larval somatocoel Left larval somatocoel Haemal structure	Located between madreporic plate/hydropore and ring canal, within interradius CD below genital plate 2 (sensu Lovén), lodged within the dorso-ventral mesentery, surrounded by oral and aboral somatocoel
Madreporic ampulla	Secondary body cavity	Left larval axocoel	Small space beneath the madreporic plate, connected to the exterior by madreporic pore canals, adorally gives rise to stone canal and axial coelom
Stone canal	Secondary body cavity	Left larval hydrocoel	Single tube arising from lower end of madreporic ampulla, descending towards ring canal, can be calcified, in some irregular taxa divided into three distinct parts, can be pulsatile
Dorsal sac	Secondary body cavity	Right larval axocoel	Closed cavity enclosing the head process, with muscularized epithelium, lateral to madreporic ampulla
Head process	Primary body cavity & connective tissue matrix	Haemal structure	Aboral extension of the axial organ, surrounded by the dorsal sac, pulsatile, perforated by canaliculi and haemal lacunae
Axial coelom	Secondary body cavity	Left larval axocoel	Orally oriented blindly-ending part of the axocoel, partly enwraps stone canal as well as axial organ, connects adapically to madreporic ampulla, podocyte lining
Axial organ	Primary body cavity & connective tissue matrix	Haemal structure	Parallel to axial coelom, partially surrounded by somatocoel, connected to dorso-ventral mesentery, crossed by numerous canaliculi and haemal lacunae
Pulsating vessel	Primary body cavity	Haemal structure	(Pulsatile) haemal structure running along the outside of the axial organ, protruding into the axial coelom, can be lined by muscularized epithelium, adoral extension of head process
Canaliculus	Secondary body cavity	Left larval axocoel Right larval somatocoel Left larval somatocoel	Randomly distributed small invagination formed through infolding of coelomic epithelium, ending blindly, found inside the matrix of axial organ and head process
Haemal lacuna	Primary body cavity	Haemal structure	Randomly distributed anastomosing compartments within axial organ, head process and mesenteries, not lined by epithelium, part of the haemal system

Table 3

English	French	German
<b>Axial complex</b> Axial gland complex (Booolootian & Campbell 1966) Axial hemal complex Madreporite-axial-complex	Complexe axial	Axialer Organkomplex Axial-Hydrocoel-Komplex (Kaburek & Hilgers 1999) Axialkomplex (Fedotov 1924) Axo-Hydrocoel-Komplex (Strenger 1973)
<b>Madreporic plate</b> Calcareous disc (Sharpey 1836) Madrepore Madrepore plate Madreporic body Madreporic tubercle Madreporite (Huxley 1878) Madreporitic body Madreporitic plate Madreporite plate Sieve plate	Plaque madréporique Madréporé Madréporite	Madreporenplatte (Tiedemann 1816) Madreporit Siebplatte
<b>Madreporic pore canal</b> Hydropore Labyrinthine canal Madreporic canal Madreporic duct Madreporite pore canal	Canalicule du madréporite Canal madréporique Pore madréporique	Hydroporus Kanal der Madreporenplatte Labyrinthkanal Madreporenkanal Porenkanal Porenkanälchen (Hamann 1887) Wimperkanal
<b>Madreporic ampulla</b> Ampulla Ampulla of madreporite Ampulla of the stone canal Madreporic chamber Madreporic vesicle Madreporitic ampulla Sub-madreporite ampulla	Ampoule Ampoule collectrice Ampoule madréporique Ampoule sous-madréporique Canal excréteure Canal ramifié aquifère Espace infundibuliforme (Perrier 1875) Orifice de communication	Ampulla Ampulle (Hamann 1887) Madreporenblase Madreporit Protoceolampulle Sammelblase (Leipoldt 1893)
<b>Stone canal</b> Calcareous tube (Sharpey 1836) Madreporic canal Madreporic tube Sand-canal Water canal Water tube	Canal du sable Canal hydrophore Canal madréporique Canal onduleux Canal pierreux Cœur acquifère Tube acquifère Tube hydrophore (Perrier 1887)	Axiales Wassergefäß Axialwassergefäß Steincanal (Tiedemann 1816) Steinkanal Wassergefäßkanal Wasserkanal
<b>Dorsal sac</b> Axocoel Dorsal ampulla Heart Heart lumen Madreporic vesicle Pericardial cavity Pericardium Terminal coelom Terminal sinus	Espace sous-madréporique (Prouho 1887) Expansion terminale du sinus axial Hydrocoele droite Rudiment de l'hydrocoele droite Sinus terminal Vésicule madréporique (Jangoux & Schaltin 1977)	Axocoel Dorsalblase Dorsalsack (v. Ubisch 1913) Fortsatzcoelom (Leipoldt 1893) Fortsatzsinus Hohlraum unterhalb des Madreporiten Rechter Axialsinus Sinus dextra Terminalsack
<b>Head process (Chadwick 1923)</b> Aboral diverticulum Aboral part Aboral terminus (Farmanfarmaian 1968) Dorsal organ Head piece Heart coelom	Diverticule aboral (Jangoux & Schaltin 1977) Organe dorsal Processus glandulaire (Prouho 1887) Prolongement de l'organe axial Prolongement terminal	Aboraler Fortsatz (Leipoldt 1893) Drüsenfortsatz Eiförmiger Anhang (Pietschmann 1906) Fortsatz Fortsatz des Achsenorgans Fortsatz des Axialorgans Nebenniere (Sarasin & Sarasin)

Heart lumen Internal ridge Pericardium Terminal process (Bachmann & Goldschmid 1978a)		1887) Terminalfortsatz
<b>Axial coelom</b> Axial canal Axial gland lumen Axial sinus Axocoel Central cavity Central lumen Lumen of axial gland	Canal excréteure de la glande Canal glandulaire Canal ovoïde Cavité de la glande brune Cavité de l'organe ovoïde Cœlom axial (Cuénot 1891) Cœlom glandulaire (Cuénot 1886) Cœur Organe d'excrétion Sac fusiforme (Jourdain 1867) Sinus axial Sinus glandulaire	Axialcoelom Axialer Hohlraum Axialkanal Axialsinus Axocoel Drüsenhohlraum Höhle des sichelförmigen Bandes (Tiedemann 1816) Hohlraum Hohlraum der Niere Hohlraum des Dorsalorgans Linker Axialsinus Problematischer Kanal Schlauchförmiger Kanal (Vogt & Yung 1888) Sinus sinistra Ureter (Sarasin & Sarasin 1887)
<b>Axial organ</b> Axial gland Axial haemal duct Axial haemal vessel Brown gland Central plexus Dorsal organ Fusiform body Genital stolon Glandular organ Kidney Oral part Ovoid gland Plexiform gland (Carpenter 1883) Mysterious gland Septal gland Spongy body Tubular axial organ	Canal glandulaire Cavité de l'organe ovoïde Cœur (Valentin 1841) Corps plastidogène (Perrier 1887) Corps pyriforme (Jourdain 1867) Glande brune (Jourdain 1867) Glande excrétrice Glande madréporique (Koehler 1883) Glande ovoïde (Perrier 1875) Lacune axiale Organe axial (Cuénot 1886) Organe d'excrétion Organe plastidogène Rein lymphoïde (Cuénot 1886)	Achsenorgan Axialdrüse Axialorgan Braune Drüse Chromatogenes Organ (Hamann 1885) Dorsalorgan (Vogt & Yung 1888) Drüse Drüsiges Organ (Hamann 1887) Herz Herzförmiger Kanal (Tiedemann 1816) Lymphoides Organ Niere (Sarasin & Sarasin 1887) Ovoïde Drüse Septalorgan Wassergefäßherz (Hoffmann 1871) Zentralplexus (Ludwig 1878)
<b>Pulsating vessel</b> Axial blood vessel Central contractile vessel Contractile vessel Internal ridge Irregular vessel Pulsatile vessel	Vaisseau pulsatile Cordon axial	Herz Pulsierendes Gefäß
<b>Canaliculus</b>	Canaliculus Diverticule du sinus axial	Canaliculus Drüsenschläuche Nebenhohlräume
<b>Haemal lacuna</b> Blood lacuna Blood vessel Haemal vessel Lacunar system	Lacune hémale Système hémal	Blutlakune Epithellose Masche Hämalkanal Lakunennetz

## 8. Sea Urchin Comparative Soft Tissue Anatomy

Apart from the axial complex, further soft tissue structures might be of interest for an extension of the morphological matrix used for cladistic analyses. In this chapter, I will present a set of data on the internal anatomy of sea urchins. As in the previous chapter, these combined analyses involve magnetic resonance imaging, dissection, and a thorough literature search. However, the focus here is to evaluate the potential applicability of sea urchin internal anatomical features to supplement the existing set of characters. The major findings will be presented in taxonomic order and for each family in a pooled form to simplify an overview. A character matrix based entirely on soft tissue characters is in preparation and will then be combined with the existing matrices based on larval and hard-part characters as well as molecular findings.

The following sections are headed by the designation of the order and the number of extant species currently assigned to it. Species analyzed are listed by family including the techniques employed to gather the data: magnetic resonance imaging (MRI) with dataset resolution and accession number for the datasets deposited at MorphDBase ([www.morphdbase.de](http://www.morphdbase.de)) in brackets, dissection, histology, and literature with the respective source in brackets. Representative images derived from the various sources will be presented for the internal anatomy of selected taxa. A short list of definitions of the major soft tissue characters is provided at the end of the descriptions.

### **Cidaroida Claus, 1880 (~140 extant species)**

#### **Histocidaridae Lambert, 1900**

*Histocidaris elegans* (Agassiz, 1879)

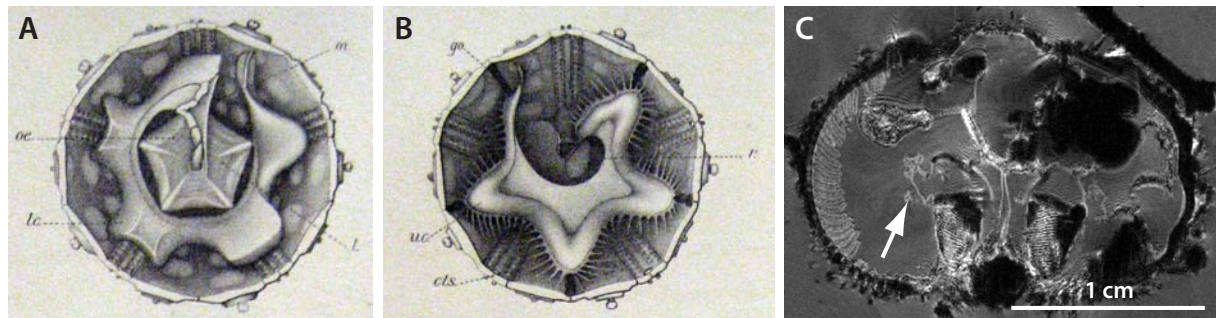
MRI (81  $\mu\text{m}$ )<sup>3</sup> (MorphDBase: A\_Ziegler\_20081116-M-51.1)

*Histocidaris variabilis* (Agassiz & Clark, 1907)

Literature (Agassiz & Clark 1908)

Histocidarids possess a cylindrical digestive tract with festoons present only in the stomach. The oesophagus is short and straight, a primary siphon could not be detected. The presence of a siphonal groove is likely in all taxa, a secondary siphon is absent. A small caecum is present at the start of the anterior stomach. The smooth-walled stomach and intestine make a full turn each. An intestinal caecum as well as Gregory's diverticulum could not be detected. The rectum is ascending towards the aborally located anus. An anal cone is absent. The axial complex is straight in its lateral aspect, the axial organ is oriented vertically. A peripharyngeal coelom surrounds Aristotle's lantern, buccal sacs are absent. Stewart's organs are large and bushy with two lateral diverticula. Five stalked gonads are present, the aboral sinuses are discreet. The lantern protractor muscles are smooth, longitudinal body wall muscles are

absent, compass elevator muscles are present. The perioesophageal haemal system consists of a spongy ring; a collateral duct of the digestive tract haemal system is absent. The primary spines are not covered with epidermis. Fig. 1 depicts selected internal views.



**Fig. 1:** Histocidaridae, internal anatomy. **A** *Histocidaris variabilis*, stomach, aboral view. **B** *Histocidaris variabilis*, intestine, oral view. **A, B** from Agassiz & Clark (1908). **C** *Histocidaris elegans*, MRI, lateral view. Arrow depicts bushy Stewart's organ.

## Cidaridae Gray, 1825

*Aporocidaris milleri* (Agassiz, 1898)

Literature (Lovén 1892)

*Austrocidaris canaliculata* (Agassiz, 1863)

Literature (Lovén 1892)

*Cidaris cidaris* (Linnaeus, 1758)

MRI ( $81 \mu\text{m}^3$ ) (MorphDBase: A\_Ziegler\_20081116-M-62.1) and literature (Koehler 1883, Prouho 1887, Leipoldt 1893)

*Eucidaris metularia* (Lamarck, 1816)

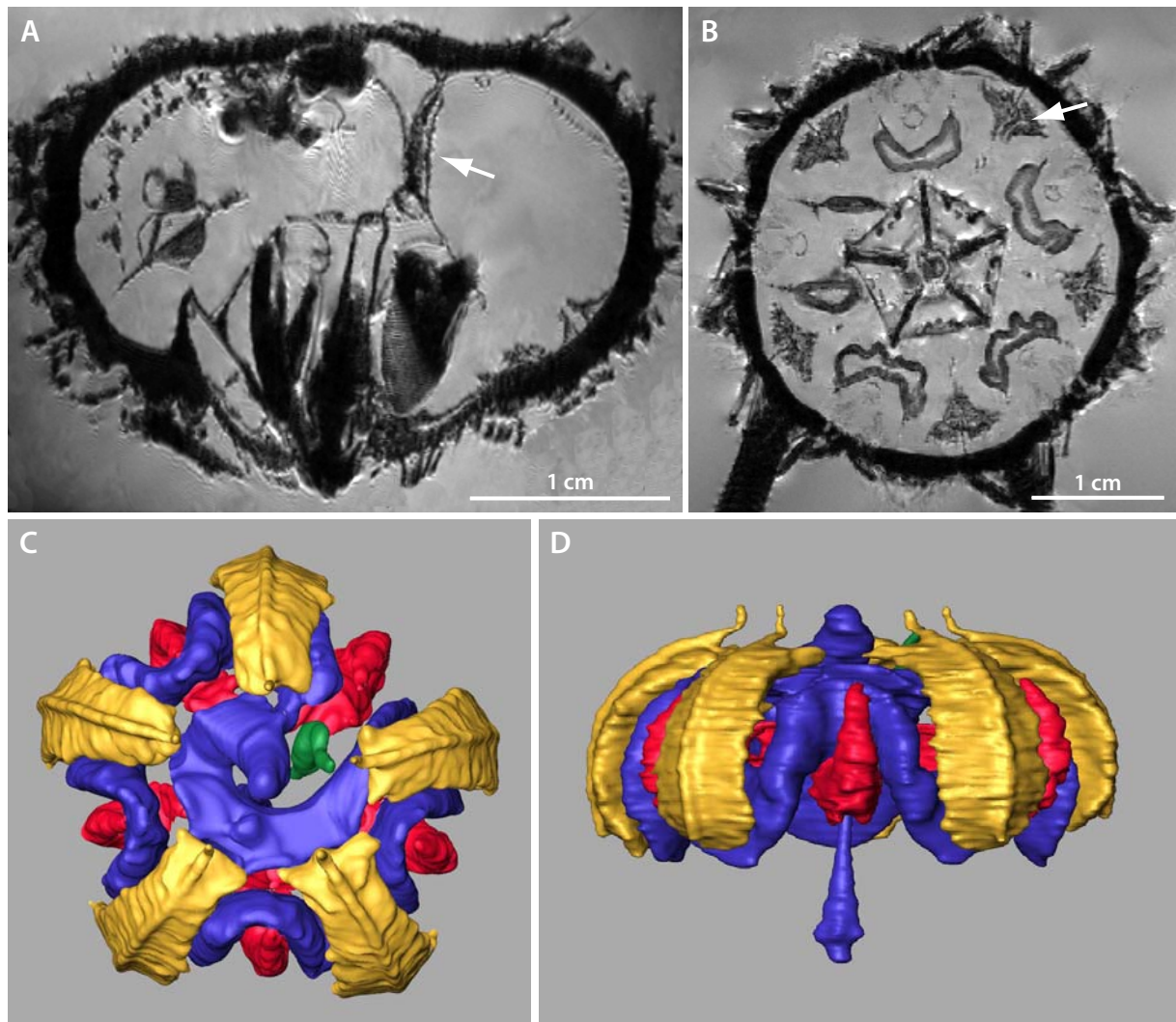
MRI ( $44 \mu\text{m}^3$ ), MRI ( $81 \mu\text{m}^3$ ) (MorphDBase: A\_Ziegler\_20081116-M-72.1), and MRI ( $117 \mu\text{m}^3$ )

*Eucidaris tribuloides* Desmoulins, 1835

Dissection, histology, and literature (Agassiz 1872-1873, Ludwig 1877)

Cidarids possess a cylindrical digestive tract with festoons present only in the stomach. The oesophagus is short and straight, a primary siphon could not be detected. The presence of a siphonal groove is known for some taxa, a secondary siphon is generally absent. The smooth-walled stomach and intestine make a full turn each. An intestinal caecum could not be detected as well as Gregory's diverticulum. The rectum is ascending towards the aborally located anus. An anal cone is absent. The axial complex is straight in its lateral aspect, the axial organ is oriented vertically. A peripharyngeal coelom surrounds Aristotle's lantern, buccal sacs are absent. Stewart's organs are large and bushy with two lateral diverticula. Five stalked gonads are present, the aboral sinuses are discreet. The lantern protractor muscles are smooth, longitudinal body wall muscles are absent, compass elevator muscles are present. The perioesophageal haemal system consists of a spongy ring; a collateral duct of

the digestive tract haemal system is absent. The primary spines are not covered with epidermis. Fig. 2 depicts selected internal views.



**Fig. 2:** Cidaridae, internal anatomy. **A** *Cidaris cidaris*, MRI, lateral view. Arrow depicts axial complex. **B** *Eucidaris metularia*, MRI, aboral view. Arrow depicts stalked gonad. **C** *Eucidaris metularia*, 3D model of the internal anatomy, aboral view. **D** *Eucidaris metularia*, 3D model of the internal anatomy, lateral view. Colour legend on page 32.

## Echinothurioida Claus, 1880 (~45 extant species)

### Phormosomatidae Mortensen, 1934

*Phormosoma bursarium* Agassiz, 1881

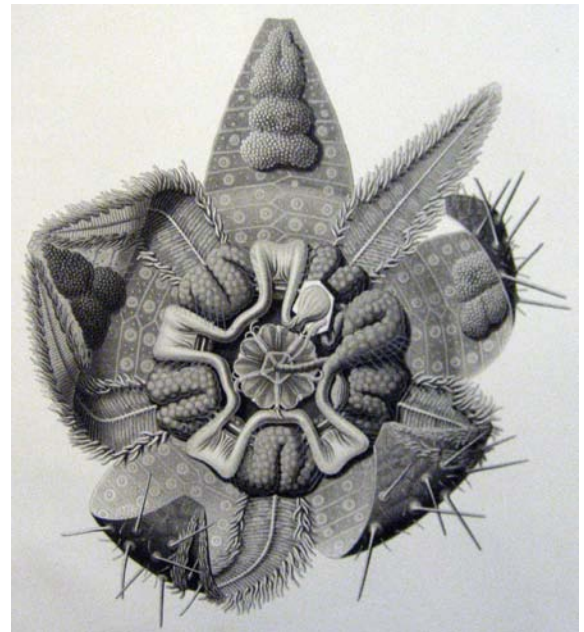
Literature (Schurig 1906, Agassiz & Clark 1909)

*Phormosoma placenta* Wyville Thomson, 1872

Dissection

Phormosomatids possess a cylindrical digestive tract, both stomach and intestine are festooned. The oesophagus is long and extends over several ambulacra before entering the

stomach. The presence of a primary siphon has been reported, a siphonal groove is presumably absent. A secondary siphon is absent. The caecum at the beginning of the stomach is enlarged. Stomach and intestine both make full turns. The stomach wall is smooth. Intestinal caecum as well as Gregory's diverticulum are absent. The rectum is enlarged and ascends aborally towards the anus. An anal cone is absent. The axial complex is straight and winding in its lateral form, the axial organ is oriented vertically. Aristotle's lantern is surrounded by a peripharyngeal coelom; buccal sacs are present as small bushy structures. Stewart's organs are present as tubular structures without lateral diverticula. The aboral sinuses are discreet, five gonads are present. The protractor muscles are smooth, compass elevator as well as weak longitudinal body wall muscles are present. The perioesophageal haemal system consists of a spongy ring; the presence of a collateral duct of the haemal system could not be verified. Both primary and secondary spines are covered with epidermis. Fig. 3 depicts a selected internal view.



**Fig. 3:** Phormosomatidae, internal anatomy. *Phormosoma bursarium*, digestive tract and gonads, aboral view. From Schurig (1906).

### **Echinothuriidae Wyville Thomson, 1872**

*Araeosoma fenestratum* (Wyville Thomson, 1872)

Literature (Wyville Thomson 1874)

*Asthenosoma ijimai* Yoshiwara, 1897

Literature (Agassiz & Clark 1909)

*Asthenosoma varium* Grube, 1868

Literature (Sarasin & Sarasin 1887, Schurig 1906)

*Hygrosoma hoplacantha* (Wyville Thomson, 1877)

Literature (Agassiz 1881, Schurig 1906)

*Sperosoma biseriatum* Döderlein, 1901

Literature (Schurig 1906)



*Sperosoma obscurum* (Agassiz & Clark, 1907)

Literature (Agassiz & Clark 1909)

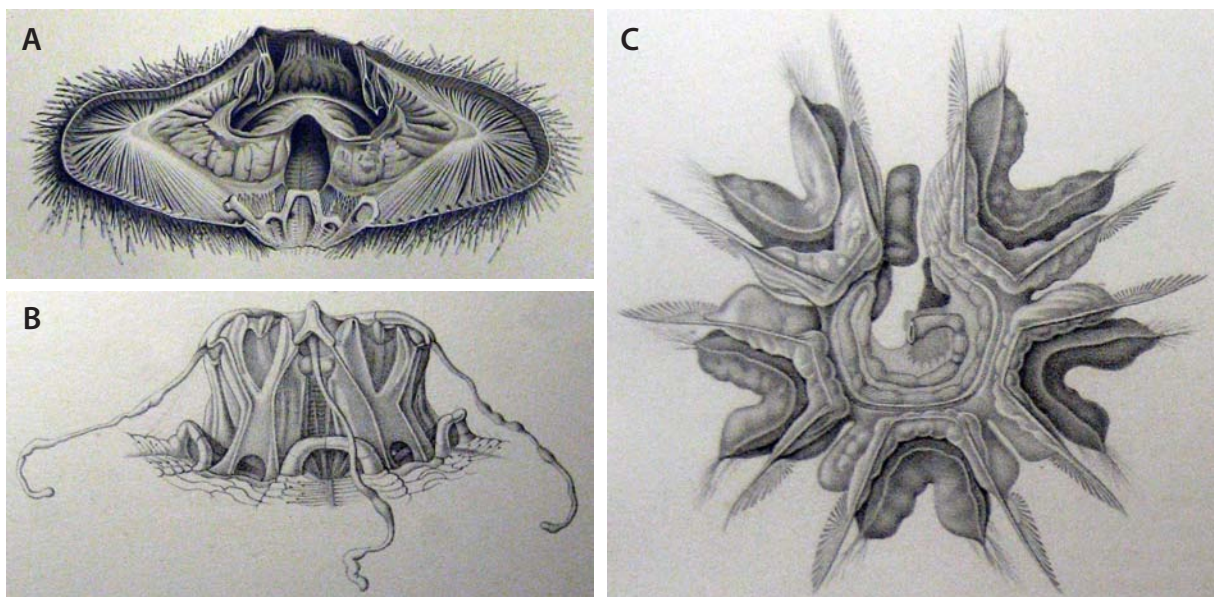
*Tromikosoma hispidum* (Agassiz, 1898)

Literature (Agassiz & Clark 1909)

*Tromikosoma tenue* (Agassiz, 1879)

Literature (Agassiz 1881)

Echinothuriids possess a cylindrical digestive tract; both stomach and intestine are festooned. The oesophagus is long and extends over several ambulacra before entering the stomach. In some taxa the oesophagus is even more extended, bending back on itself. The presence of a primary siphon has been reported, a siphonal groove is presumably absent. A secondary siphon is absent. The caecum at the beginning of the stomach is enlarged or even consists of a separate festoon. Stomach and intestine both make full turns. The stomach wall is smooth. Intestinal caecum as well as Gregory's diverticulum are absent. The rectum is enlarged and ascends aborally towards the anus. An anal cone is presumably absent. The axial complex is straight and winding in lateral form, the axial organ is oriented vertically. Aristotle's lantern is surrounded by a peripharyngeal coelom; buccal sacs are present as small bushy structures, but are larger in some taxa. Stewart's organs are present as tubular structures without lateral diverticula. The aboral sinuses are discreet, five gonads are present. The protractor muscles are smooth, compass elevator as well as pronounced longitudinal body wall muscles are present. The perioesophageal haemal system consists of a spongy ring; the presence of a collateral duct of the haemal system could not be verified. Both primary and secondary spines are covered with epidermis. Fig. 4 depicts selected internal views.



**Fig. 4:** Echinothuriidae, internal anatomy. **A** *Asthenosoma varium*, longitudinal body wall muscles and digestive tract, lateral view. From Sarasin & Sarasin (1887). **B** *Asthenosoma ijimai*, Aristotle's lantern with tubular Stewart's organs, lateral view. **C** *Asthenosoma ijimai*, digestive tract with siphon and extended oesophagus, oral view. **B, C** from Agassiz & Clark (1909).

## Pedinoida Mortensen, 1939 (~10 extant species)

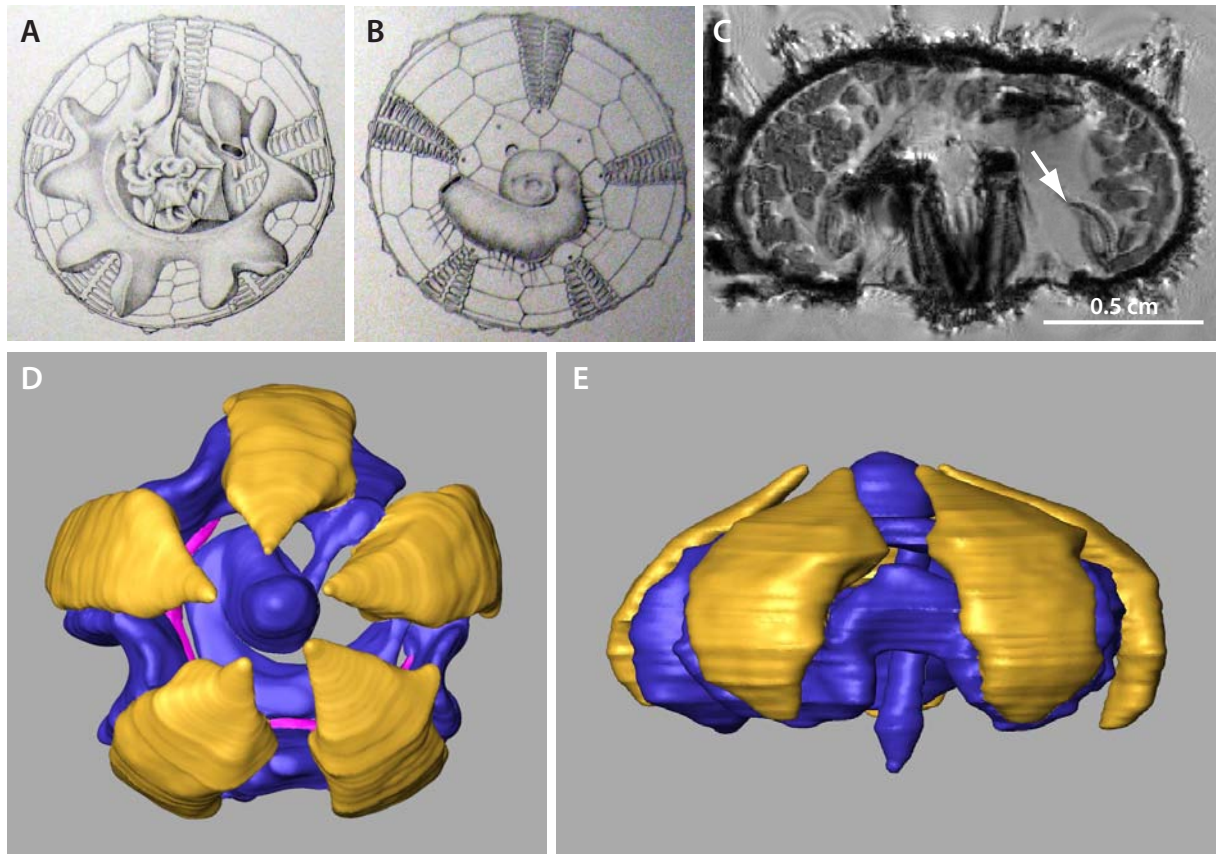
### Pedinidae Pomel, 1883

*Caenopedina hawaiiensis* Clark, 1907

Literature (Clark 1912)

*Caenopedina mirabilis* (Döderlein, 1885)

MRI (81  $\mu\text{m}$ )<sup>3</sup> (MorphDBase: A\_Ziegler\_20081116-M-65.1) and dissection



**Fig. 5:** Pedinidae, internal anatomy. **A** *Caenopedina hawaiiensis*, stomach with caecum and oesophagus, aboral view. **B** *Caenopedina hawaiiensis*, intestine, oral view. **A, B** from Clark (1912). **C** *Caenopedina mirabilis*, MRI, lateral view. Arrow depicts stomach. **D** *Caenopedina mirabilis*, 3D model of the internal anatomy, aboral view. **E** *Caenopedina mirabilis*, 3D model of the internal anatomy, lateral view. Colour legend on page 32.

Pedinids possess a cylindrical digestive tract, the stomach is festooned, whereas the intestine is not. The oesophagus extends over one to two ambulacra. A primary siphon was shown not to be present. Instead, a siphonal groove can be found as part of the pedinid digestive tract. Pedinids do not possess a secondary siphon. A prominent caecum marks the beginning of the stomach. Stomach and intestine both make a full turn. The stomach is smooth-walled. An intestinal caecum and Gregory's diverticulum are both absent. The rectum ascends aborally towards the anus; an anal cone is not present. The axial complex is straight to oblique in lateral view; the axial organ is oriented vertically. A peripharyngeal coelom engulfs the Aristotle's lantern; buccal sacs are present as small branched appendages. Stewart's organs are present as miniscule small sacs without lateral diverticula. The aboral sinuses are discreet.

Five gonads are present. The structure of the lantern protractor muscles is smooth. Compass elevator muscles are present, longitudinal body wall muscles are absent. The perioesophageal haemal system consists of five spongy bodies; a small collateral duct is present. All spines are covered with epidermis. Fig. 5 depicts selected internal views.

## Diadematoidea Duncan, 1889 (~45 extant species)

### Aspidodiadematidae Duncan, 1889

*Aspidodiadema hawaiiense* Mortensen, 1939

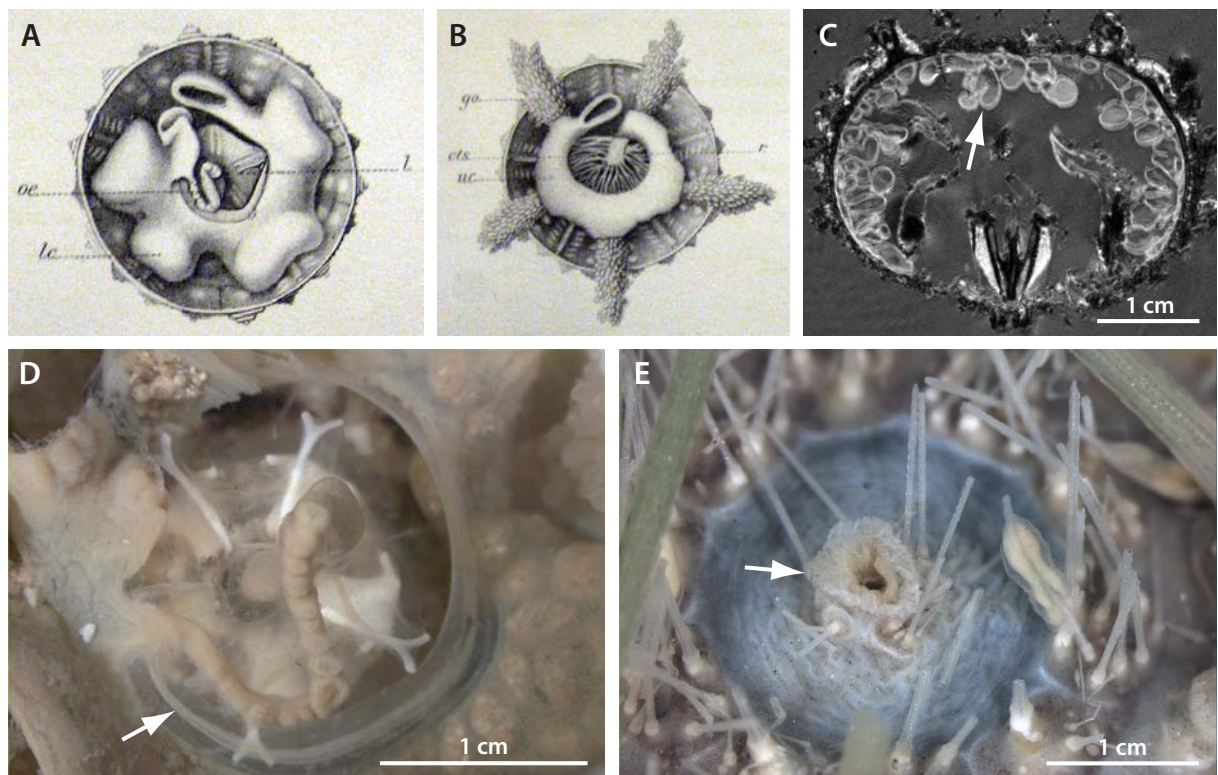
MRI (81  $\mu\text{m}$ )<sup>3</sup> (MorphDBase: A\_Ziegler\_20081116-M-53.1) and dissection

*Aspidodiadema meijerei* Döderlein, 1906

Literature (Agassiz & Clark 1908)

*Plesiadiadema indicum* (Döderlein, 1901)

MRI (81  $\mu\text{m}$ )<sup>3</sup> (MorphDBase: A\_Ziegler\_20081116-M-54.1)



**Fig. 6:** Aspidodiadematidae, internal anatomy. **A** *Aspidodiadema meijerei*, stomach with caecum and oesophagus, aboral view. **B** *Aspidodiadema meijerei*, intestine and gonads, oral view. **A**, **B** from Agassiz & Clark (1908). **C** *Aspidodiadema hawaiiense*, MRI, lateral view. Arrow depicts gonad. **D** *Aspidodiadema hawaiiense*, dissection, Aristotle's lantern with oesophagus. Arrow depicts primary siphon. **E** *Aspidodiadema hawaiiense*, periproct, aboral view. Arrow depicts anal cone.

Aspidodiadematids possess a cylindrical digestive tract; the stomach is festooned whereas the intestine is not. The oesophagus extends over one to two ambulacra. A primary siphon was shown to be present in the form of a hemisiphon or as a true siphon. A siphonal groove is therefore presumably not present. No secondary siphon can be found in aspidodiadematids.

A prominent caecum marks the beginning of the stomach. Stomach and intestine both make a full turn. The stomach is smooth-walled. An intestinal caecum and Gregory's diverticulum are both absent. The rectum ascends aborally towards the anus, an anal cone is present. The rectum is heavily suspended by numerous mesenterial strands. The axial complex is straight to oblique in lateral view; the axial organ is oriented vertically. A peripharyngeal coelom engulfs Aristotle's lantern; buccal sacs are present as small branched appendages. Stewart's organs are present as miniscule small to medium large sacs without lateral diverticula. The aboral sinuses are discreet. Five gonads are present. The structure of the lantern protractor muscles is smooth. Compass elevator muscles are present, longitudinal body wall muscles are absent. The perioesophageal haemal system consists of five spongy bodies; a small collateral duct is present. All spines are covered with epidermis. Fig. 6 depicts selected internal views.

### **Diadematidae Gray, 1855**

*Astropyga radiata* (Leske, 1778)

Literature (Agassiz & Clark 1909)

*Centrostephanus longispinus* (Philippi, 1845)

MRI (66 µm)<sup>3</sup> (MorphDBase: A\_Ziegler\_20081116-M-64.1)

*Chaetodiadema pallidum* (Agassiz & Clark, 1907)

Literature (Agassiz & Clark 1908)

*Diadema savignyi* Michelin, 1845

MRI (40 µm)<sup>3</sup> (MorphDBase: A\_Ziegler\_20081116-M-33.1)

*Diadema setosum* (Leske, 1778)

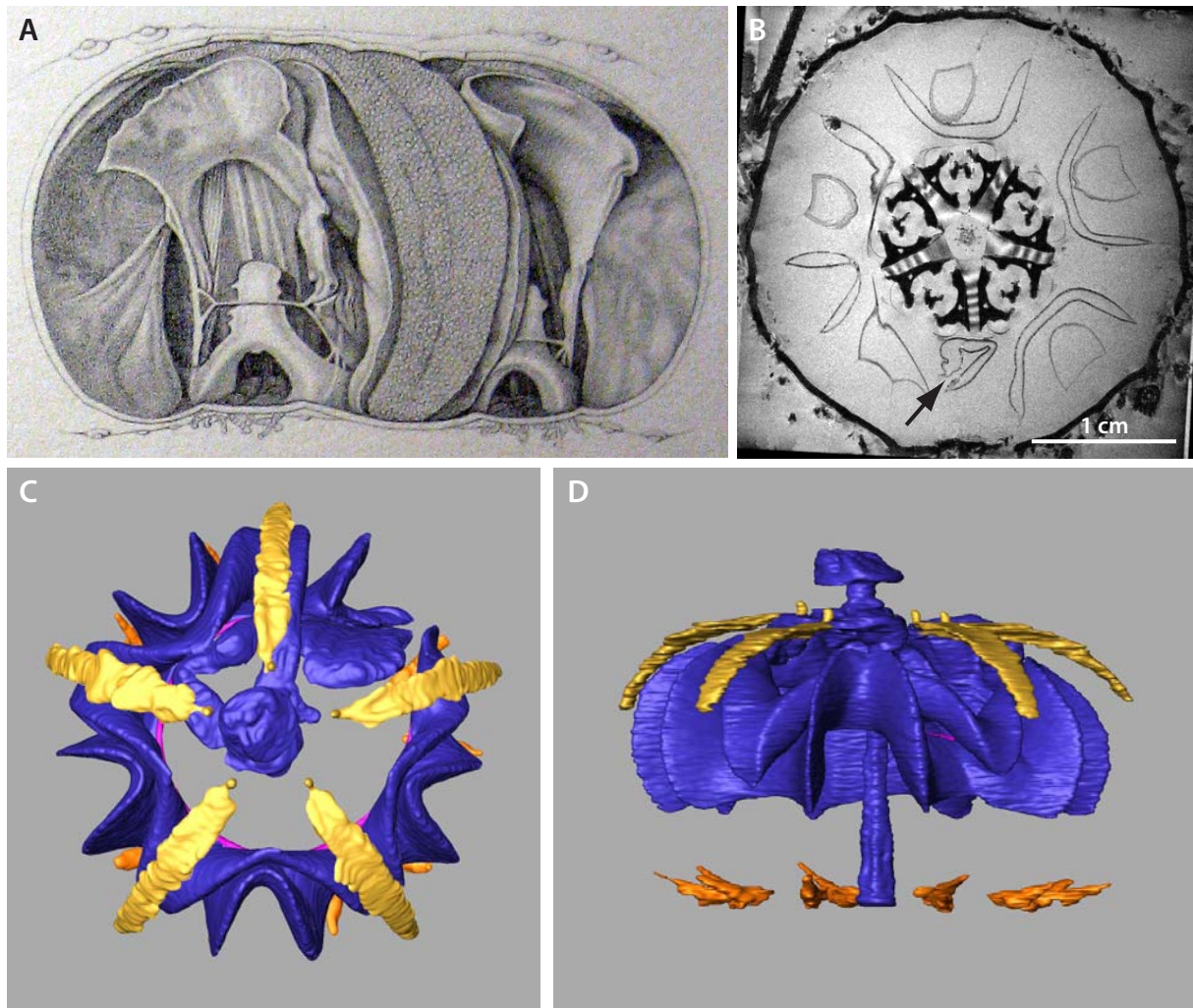
Dissection, histology, and literature (Agassiz 1872-1873)

*Echinothrix diadema* (Linnaeus, 1758)

Literature (Agassiz & Clark 1909)

Diadematids possess a cylindrical digestive tract; the stomach as well as the intestine are both festooned. The oesophagus extends over one to several ambulacra. A primary siphon was shown to be absent; instead, a siphonal groove is present. No secondary siphon can be found in diadematids. A prominent caecum marks the beginning of the stomach. Stomach and intestine both make a full turn. The stomach is smooth-walled. An intestinal caecum as well as Gregory's diverticulum are both absent. The rectum ascends aborally towards the anus, an anal cone is present. The axial complex is straight to oblique in lateral view; the axial organ is oriented vertically. A peripharyngeal coelom engulfs Aristotle's lantern; buccal sacs are present as extended and enlarged appendages. Stewart's organs are present as miniscule sacs in some species, always without lateral diverticula. The aboral sinuses are discreet. Five gonads are present. The structure of the lantern protractor muscles is smooth. Compass elevator muscles are present, longitudinal body wall muscles are absent. The peri-

oesophageal haemal system consists of five spongy bodies; a well-developed collateral duct is present. All spines are covered with epidermis. Fig. 7 depicts selected internal views.



**Fig. 7:** Diadematidae, internal anatomy. **A** *Echinothrix diadema*, gonads, digestive tract with collateral duct of the digestive tract haemal system, lateral view. From Agassiz & Clark (1909). **B** *Diadema savignyi*, MRI, aboral view. Arrow depicts enlarged caecum. **C** *Diadema savignyi*, 3D model of the internal anatomy, aboral view. **D** *Diadema savignyi*, 3D model of the internal anatomy, lateral view. Colour legend on page 32.

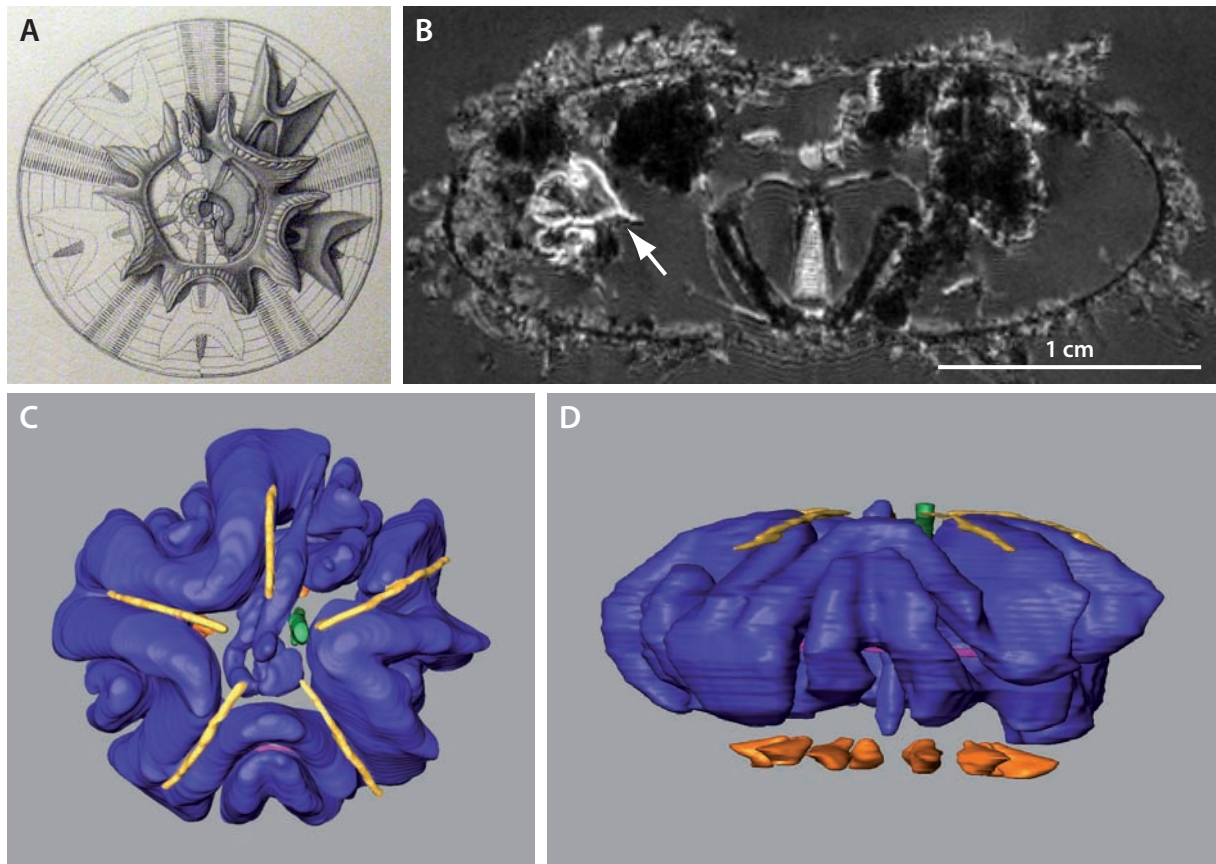
### **Micropygidae Duncan, 1889**

*Micropyga tuberculata* Agassiz, 1879

MRI (81  $\mu\text{m}$ )<sup>3</sup> (MorphDBase: A\_Ziegler\_20081116-M-38.1) and literature (Agassiz & Clark 1909)

*Micropyga tuberculata* possesses a cylindrical digestive tract; the stomach as well as the intestine are both festooned. The oesophagus extends over several ambulacra. A primary siphon is presumably present in the form of a hemisiphon. A secondary siphon is presumably absent in this species. A prominent caecum marks the beginning of the stomach. Stomach and intestine both make a full turn. The stomach is smooth-walled. An intestinal caecum as

well as Gregory's diverticulum are both absent. The rectum ascends aborally towards the anus; an anal cone is slightly developed. The axial complex is straight in lateral view; the axial organ is oriented vertically. A peripharyngeal coelom engulfs Aristotle's lantern; buccal sacs are present as extended and enlarged appendages. Stewart's organs are present as miniscule sacs without lateral diverticula. The aboral sinuses are discreet. Five gonads are present. The structure of the lantern protractor muscles is smooth. Compass elevator muscles are present, longitudinal body wall muscles are absent. The perioesophageal haemal system consists of five spongy bodies; a well-developed collateral duct is present. All spines are covered with epidermis. Fig. 8 depicts selected internal views.



**Fig. 8:** Micropygidae, internal anatomy. **A** *Micropyga tuberculata*, digestive tract, oral view. From Agassiz & Clark (1909). **B** *Micropyga tuberculata*, MRI, lateral view. Arrow depicts stomach. **C** *Micropyga tuberculata*, 3D model of the internal anatomy, aboral view. **D** *Micropyga tuberculata*, 3D model of the internal anatomy, lateral view. Colour legend on page 32.

## Salenioida Delage & Hérouard, 1903 (~15 extant species)

### Saleniidae Agassiz, 1838

*Bathysalenia goesiana* (Lovén, 1874)

MRI (81  $\mu\text{m}$ )<sup>3</sup> (MorphDBase: A\_Ziegler\_20081116-M-63.1) and literature (Agassiz & Clark 1908)

*Salenocidaris hastigera* (Agassiz, 1869)

MRI (81  $\mu\text{m}$ )<sup>3</sup> (MorphDBase: A\_Ziegler\_20081116-M-58.1) and dissection

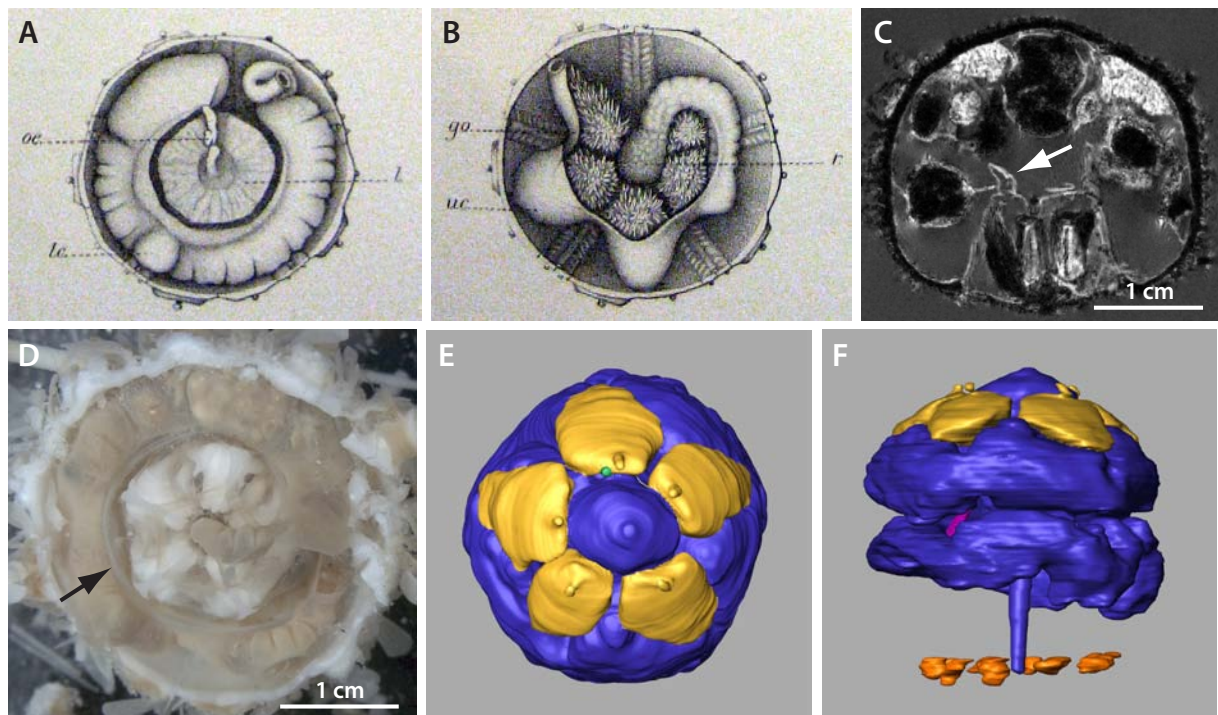
*Salenocidaris miliaris* (Agassiz, 1869)

Literature (Agassiz & Clark 1908)

*Salenocidaris varispina* Agassiz, 1869

MRI (66  $\mu\text{m}$ )<sup>3</sup> (MorphDBase: A\_Ziegler\_20081116-M-59.1)

Saleniids possess a cylindrical digestive tract; the stomach as well as the intestine are both slightly festooned. The oesophagus is short and straight. A well-developed primary siphon is present; a siphonal groove is presumably absent. No secondary siphon can be found in saleniids. A small caecum marks the beginning of the stomach. Stomach and intestine both make a full turn. The stomach is slightly sacculated. An intestinal caecum as well as Gregory's diverticulum are both absent. The rectum ascends aborally towards the anus, an anal cone is absent. The rectum is conspicuously suspended by several mesenteric strands. The axial complex is straight in lateral view; the axial organ is oriented vertically. A peripharyngeal coelom engulfs Aristotle's lantern; buccal sacs are present as small appendages. Stewart's organs are not present in saleniids. The aboral sinuses are discreet. Five gonads are present. The structure of the lantern protractor muscles is smooth. Compass elevator muscles are present, longitudinal body wall muscles are absent. The perioesophageal haemal system consists of five spongy bodies; a collateral duct is present. All spines are covered with epidermis. Fig. 9 depicts selected internal views.



**Fig. 9:** Saleniidae, internal anatomy. **A** *Salenocidaris miliaris*, stomach and oesophagus, aboral view. **B** *Salenocidaris miliaris*, intestine, enlarged rectum, and gonads, oral view. **A**, **B** from Agassiz & Clark (1908). **C** *Bathysalenia goesiana*, MRI, lateral view. Arrow depicts dental sac. **D** *Salenocidaris hastigera*, dissection, Aristotle's lantern, stomach, and oesophagus. Arrow depicts primary siphon. **E** *Salenocidaris hastigera*, 3D model of the internal anatomy, aboral view. **F** *Salenocidaris hastigera*, 3D model of the internal anatomy, lateral view. Colour legend on page 32.

## Arbacioida Gregory, 1900 (~25 extant species)

### Arbaciidae Gray, 1855

*Arbacia lixula* (Linnaeus, 1758)

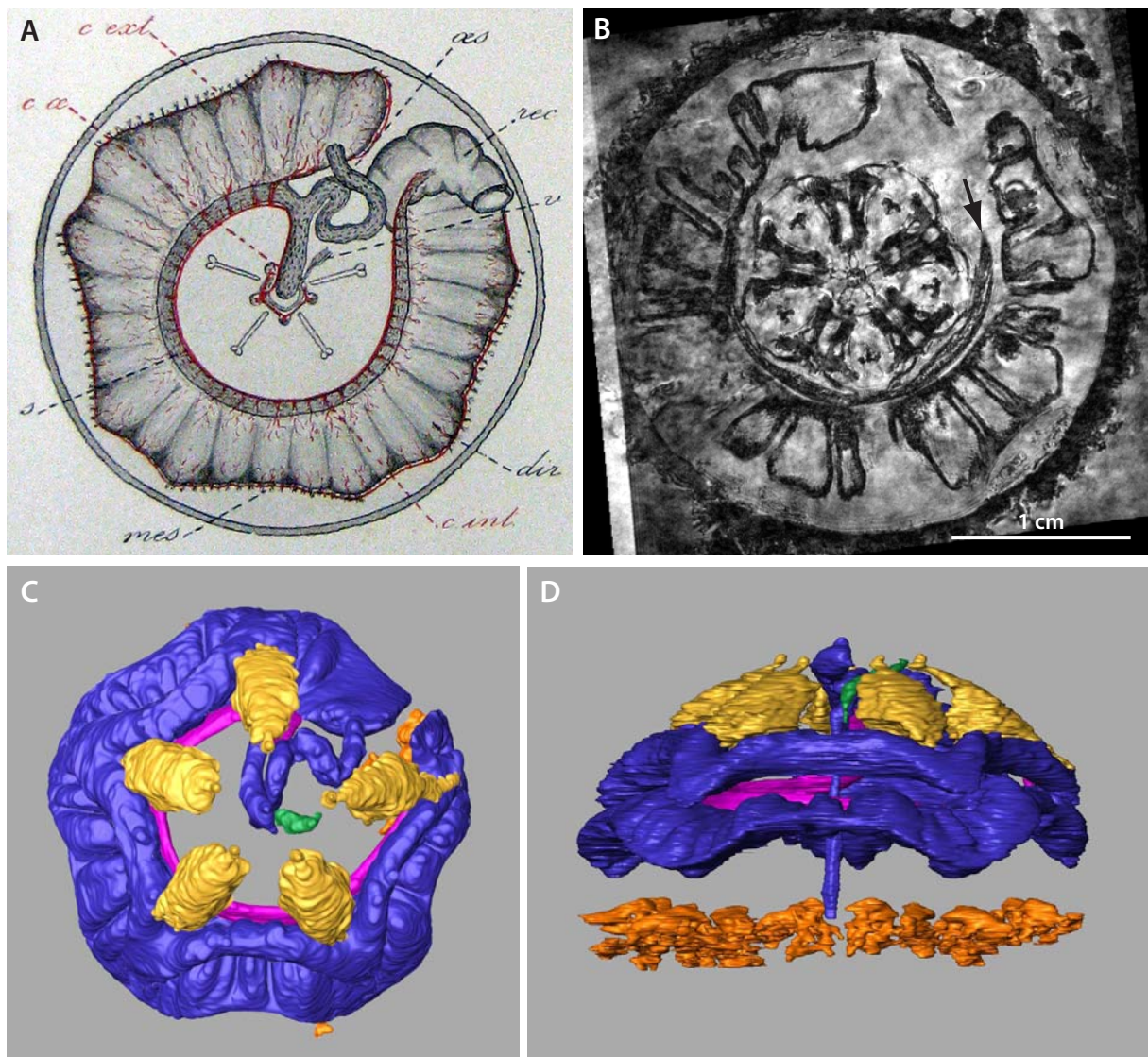
MRI (81  $\mu\text{m}$ )<sup>3</sup> (MorphDBase: A\_Ziegler\_20081116-M-41.1) and literature (Agassiz 1872-1873, Hamann 1887, Bonnet 1925)

*Arbacia punctulata* (Lamarck, 1816)

Literature (Coe 1912, von Ubisch 1913)

*Coelopleurus floridanus* Agassiz, 1872

Literature (Agassiz & Clark 1908)



**Fig. 10:** Arbaciidae, internal anatomy. **A** *Arbacia lixula*, sacculated stomach and well-developed primary siphon, aboral view. From Bonnet (1925). **B** *Arbacia lixula*, MRI, Aristotle's lantern and digestive tract, aboral view. Arrow depicts primary siphon. **C** *Arbacia lixula*, 3D model of the internal anatomy, aboral view. **D** *Arbacia lixula*, 3D model of the internal anatomy, lateral view. Colour legend on page 32.

Arbaciids possess a cylindrical digestive tract; the stomach as well as the intestine are both



well-festooned. The oesophagus is prolonged and extends clockwise over one ambulacrum. A well-developed primary siphon is present, a siphonal groove is absent. No secondary siphon can be found in arbaciids. A small caecum marks the beginning of the stomach. Stomach and intestine both make a full turn. The stomach is heavily sacculated. An intestinal caecum as well as Gregory's diverticulum are both absent. The rectum ascends aborally towards the anus, an anal cone is absent. The axial complex is straight in lateral view; the axial organ is oriented vertically. A peripharyngeal coelom surrounds Aristotle's lantern; buccal sacs are present as well-developed appendages. Stewart's organs are not present in arbaciids. The aboral sinuses are discreet. Five gonads are present. The structure of the lantern protractor muscles is smooth. Compass elevator muscles are present, longitudinal body wall muscles are absent. The perioesophageal haemal system consists of five spongy bodies; a collateral duct is present. All spines are covered with epidermis. Fig. 10 depicts selected internal views.

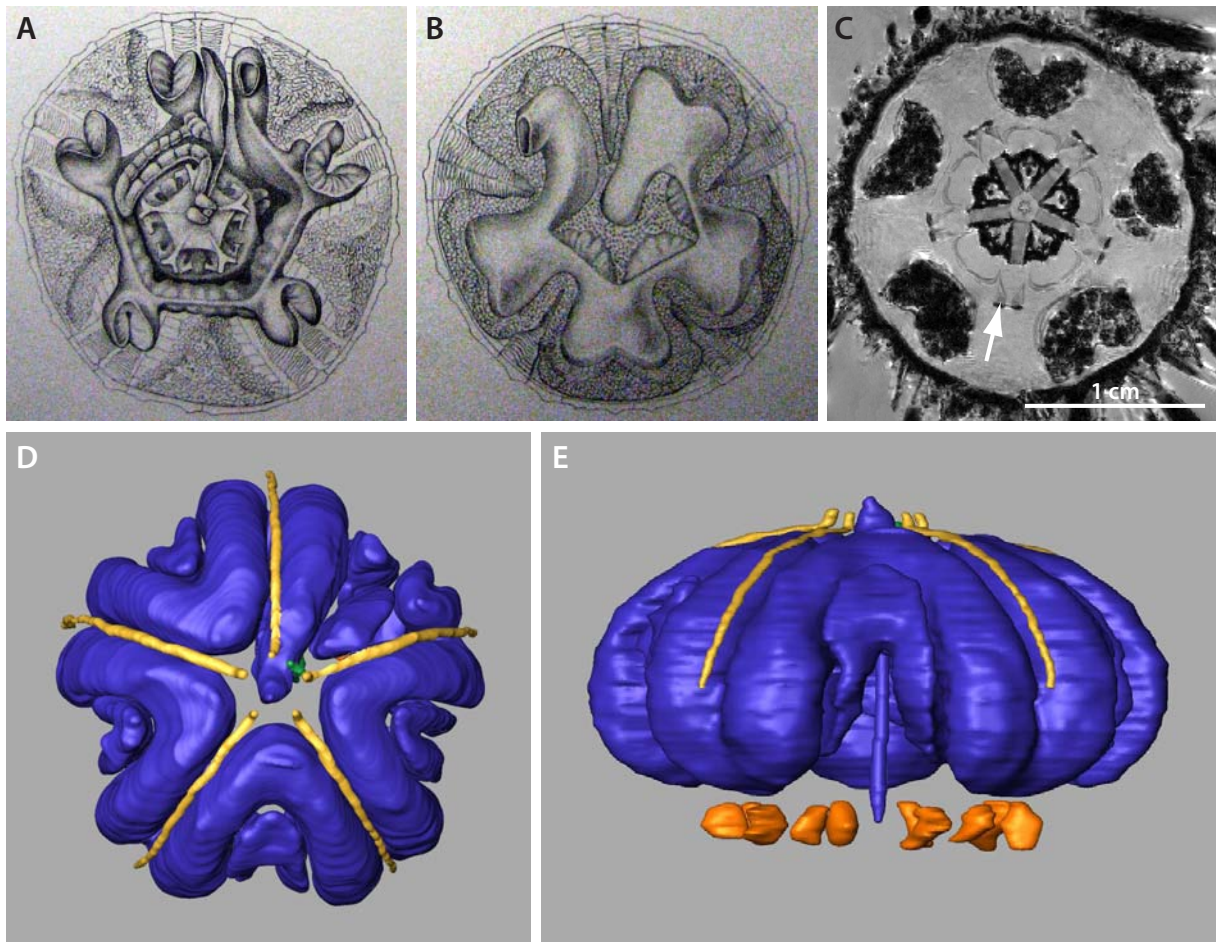
### **Incerta sedis (2 extant species)**

#### **Stomopneustidae Mortensen, 1903**

*Stomopneustes variolaris* (Lamarck, 1816)

MRI (81  $\mu\text{m}$ )<sup>3</sup> (MorphDBase: A\_Ziegler\_20081116-M-68.1), dissection, and literature (Clark 1912)

*Stomopneustes variolaris* possesses a cylindrical digestive tract; the stomach as well as the intestine are both well-festooned. The oesophagus is prolonged and extends over several ambulacra. A thin-walled primary siphon is present; a siphonal groove is presumably absent. No secondary siphon can be found in this species. A large caecum marks the beginning of the stomach. Stomach and intestine both make a full turn. The stomach is slightly sacculated. An intestinal caecum as well as Gregory's diverticulum are both absent. The rectum ascends aborally towards the anus, an anal cone is absent. The axial complex is straight in lateral view; the axial organ is oriented vertically. A peripharyngeal coelom surrounds Aristotle's lantern; buccal sacs are present as well-developed appendages. Stewart's organs are present as miniscule sacs without lateral diverticula. The aboral sinuses are discreet. Five gonads are present. The structure of the lantern protractor muscles is smooth. Compass elevator muscles are present, longitudinal body wall muscles are absent. The perioesophageal haemal system consists of five spongy bodies; a collateral duct is present. All spines are covered with epidermis. Fig. 11 depicts selected internal views.



**Fig. 11:** Stomopneustidae, internal anatomy. **A** *Stomopneustes variolaris*, stomach and oesophagus, aboral view. **B** *Stomopneustes variolaris*, intestine and gonads, oral view. **A, B** from Clark (1912). **C** *Stomopneustes variolaris*, MRI, Aristotle's lantern with muscles and digestive tract, aboral view. Arrow depicts lantern retractor muscle. **D** *Stomopneustes variolaris*, 3D model of the internal anatomy, aboral view. **E** *Stomopneustes variolaris*, 3D model of the internal anatomy, lateral view. Colour legend on page 32.

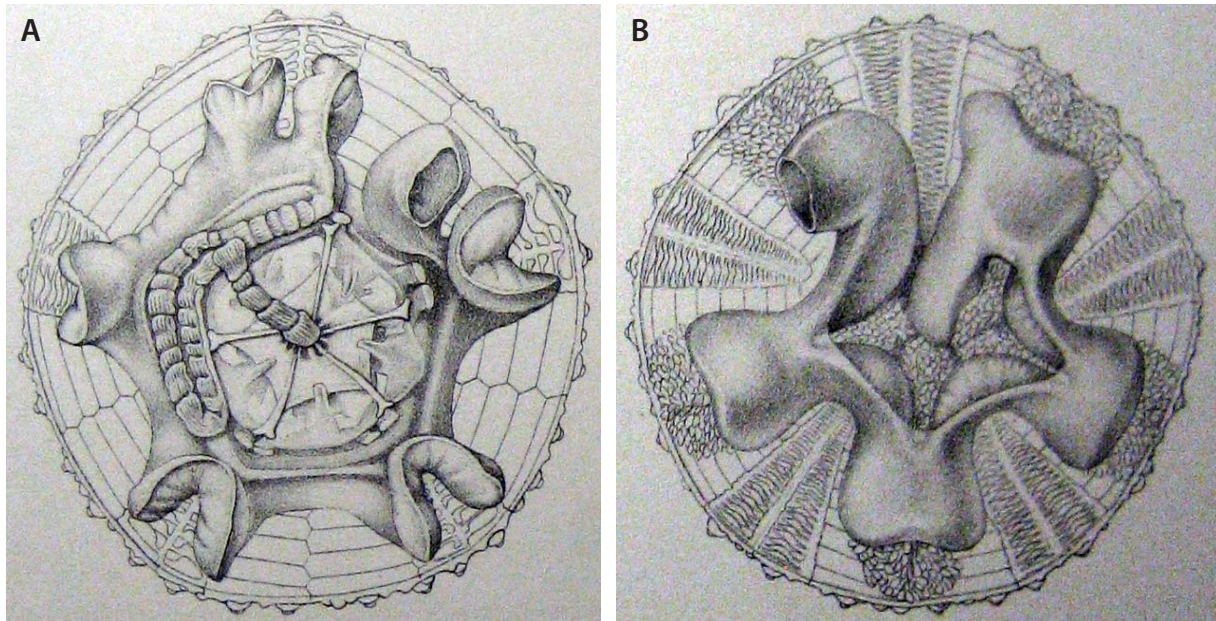
## N.N.

*Glyptocidaris crenularis* Agassiz, 1853

Literature (Clark 1912)

*Glyptocidaris crenularis* possesses a cylindrical digestive tract; the stomach as well as the intestine are both well-festooned. The oesophagus is prolonged and extends over several ambulacra. A primary siphon is present; a siphonal groove is presumably absent. No secondary siphon can be found in this species. A large caecum marks the beginning of the stomach. Stomach and intestine both make a full turn. The stomach is smooth-walled. An intestinal caecum and Gregory's diverticulum are both absent. The rectum ascends aborally towards the anus, an anal cone is absent. The axial complex is straight in lateral view; the axial organ is oriented vertically. A peripharyngeal coelom surrounds Aristotle's lantern; buccal sacs are present and well-developed. Stewart's organs are entirely missing. The aboral sinuses are discreet. Five gonads are present. The structure of the lantern protractor muscles is smooth.

Compass elevator muscles are present, longitudinal body wall muscles are absent. The peri-oesophageal haemal system consists of five spongy bodies; a collateral duct is present. All spines are covered with epidermis. Fig. 12 depicts selected internal views.



**Fig. 12:** *Glyptocidaris crenularis*, internal anatomy. **A** Stomach and extended oesophagus, aboral view. **B** Intestine and gonads, oral view. **A, B** from Clark (1912).

## Echinoida Troschel, 1872 (~65 extant species)

### Parechinidae Mortensen, 1903

*Paracentrotus lividus* (Lamarck, 1816)

MRI (81  $\mu\text{m}$ )<sup>3</sup> (MorphDBase: A\_Ziegler\_20081116-M-42.1), dissection, and literature (Tiedemann 1816, Valentin 1841, Prouho 1887, Vogt & Yung 1888, von Ubisch 1913, Bonnet 1925)

*Psammechinus microtuberculatus* (Blainville, 1825)

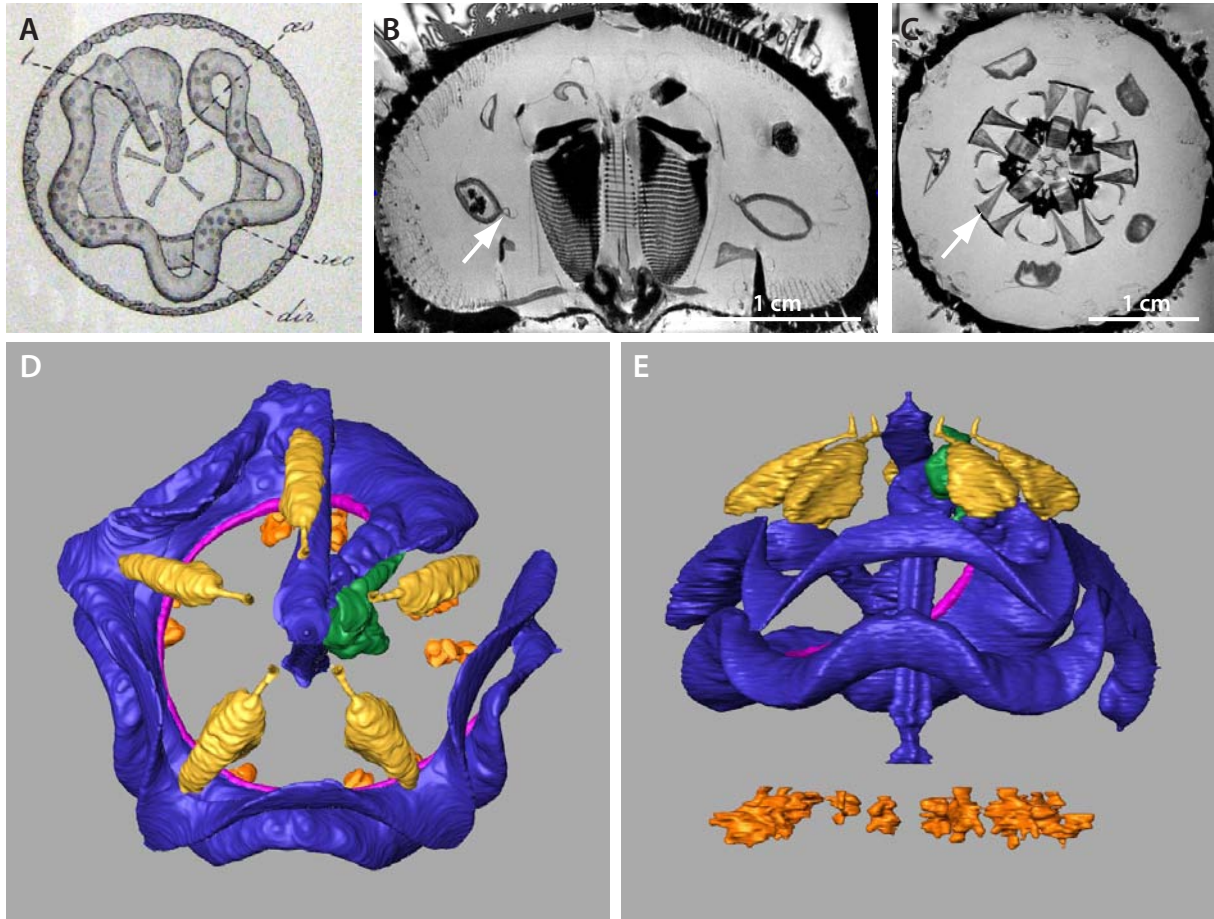
Literature (Ludwig & Hamann 1904, von Ubisch 1913)

*Psammechinus miliaris* (Müller, 1771)

MRI (44  $\mu\text{m}$ )<sup>3</sup> (MorphDBase: A\_Ziegler\_20081116-M-60.1), MRI (81  $\mu\text{m}$ )<sup>3</sup>, MRI (117  $\mu\text{m}$ )<sup>3</sup>, dissection, and literature (Tiedemann 1816, Perrier 1875, Bonnet 1925)

Parechinids possess a cylindrical digestive tract; the stomach as well as the intestine are both well-festooned. The oesophagus is rather short. A well-developed primary siphon is present, a siphonal groove is absent. No secondary siphon can be found in parechinids. A small caecum marks the beginning of the stomach. Stomach and intestine both make a full turn. The stomach is slightly sacculated. An intestinal caecum as well as Gregory's diverticulum are both absent. The rectum ascends aborally towards the anus, an anal cone is absent. The axial

complex is straight in lateral view; the axial organ is oriented vertically. A peripharyngeal coelom surrounds Aristotle's lantern; buccal sacs are present and well-developed. Stewart's organs are entirely missing. The aboral sinuses are discreet. Five gonads are present. The structure of the lantern protractor muscles can be smooth or frilled. Compass elevator muscles are present, longitudinal body wall muscles are absent. The perioesophageal haemal system consists of five spongy bodies; a well-developed collateral duct is present. All spines are covered with epidermis. Fig. 13 depicts selected internal views.



**Fig. 13:** Parechinidae, internal anatomy. **A** *Psammechinus miliaris*, digestive tract with festoons and primary siphon, aboral view. From Bonnet (1925). **B** *Psammechinus miliaris*, MRI, lateral view. Arrow depicts primary siphon. **C** *Psammechinus miliaris*, MRI, aboral view. Arrow depicts lantern retractor muscle. **D** *Psammechinus miliaris*, 3D model of the internal anatomy, aboral view. **E** *Psammechinus miliaris*, 3D model of the internal anatomy, lateral view. Colour legend on page 32.

## Echinidae Gray, 1825

*Echinus esculentus* Linnaeus, 1758

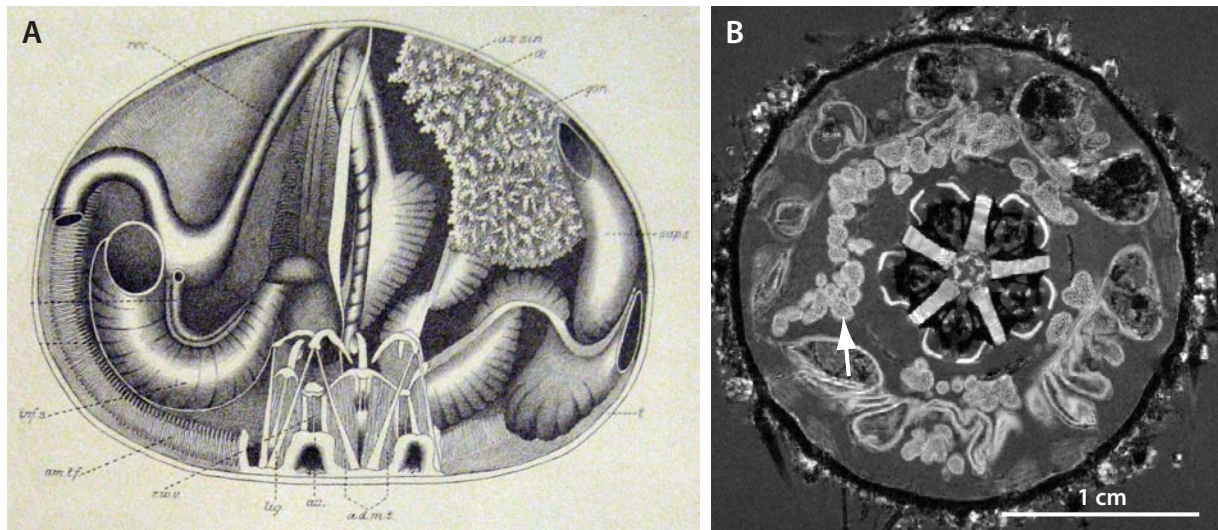
MRI (81  $\mu\text{m}$ )<sup>3</sup> (MorphDBase: A\_Ziegler\_20081116-M-47.1) and literature (Perrier 1875, Valentin 1841, Chadwick 1900, Wagner 1903, MacBride 1906, Bamber 1920, Cuénot 1948, Stott 1955, Fechter 1972)

*Echinus melo* Lamarck, 1816

Literature (Bonnet 1925)

*Gracilechinus acutus* (Lamarck, 1816)

Literature (Hamann 1887, Prouho 1887)



**Fig. 14:** Echinidae, internal anatomy. **A** *Echinus esculentus*, digestive tract and gonads, lateral view. From Chadwick (1900). **B** *Echinus esculentus*, MRI, Aristotle's lantern and digestive tract, aboral view. Arrow depicts gonad.

Echinids possess a cylindrical digestive tract; the stomach as well as the intestine are both well-festooned. The oesophagus extends over one to two ambulacra. A well-developed primary siphon is present, a siphonal groove is absent. No secondary siphon can be found in echinids. A small caecum marks the beginning of the stomach. Stomach and intestine both make a full turn. The stomach is slightly sacculated. An intestinal caecum as well as Gregory's diverticulum are both absent. The rectum ascends aborally towards the anus, an anal cone is absent. The axial complex is straight in lateral view; the axial organ is oriented vertically. A peripharyngeal coelom surrounds Aristotle's lantern; buccal sacs are present and well-developed. Stewart's organs are entirely missing. The aboral sinuses are discreet. Five gonads are present. The structure of the lantern protractor muscles is smooth. Compass elevator muscles are present, longitudinal body wall muscles are absent. The perioesophageal haemal system consists of five spongy bodies; a well-developed collateral duct is present. All spines are covered with epidermis. Fig. 14 depicts selected internal views.

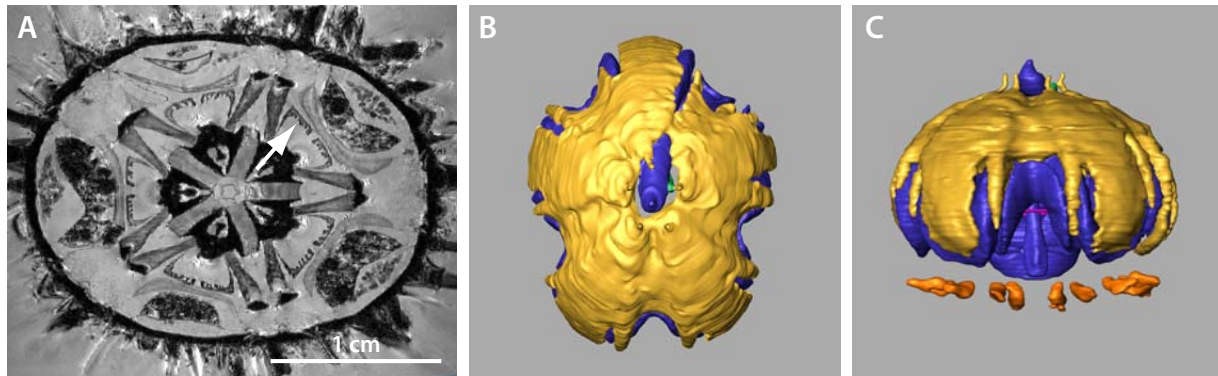
### **Echinometridae Gray, 1855**

*Echinometra mathaei* (Blainville, 1825)

MRI (81  $\mu\text{m}$ )<sup>3</sup> (MorphDBase: A\_Ziegler\_20081116-M-40.1) and dissection

Echinometrids possess a cylindrical digestive tract; the stomach as well as the intestine are both well-festooned. The oesophagus extends over one to two ambulacra. A well-developed primary siphon is present, a siphonal groove is absent. No secondary siphon can be found in echinometrids. A small caecum marks the beginning of the stomach. Stomach and intestine

both make a full turn. The stomach is slightly sacculated. An intestinal caecum as well as Gregory's diverticulum are both absent. The rectum ascends aborally towards the anus, an anal cone is absent. The axial complex is straight in lateral view; the axial organ is oriented vertically. A peripharyngeal coelom surrounds Aristotle's lantern; buccal sacs are present and well-developed. Stewart's organs are entirely missing. The aboral sinuses are discreet. Five gonads are present. The structure of the lantern protractor muscles is frilled. Compass elevator muscles are present, longitudinal body wall muscles are absent. The perioesophageal haemal system consists of five spongy bodies; a well-developed collateral duct is present. All spines are covered with epidermis. Fig. 15 depicts selected internal views.



**Fig. 15:** Echinometridae, internal anatomy. **A** *Echinometra mathaei*, MRI, Aristotle's lantern and digestive tract, aboral view. Arrow depicts frilled lantern protractor muscles. **B** *Echinometra mathaei*, 3D model of the internal anatomy, aboral view. **C** *Echinometra mathaei*, 3D model of the internal anatomy, lateral view. Colour legend on page 32.

### Strongylocentrotidae Gregory, 1900

*Strongylocentrotus dröbachiensis* (Müller, 1776)

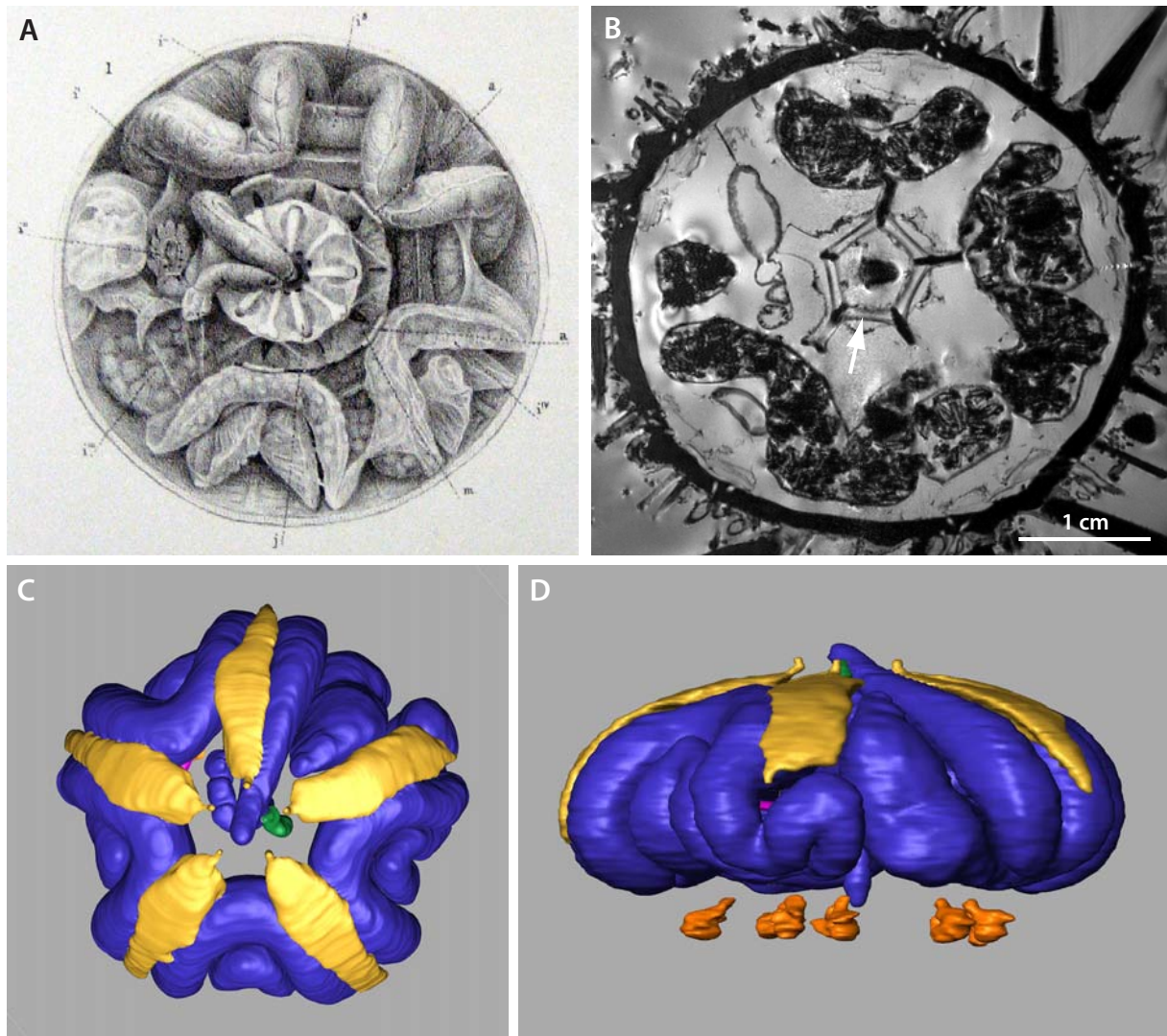
Dissection and literature (Agassiz 1872-1873, Fedotov 1924)

*Strongylocentrotus purpuratus* (Stimpson, 1857)

MRI (42  $\mu\text{m}$ )<sup>3</sup> (MorphDBase: A\_Ziegler\_20081116-M-69.1), MRI (81  $\mu\text{m}$ )<sup>3</sup>, and dissection

Strongylocentrotids possess a cylindrical digestive tract; the stomach as well as the intestine are both well-festooned. The oesophagus extends over one or two ambulacra. A well-developed primary siphon is present, a siphonal groove is absent. No secondary siphon can be found in strongylocentrotids. A small caecum marks the beginning of the stomach. Stomach and intestine both make a full turn. The stomach is slightly sacculated. An intestinal caecum as well as Gregory's diverticulum are both absent. The rectum ascends aborally towards the anus, an anal cone is absent. The axial complex is straight in lateral view; the axial organ is oriented vertically. A peripharyngeal coelom surrounds Aristotle's lantern; buccal sacs are present and well-developed. Stewart's organs are entirely missing. The aboral sinuses are discreet. Five gonads are present. The structure of the lantern protractor muscles is smooth.

Compass elevator muscles are present, longitudinal body wall muscles are absent. The peri-oesophageal haemal system consists of five spongy bodies; a well-developed collateral duct is present. All spines are covered with epidermis. Fig. 16 depicts selected internal views.



**Fig. 16:** Strongylocentrotidae, internal anatomy. **A** *Strongylocentrotus dröbachiensis*, digestive tract and Aristotle's lantern, aboral view. From Agassiz (1872-1873). **B** *Strongylocentrotus purpuratus*, MRI, digestive tract, aboral view. Arrow depicts compass elevator muscle. **C** *Strongylocentrotus purpuratus*, 3D model of the internal anatomy, aboral view. **D** *Strongylocentrotus purpuratus*, 3D model of the internal anatomy, lateral view. Colour legend on page 32.

### Toxopneustidae Troschel, 1872

*Lytechinus variegatus* (Lamarck, 1816)

MRI (81  $\mu\text{m}$ )<sup>3</sup> (MorphDBase: A\_Ziegler\_20081116-M-48.1)

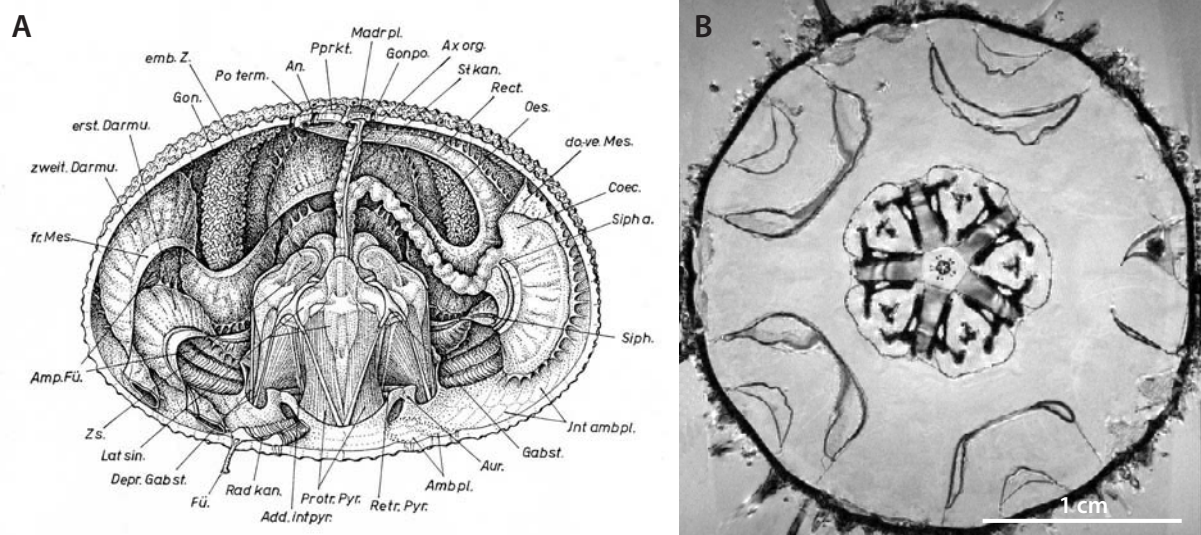
*Sphaerechinus granularis* (Lamarck, 1816)

MRI (81  $\mu\text{m}$ )<sup>3</sup> (MorphDBase: A\_Ziegler\_20081116-M-67.1), MRI (117  $\mu\text{m}$ )<sup>3</sup>, dissection, and literature (Valentin 1841, Koehler 1883, Ludwig 1889-1892, Leipoldt 1893, Bonnet 1925, Strenger 1973)

*Tripneustes esculentus* (Leske, 1778)

## Literature (Hyman 1955)

Toxopneustids possess a cylindrical digestive tract; the stomach as well as the intestine are both well-festooned. The oesophagus extends over one to two ambulacra. A well-developed primary siphon is present, a siphonal groove is absent. No secondary siphon can be found in toxopneustids. A small caecum marks the beginning of the stomach. Stomach and intestine both make a full turn. The stomach is slightly sacculated. An intestinal caecum as well as Gregory's diverticulum are both absent. The rectum ascends aborally towards the anus, an anal cone is absent. The axial complex is straight in lateral view; the axial organ is oriented vertically. A peripharyngeal coelom surrounds Aristotle's lantern; buccal sacs are present and well-developed. Stewart's organs are entirely missing. The aboral sinuses are discreet. Five gonads are present. The structure of the lantern protractor muscles can be smooth or frilled. Compass elevator muscles are present, longitudinal body wall muscles are absent. The peri-oesophageal haemal system consists of five spongy bodies; a well-developed collateral duct is present. All spines are covered with epidermis. Fig. 17 depicts selected internal views.



**Fig. 17:** Toxopneustidae, internal anatomy. **A** *Sphaerechinus granularis*, Aristotle's lantern and digestive tract, lateral view. From Strenger (1973). **B** *Lytechinus variegatus*, MRI, Aristotle's lantern and digestive tract, aboral view.

## Temnopleuroidea Mortensen, 1942 (~120 extant species)

### Trigonocidaridae Mortensen, 1903

*Genocidaris maculata* Agassiz, 1869

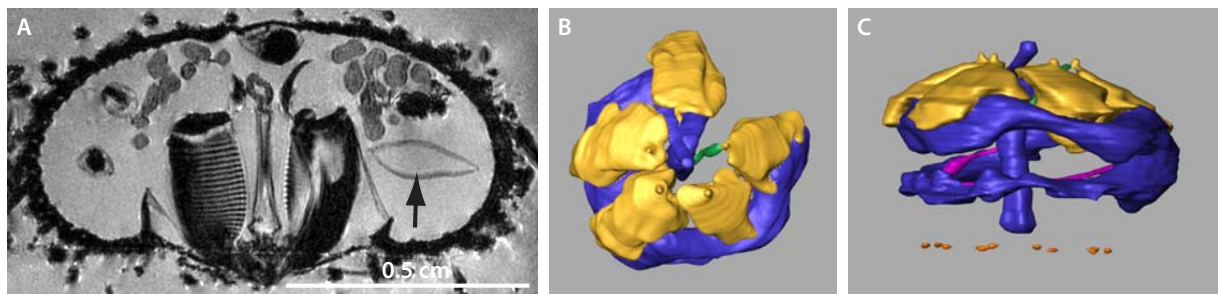
MRI (36  $\mu\text{m}$ )<sup>3</sup> (MorphDBase: A\_Ziegler\_20081116-M-43.1)

*Trigonocidaris albida* Agassiz, 1869

MRI (32  $\mu\text{m}$ )<sup>3</sup> (MorphDBase: A\_Ziegler\_20081116-M-70.1)



Trigonocidarids possess a cylindrical to flattened digestive tract; the stomach as well as the intestine are both only slightly festooned. The oesophagus is rather short. A thin-walled primary siphon is present; a siphonal groove is presumably absent. No secondary siphon can be found in this taxon. A small caecum marks the beginning of the stomach. Stomach and intestine both make a full turn. The stomach is smooth-walled. An intestinal caecum as well as Gregory's diverticulum are both absent. The rectum ascends aborally towards the anus, an anal cone is absent. The axial complex is straight to oblique in lateral view; the axial organ is oriented vertically. A peripharyngeal coelom surrounds Aristotle's lantern; buccal sacs are present and rather small. Stewart's organs are entirely missing. The aboral sinuses are discreet. Five gonads are present. The structure of the lantern protractor muscles is smooth. Compass elevator muscles are present, longitudinal body wall muscles are absent. The perioesophageal haemal system consists of five spongy bodies; a slightly developed collateral duct is present. All spines are covered with epidermis. Fig. 18 depicts selected internal views.



**Fig. 18:** Trigonocidaridae, internal anatomy. **A** *Trigonocidaris albida*, MRI, lateral view. Arrow depicts stomach. **B** *Genocidaris maculata*, 3D model of the internal anatomy, aboral view. **C** *Genocidaris maculata*, 3D model of the internal anatomy, lateral view. Colour legend on page 32.

### **Temnopleuridae Agassiz, 1872**

*Mespilia globulus* (Linnaeus, 1758)

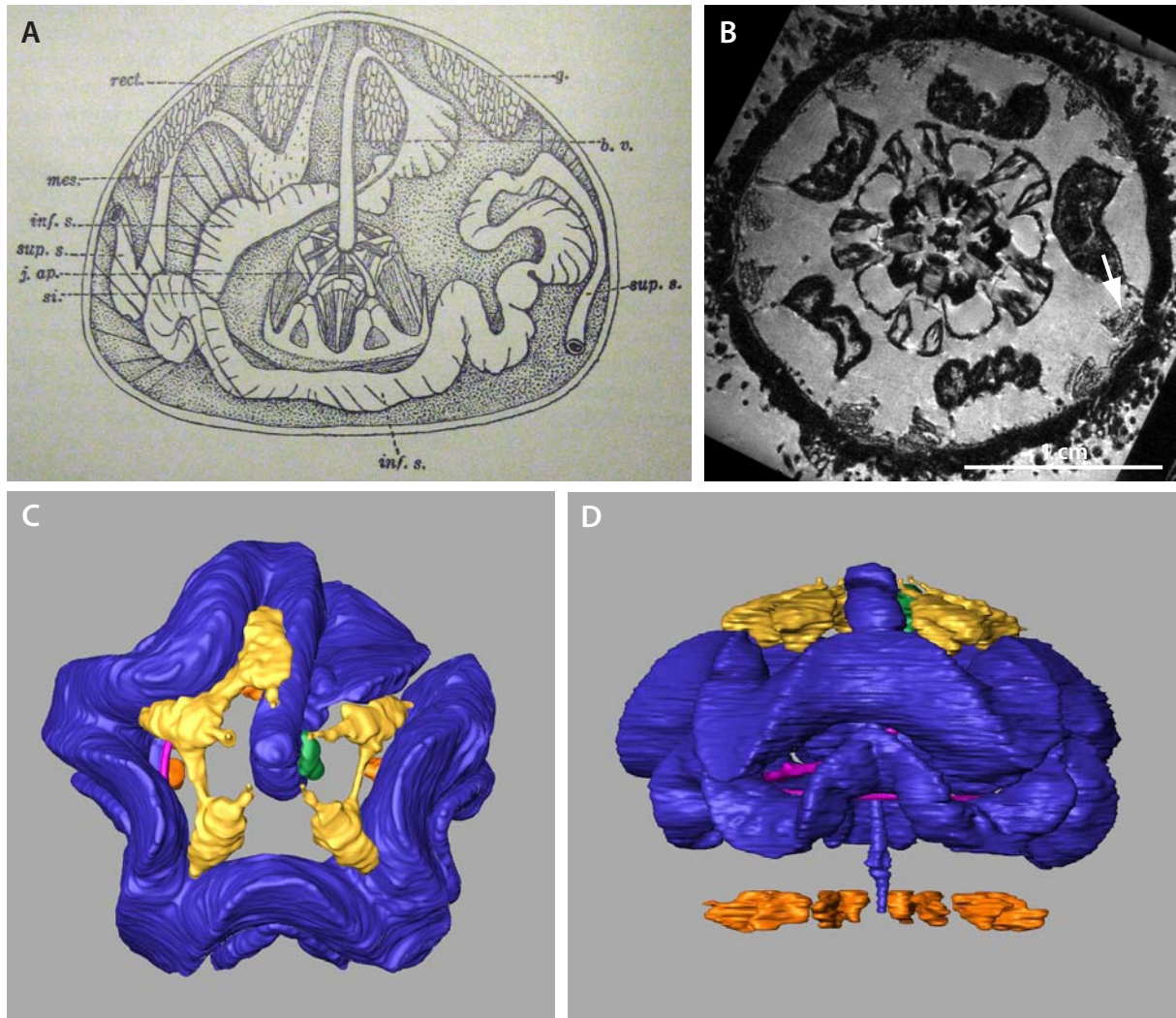
MRI (44  $\mu\text{m}$ )<sup>3</sup> (MorphDBase: A\_Ziegler\_20081116-M-52.1) and MRI (81  $\mu\text{m}$ )<sup>3</sup>

*Salmacis bicolor* (Agassiz, 1846)

Literature (Aiyar 1938)

Temnopleurids possess a cylindrical digestive tract; the stomach as well as the intestine are both well-festooned. The oesophagus is rather short. A well-developed primary siphon is present, a siphonal groove is absent. No secondary siphon can be found in temnopleurids. A small caecum marks the beginning of the stomach. Stomach and intestine both make a full turn. The stomach is smooth-walled. An intestinal caecum as well as Gregory's diverticulum are both absent. The rectum ascends aborally towards the anus, an anal cone is absent. The axial complex is straight in lateral view; the axial organ is oriented vertically. A peripharyngeal coelom surrounds Aristotle's lantern; buccal sacs are present and well-developed. Stewart's organs are entirely missing. The aboral sinuses are discreet. Five gonads are present. The

structure of the lantern protractor muscles is smooth. Compass elevator muscles are present, longitudinal body wall muscles are absent. The perioesophageal haemal system consists of five spongy bodies; a well-developed collateral duct is present. All spines are covered with epidermis. Fig. 19 depicts selected internal views.



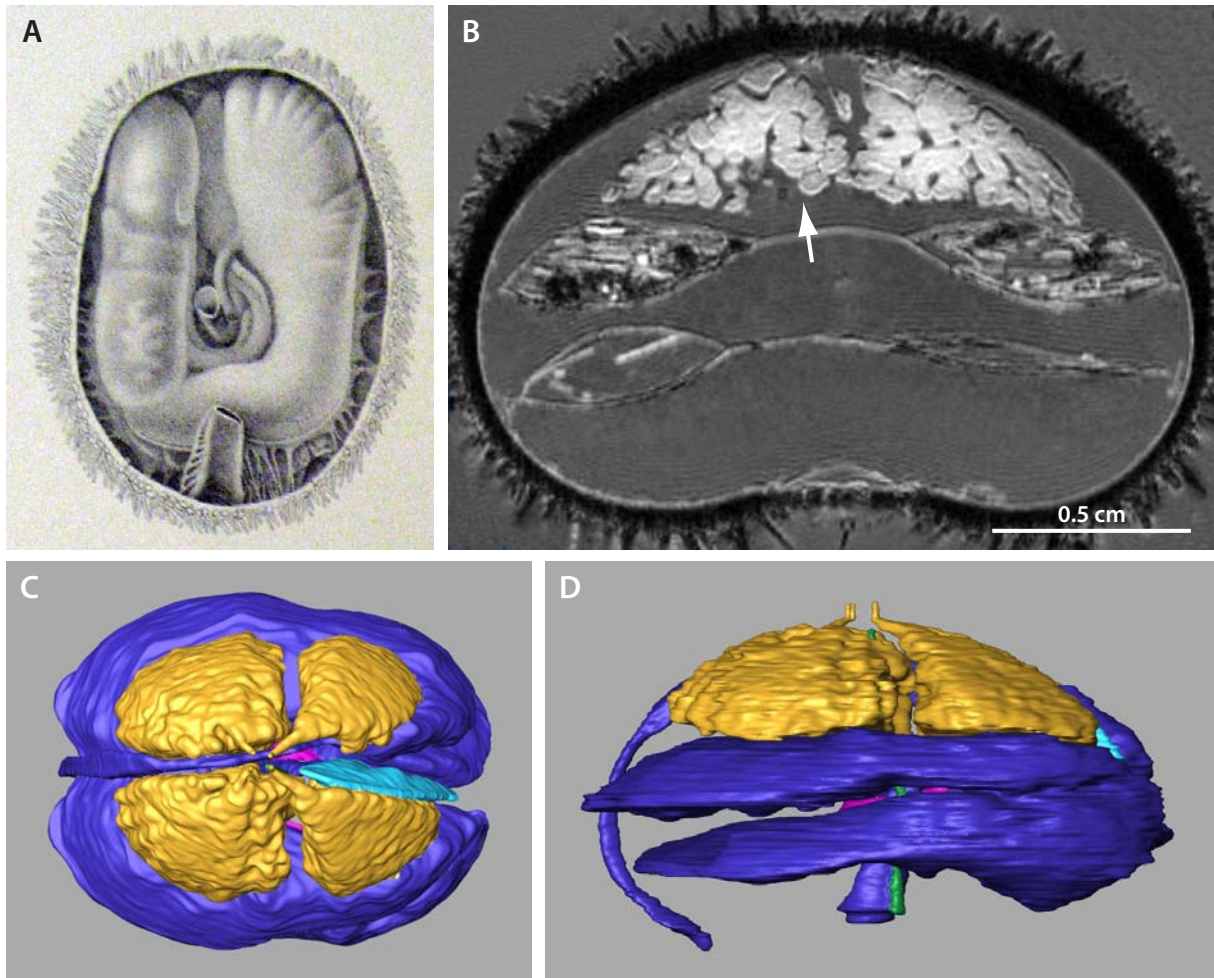
**Fig. 19:** Temnopleuridae, internal anatomy. **A** *Salmacis bicolor*, Aristotle's lantern, gonads, and digestive tract, lateral view. From Aiyar (1938). **B** *Mespilia globulus*, MRI, digestive tract and Aristotle's lantern, aboral view. Arrow depicts ampulla of the water vascular system. **C** *Mespilia globulus*, 3D model of the internal anatomy, aboral view. **D** *Mespilia globulus*, 3D model of the internal anatomy, lateral view. Colour legend on page 32.

## Holactypoida Duncan, 1889 (3 extant species)

### Echinoneidae Agassiz & Desor, 1847

*Echinoneus cyclostomus* Leske, 1778

MRI (66  $\mu\text{m}$ )<sup>3</sup>, MRI (86  $\mu\text{m}$ )<sup>3</sup> (MorphDBase: A\_Ziegler\_20081116-M-46.1), MRI (93  $\mu\text{m}$ )<sup>3</sup>, MRI (126  $\mu\text{m}$ )<sup>3</sup>, and literature (Westergren 1911)



**Fig. 20:** Echinoneidae, internal anatomy. **A** *Echinoneus cyclostomus*, stomach, oesophagus, and rectum, oral view. From Westergren (1911). **B** *Echinoneus cyclostomus*, MRI, digestive tract, fronto-lateral view. Arrow depicts gonad. **C** *Echinoneus cyclostomus*, 3D model of the internal anatomy, aboral view. **D** *Echinoneus cyclostomus*, 3D model of the internal anatomy, lateral view. Colour legend on page 33.

Echinoneids possess a cylindrical digestive tract, festoons are entirely absent. The oesophagus is short and oriented towards ambulacrum III. A primary siphon is present and attached to the stomach throughout its entire course. A siphonal groove is absent. Members of this taxon do not possess a secondary siphon. The gastric caecum is ovoid in form; its connection with the stomach is located in its adoral middle part. Stomach and intestine both make a full turn; the stomach is smooth-walled. The mesenterial connection of the first gut loop is not extended towards ambulacrum III. An intestinal caecum as well as Gregory's diverticulum are not present. The rectum initially extends towards interambulacrum 5 and later towards the adorally located anus. An anal cone is absent. The form of the axial complex is straight in lateral view; the axial organ is oriented vertically. The stone canal shows a distinct swelling in its adoral part. A peripharyngeal coelom surrounds Aristotle's lantern in juvenile specimens; a small peripharyngeal coelom is present in the adult. Buccal sacs as well as Stewart's organs are absent. The aboral sinuses are fused into a single pentagonal membrane. Four gonads are present; the anterior pair is slightly smaller than the posterior one. Longitudinal body wall muscles are absent, compass elevator muscles are present in

juvenile specimens. The peripharyngeal haemal system is not differentiated. A collateral duct of the digestive tract haemal system is absent. All spines are covered by an epidermis. Fig. 20 depicts selected internal views.

## „Cassiduloida“ Agassiz & Desor, 1847 (~30 extant species)

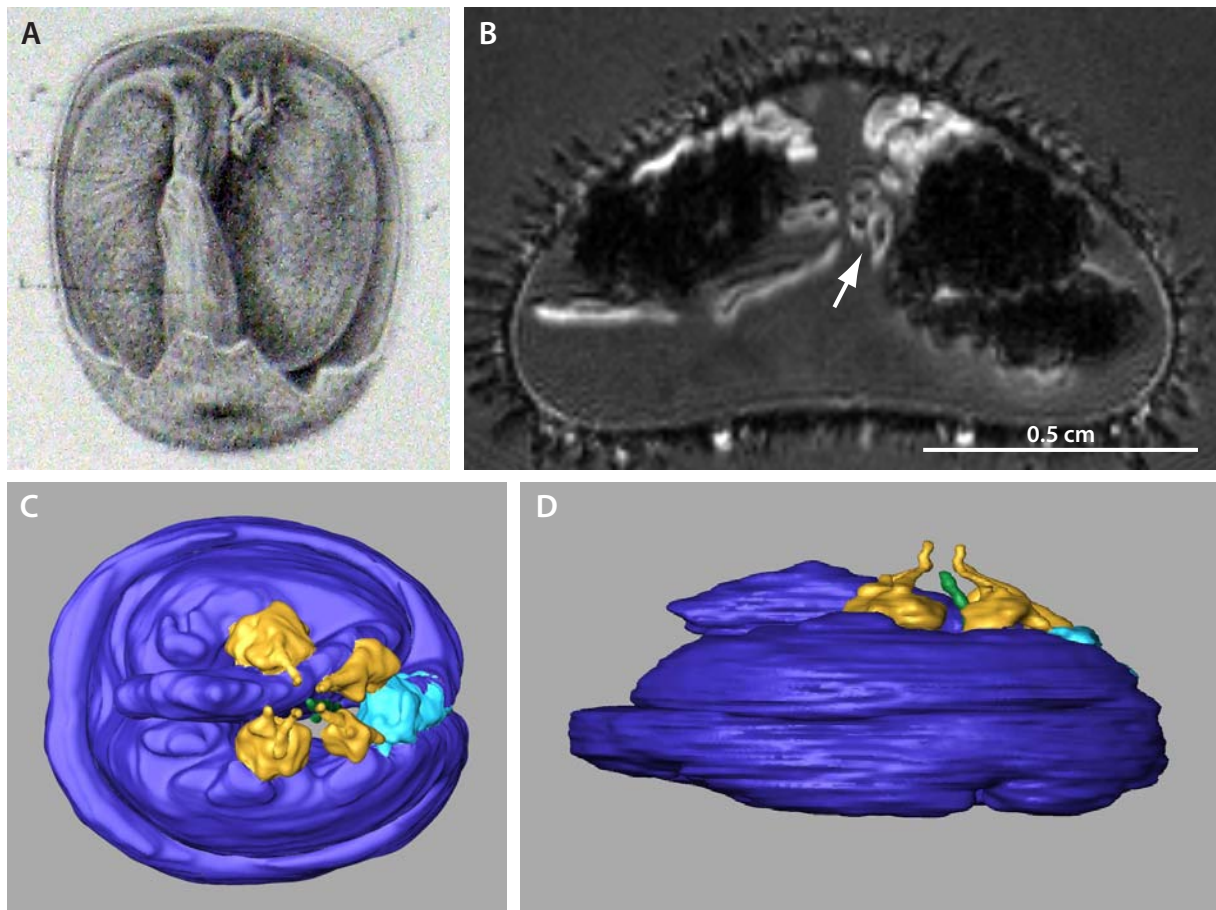
### Cassidulidae Agassiz & Desor, 1847

*Cassidulus caribaeorum* Lamarck, 1801

MRI (81  $\mu\text{m}$ )<sup>3</sup> (MorphDBase: A\_Ziegler\_20081116-M-66.1) and literature (Gladfelter 1978)

*Rhyncholampas pacificus* (Agassiz, 1863)

Literature (Agassiz 1872-1873)



**Fig. 21:** Cassidulidae, internal anatomy. **A** *Rhyncholampas pacificus*, rectum, intestine, and gastric caecum, aboral view. From Agassiz (1872-1873). **B** *Cassidulus caribaeorum*, MRI, digestive tract and gonads, fronto-lateral view. Arrow depicts gastric caecum. **C** *Cassidulus caribaeorum*, 3D model of the internal anatomy, aboral view. **D** *Cassidulus caribaeorum*, 3D model of the internal anatomy, lateral view. Colour legend on page 33.

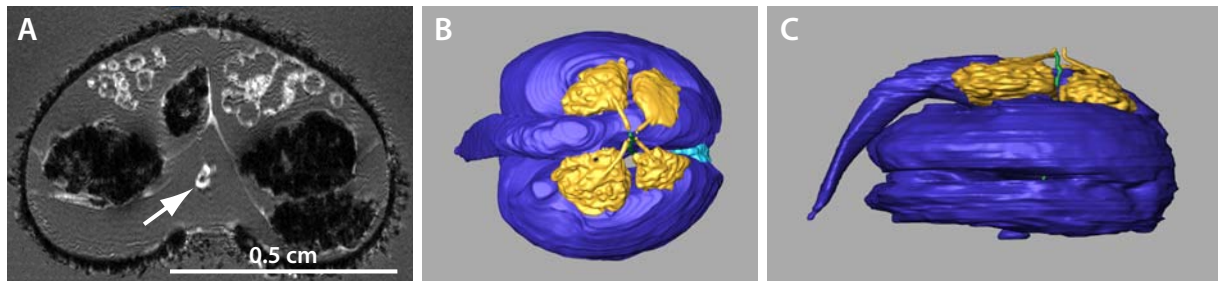
Cassidulids possess a cylindrical digestive tract, festoons are entirely absent. The oesophagus is short and oriented towards ambulacrum III. A primary siphon is present and attached to the stomach throughout its entire course. A siphonal groove is absent. Members of this

taxon do not possess a secondary siphon. The gastric caecum is characterized by numerous small tubular structures, each attaching to the anterior part of the stomach. Stomach and intestine both make a full turn; the stomach is smooth-walled. The mesenterial connection of the first gut loop is not extended towards ambulacrum III. An intestinal caecum as well as Gregory's diverticulum are not present. The rectum extends towards interambulacrum 5. An anal cone is absent. The axial complex is bent towards ambulacrum III; the axial organ is oriented more or less vertically. The stone canal shows a distinct swelling in its adoral part. A peripharyngeal coelom surrounds Aristotle's lantern in juvenile specimens; a small peripharyngeal coelom is present in the adult. Buccal sacs as well as Stewart's organs are absent. The aboral sinuses are fused into a single pentagonal membrane. Four gonads are present; the anterior pair is conspicuously smaller than the posterior one. Longitudinal body wall muscles are absent, compass elevator muscles are present in the juvenile specimens. The peripharyngeal haemal system is not differentiated. A collateral duct of the digestive tract haemal system is absent. All spines are covered by an epidermis. Fig. 21 depicts selected internal views.

### Echinolampadidae Gray, 1851

*Echinolampas depressa* Gray, 1851

MRI (81  $\mu\text{m}$ )<sup>3</sup> (MorphDBase: A\_Ziegler\_20081116-M-37.1) and dissection



**Fig. 22:** Echinolampadidae, internal anatomy. **A** *Echinolampas depressa*, MRI, digestive tract, mesenteries, and gonads, fronto-lateral view. Arrow depicts oesophagus. **B** *Echinolampas depressa*, 3D model of the internal anatomy, aboral view. **C** *Echinolampas depressa*, 3D model of the internal anatomy, lateral view. Colour legend on page 33.

Echinolampadids possess a cylindrical digestive tract, festoons are entirely absent. The oesophagus is short and oriented towards ambulacrum III. A primary siphon is present and attached to the stomach throughout its course. A siphonal groove is absent. Members of this taxon presumably do not possess a secondary siphon, although the histology of a thin-walled structure paralleling stomach and primary siphon still needs to be ascertained. The gastric caecum is characterized by numerous small tubular structures, each attaching to the anterior part of the stomach. Stomach and intestine both make a full turn; the stomach is smooth-walled. The mesenterial connection of the first gut loop is not extended towards ambulacrum III. An intestinal caecum as well as Gregory's diverticulum are not present. The rectum extends towards interambulacrum 5 and descends towards the adorally located anus.

An anal cone is absent. The axial complex is bent towards ambulacrum III; the axial organ is oriented more or less vertically. The stone canal does not show a distinct swelling in its adoral part. A peripharyngeal coelom surrounds Aristotle's lantern in juvenile specimens; a small peripharyngeal coelom is present in the adult. Buccal sacs as well as Stewart's organs are absent. The aboral sinuses are fused into a single pentagonal membrane. Four gonads are present; the anterior pair is conspicuously smaller than the posterior one. Longitudinal body wall muscles are absent. Compass elevator muscles are absent in the juvenile specimens. The peripharyngeal haemal system is not differentiated. A collateral duct of the digestive tract haemal system is absent. All spines are covered by an epidermis. Fig. 22 depicts selected internal views.

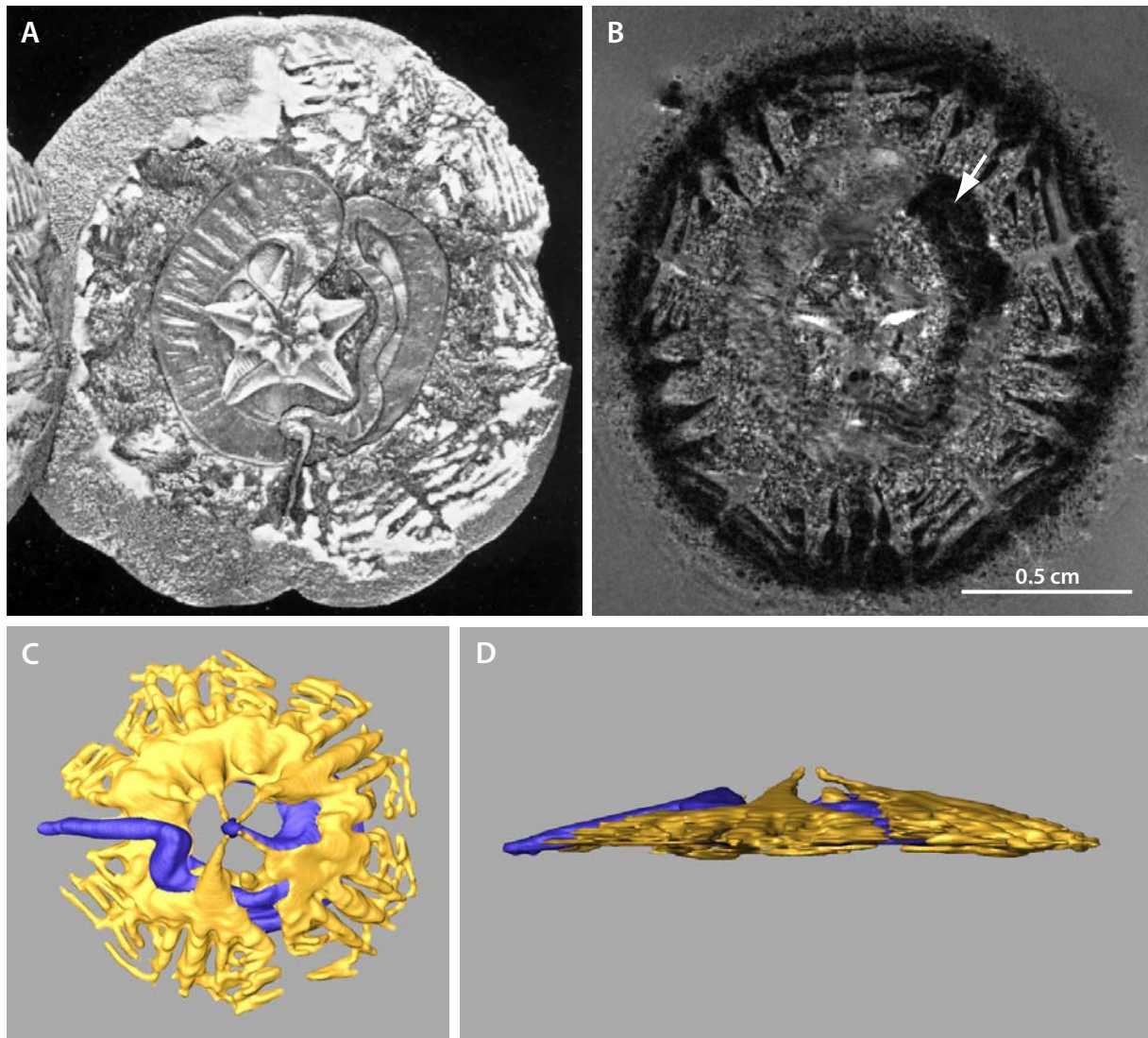
### **Clypeasteroida Agassiz, 1835 (~125 extant species)**

#### **Arachnoididae Duncan, 1889**

*Arachnoides placenta* (Linnaeus, 1758)

MRI (81  $\mu\text{m}$ )<sup>3</sup> (MorphDBase: A\_Ziegler\_20081116-M-39.1) and literature (Koehler 1922)

Arachnoidids possess a flattened digestive tract, festoons are entirely absent. The oesophagus is short and oriented towards ambulacrum III. A primary siphon is present and not attached to the stomach during its first half. A siphonal groove is absent. Members of this taxon presumably do not possess a secondary siphon. The gastric caecum is characterized by numerous small spherical structures located near the anterior part of the stomach. Stomach and intestine both make a half turn, the stomach is slightly sacculated. An intestinal caecum as well as Gregory's diverticulum are not present. The rectum extends towards interambulacrum 5. An anal cone is absent. The axial complex is straight in lateral view; the axial organ is oriented vertically. A peripharyngeal coelom surrounds Aristotle's lantern. Buccal sacs as well as Stewart's organs are absent. The aboral sinuses are fused into a single pentagonal membrane. Four gonads are present. Longitudinal body wall and compass elevator muscles are absent. The peripharyngeal haemal system consists of five spongy bodies. A collateral duct of the digestive tract haemal system is absent. All spines are covered by an epidermis. Fig. 23 depicts selected internal views.



**Fig. 23:** Arachnoididae, internal anatomy. **A** *Arachnoides placenta*, digestive tract, primary siphon, and gonads, aboral view. From Koehler (1922). **B** *Arachnoides placenta*, MRI, aboral view. Arrow depicts sediment-filled intestine. **C** *Arachnoides placenta*, 3D model of the internal anatomy, aboral view. **D** *Arachnoides placenta*, 3D model of the internal anatomy, lateral view. Colour legend on page 33.

### Clypeasteridae Agassiz, 1835

*Clypeaster humilis* (Leske, 1778)

Literature (Koehler 1922)

*Clypeaster reticulatus* (Linnaeus, 1758)

MRI ( $81 \mu\text{m}$ )<sup>3</sup> (MorphDBase: A\_Ziegler\_20081116-M-31.1) and literature (Koehler 1922)

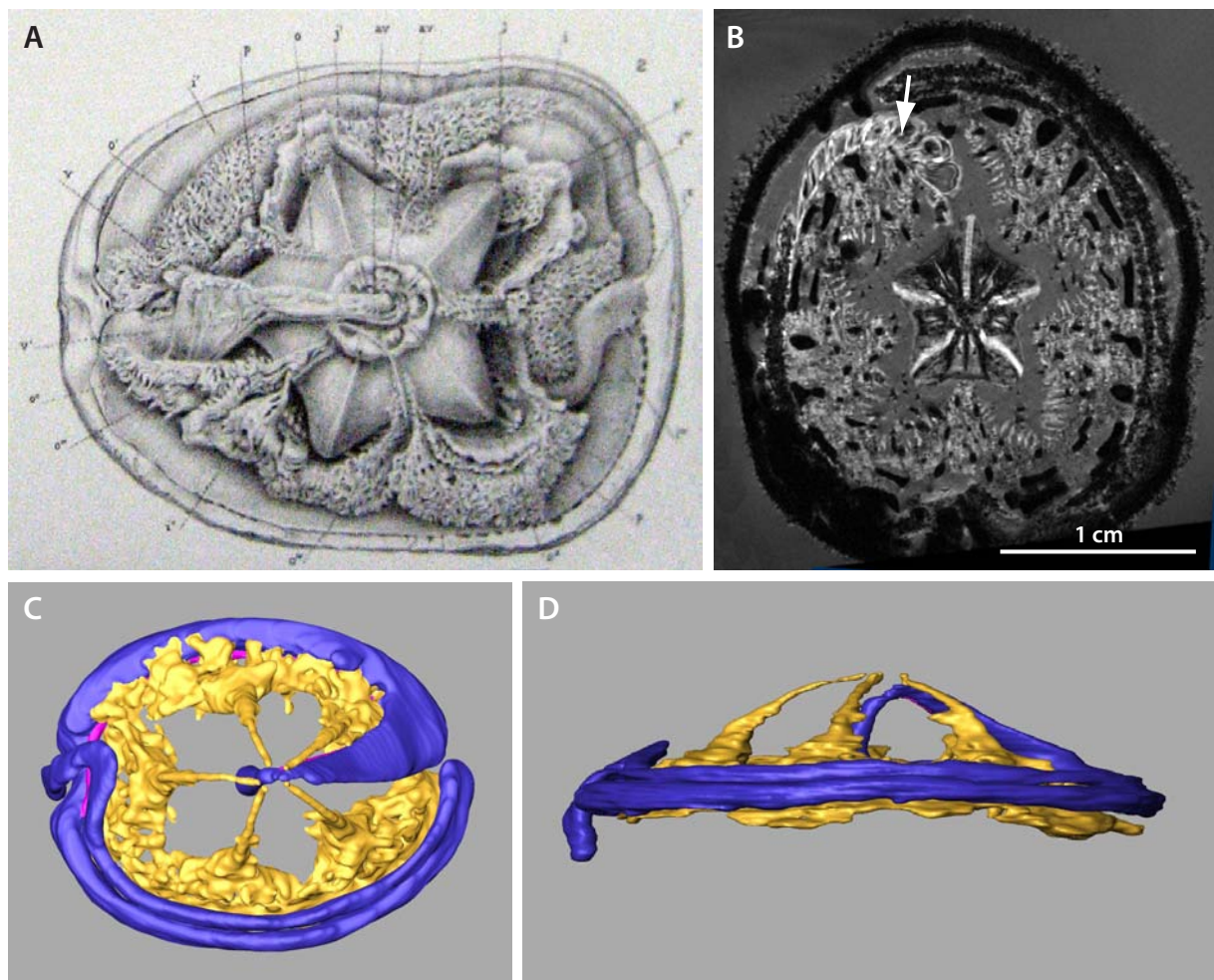
*Clypeaster rosaceus* (Linnaeus, 1758)

MRI ( $96 \mu\text{m}$ )<sup>3</sup> (MorphDBase: A\_Ziegler\_20081116-M-32.1) and literature (Agassiz 1872-1873)

*Clypeaster subdepressus* (Gray, 1825)

Literature (Agassiz 1872-1873)

Clypeasterids possess a flattened digestive tract, festoons are entirely absent. The oesophagus is short and oriented towards ambulacrum III. A primary siphon is present and attached to the stomach during its entire course. A siphonal groove is absent. Members of this taxon do not possess a secondary siphon. The gastric caecum is characterized by numerous small spherical structures located near the anterior part of the stomach. Stomach and intestine both make a half turn, the stomach is slightly sacculated. An intestinal caecum as well as Gregory's diverticulum are not present. The rectum extends towards interambulacrum 5. An anal cone is absent. The axial complex is straight in lateral view; the axial organ is oriented vertically. A peripharyngeal coelom surrounds Aristotle's lantern. Buccal sacs as well as Stewart's organs are absent. The aboral sinuses are fused into a single pentagonal membrane. Five gonads are present. Longitudinal body wall and compass elevator muscles are absent. The peripharyngeal haemal system consists of five spongy bodies. A collateral duct of the digestive tract haemal system is absent. All spines are covered by an epidermis. Fig. 24 depicts selected internal views.

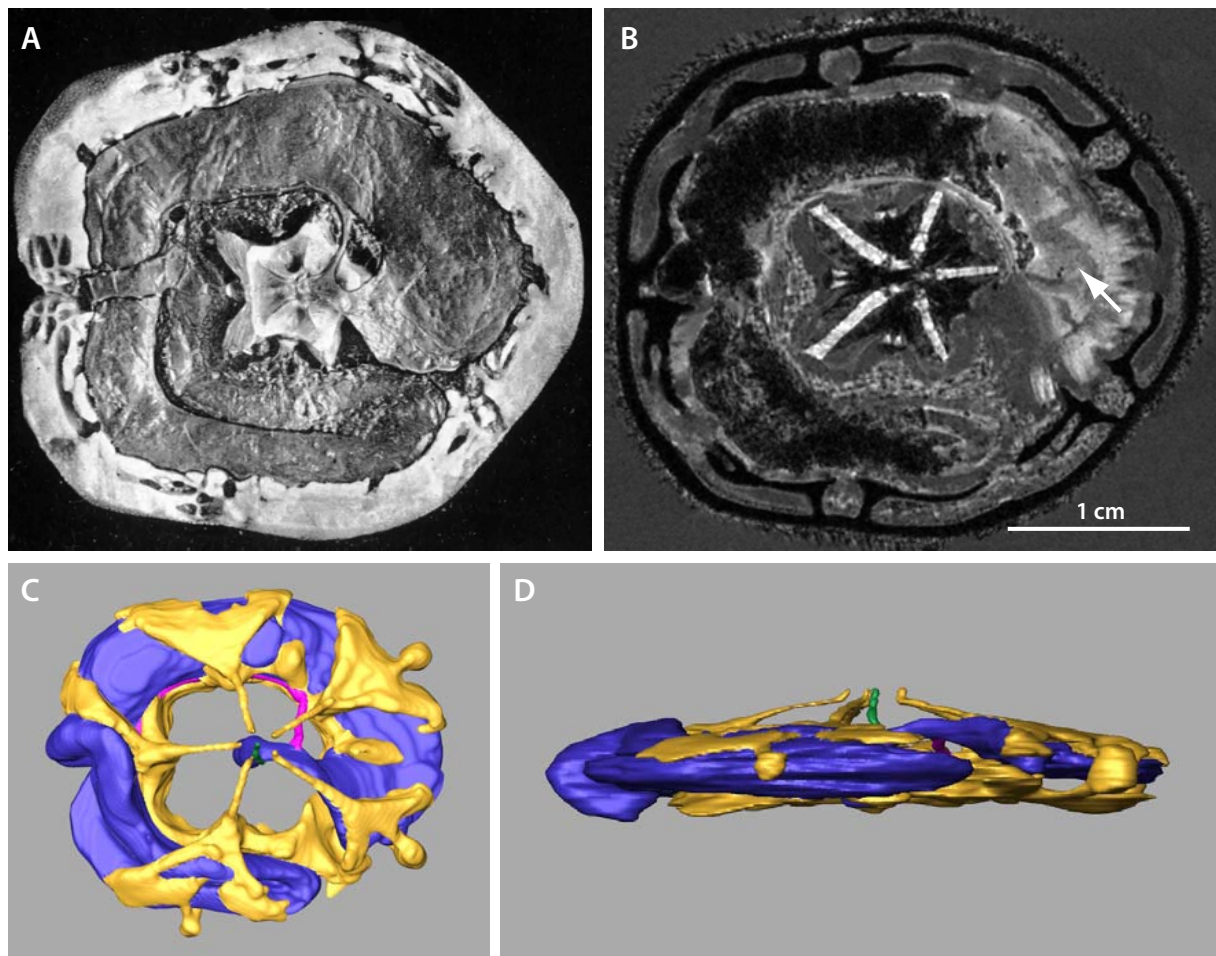


**Fig. 24:** Clypeasteridae, internal anatomy. **A** *Clypeaster rosaceus*, Aristotle's lantern, anterior stomach, and gonads, aboral view. From Agassiz (1872-1873). **B** *Clypeaster rosaceus*, MRI, aboral view. Arrow depicts anterior stomach. **C** *Clypeaster reticulatus*, 3D model of the internal anatomy, aboral view. **D** *Clypeaster reticulatus*, 3D model of the internal anatomy, lateral view. Colour legend on page 33.



**Laganidae Agassiz, 1873***Hupea decagonale* (Blainville, 1827)

Literature (Koehler 1922)

*Jacksonaster depressum* (Agassiz, 1841)MRI (86  $\mu\text{m}$ )<sup>3</sup> (MorphDBase: A\_Ziegler\_20081116-M-50.1), MRI (91  $\mu\text{m}$ )<sup>3</sup>, and literature (Koehler 1922)*Laganum laganum* (Leske, 1778)MRI (81  $\mu\text{m}$ )<sup>3</sup> (MorphDBase: A\_Ziegler\_20081116-M-49.1)*Laganum joubini* Koehler 1922MRI (44  $\mu\text{m}$ )<sup>3</sup>*Peronella lesueuri* Agassiz, 1841MRI (81  $\mu\text{m}$ )<sup>3</sup> (MorphDBase: A\_Ziegler\_20081116-M-44.1) and literature (Koehler 1922)*Peronella orbicularis* Leske, 1778MRI (81  $\mu\text{m}$ )<sup>3</sup> (MorphDBase: A\_Ziegler\_20081116-M-45.1) and literature (Cuénot 1891)

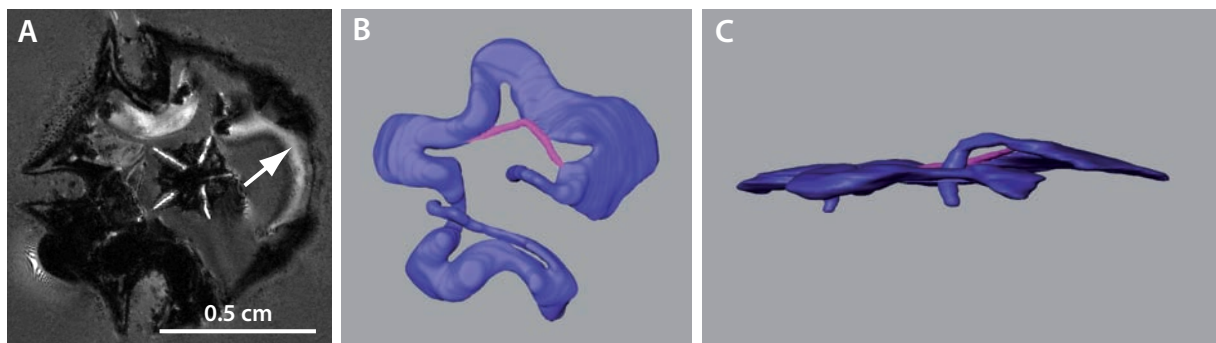
**Fig. 25:** Laganidae, internal anatomy. **A** *Jacksonaster depressum*, digestive tract with partially detached primary siphon, aboral view. From Koehler (1922). **B** *Laganum laganum*, MRI, Aristotle's lantern and digestive tract, aboral view. Arrow depicts anterior stomach. **C** *Laganum laganum*, 3D model of the internal anatomy, aboral view. **D** *Laganum laganum*, 3D model of the internal anatomy, lateral view. Colour legend on page 33.

Laganids possess a flattened digestive tract, festoons are entirely absent. The oesophagus is short and oriented towards ambulacrum III. A primary siphon is present and is not attached to the stomach during its first half. A siphonal groove is absent. Members of this taxon do not possess a secondary siphon. The gastric caecum is presumably absent. Stomach and intestine both make a half turn, the stomach is slightly sacculated. An intestinal caecum as well as Gregory's diverticulum are not present. The rectum extends towards interambulacrum 5. An anal cone is absent. The axial complex is straight in lateral view; the axial organ is oriented vertically. A peripharyngeal coelom surrounds Aristotle's lantern. Buccal sacs as well as Stewart's organs are absent. The aboral sinuses are fused into a single pentagonal membrane. Five gonads are present. Longitudinal body wall and compass elevator muscles are absent. The peripharyngeal haemal system consists of five spongy bodies. A collateral duct of the digestive tract haemal system is absent. All spines are covered by an epidermis. Fig. 25 depicts selected internal views.

### Rotulidae Gray, 1855

*Rotula multiloba* Schuhmacher, 1817

MRI (81  $\mu\text{m}$ )<sup>3</sup> (MorphDBase: A\_Ziegler\_20081116-M-57.1)



**Fig. 26:** Rotulidae, internal anatomy. **A** *Rotula multiloba*, juvenile specimen, MRI, Aristotle's lantern and digestive tract, aboral view. Arrow depicts anterior stomach. **B** *Rotula multiloba*, 3D model of the internal anatomy, aboral view. **C** *Rotula multiloba*, 3D model of the internal anatomy, lateral view. Colour legend on page 33.

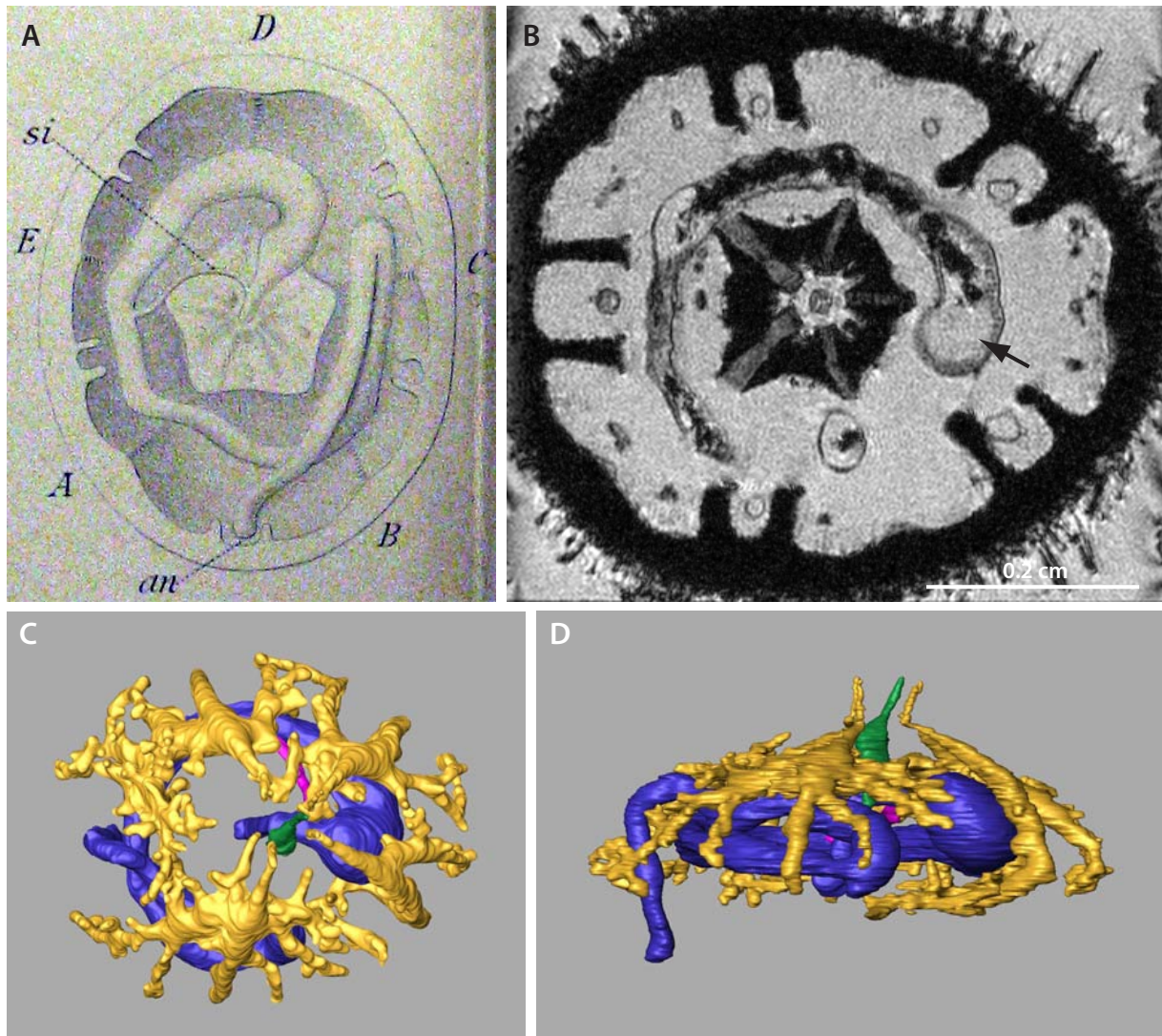
Rotulids possess a flattened digestive tract, festoons are entirely absent. The oesophagus is short and oriented towards ambulacrum III. A primary siphon is present and is not attached to the stomach during its first half. A siphonal groove is absent. Members of this taxon do not possess a secondary siphon. The gastric caecum is presumably absent. Stomach and intestine both make a half turn, the stomach is slightly sacculated. An intestinal caecum as well as Gregory's diverticulum are not present. The rectum extends towards interambulacrum 5. An anal cone is absent. The axial complex is straight in lateral view; the axial organ is oriented vertically. A peripharyngeal coelom surrounds Aristotle's lantern. Buccal sacs as well as Stewart's organs are absent. The aboral sinuses are fused into a single pentagonal membrane. Four gonads are present. Longitudinal body wall and compass elevator muscles are absent. The peripharyngeal haemal system consists of five spongy bodies. A collateral

duct of the digestive tract haemal system is absent. All spines are covered by an epidermis. Fig. 26 depicts selected internal views.

### Fibulariidae Duncan, 1889

*Echinocyamus pusillus* (Müller, 1776)

MRI 20 x 18 x 18  $\mu\text{m}^3$  (MorphDBase: A\_Ziegler\_20081116-M-36.1), histology, and literature (Cuénot 1891, Telford 1983)



**Fig. 27:** Fibulariidae, internal anatomy. **A** *Echinocyamus pusillus*, Aristotle's lantern and digestive tract, aboral view. From Cuénot (1891). **B** *Echinocyamus pusillus*, MRI, digestive tract, Aristotle's lantern, and gonads, aboral view. Arrow depicts anterior stomach. **C** *Echinocyamus pusillus*, 3D model of the internal anatomy, aboral view. **D** *Echinocyamus pusillus*, 3D model of the internal anatomy, lateral view. Colour legend on page 33.

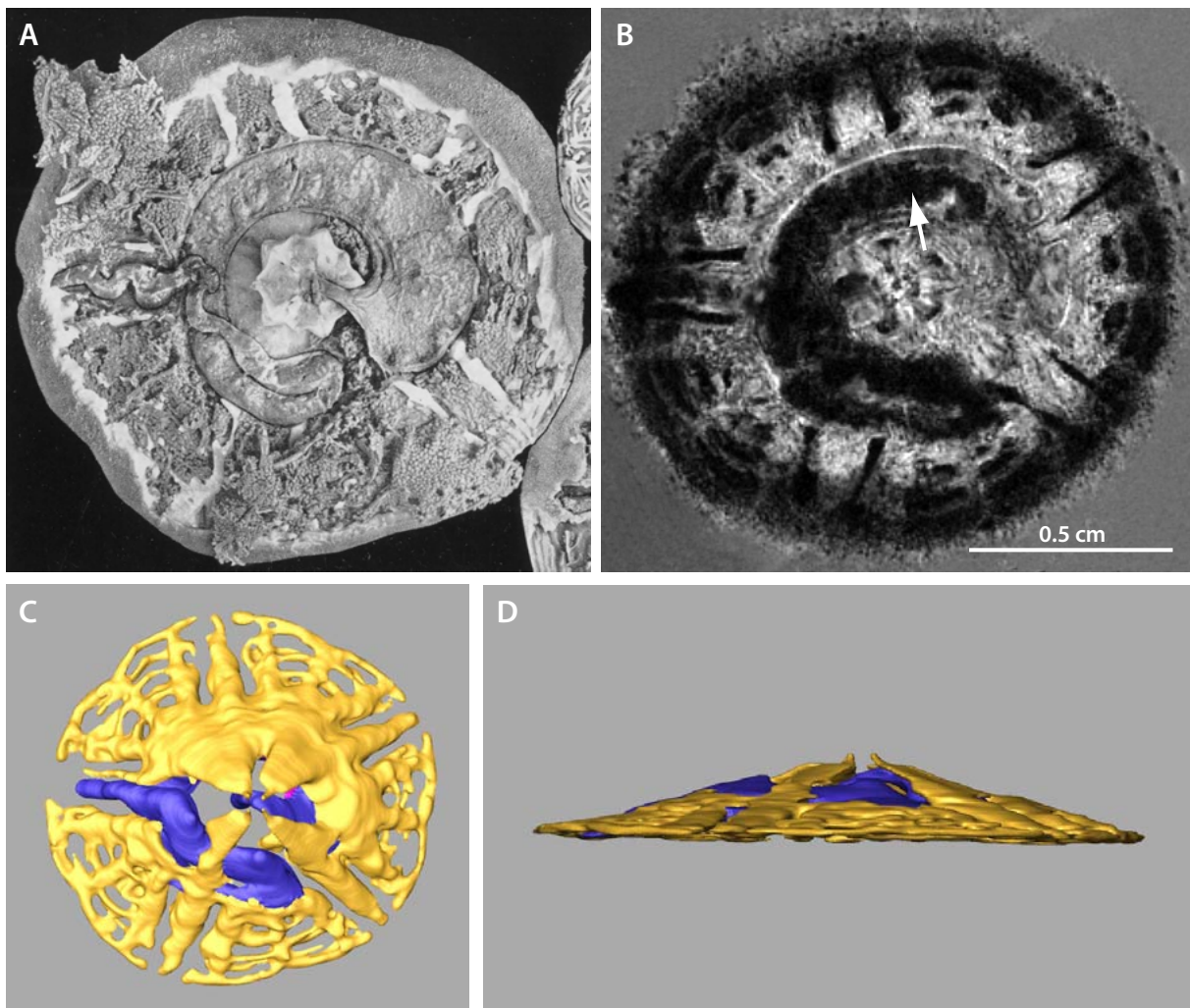
Fibulariids possess a flattened to cylindrical digestive tract, festoons are entirely absent. The oesophagus is short and oriented towards ambulacrum III. A primary siphon is present and is not attached to the stomach during its first half. A siphonal groove is absent. Members of this taxon do not possess a secondary siphon. The gastric caecum is presumably

absent. Stomach and intestine both make a half turn, the stomach is slightly sacculated. An intestinal caecum as well as Gregory's diverticulum are not present. The rectum extends towards interambulacrum 5. An anal cone is absent. The axial complex is straight in lateral view; the axial organ is oriented vertically. A peripharyngeal coelom surrounds Aristotle's lantern. Buccal sacs as well as Stewart's organs are absent. The aboral sinuses are fused into a single pentagonal membrane. Five gonads are present. Longitudinal body wall and compass elevator muscles are absent. The peripharyngeal haemal system consists of five spongy bodies. A collateral duct of the digestive tract haemal system is absent. All spines are covered by an epidermis. Fig. 27 depicts selected internal views.

### Echinarachniidae Lambert, 1914

*Echinarachnius parma* (Lamarck, 1816)

MRI (44  $\mu\text{m}$ )<sup>3</sup>, MRI (81  $\mu\text{m}$ )<sup>3</sup> (MorphDBase: A\_Ziegler\_20081116-M-34.1), and literature (Agassiz 1872-1873, MacBride 1906, Gregory 1911, Coe 1912, Koehler 1922)



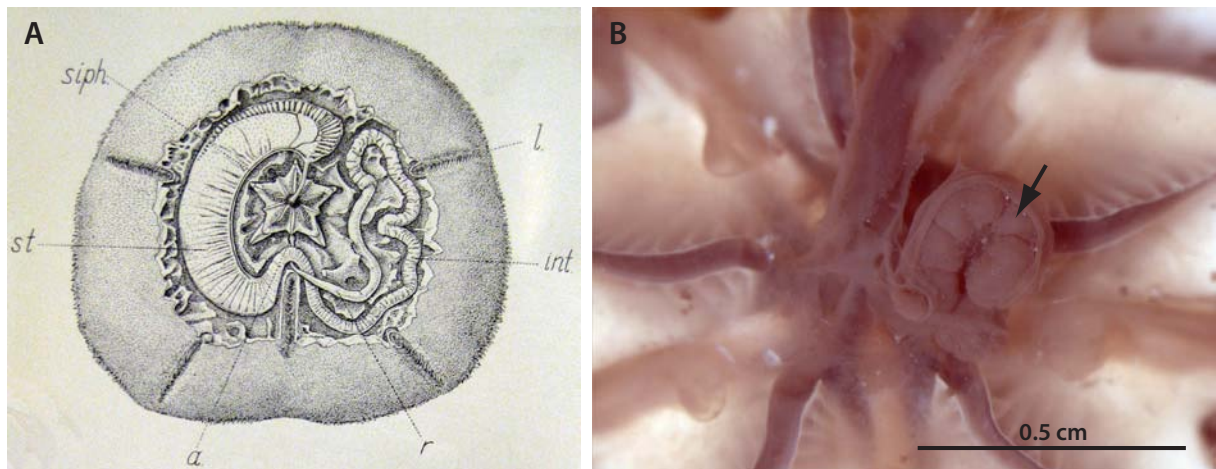
**Fig. 28:** Echinarachniidae, internal anatomy. **A** *Echinarachnius parma*, digestive tract and gonads, aboral view. From Koehler (1922). **B** *Echinarachnius parma*, MRI, digestive tract and gonads, aboral view. Arrow depicts stomach. **C** *Echinarachnius parma*, 3D model of the internal anatomy, aboral view. **D** *Echinarachnius parma*, 3D model of the internal anatomy, lateral view. Colour legend on page 33.

Echinarachniids possess a flattened digestive tract, festoons are entirely absent. The oesophagus is short and oriented towards ambulacrum III. A primary siphon is present and is attached to the stomach during its entire course. A siphonal groove is absent. Members of this taxon do not possess a secondary siphon. The gastric caecum is presumably absent. Stomach and intestine both make a half turn; the stomach is heavily sacculated on its external side. An intestinal caecum is absent. Gregory's diverticulum is present in juvenile specimens. The rectum extends towards interambulacrum 5. An anal cone is absent. The axial complex is straight in lateral view; the axial organ is oriented vertically. A peripharyngeal coelom surrounds Aristotle's lantern. Buccal sacs as well as Stewart's organs are absent. The aboral sinuses are fused into a single pentagonal membrane. Four gonads are present. Longitudinal body wall and compass elevator muscles are absent. The peripharyngeal haemal system consists of five spongy bodies. A collateral duct of the digestive tract haemal system is absent. All spines are covered by an epidermis. Fig. 28 depicts selected internal views.

### Mellitidae Stephanini, 1914

*Mellita quinquesperforata* (Leske, 1778)

Dissection and literature (Agassiz 1841, Coe 1912)



**Fig. 29:** Mellitidae, internal anatomy. **A** *Mellita quinquesperforata*, Aristotle's lantern and digestive tract, aboral view. From Coe (1912). **B** *Mellita quinquesperforata*, dissection, aboral part of Aristotle's lantern, aboral view. Arrow depicts axial organ.

Mellitids possess a flattened digestive tract, festoons are entirely absent. The oesophagus is short and oriented towards ambulacrum III. A primary siphon is present and is attached to the stomach during its entire course. A siphonal groove is absent. Members of this taxon do not possess a secondary siphon. The gastric caecum is presumably absent. Stomach and intestine both make a half turn; the stomach is conspicuously sacculated on its anterior external side. An intestinal caecum is absent. Gregory's diverticulum is present in juvenile specimens. The rectum extends towards interambulacrum 5. An anal cone is absent. The axial complex is straight in lateral view; the axial organ is oriented vertically. A peripharyngeal coelom surrounds Aristotle's lantern. Buccal sacs as well as Stewart's organs are absent.

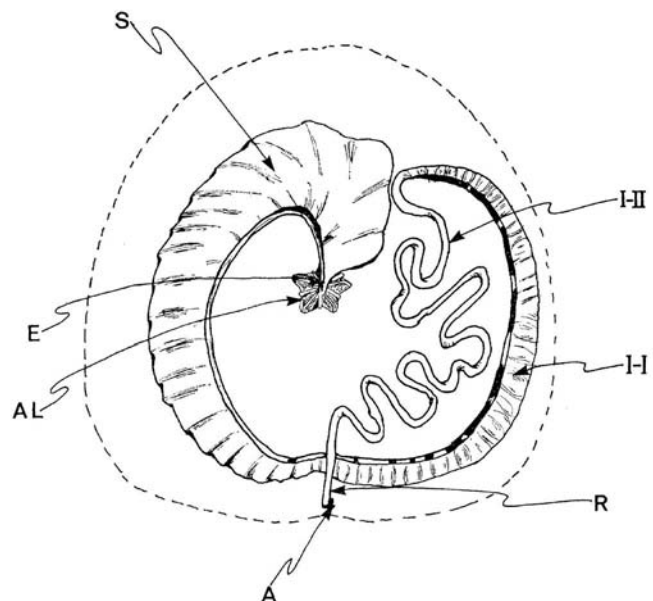
The aboral sinuses are fused into a single pentagonal membrane. Five gonads are present. Longitudinal body wall and compass elevator muscles are absent. The peripharyngeal haemal system consists of five spongy bodies. A collateral duct of the digestive tract haemal system is absent. All spines are covered by an epidermis. Fig. 29 depicts selected internal views.

### Dendrasteridae Lambert, 1889

*Dendraster excentricus* (Eschscholtz, 1831)

Literature (Timko 1976)

Dendrasterids possess a flattened digestive tract, festoons are entirely absent. The oesophagus is short and oriented towards ambulacrum III. A primary siphon is present and is attached to the stomach during its entire course. A siphonal groove is absent. Members of this taxon do not possess a secondary siphon. The gastric caecum is presumably absent. Stomach and intestine both make a half turn, the stomach is slightly sacculated. An intestinal caecum is absent. Gregory's diverticulum is present in juvenile specimens. The rectum extends towards interambulacrum 5. An anal cone is absent. The axial complex is straight in lateral view; the axial organ is oriented vertically. A peripharyngeal coelom surrounds Aristotle's lantern. Buccal sacs as well as Stewart's organs are absent. The aboral sinuses are fused into a single pentagonal membrane. Four gonads are present. Longitudinal body wall and compass elevator muscles are absent. The peripharyngeal haemal system consists of five spongy bodies. A collateral duct of the digestive tract haemal system is absent. All spines are covered by an epidermis. Fig. 30 depicts a selected internal view.



**Fig. 30:** Dendrasteridae, internal anatomy. *Dendraster excentricus*, Aristotle's lantern and digestive tract, aboral view. From Timko (1976).

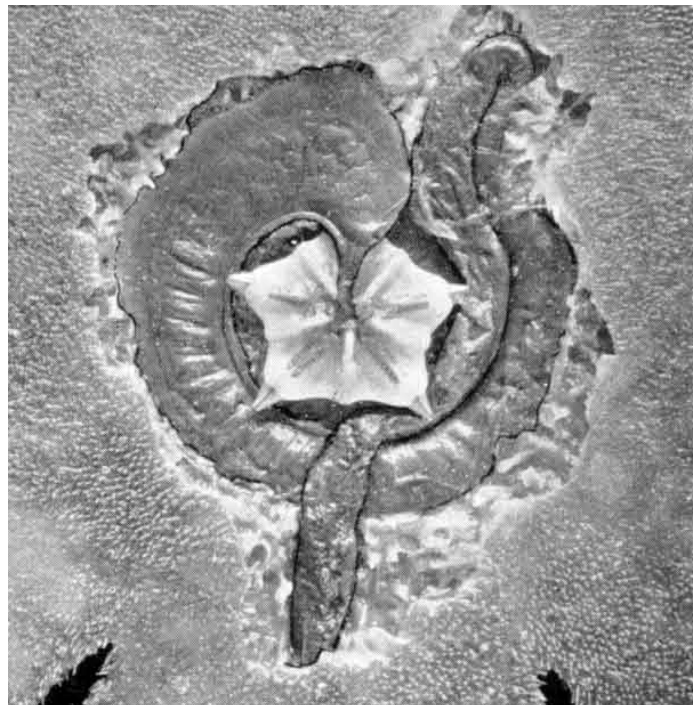
**Astriclypeidae Stephanini, 1911***Echinodiscus auritus* Leske, 1778

Literature (Koehler 1922)

*Echinodiscus bisperforatus* Leske, 1778

Dissection and literature (Cuénot 1891, Koehler 1922)

Astriclypeids possess a flattened digestive tract, festoons are entirely absent. The oesophagus is short and oriented towards ambulacrum III. A primary siphon is present and is attached to the stomach during its entire course. A siphonal groove is absent. Members of this taxon do not possess a secondary siphon. The gastric caecum is presumably absent. Stomach and intestine both make a half turn, the stomach is slightly sacculated. An intestinal caecum is absent. Gregory's diverticulum is present in juvenile specimens. The rectum extends towards interambulacrum 5. An anal cone is absent. The axial complex is straight in lateral view, the axial organ is oriented vertically. A peripharyngeal coelom surrounds Aristotle's lantern. Buccal sacs as well as Stewart's organs are absent. The aboral sinuses are fused into a single pentagonal membrane. Four gonads are present. Longitudinal body wall and compass elevator muscles are absent. The peripharyngeal haemal system consists of five spongy bodies. A collateral duct of the digestive tract haemal system is absent. All spines are covered by an epidermis. Fig. 31 depicts a selected internal view.



**Fig. 31:** Astriclypeidae, internal anatomy. *Echinodiscus auritus*, Aristotle's lantern and digestive tract, aboral view. From Koehler (1922).

**Holasteroidea Durham & Melville, 1957 (~30 extant species)****Pourtalesiidae Agassiz, 1881***Ceratopyhsa ceratopyga* Agassiz, 1879

Literature (Agassiz 1881)

*Echinochrepis cuneata* Agassiz, 1879

Literature (Agassiz 1881)

*Echinosigra phiale* (Wyville Thomson, 1873)

Literature (Mortensen 1907)

*Helgocystis carinata* (Agassiz, 1879)

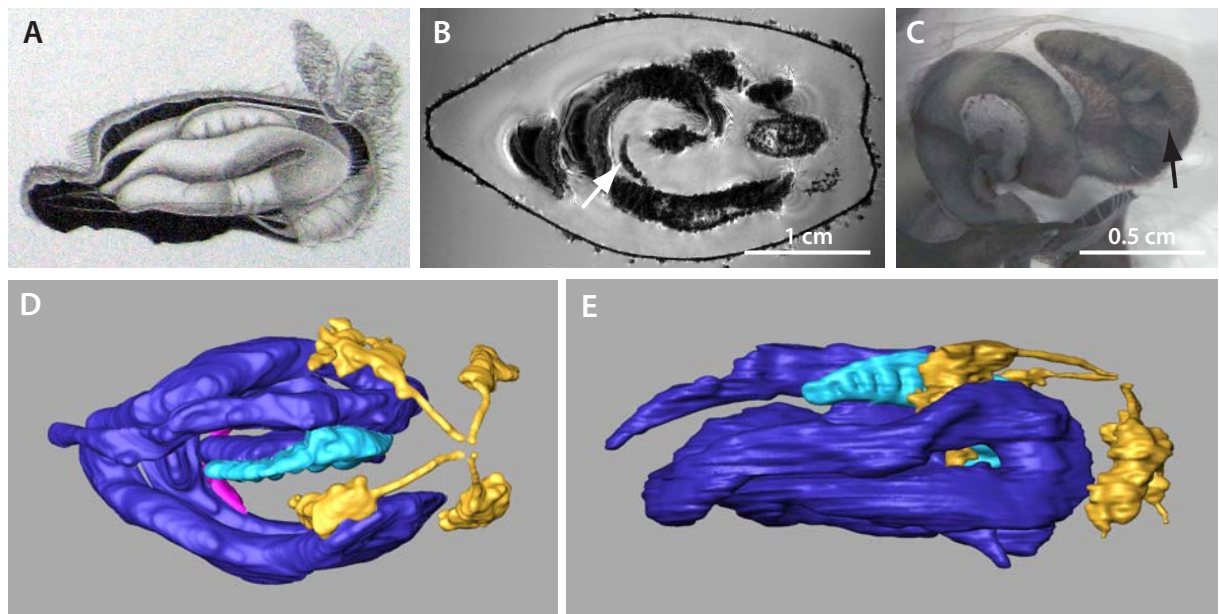
Literature (Agassiz 1881)

*Pourtalesia hispida* Agassiz, 1879

Dissection

*Pourtalesia jeffreysi* Wyville Thomson, 1873MRI ( $81\ \mu\text{m}$ )<sup>3</sup> (MorphDBase: A\_Ziegler\_20081116-M-55.1) and literature (Agassiz 1881, Mortensen 1907)*Pourtalesia wandeli* Mortensen, 1905MRI ( $86\ \mu\text{m}$ )<sup>3</sup> (MorphDBase: A\_Ziegler\_20081116-M-56.1), MRI ( $126\ \mu\text{m}$ )<sup>3</sup>, dissection, and literature (Mortensen 1907)*Spatagocystis challengerii* Agassiz, 1879

Literature (Agassiz 1881)



**Fig. 32:** Pourtalesiidae, internal anatomy. **A** *Pourtalesia jeffreysi*, gonads and digestive tract, lateral view. From Mortensen (1907). **B** *Pourtalesia wandeli*, MRI, digestive tract, aboral view. Arrow depicts primary siphon. **C** *Pourtalesia hispida*, dissection, digestive tract, lateral view. Arrow depicts horn-shaped gastric caecum. **D** *Pourtalesia wandeli*, 3D model of the internal anatomy, aboral view. **E** *Pourtalesia wandeli*, 3D model of the internal anatomy, lateral view. Colour legend on page 33.



Pourtalesiids possess a cylindrical digestive tract, festoons are entirely absent. The oesophagus is short and oriented towards interambulacrum 5. A primary siphon is present and dilated at its posterior end. A siphonal groove is absent. A secondary siphon is present. The gastric caecum is horn-shaped in form; its connection with the stomach is located at its adoral anterior part. Stomach and intestine both make a full turn; the stomach is smooth-walled. The mesenterial connection of the first gut loop is not extended towards ambulacrum III. An intestinal caecum as well as Gregory's diverticulum are not present. The rectum extends towards interambulacrum 5. An anal cone is absent. The form of the axial complex is C-shaped in lateral view; the axial organ is oriented horizontally. The stone canal does not show a distinct swelling in its adoral part. A small peripharyngeal coelom is present. Buccal sacs as well as Stewart's organs are absent. The aboral sinuses are fused into a single pentagonal membrane. Four gonads are present and display a considerable sexual dimorphism. The gonoducts are distinctly extended. Longitudinal body wall muscles are absent. Aristotle's lantern is absent in juvenile and adult specimens. The peripharyngeal haemal system is not differentiated; a collateral duct of the digestive tract haemal system is absent. All spines are covered by an epidermis. Fig. 32 depicts selected internal views.

### **Urechinidae Duncan, 1889**

*Antrechinus nordenskjöldi* (Mortensen, 1905)

Dissection

*Cystechinus wyvillei* Agassiz, 1879

Literature (Agassiz 1881)

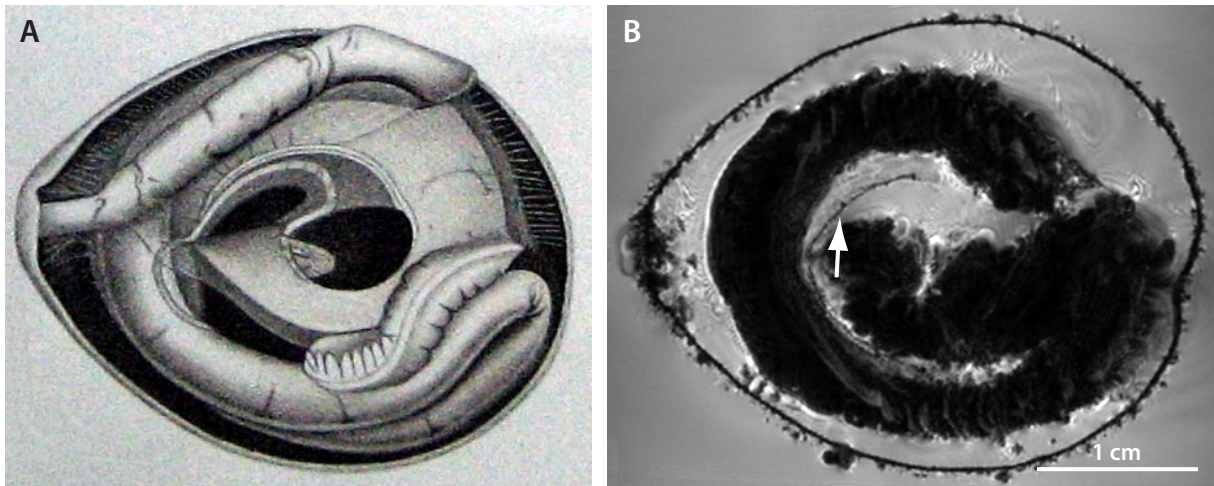
*Pilematechinus vesica* (Agassiz, 1898)

Literature (Agassiz 1881)

*Urechinus naresianus* Agassiz, 1879

MRI (81  $\mu\text{m}$ )<sup>3</sup> (MorphDBase: A\_Ziegler\_20081116-M-71.1), dissection, and literature (Mortensen 1907)

Urechinids possess a cylindrical digestive tract, festoons are entirely absent. The oesophagus is short and oriented towards interambulacrum 5. A primary siphon is present. A siphonal groove is absent. A secondary siphon is present. The gastric caecum is sac-shaped in form, its connection with the stomach is located at its adoral anterior part. Stomach and intestine both make a full turn; the stomach is smooth-walled. The mesenterial connection of the first gut loop is not extended towards ambulacrum III. An intestinal caecum as well as Gregory's diverticulum are not present. The rectum extends towards interambulacrum 5. An anal cone is absent. The form of the axial complex is C-shaped in lateral view; the axial organ is oriented horizontally. The stone canal shows a distinct swelling in its adoral part. A small peripharyngeal coelom is present. Buccal sacs as well as Stewart's organs are absent. The aboral sinuses are fused into a single pentagonal membrane. Four gonads are present and display a



**Fig. 33:** Urechinidae, internal anatomy. **A** *Urechinus naresianus*, gastric caecum, primary and secondary siphon, digestive tract, aboral view. From Mortensen (1907). **B** *Urechinus naresianus*, MRI, digestive tract with strong artefacts caused by paramagnetic gut content, aboral view. Arrow depicts primary siphon.

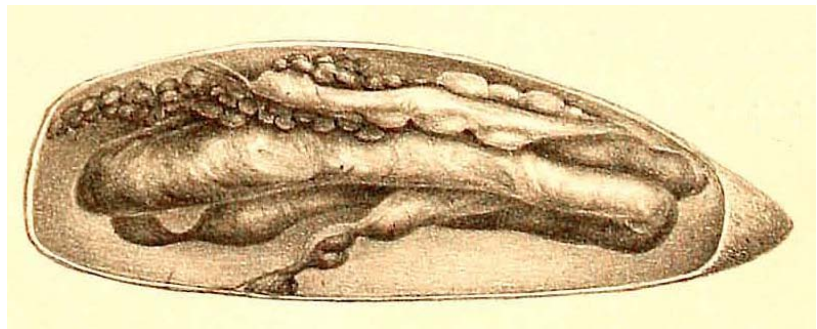
considerable sexual dimorphism. The gonoducts are distinctly extended. Longitudinal body wall muscles are absent. Aristotle's lantern is absent in juvenile and adult specimens. The peripharyngeal haemal system is not differentiated; a collateral duct of the digestive tract haemal system is absent. All spines are covered by an epidermis. Fig. 33 depicts selected internal views.

## Spatangoida Agassiz, 1840 (~225 extant species)

### Aeropsidae Lambert, 1896

*Aeropsis rostrata* (Wyville Thomson, 1877)

Literature (Agassiz 1881)



**Fig. 34:** Aeropsidae, internal anatomy. *Aeropsis rostrata*, digestive tract and gonads, lateral view. From Agassiz (1881).

Aeropsids possess a cylindrical digestive tract, festoons are entirely absent. The oesophagus is short and oriented towards interambulacrum 5. A primary siphon is present. A siphonal groove is absent. A secondary siphon is presumably present. The gastric caecum is sac-shaped in form; its connection with the stomach is located at its adoral anterior part. Stomach and intestine both make a full turn; the stomach is smooth-walled. The mesenterial connection of the first gut loop is not extended towards ambulacrum III. An intestinal caecum as well

as Gregory's diverticulum are not present. The rectum extends towards interambulacrum 5. An anal cone is absent. The form of the axial complex is C-shaped in lateral view; the axial organ is oriented horizontally. A small peripharyngeal coelom is present. Buccal sacs as well as Stewart's organs are absent. The aboral sinuses are fused into a single pentagonal membrane. Two gonads are present. Longitudinal body wall muscles are absent. Aristotle's lantern is absent in juvenile and adult specimens. The peripharyngeal haemal system is not differentiated; a collateral duct of the digestive tract haemal system is absent. All spines are covered by an epidermis. Fig. 34 depicts a selected internal view.

### **Hemiasteridae Clark, 1917**

*Hemiaster expergitus* (Lovén, 1874)

Dissection

Hemiasterids possess a cylindrical digestive tract, festoons are entirely absent. The oesophagus is short and oriented towards interambulacrum 5. A primary siphon is present, free from the gut and dilated in its anterior part. A siphonal groove is absent. A secondary siphon is presumably present. The gastric caecum is sac-shaped in form; its connection with the stomach is located at its adoral anterior part. Stomach and intestine both make a full turn; the stomach is smooth-walled. The mesenterial connection of the first gut loop is not extended towards ambulacrum III. An intestinal caecum as well as Gregory's diverticulum are not present. The rectum extends towards interambulacrum 5. An anal cone is absent. The form of the axial complex is C-shaped in lateral view; the axial organ is oriented horizontally. A small peripharyngeal coelom is present. Buccal sacs as well as Stewart's organs are absent. The aboral sinuses are fused into a single pentagonal membrane. Four gonads are present. Longitudinal body wall muscles are absent. Aristotle's lantern is absent in juvenile and adult specimens. The peripharyngeal haemal system is not differentiated; a collateral duct of the digestive tract haemal system is absent. All spines are covered by an epidermis.

### **Schizasteridae Lambert, 1905**

*Abatus cavernosus* (Philippi, 1845)

MRI (81  $\mu\text{m}$ )<sup>3</sup> (MorphDBase: A\_Ziegler\_20081116-M-30.1) and MRI (117  $\mu\text{m}$ )<sup>3</sup>

*Aceste ovata* Agassiz & Clark, 1907

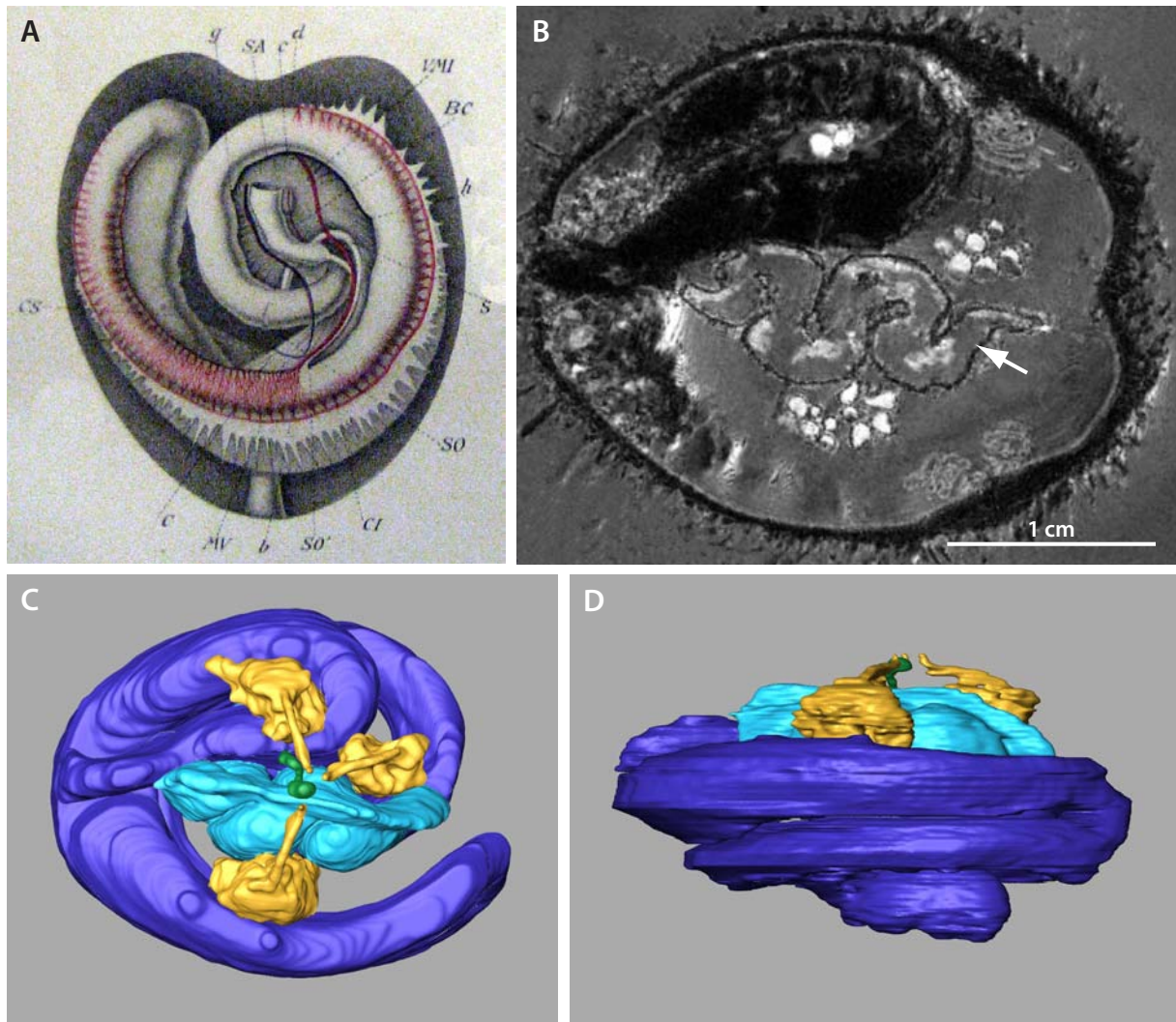
Literature (Koehler 1914)

*Schizaster canaliferus* (Lamarck, 1816)

Literature (Koehler 1883, Kaburek & Hilgers 1999)

*Schizaster lacunosus* (Linnaeus, 1758)

Dissection



**Fig. 35:** Schizasteridae, internal anatomy. **A** *Schizaster canaliferus*, digestive tract with primary siphon and axial complex, oral view. From Koehler (1883). **B** *Abatus cavernosus*, MRI, digestive tract and gonads, aboral view. Arrow depicts massive gastric caecum. **C** *Abatus cavernosus*, 3D model of the internal anatomy, aboral view. **D** *Abatus cavernosus*, 3D model of the internal anatomy, lateral view. Colour legend on page 33.

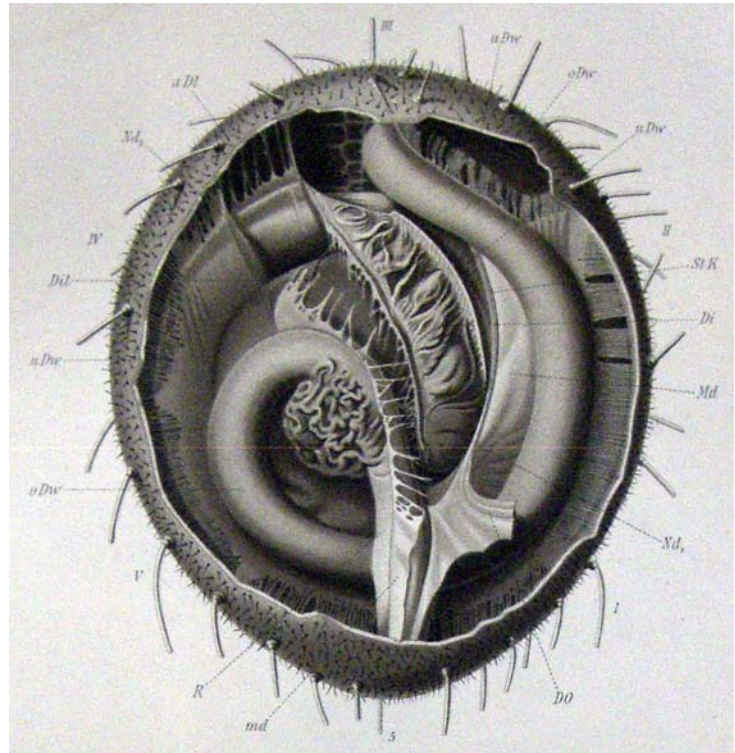
Schizasterids possess a cylindrical digestive tract, festoons are entirely absent. The oesophagus is short and oriented towards interambulacrum 5. A primary siphon is present, free from the gut and dilated in its anterior part. A siphonal groove is absent. A secondary siphon is present. The gastric caecum is sac-shaped in form; its connection with the stomach is located at its adoral anterior part. Stomach and intestine both make a full turn; the stomach is smooth-walled. The mesenterial connection of the first gut loop is not extended towards ambulacrum III. An intestinal caecum is present in some taxa. Gregory's diverticulum is not present. The rectum extends towards interambulacrum 5. An anal cone is absent. The form of the axial complex is C-shaped in lateral view; the axial organ is oriented horizontally. The stone canal is tri-partite. A small peripharyngeal coelom is present. Buccal sacs as well as Stewart's organs are absent. The aboral sinuses are fused into a single pentagonal membrane. Two to four gonads are present. Longitudinal body wall muscles are absent. Aristotle's lantern is absent in juvenile and adult specimens. The peripharyngeal haemal system is not

differentiated; a collateral duct of the digestive tract haemal system is absent. All spines are covered by an epidermis. Fig. 35 depicts selected internal views.

### **Incerta sedis**

*Heterobrissus niasicus* (Döderlein, 1901)

Literature (Wagner 1903)



**Fig. 36:** *Heterobrissus niasicus*, internal anatomy. Digestive tract with gastric and intestinal caecum. From Wagner (1903).

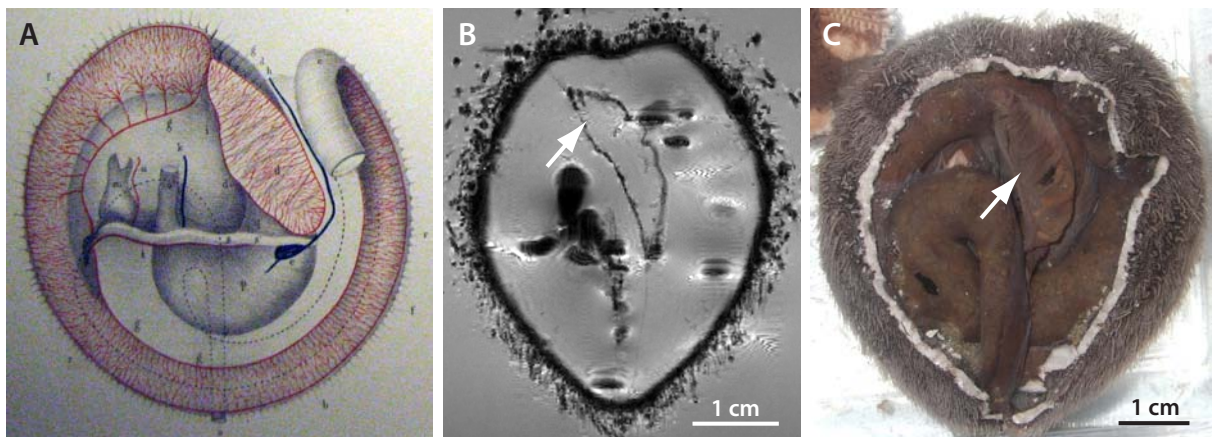
*Heterobrissus niasicus* possesses a cylindrical digestive tract, festoons are entirely absent. The oesophagus is short and oriented towards interambulacrum 5. A primary siphon is present, free from the gut and dilated in its anterior part. A siphonal groove is absent. A secondary siphon is present. The gastric caecum is sac-shaped in form; its connection with the stomach is located at its adoral anterior part. Stomach and intestine both make a full turn; the stomach is smooth-walled. The mesenterial connection of the first gut loop is extended towards ambulacrum III. An intestinal caecum is present. Gregory's diverticulum is not present. The rectum extends towards interambulacrum 5. An anal cone is absent. The form of the axial complex is S-shaped in lateral view; the axial organ is oriented horizontally. The stone canal is tri-partite. A small peripharyngeal coelom is present. Buccal sacs as well as Stewart's organs are absent. The aboral sinuses are fused into a single pentagonal membrane. Four gonads are present. Longitudinal body wall muscles are absent. Aristotle's lantern is absent in juvenile and adult specimens. The peripharyngeal haemal system is not differentiated; a collateral duct of the digestive tract haemal system is absent. All spines are covered by an epidermis. Fig. 36 depicts a selected internal view.

## Spatangidae Gray, 1825

*Spatangus purpureus* Müller, 1776

MRI (81  $\mu\text{m}$ )<sup>3</sup> (MorphDBase: A\_Ziegler\_20081116-M-61.1), dissection, and literature (Hoffmann 1871, Agassiz 1872-1873, Koehler 1883, Hamann 1887, Prouho 1887, Eichelbaum 1909, Klinghardt 1911)

Spatangids possess a cylindrical digestive tract, festoons are entirely absent. The oesophagus is short and oriented towards interambulacrum 5. A primary siphon is present, free from the gut and dilated in its anterior part. A siphonal groove is absent. A secondary siphon is absent. The gastric caecum is sac-shaped in form; its connection with the stomach is located at its adoral anterior part. Stomach and intestine both make full turns; the stomach is smooth-walled. The mesenterial connection of the first gut loop is extended towards ambulacrum III. An intestinal caecum as well as Gregory's diverticulum are not present. The rectum extends towards interambulacrum 5. An anal cone is absent. The form of the axial complex is S-shaped in lateral view; the axial organ is oriented horizontally. The stone canal is tripartite. A small peripharyngeal coelom is present. Buccal sacs as well as Stewart's organs are absent. The aboral sinuses are fused into a single pentagonal membrane. Four gonads are present. Longitudinal body wall muscles are absent. Aristotle's lantern is absent in juvenile and adult specimens. The peripharyngeal haemal system is not differentiated; a collateral duct of the digestive tract haemal system is absent. All spines are covered by an epidermis. Fig. 37 depicts selected internal views.



**Fig. 37:** Spatangidae, internal anatomy. **A** *Spatangus purpureus*, digestive tract with haemal system and axial complex, aboral view. From Hoffmann (1871). **B** *Spatangus purpureus*, MRI, rectum, aboral view. Arrow depicts gastric caecum. **C** *Spatangus purpureus*, dissection, digestive tract, aboral view. Arrow depicts gastric caecum.

## Brissidae Gray, 1855

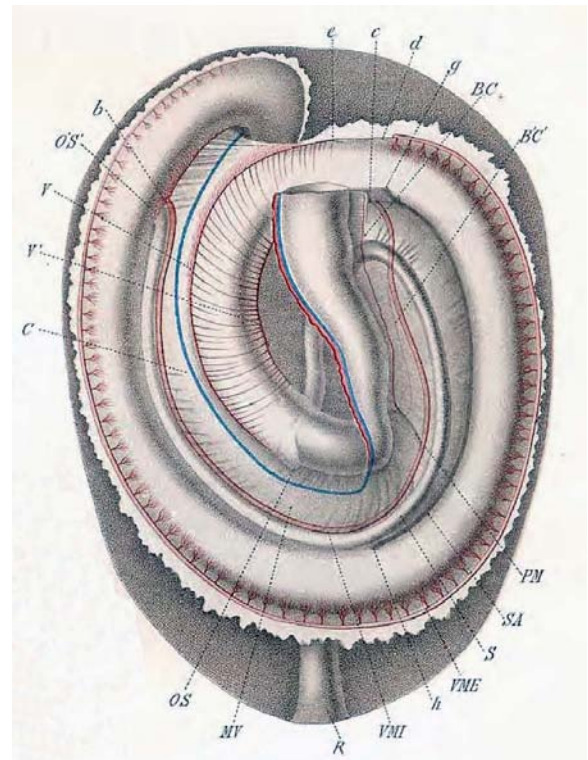
*Brissus unicolor* (Leske, 1778)

Literature (Koehler 1883, Hamann 1887)

*Meoma ventricosa* (Lamarck, 1816)

Literature (Hyman 1955, Chesher 1963)

Brissids possess a cylindrical digestive tract, festoons are entirely absent. The oesophagus is short and oriented towards interambulacrum 5. A primary siphon is present, free from the gut and dilated in its anterior part. A siphonal groove is absent. A secondary siphon is present. The gastric caecum is sac-shaped in form; its connection with the stomach is located at its adoral anterior part. Stomach and intestine both make a full turn; the stomach is smooth-walled. The mesenterial connection of the first gut loop is extended towards ambulacrum III. An intestinal caecum as well as Gregory's diverticulum are not present. The rectum extends towards interambulacrum 5. An anal cone is absent. The form of the axial complex is S-shaped in lateral view; the axial organ is oriented horizontally. The stone canal is tripartite. A small peripharyngeal coelom is present. Buccal sacs as well as Stewart's organs are absent. The aboral sinuses are fused into a single pentagonal membrane. Four gonads are present. Longitudinal body wall muscles are absent. Aristotle's lantern is absent in juvenile and adult specimens. The peripharyngeal haemal system is not differentiated; a collateral duct of the digestive tract haemal system is absent. All spines are covered by an epidermis. Fig. 38 depicts a selected internal view.



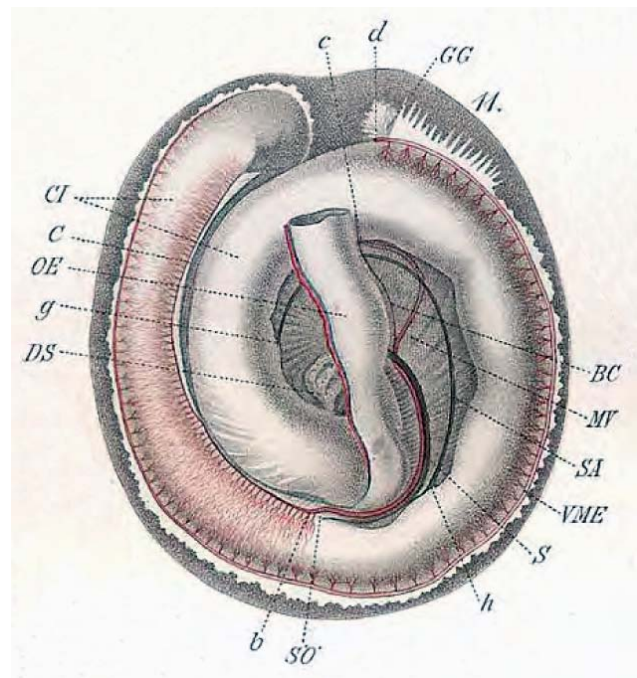
**Fig. 38:** Brissidae, internal anatomy. *Brissus unicolor*, digestive tract with primary and secondary siphon, axial complex, oral view. From Koehler (1883).

### **Brissopsidae Lambert, 1905**

*Brissopsis lyrifera* (Forbes, 1841)

Dissection and literature (Koehler 1883)

Brissopsids possess a cylindrical digestive tract, festoons are entirely absent. The oesophagus is short and oriented towards interambulacrum 5. A primary siphon is present, free from the gut and dilated in its anterior part. A siphonal groove is absent. A secondary siphon is present. The gastric caecum is sac-shaped in form; its connection with the stomach is located at its adoral anterior part. Stomach and intestine both make a full turn; the stomach is smooth-walled. The mesenterial connection of the first gut loop is extended towards ambulacrum III. An intestinal caecum as well as Gregory's diverticulum are not present. The rectum extends towards interambulacrum 5. An anal cone is absent. The form of the axial complex is S-shaped in lateral view; the axial organ is oriented horizontally. The stone canal is tripartite. A small peripharyngeal coelom is present. Buccal sacs as well as Stewart's organs are absent. The aboral sinuses are fused into a single pentagonal membrane. Four gonads are present. Longitudinal body wall muscles are absent. Aristotle's lantern is absent in juvenile and adult specimens. The peripharyngeal haemal system is not differentiated; a collateral duct of the digestive tract haemal system is absent. All spines are covered by an epidermis. Fig. 39 depicts a selected internal view.



**Fig. 39:** Brissopsidae, internal anatomy. *Brissopsis lyrifera*, digestive tract with primary and secondary siphon as well as axial complex. From Koehler (1883).

### **Echinocardiidae Wythe Cooke, 1942**

*Echinocardium cordatum* (Pennant, 1777)

MRI (81  $\mu\text{m}$ )<sup>3</sup> (MorphDBase: A\_Ziegler\_20081116-M-35.1), MRI (117  $\mu\text{m}$ )<sup>3</sup>, dissection, and literature (MacBride 1906, Eichelbaum 1909, De Ridder & Jangoux 1993, Thorsen 1998)

*Echinocardium flavescens* (Müller, 1776)

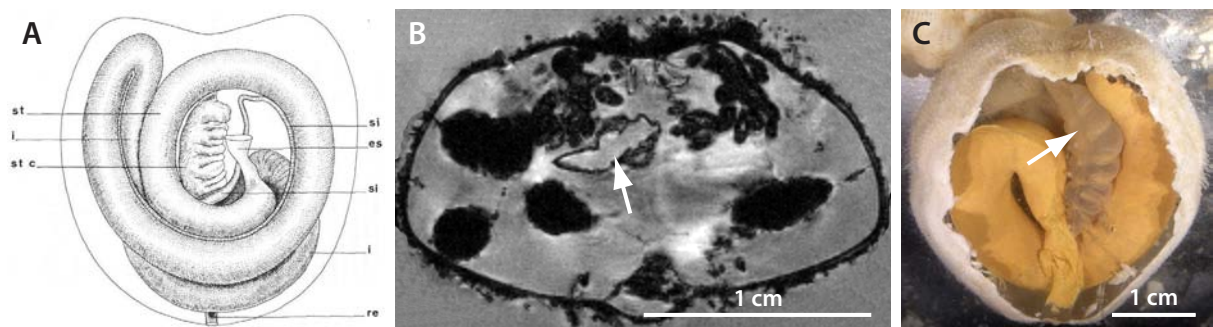
Literature (Koehler 1883)

*Echinocardium mediterraneum* (Forbes, 1844)

Literature (Hamann 1887)



Echinocardiids possess a cylindrical digestive tract, festoons are entirely absent. The oesophagus is short and oriented towards interambulacrum 5. A primary siphon is present, free from the gut and dilated in its anterior part. A siphonal groove is absent. A secondary siphon is absent. The gastric caecum is sac-shaped; its connection with the stomach is located at its adoral anterior part. Stomach and intestine both make a full turn; the stomach is smooth-walled. The mesenterial connection of the first gut loop is extended towards ambulacrum III. An intestinal caecum is present. Gregory's diverticulum is not present. The rectum extends towards interambulacrum 5. An anal cone is absent. The form of the axial complex is S-shaped in lateral view; the axial organ is oriented horizontally. The stone canal is tripartite. A small peripharyngeal coelom is present. Buccal sacs as well as Stewart's organs are absent. The aboral sinuses are fused into a single pentagonal membrane. Four gonads are present. Longitudinal body wall muscles are absent. Aristotle's lantern is absent in juvenile and adult specimens. The peripharyngeal haemal system is not differentiated; a collateral duct of the digestive tract haemal system is absent. All spines are covered by an epidermis. Fig. 40 depicts selected internal views.



**Fig. 40:** Echinocardiidae, internal anatomy. **A** *Echinocardium cordatum*, digestive tract with gastric caecum and primary siphon, oral view. From De Ridder & Jangoux (1993). **B** *Echinocardium cordatum*, MRI, digestive tract and gonads, fronto-lateral view. Arrow depicts gastric caecum. **C** *Echinocardium cordatum*, dissection, digestive tract. Arrow depicts gastric caecum.

## 9. Final Discussion and Conclusions

The overall aim of the study presented here was to evaluate the potential of non-invasive imaging techniques in combination with advanced 3D modeling protocols to visualize internal structures of representative species of a marine invertebrate taxon, the Echinoidea. Sea urchins were chosen because our knowledge of their soft tissue anatomy is still fragmentary. Furthermore, since the current hypotheses on the phylogeny of this taxon are almost entirely restricted to hard-part anatomy, an in-depth analysis of sea urchin soft tissues could be expected to yield additional characters that would supplement the existing morphological matrices. In order not to overly repeat the discussions in the articles previously presented, I will concentrate here on the three most comprehensive aspects of this work, namely (i) the principal feasibility of applying MRI and  $\mu$ CT for large-scale comparative soft tissue studies, (ii) the improvement of the communication of digital 3D datasets in general, and (iii) the evaluation of the suitability of sea urchin soft tissue structures to extend the existing character sets.

### 9.1. Comparative morphological analyses using MRI and $\mu$ CT

A correlation of the results derived from the MRI experiments with results based on histological data reveals that this non-invasive imaging technique can be used for reliable soft tissue detection and imaging in sea urchins. The resolution achievable with the selected imaging sequences was well below the isotropic resolution of 100  $\mu$ m that was deemed essential for large-scale comparative anatomical studies in this taxon. However, the resolutions that were achieved (isotropically down to approximately 20  $\mu$ m) cannot compete with the maximum resolution of classical light microscopy of 0.2  $\mu$ m. Technical and physical limitations currently do not permit isotropic resolutions higher than approximately 5  $\mu$ m to be obtained by MRI. However, since the present applications of NMR techniques range from the detection of protein structures to imaging of whole human bodies, a considerable amount of research is devoted to an improvement of the instruments and protocols (e.g. Boesch 2001). The steady increase in isotropic resolution of MRI systems is an important aspect of developments in the future and must be regarded to be of utmost importance for a broad acceptance of this technique in invertebrate morphology.

Image contrast largely depends on the MRI sequence employed as well as on the application of a contrast agent. For the large-scale comparative analysis described in Chapter 4, a combination of FLASH and RARE sequences was selected, with the former being employed on the 7 T scanner and the latter on the 17.6 T scanner. The FLASH sequence (15 h scan time) permitted to optimally use the available scan time during overnight scans, whereas the RARE sequence was used during scans over the weekend (18 – 33 h scan time). In this way, both scanners were used during off-peak hours, leading to an optimal use of the instruments. The contrast agent employed during the analyses (Magnevist) readily perfused into

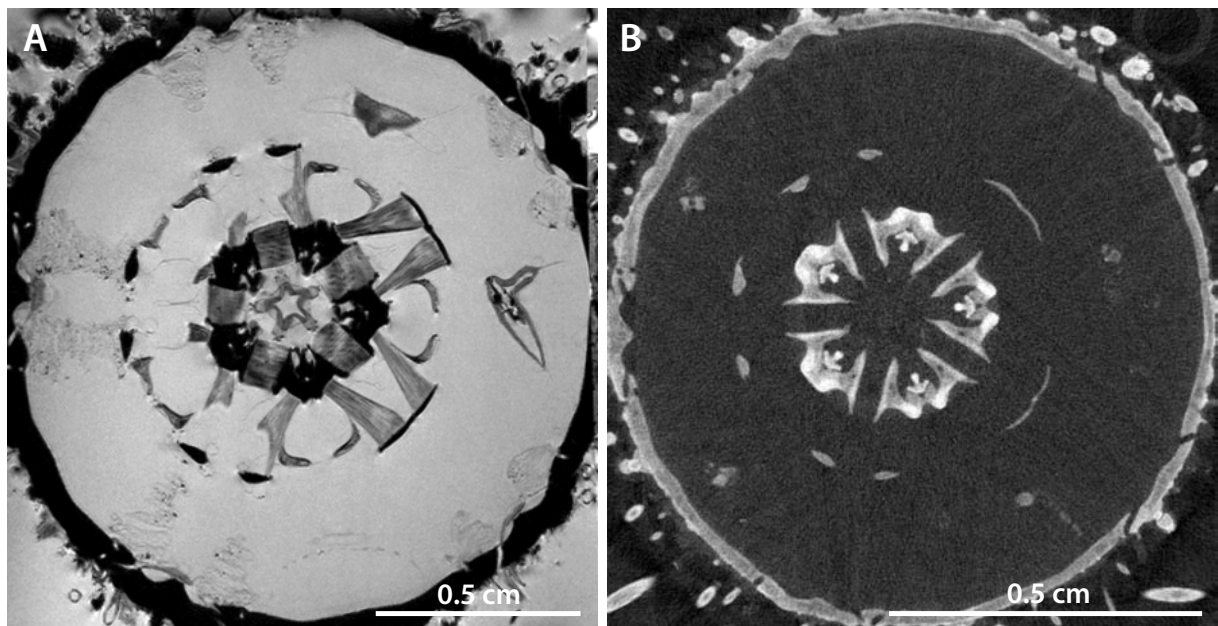
the large fluid-filled coelomic compartments and allowed to obtain better contrast of both soft and hard parts. However, in some cases, the application of the contrast agent resulted in an overly strong signal which in turn led to reduced contrast between soft tissues. Therefore, whenever possible, specimens were analyzed before and after the application of the contrast agent to further improve the gathering of morphological data that are principally available for each species. An increased use of contrast agents (e.g. manganese, Magnevist) will certainly extend the range of applications for MRI analyses of invertebrates in the future, both *in vivo* and *in vitro*.

The artefacts observed in a number of scans played an important role during the imaging experiments. Artefacts can be divided into those that are caused by the specimen (or substances within the specimen) and artefacts that are inherent in imaging at high magnetic fields. Experiments with life animals are further complicated by possible movement artefacts, demanding the application of anaesthetic substances during the long scan times that are currently required to achieve high isotropic resolutions. The important aspect of anaesthesia could not be treated in this study because most specimens were only available as fixed material, but this field certainly merits further studies. The dominant artefact that could be attributed to the biology of the specimens was an alteration in the homogeneity of the magnetic field inside the scanner due to (para-) magnetic content of the gut. Such disturbances were also caused by the presence of magnetite-accumulating symbionts located in Gregory's diverticulum in scutelline sand dollars (Echinarachniidae, Mellitidae, Dendrasteridae, and Astriclypeidae). The tendency of some spatangoid sea urchins to accumulate iron phosphate in the epithelia of their digestive tracts made imaging of certain taxa almost impossible (e.g. Aeropsidae, Hemiasteridae, Brissidae, Brissopsidae, Spatangidae, Echinocardiidae). A partial solution to these problems was to scan several specimens of a given species to select the best-suited material. In a few cases, 3D modeling had to be based on a combination of scans of several specimens to overcome partial information loss. Artefacts caused by the imaging modalities themselves included Gibbs artefacts typically occurring at high and ultra-high magnetic fields, susceptibility artefacts inherent in this approach in general, artefacts at material boundaries, as well as image distortions caused by small air bubbles trapped inside the specimen or attached to its outside (please refer to Callaghan (1991) for further information regarding MRI and artefacts).

In spite of the technical problems encountered during the preliminary studies, MRI proved to be a technique with extremely simple specimen preparation. Consequently, a rapid specimen turnover was possible. In particular, the opportunity to analyze valuable museum material, including type material, further complements the advantages of MRI for large-scale comparative soft tissue analyses of invertebrates.

In contrast to MRI,  $\mu$ CT studies using conventional scanners and established protocols lack the potential to display soft tissue structures (Fig. 1). This applies especially to sea urchins, where the strong X-rays have to penetrate the calcite endoskeleton twice, making the

analysis of soft tissues in this taxon with conventional desktop  $\mu$ CT equipment practically impossible. However, more advanced CT methods such as synchrotron radiation tomography and very-high-resolution X-ray computed tomography have been shown to be capable of soft tissue imaging in specimens with strong endo- and exoskeletons (Tafforeau et al. 2006, Betz et al. 2007, Socha 2007). Unfortunately, the allocated scanning times at synchrotron facilities are extremely limited. Nonetheless, the  $\mu$ CT data gathered in the present study complement the MRI datasets with regard to hard-part anatomy. One of the future aspects of my work will therefore be to integrate the acquired MRI and  $\mu$ CT datasets of a given species into a single 3D model.



**Fig. 1:** Direct comparison of results derived from non-invasive imaging techniques using freshly fixed specimens of *Psammechinus miliaris* (Müller, 1771). **A** Almost horizontal section at the level of Aristotle's lantern and perignathic girdle using MRI. Soft tissue structures are well visible: e.g. muscles, digestive tract components, water vascular system, and nervous system. Isotropic resolution: 44  $\mu$ m. **B** Almost horizontal section at the level of Aristotle's lantern and perignathic girdle using  $\mu$ CT. Only calcified structures (and sediment in the gut) are visible. Isotropic resolution: 17.4  $\mu$ m. It is immediately obvious that the two datasets complement each other.

## 9.2. Communicating 3D datasets

For centuries, scientists have communicated their observations on biological specimens through written text, elaborate or simplified drawings, and later photographs. Depending on the individual talent of the author (or the person commissioned to do the work), these descriptions more or less successfully convey the essential information. Due to the dominant media for scientific communication, i.e. books and journals, the drawings and photographs were naturally restricted to 2D representations. However, since anatomical structures are usually complex, a three-dimensional representation would greatly facilitate their understanding.

The improvements in 3D modeling and visualization during the last decade permit now to use even conventional desktop and laptop PC systems to display and interactively manipu-

late 3D models. This technological quantum leap permits a considerable range of novel applications for morphological studies, including 3D modeling based on digitally acquired tomographic datasets. These data can then be used for a large variety of secondary analyses such as volume and surface measurements. The Volume Viewer plug-in of the freely available ImageJ software proved to be particularly useful for the analysis of isotropic datasets: this program permits to manipulate the original MRI datasets in an interactive manner. Any desired view of the specimen's internal anatomy can thus be selected and saved as a separate image file (see Figs. 3 and 4 in Chapter 7). Regarding the modeling process, it has to be noted that the 3D models based on morphological datasets still contain elements of structural interpretation. It is therefore possible that a second person repeating the analyses might come to slightly different conclusions. Although highly desirable, automated segmentation algorithms are not yet available for this purpose (see also the Discussion in Chapter 4). However, using digital data gathering techniques such as  $\mu$ CT, MRI, CLSM, and OCT, the difficult and lengthy process of image alignment, necessary for a 3D analysis of histological sections, can be overcome.

In spite of the restrictions of conventional scientific publications to the 2D format, semi-interactive movies of rotating 3D models have become a standard, but only as supplementary material. Even fully interactive 3D models, for example of entire molecules, could be accessed since some years, but the reader needed to be constantly online during this procedure. In order to facilitate the communication of 3D content between authors and readers, we described how fully interactive 3D models can be integrated into a PDF-based scientific publication (Chapter 6). Thereby, the need for constant online access and large supplementary data packages could be circumvented. The advantages offered by this approach are obvious, since the reader can now independently and interactively access 3D content within a publication. Apart from the 3D models, the latest version of the Adobe Acrobat package also permits the integration of video (Ziegler et al. 2008) and audio content into PDF documents. The range of applications for embedded media can thus be considerably extended.

It is particularly important to point out that the novel technique permits also the unlimited duplication and storage of the acquired data, since these are present as digital files. Once available online, the same datasets can also be used by other researchers, inevitably leading to a heightened awareness for morphological findings. I foresee an enormous increase in the application of this procedure also because of this drastic increment in data transparency. This is a field where morphology is currently far behind the advances in other fields such as genetics and proteomics.

### **9.3. Suitability of echinoid soft tissues for phylogenetic inferences**

Based on the acquired MRI datasets as well as results derived from dissection, the morphological findings on the echinoid soft tissue anatomy were combined with the information

available from a comprehensive literature search (see Chapters 7, 8). This combination of all available data suggests that a number of internal and external soft tissue structures might serve as an extension to the existing hard-part character matrices currently available for this taxon. The data were collected at the level of species, but were then pooled for every family in order to facilitate an overview of the essential components and their variation across high-ranking echinoid subtaxa. A species-based character matrix is currently in preparation which is expected to lead to a considerable extension of the existing hard-part matrices due to the inclusion of newly analyzed taxa that provide phylogenetically relevant information.

The results presented in Chapter 8 are restricted to a description of the main soft tissue characters that I consider to have the greatest potential to extend the present morphological character matrices. Based on these preliminary results, a number of key taxa became obvious that should be included in a combined hard-part, larval, and soft tissue morphological character matrix. For an independent comparison, the selected soft tissue characters suggested here will be mapped onto the latest cladogram based on molecular evidence (Fig. 2).

- (1) Stewart's organs are internal extensions of the peripharyngeal coelom and can be found in different shapes, primarily in the more basal echinoid taxa: Cidaroida, Echinothurioida, Pedinoida, and Diadematoida. Further extensions of Stewart's organs, the so-called lateral diverticula, on top of the peripharyngeal coelom, are present only in cidaroid sea urchins.
- (2) A siphonal groove, i.e. a lateral outgrowth of the stomach, can be found in Cidaroida, Pedinoida, and Diadematidae. It is considered to be the plesiomorphic condition of the siphonal groove/primary siphon character complex (Holland & Ghiselin 2008). However, the MRI results presented online on The Echinoid Directory (Chapter 5) as well as a recent article (Campos & Moura 2008) resulted in a controversy regarding the presence or absence of the siphon in several "regular" echinoid taxa. In the course of the discussion, Holland and Ghiselin (2008) convincingly showed that the presence of a siphon in Diadematidae and Pedinidae, as suggested on The Echinoid Directory, can be ruled out. These conflicting interpretations clearly illustrate the limitations of current MRI protocols' capacity to permit a differentiation between thin structures in some cases and demonstrates that great care has to be taken when conclusions are reached that are based on insufficient data.
- (3) Although the echinoid ancestor is believed to have possessed, as observed also in the echinoid sister taxon Holothuroidea, a single gonad only, the presence of five gonads is still considered a plesiomorphic condition for extant sea urchins (Littlewood & Smith 1995). Indeed, all "regular" sea urchin taxa possess five discreet gonads.
- (4) The differentiation of the perioesophageal haemal system into a spongy ring can be observed in the basal echinoid taxa Cidaroida and Echinothurioida (Prouho 1887, Schurig 1906).
- (5) Festoons characterize the stomach of all "regular" sea urchin taxa. This character is lost in the irregular groups.

(6) An apomorphy of the Cidaroida is presented by the loss of the epidermal covering of the primary spines. This character has not been observed in any other extant sea urchin taxon (Littlewood & Smith 1995).

(7) The primary siphon, also termed Hoffmann's organ, is an intricate structure paralleling the stomach. Presumably, it constitutes a morphological advancement of the previously mentioned siphonal groove. Nevertheless, the current concept of echinoid phylogeny suggests a convergent evolution of this organ (Holland & Ghiselin 2008). It can be found in all taxa not possessing a siphonal groove.

(8) The enlarged caecum following the intersection of oesophagus and anterior stomach can be found in Echinothurioida, Pedinoida, Diadematoida, *Stomopneustes variolaris*, and *Glyptocidaris crenularis*. Less enlarged caeca are present in many echinacean taxa. This confined area of the anterior stomach of the "regular" taxa has been shown to possess largely the same histological characteristics as the subsequent stomach regions. The location and size of the enlarged caecum hint at its possible precursor function of the highly specialized gastric caecum that is found in the Irregularia.

(9) The echinoid buccal sacs, also termed gills, constitute external extensions of the peripharyngeal coelom. Their function is still not fully understood, although a dominant role in gas exchange has been ruled out. These structures are present in different shapes and sizes in all "regular" taxa except for the Cidaroida.

(10) Except for Cidaroida, Pedinoida, and Aspidodiadematidae, all "regular" sea urchin taxa possess a festooned intestine. This character is absent in Irregularia and supports a close relationship of Pedinidae and Aspidodiadematidae as well as Diadematidae and Micropygidae.

(11) The longitudinal body wall muscles constitute an apomorphy of the Echinothurioida. The more basal Phormosomatidae seem to have weakly developed longitudinal muscles in comparison to the pronounced muscles found in their sister group, the Echinothuriidae.

(12) The presence of five leaf-shaped, discrete spongy bodies, also termed Tiedemann's bodies, is a joint feature of acroechinoid sea urchins - except for the irregular taxa. However, some clypeasteroid groups show slightly altered spongy bodies, but whether these structures are homologous to the spongy bodies found in "regular" taxa remains unclear. For further clarification, the soft tissue structures surrounding Aristotle's lantern that is still present in juvenile holactypoids and "cassiduloids" also merit a closer look in this context.

(13) The outer marginal duct of the digestive tract haemal system can be found in all acroechinoid taxa, again except for the Irregularia. The outer marginal duct displays a certain variation and is less developed in the basal acroechinoid taxa, e.g. Pedinoida and Aspidodiadematidae.

(14) A pronounced, muscularized anal cone can be found in Diadematidae and Aspidodiadematidae, while Micropygidae possess a less conspicuous anal cone. This character

presumably constitutes an apomorphy of the Diadematacea and is therefore considered to have been lost in the Pedinoida.

(15) The heavily sacculated stomach of the Arbacioida clearly distinguishes them from their presumed sister taxon, the Stomopneustidae. However, some salenioids (not shown in Fig. 2) also display a sacculated stomach, hinting at a potential convergent evolution of this architectural feature.

(16) The presence of four gonads, i.e. the reduction of the fifth gonad, is a character that evolved along with the secondarily acquired bilateral symmetry of the Irregularia. Although some derived irregular taxa possess more (five) or less (two to three) than four gonads, this character is considered an apomorphy of the Irregularia.

(17) Another apomorphy of this group of sea urchins is the pentagonal membrane, a structure composed of coelomic epithelia engulfing the apical region underneath the madreporic plate. Further histological analyses will be required to unravel the complex mesenterial connections that this structure is based upon. The homologies of the various mesenteries of “regular” and irregular taxa will be a future aspect of my work.

(18) The highly specialized gastric caecum constitutes another apomorphy of the Irregularia. It can be found in different shapes and sizes throughout the irregular groups. Whether the gastric caecum is really absent in laganine and scutelline sand dollars needs to be further analyzed using histology, since the presence of a haemal strand between the sacculated lateral and the smooth main part of the laganine and scutelline stomach might be indicative of the presence of a gastric caecum.

(19) A flattened digestive tract is a prominent feature of sand dollars and is considered an apomorphy of this group.

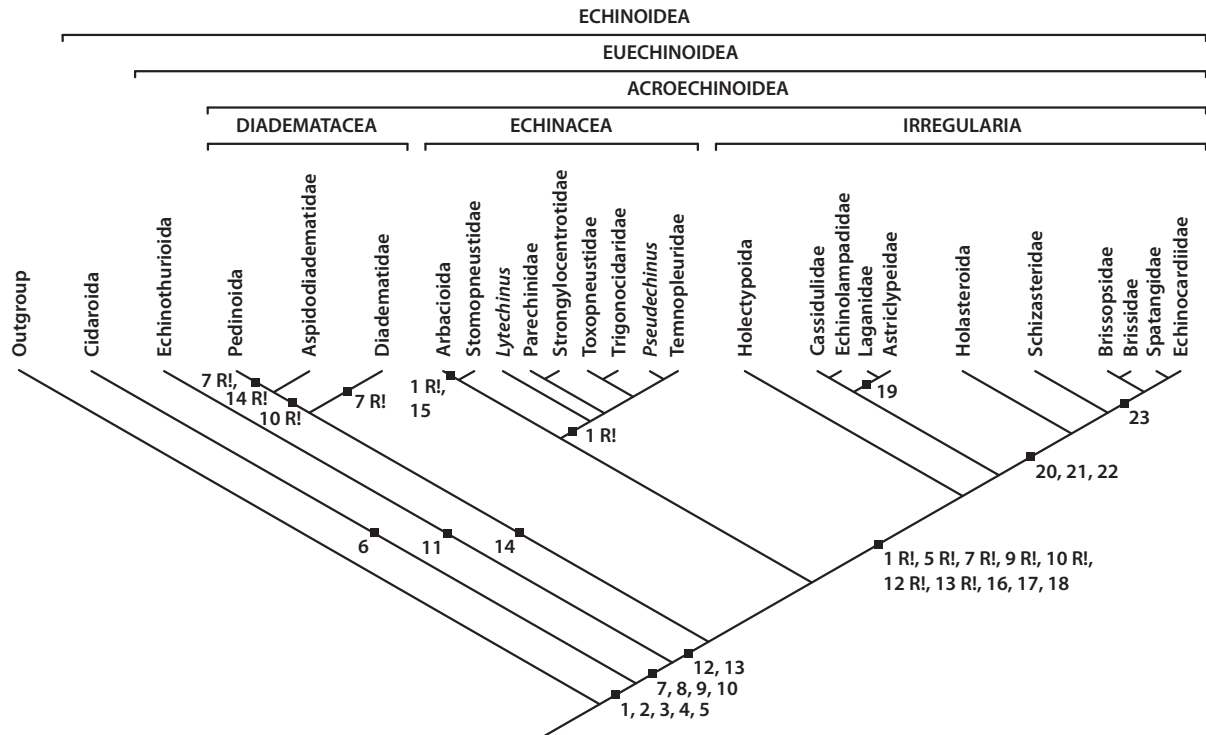
(20) The axial complex is C- to S-shaped in holasteroid and spatangoid sea urchins when seen in lateral view. This character is considered an apomorphy of the Atelostomata, a taxon uniting the highly derived Holasteroida and Spatangoida.

(21) Another apomorphy of this group of sea urchins is the presence of a secondary siphon. However, the presence of this structure could also be possible in Echinolampadidae, which then would hint at a convergent evolution. Further analyses will be needed to clarify this situation.

(22) In the Atelostomata, the oesophagus is initially directed towards interambulacrum 5, whereas in all other sea urchin groups, the oesophagus is initially directed towards ambulacrum III.

(23) An apomorphy of the Micrasterina, a spatangoid subtaxon, is the characteristic enlargement of the mesenterial strand suspending the stomach. In this taxon, this structure extends far towards ambulacrum III. All other irregular groups lack this extended mesentery.





**Fig. 2:** Phylogeny of the Echinozoa based on a cladistic analysis of molecular characters. Modified after Smith et al. (2006). Several of the taxa mentioned in Chapters 8 and 9 have not been included into the analysis because of the absence of suitable tissue material for sequencing (e.g. *Micropyga tuberculata*, *Glyptocidaris crenularis*, Salenioida). The splitting of the Echinozoa and Temnopleurozoa as well as the position of *Lytechinus* are unexpected consequences of the molecular character-based studies and contradict hypotheses based entirely upon morphological data. The numbers refer to characters described in the text. R! = character reduction.

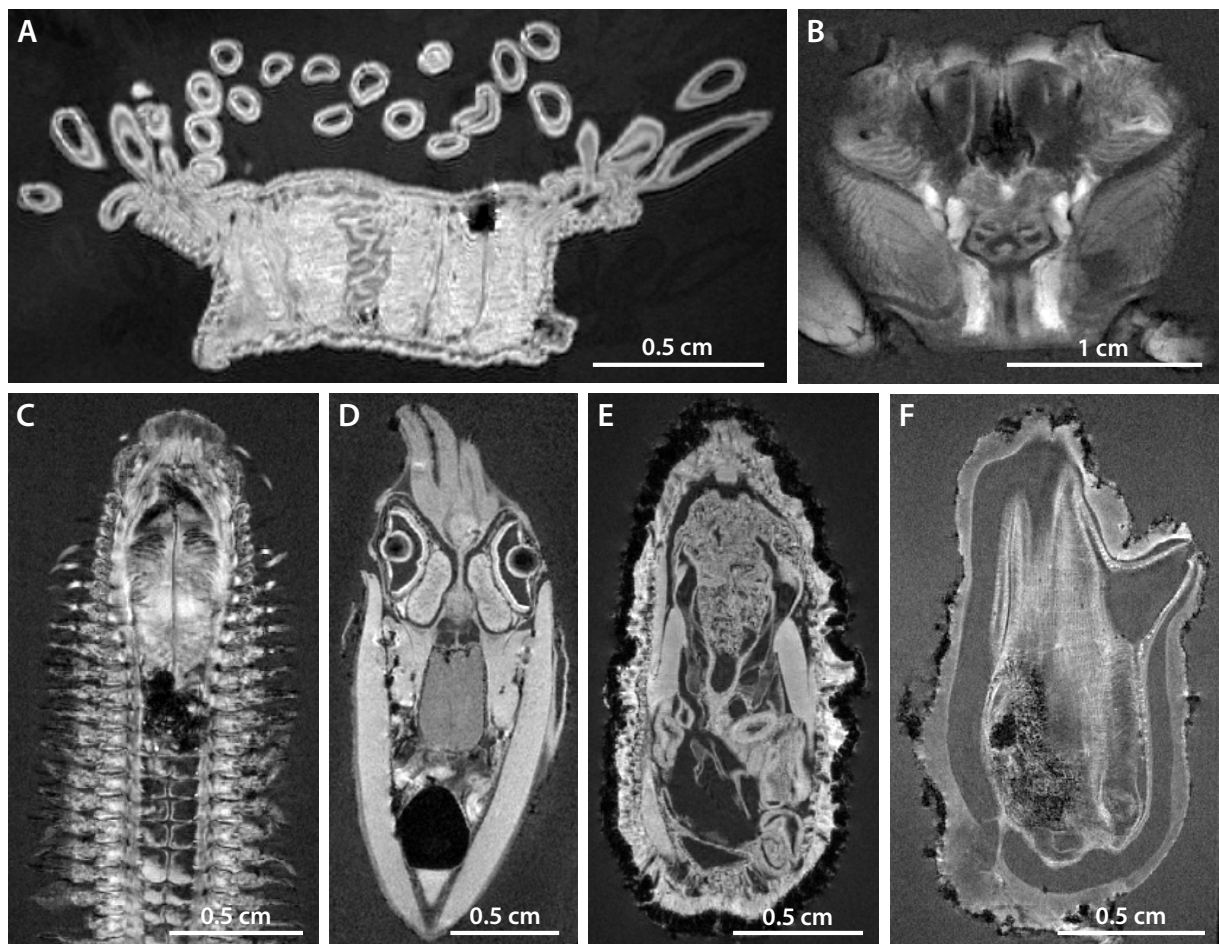
The comprehensive MRI analyses, in combination with dissection and histology, have the potential to lead to the reappraisal of certain internal organs in a number of groups, e.g. the gastric caecum in Clypeasteroidea and the primary siphon in Aspidodiadematidae. However, and maybe not surprisingly considering the extensive previous studies of this animal group, no completely new internal organ could be described for sea urchins. A first idea of potentially homologous and convergent characters will hopefully be obtained using cladistic methods based on the combined hard-part, larval and soft tissue matrix. Using this approach, the complex characters currently conflicting in terms of parsimony in a given scenario (e.g. the digestive tract festoons and the primary siphon) might be united to deduce a single consistent hypothesis of echinoid phylogeny.

It must be pointed out, however, that the presented set of selected soft tissue characters (1-23) does not appear to provide additional information which could help in solving the existing discrepancies in the current phylogenetic hypotheses of several of the more derived “regular” taxa, e.g. Echinozoa, Temnopleurozoa, Salenioida and Arbacioida. In spite of these cautionary remarks, a number of soft tissue structures supports existing hypotheses regarding the monophyly of various other taxa, e.g. of the Irregularia (presence of four gonads, presence of the gastric caecum), the Atelostomata (presence of a secondary siphon), the Micrasterina (presence of an extended mesentery), the Acroechinozoa (presence of five

discreet spongy bodies), etc. A careful selection of soft tissue structures for phylogenetic inferences and their amalgamation with existing phylogenetic trees will therefore almost certainly result in a refined hypothesis of sea urchin evolution.

#### 9.4. Concluding remarks

The MRI analyses of selected representative sea urchin taxa carried out as part of this work have led to an improved understanding of sea urchin internal anatomy in general. Furthermore, through the inclusion of museum specimens, the taxon sampling could be considerably increased. It appears that combined analyses involving MRI,  $\mu$ CT, dissection, and a thorough literature search have the potential to trigger the renaissance of morphological research on a macroscopic scale - a field where, according to a widely held belief, everything had already been said and done. In the light of the extensive fossil, larval, hard-part, and soft tissue datasets, sea urchins have become one of the best-studied groups of marine invertebrates. The model character of this group was recently underlined through the sequencing of the entire genome of the purple sea urchin, *Strongylocentrotus purpuratus* (Sea Urchin Genome Sequencing Consortium 2006).



**Fig. 3:** Virtual sections through MRI datasets of selected non-echinoid invertebrates. Isotropic resolution of each image stack: 81  $\mu$ m. **A** Sea anemone (Cnidaria: Actinaria). **B** Crab (Crustacea: Brachyura). **C** Ragworm (Annelida: Nereididae). **D** Cuttlefish (Mollusca: Sepiida). **E** Sea cucumber (Echinodermata: Holothuroidea). **F** Sea squirt (Tunicata: Ascidiacea).

---

Clearly, the extended application of MRI will lead to a renewed interest in soft tissue structures in other invertebrate taxa and, possibly, even in vertebrates. A preliminary analysis to find potential candidates for further large-scale comparative MRI studies on invertebrates has already shown that this technique can be employed to study many other taxa (Fig. 3). Further experiments will therefore involve a combination of various non-invasive imaging techniques, especially MRI and  $\mu$ CT, and allow the scanning of considerable numbers of specimens. The storage, dissemination and communication of these data have already been shown to be possible using the various approaches described in the study presented here.

## Bibliography (Chapters 1, 8, 9)

- Agassiz A. 1872-1873. Revision of the Echini. Illustrated Catalogue of the Museum of Comparative Zoology 7: 1-762
- Agassiz A. 1881. Report on the Echinoidea dredged by HMS Challenger during the years 1873-1876. Challenger Report, Zoology 9: 1-321
- Agassiz L. 1841. *Livraison des Monographies d'Echinodermes vivants et fossiles*. Neuchatel: Petitpierre
- Agassiz A, Clark HL. 1908. Hawaiian and other Pacific Echini. The Salenidae, Arbaciidae, Aspidodiadematidae, and Diadematidae. Memoirs of the Museum of Comparative Zoology 34 (2)
- Agassiz A, Clark HL. 1909. Hawaiian and other Pacific Echini. The Echinothuridae. Memoirs of the Museum of Comparative Zoology 34 (3)
- Aiyar RG. 1938. Salmacis - The Indian sea urchin. In: Bahl KN, ed. *The Indian Zoological Memoirs on Indian Animal Types, Vol. 7*. Lucknow: Lucknow Publishing House
- Aldrovandi U. 1606. *De Reliquis Animalibus Exsanguinibus*
- Amos WB, White JG. 2003. How the confocal laser scanning microscope entered biological research. *Biology of the Cell* 95: 335-342
- Attwood D. 2006. Nanotomography comes of age. *Nature* 442: 642-643
- Bamber RC. 1921. Note on some experiments on the water vascular system of *Echinus*. *Proceedings of the Liverpool Biological Society* 35: 64-70
- Betz O, Wegst U, Weide D, Heethoff M, Helfen L, Lee WK, Cloetens P. 2007. Imaging applications of synchrotron X-ray phase-contrast microtomography in biological morphology and biomaterials science. I. General aspects of the technique and its advantages in the analysis of millimetre-sized arthropod structure. *Journal of Microscopy* 227: 51-71
- Bock C, Frederich M, Wittig RM, Pörtner HO. 2001. Simultaneous observations of haemolymph flow and ventilation in marine spider crabs at different temperatures: a flow weighted MRI study. *Magnetic Resonance Imaging* 19: 1113-1124
- Boesch C. 2001. How MRI and MRS can probe tissue microstructure far below the spatial dimensions of a voxel. *NMR in Biomedicine* 14: 55-56
- Bonnet A. 1925. Documents pour servir à l'étude de la variation chez les échinides. *Bulletin de l'Institut Oceanographique a Monaco* 462: 1-18
- Breyne JP. 1732. *Schediasma de Echinis*. Gedani: Dissertatio
- Brouwer M, Engel DW, Bonaventura J, Johnson GA. 1992. In vivo magnetic resonance imaging of the blue crab, *Callinectes sapidus*: effect of cadmium accumulation in tissues on protein relaxation properties. *Journal of Experimental Zoology* 263: 32-40

- Bushberg JT, Seibert JA, Leidoldt EM, Boone JM. 2002. *The essential physics of medical imaging*. Lippincott Williams & Wilkins
- Callaghan PT. 1991. *Principles of Nuclear Magnetic Resonance Microscopy*. Oxford: Clarendon Press
- Calman WT. 1941. Ernest William MacBride. 1866-1940. Obituary Notices of Fellows of the Royal Society 3: 747-759.
- Campos LS, Moura RB. 2008. Macrostructure and evolution of the digestive system in Echinoida. *Zoomorphology* 127: 135-141
- Chadwick HC. 1900. *Echinus*. In: Liverpool Marine Biology Committee Memoir III. Liverpool: University Press
- Chesher RH. 1963. Contributions to the biology of *Meoma ventricosa* (Echinoidea: Spatangoida). *Bulletin of Marine Science* 19: 72-110
- Clark HL. 1912. Hawaiian and other Pacific Echini. The Pedinidae, Phymosomatidae, Stomopneustidae, Echinidae, Temnopleuridae, Strongylocentrotidae, and Echinometridae. *Memoirs of the Museum of Comparative Zoology* 34 (4)
- Coe WR. 1912. Echinoderms of Connecticut. Connecticut State Geological and Natural History Survey Bulletin 19: 1-152
- Cuénot L. 1891. Etudes morphologiques sur les échinodermes. *Archives de Biologie (Paris, Bruxelles)* 11: 303-680
- Cuénot L. 1948. Anatomie, éthologie et systématique des Echinodermes. In: Grassé PP, ed. *Traité de Zoologie, vol. II*. Paris: Masson
- Davenel A, Quéllec S, Pouvreau S. 2006. Noninvasive characterization of gonad maturation and determination of the sex of Pacific oysters by MRI. *Magnetic Resonance Imaging* 24: 1103-1110
- De Ridder C, Jangoux M. 1993. The digestive tract of the spatangoid echinoid *Echinocardium cordatum* (Echinodermata): morphofunctional study. *Acta Zoologica (Stockholm)* 74: 337-351
- Eichelbaum E. 1910. Über Nahrung und Ernährungsorgane von Echinodermen. *Wissenschaftliche Meeresuntersuchungen/Abteilung Kiel* 11: 187-274
- Fechter H. 1972. Untersuchungen über den Wasserwechsel der Seeigel und seine Bedeutung für Atmung und Exkretion. *Helgoländer Meeresuntersuchungen* 23: 80-89
- Fedotov DM. 1924. Zur Morphologie des axialen Organkomplexes der Echinodermen. *Zeitschrift für wissenschaftliche Zoologie* 123: 209-305
- Gesner C. 1558. De Piscium et Aquatilium Animantium Natura. In: *Historia animalium Liber IV*. Tiguri
- Gesner C. 1563. *Fischbuch*. Franckfurt am Meyn: Cambier

- Gladfelter WB. 1978. General ecology of the cassiduloid urchin *Cassidulus cariboeorum*. *Marine Biology* 47: 149-160
- Goldschmid A. 2007. Echinodermata, Stachelhäuter. In: Westheide W, Rieger RM, eds. *Spezielle Zoologie. Teil 1: Einzeller und Wirbellose Tiere*. Heidelberg: Spektrum Akademischer Verlag
- Gozansky EK, Ezell EL, Budelmann BU, Quast MJ. 2003. Magnetic resonance histology: in situ single cell imaging of receptor cells in an invertebrate (*Loliguncula brevis*, Cephalopoda) sense organ. *Magnetic Resonance Imaging* 21: 1019-1022
- Gregory ER. 1911. Observations on the water-vascular system in *Echinarachnius parma*. *Zoologischer Anzeiger* 38: 323-326
- Haeckel E. 1904. *Kunstformen der Natur*. Leipzig und Wien: Verlag des Bibliographischen Instituts
- Hamann O. 1887. Anatomie und Histologie der Echiniden und Spatangiden. In: *Beiträge zur Histologie der Echinodermen, Heft 3*. Jena: Fischer
- Harvey EV. 1956. *The American Arbacia and Other Sea Urchins*. Princeton: Princeton University Press
- Hoffmann CK. 1871. Zur Anatomie der Echinen und Spatangen. *Niederländisches Archiv für Zoologie* 1: 11-112
- Holland ND, Ghiselin MT. 2008. Siphons and siphonal grooves in the digestive systems of the Echinoidea (Echinodermata). *Zoomorphology* 127: 259-264
- Huang D, Swanson EA, Lin CP, Schuman JS, Stinson WG, Chang W, Hee MR, Flotte T, Gregory K, Puliafito CA. 1991. Optical coherence tomography. *Science* 254: 1178-1181
- Hyman LH. 1955. IV. Echinodermata. In: *The Invertebrates*. New York: McGraw-Hill
- Jensen M. 1981. Morphology and classification of Euechinoidea Bronn, 1860 – a cladistic analysis. *Videnskabelige Meddelelser fra Dansk Naturhistorisk Forening i Kjobenhavn* 143: 7-99
- Kaburek M, Hilgers H. 1999. The axial-hydrocoel complex of the endemic Mediterranean heart urchin *Schizaster canaliferus* (Echinoidea: Spatangoida). In: Candia Carnevali MD, Bonasoro F, eds. *Echinoderm Research 1998*. Rotterdam: Balkema
- Klaus AV, Schawaroch V. 2006. Novel methodology utilizing confocal laser scanning microscopy for systematic analysis in arthropoda (Insecta). *Integrative & Comparative Biology* 46: 207-214.
- Klein JT. 1734. *Naturalis dispositio Echinodermatum*. Gedani: Schreiber
- Klinghardt F. 1911. Über die innere Organisation und Stammesgeschichte einiger irregulärer Seeigel der Oberen Kreide. Jena: PhD-thesis
- Koehler R. 1883. Recherches sur les échinides des côtes de Provence. In: *Annales du Musée d'Histoire Naturelle Marseille – Zoologie, Tome 1, Memoire No. 3*

- Koehler R. 1914. An account of the Echinoidea. I. Spatangidés. In: *Echinoderma of the Indian Museum, Part VIII, Echinoidea (I)*. Calcutta: Trustees of the Indian Museum
- Koehler R. 1922. An account of the Echinoidea. II. Clypeastridés et Cassidulidés. In: *Echinoderma of the Indian Museum, Part IX, Echinoidea (II)*. Calcutta: Trustees of the Indian Museum
- Leipoldt F. 1893. Das angebliche Exkretionsorgan der Seeigel, untersucht an *Sphaerechinus granularis* und *Dorocidaris papillata*. *Zeitschrift für wissenschaftliche Zoologie* 55: 4-50
- Littlewood DTJ, Smith AB. 1995. A combined morphological and molecular phylogeny for sea urchins (Echinoidea: Echinodermata). *Philosophical Transactions of the Royal Society B Biological Sciences* 347: 213-234
- Littlewood DTJ, Smith AB, Clough KA, Emson RH. 1997. The interrelationships of the echinoderm classes: morphological and molecular evidence. *Biological Journal of the Linnean Society* 61: 409-438
- Lovén S. 1892. Echinologica. Bihang till Kongliga Svenska Vetenskaps-Akademiens Handlingar 18: 1-73
- Ludwig H. 1877. *Morphologische Studien an Echinodermen. I. Beiträge zur Anatomie der Crinoideen*. Leipzig: Verlag von Wilhelm Engelmann
- Ludwig H. 1889-1892. Die Seewalzen. In: *Dr. H. G. Bronn's Klassen und Ordnungen des Thier-Reichs. Band 2, Abtheilung 3, Buch 1*. Leipzig: C.F. Winter'sche Verlagshandlung
- Ludwig H, Hamann O. 1904. Die Seeigel. In: *Dr. H. G. Bronn's Klassen und Ordnungen des Thier-Reichs. Band 2, Abtheilung 3, Buch 4*. Leipzig: C.F. Winter'sche Verlagshandlung
- MacBride EW. 1906. Echinodermata. In: Hamer SF, Shibly AE, eds. *The Cambridge Natural History*. London: MacMillan
- Michels J. 2007. Confocal laser scanning microscopy: using cuticular autofluorescence for high resolution morphological imaging in small crustaceans. *Journal of Microscopy* 227: 1-7
- Mortensen T. 1907. Echinoidea, Part 2. In: *The Danish Ingolf-Expedition 4*
- Mortensen T. 1928-1951. *A monograph of the Echinoidea*. Copenhagen: Reitzel
- Perrier E. 1875. Recherches sur l'appareil circulatoire des oursins. *Archives de Zoologie Experimentale et Générale* 4: 605-643
- Pohlmann A, Möller M, Decker H, Schreiber WG. 2007. MRI of tarantulas: morphological and perfusion imaging. *Magnetic Resonance Imaging* 25: 129-135
- Prouho H. 1887. Recherches sur le *Dorocidaris papillata* et quelques autres échinides de la Méditerranée. *Archives de Zoologie Expérimentale et Générale* 5: 213-380
- Rondelet G. 1554. *De Piscibus Marinis, in quibus verae piscium effigies expressae sunt*. Lugduni: Bonhomme

- Rumpf GE. 1705. *D'Amboinsche Rariteitkamer*. Amsterdam: Halma
- Ruthensteiner B. 2008. Soft part 3D visualization by serial sectioning and computer reconstruction. *Zoosymposia* 1: 63-100
- Sarasin P, Sarasin F. 1887. Ueber die Anatomie der Echinothuriden und die Phylogenie der Echinodermen. In: *Ergebnisse naturwissenschaftlicher Forschungen auf Ceylon. Band I, Heft 3*. Wiesbaden: Kreidel`s
- Schmitt JM. 1999. Optical coherence tomography (OCT): a review. *IEEE Journal of Selected Topics in Quantum Electronics* 5: 1205-1215
- Schurig W. 1906. Anatomie der Echinothuriden. In: Chun C, ed. *Wissenschaftliche Ergebnisse der deutschen Tiefsee-Expedition auf dem Dampfer „Valdivia“ 1898-1899. Fünfter Band, dritte Lieferung*. Jena: Fischer
- Sea Urchin Genome Sequencing Consortium. 2006. The genome of the sea urchin *Strongylocentrotus purpuratus*. *Science* 314: 941-952
- Smith AB, Pisani D, Mackenzie-Dodds JA, Stockley B, Webster BL, Littlewood DTJ. 2006. Testing the molecular clock: molecular and paleontological estimates of divergence times in the Echinoidea (Echinodermata). *Molecular Biology and Evolution* 23: 1832-1851
- Socha JJ, Westneat MW, Harrison JF, Waters JS, Lee WK. 2007. Real-time phase-contrast X-ray imaging: a new technique for the study of animal form and function. *BMC Biology* 5: 6
- Stott FC. 1955. The food canal of the sea-urchin *Echinus esculentus* L. and its functions. *Proceedings of the Zoological Society London* 125: 63-86
- Strenger A. 1973. *Sphaerechinus granularis* (Violetter Seeigel), Anleitung zur makroskopischen und mikroskopischen Untersuchung. In: Siewing R, ed. *Großes Zoologisches Praktikum, Band 18*. Stuttgart: Fischer
- Summers AP, Hartel KE, Koob TJ. 1999. Agassiz, Garman, *Albatross*, and the collection of deep-sea fishes. *Marine Fisheries Review* 61: 58-68.
- Tafforeau P, Boistel R, Boller E, Bravn A, Brunet M, Chaimanee Y, Cloetens P, Feist M, Hozowska J, Jaeger JJ, Kay RF, Lazzari V, Marivaux L, Nel A, Nemoz C, Thibault X, Vignaud P, Zabler S. 2006. Applications of X-ray synchrotron microtomography for non-destructive 3D studies of paleontological specimens. *Applied Physics A: Materials Science & Processing* 83: 195-202
- Telford M, Harold AS, Mooi R. 1983. Feeding structures, behavior, and microhabitat of *Echinocyamus pusillus* (Echinoidea: Clypeasteroidea). *Biological Bulletin* 165: 745-757
- Thorsen MS. 1998. Microbial activity, oxygen status and fermentation in the gut of the irregular sea urchin *Echinocardium cordatum* (Spatangoida: Echinodermata). *Marine Biology* 132: 423-433



- Tiedemann F. 1816. Anatomie der Röhren-Holothurie (*Holothuria tubulosa*), des Pomerantzfarbigen Seesterns (*Astropecten aurantiacus*) und des Stein-Seeigels (*Echinus saxatilis*). Landshut: Joseph Thomannsche Buchdruckerei, Verlag der Landshuter Zeitung
- Timko PL. 1976. Sand dollars as suspension feeders: a new description of feeding in *Dendraster excentricus*. *Biological Bulletin* 151: 247-259
- Valentin GG. 1841. Anatomie du genre *Echinus*. In: Agassiz L, ed. *Livraison des Monographies d' Echinodermes vivants et fossiles*. Neuchatel: Petitpierre
- Vogt C, Yung E. 1888. Echinodermata. In: *Lehrbuch der praktischen vergleichenden Anatomie. Zweiter Band*. Braunschweig: Druck und Verlag von Friedrich Vieweg und Sohn
- von Ubisch L. 1913. Die Entwicklung von *Strongylocentrotus lividus*. (*Echinus microtuberculatus*, *Arbacia pustulosa*). *Zeitschrift für wissenschaftliche Zoologie* 106: 409-448
- Wagner J. 1903. Anatomie des *Palaeopneustes niasicus*. In: Chun C, ed. *Wissenschaftliche Ergebnisse der Deutschen Tiefsee-Expedition auf dem Dampfer „Valdivia“ 1898-1899. Fünfter Band, erste Lieferung*. Jena: Fischer
- Westergren AM. 1911. *Echinoneus* and *Micropetalon*. In: *Echini. Reports on the scientific results of the expedition „Albatross“*. *Memoirs of the Museum of Comparative Zoology Volume 39, No. 2*
- Wyville Thomson C. 1874. On the Echinoidea of the Porcupine deep-sea dredging expeditions. *Philosophical Transactions of the Royal Society of London* 164: 719-756
- Ziegler A, Müller CA, Böckmann RA, Uchańska-Ziegler B. 2008. Low-affinity peptides and T cell selection. *Trends in Immunology*, in press